

THESIS

OCCURRENCE AND TRANSPORT OF SALINITY AND SELENIUM IN A TILE-DRAINED  
IRRIGATED AGRICULTURAL SYSTEM

Submitted by

Miles Brian Daly

Department of Civil and Environmental Engineering

In partial fulfillment of the requirements

For the Degree of Master of Science

Colorado State University

Fort Collins, Colorado

Spring, 2017

Master's Committee:

Advisor: Ryan T. Bailey

Co-Advisor: Timothy K. Gates

Gregory L. Butters

Copyright by Miles Brian Daly 2017

All Rights Reserved

## ABSTRACT

### OCCURRENCE AND TRANSPORT OF SALINITY AND SELENIUM IN A TILE-DRAINED IRRIGATED AGRICULTURAL GROUNDWATER SYSTEM

Elevated salinity and selenium (Se) concentrations in groundwater, soil water, and surface water are common environmental problems in many semi-arid irrigated stream-aquifer systems worldwide. Within these systems, inefficient irrigation practices often can lead to excessive dissolution of naturally occurring salts and trace elements from the surrounding geologic formations and their transport through the aquifer system and nearby surface water bodies, causing contamination of downstream waters.

Inadequate drainage in semi-arid irrigated areas leads to high groundwater levels, resulting in waterlogging of soils and evapo-concentration of salts in the root zone, both of which decrease crop yields and pose a major constraint in meeting the world's food demand. A common solution to waterlogging and soil salinization is the installation of tile drains as subsurface drainage systems. By exporting water and solutes out of the soil, tile drains effectively reduce the salinization of the soil, improve aeration, and maintain agricultural productivity levels. An undesired consequence of subsurface drainage is the acceleration of solute loading to the river system which, in conventional practice, bypasses riparian corridors that have been shown to facilitate chemical reduction of harmful solutes.

Se is a naturally occurring trace element in Cretaceous marine shales and is mobilized through reduction-oxidation (redox) reactions in the presence of reactant species such as nitrate ( $\text{NO}_3$ ) and dissolved oxygen (DO). The excessive application of fertilizer and water in irrigated

agricultural systems leads to the presence of  $\text{NO}_3$ , and subsequently accentuates dissolved Se, in groundwater baseflow that return to the river system. In high concentrations, dissolved Se is toxic to animals and humans and has become problematic in many aquatic systems worldwide. Due to its effective export of  $\text{NO}_3$  from irrigated groundwater systems, the consequential effect of subsurface drainage on Se transport in groundwater is of special interest and has not previously been studied in detail.

The objective of this thesis is to describe the influence of tile drains on salinity and Se transport in an irrigated groundwater system in a typical field setting. This objective is investigated within a 3700 acre (1500 ha) tile drained area of the Lower Arkansas River Valley (LARV) in southeastern Colorado, a historically productive, irrigated agricultural region that has experienced decline in crop productivity partially due to waterlogging and soil salinization, and also has a Se contamination problem in the Arkansas River network and its alluvium. The average concentration of total dissolved solids (TDS) in river water has been shown in previous studies to increase from an average of about 700 mg/L to 3600 mg/L with estimated crop yield reductions of 6% and 17% within surveyed areas along a 78 km reach of the Arkansas River extending from the town of Manzanola, CO to the Kansas state line. The Colorado Department of Public Health and Environment (CDPHE) has designated all segments of the LARV as impaired according to the U.S. Environmental Protection Agency (USEPA) 1999 Se chronic criterion for aquatic habitat protection of 4.6  $\mu\text{g/L}$  for lotic water.

To fulfil the overall objective, water samples analyzed for major salt ions, including  $\text{NO}_3$ , and dissolved Se were collected every one to three months over the course of two years from subsurface drainage effluent, applied surface water, tailwater runoff, and groundwater monitoring wells within and outside of the drained area. Additionally, salt and Se field-scale mass balances were estimated for irrigation events on three fields by measuring flow and

recording temporally detailed in-situ specific conductance readings of applied water and tailwater in order to better understand processes leading to tailwater solute loading. A soil salinity survey was conducted on one of the fields included in the mass balance to determine relationships that exist between soil salinity and the change in TDS concentration between applied water and tailwater.

Results indicate that through the export of  $\text{NO}_3$  from the groundwater system, subsurface drainage limits the mobilization of Se in groundwater and therefore limits the dissolved Se loaded to the river via groundwater baseflow. However, subsurface drainage effluent had a median concentration 3 times greater than the USEPA chronic criterion and appears to be a significant source of Se loading to the river system. There appears to be a  $\text{NO}_3$  concentration ( $\text{NO}_3\text{-N}$ ) threshold near 4 mg/L above which changes in  $\text{NO}_3$  concentration do not influence Se concentration. Subsurface drainage was shown to be a significant source of salt loading with median TDS concentrations over 5 times greater than applied water concentrations and no apparent impact on baseflow concentrations. The correlation between Se concentration and TDS concentration in tailwater runoff is much lower than it is for applied water indicating the possibility of spatially or temporally inconsistent sorption or redox reactions as water flows across the field causing the removal of dissolved Se. A weak linear relationship ( $R^2 = 0.39$ ) was found between average soil salinity to a depth of 25.6 inches (65 cm) and the change in TDS concentration between applied water and tailwater.

These results provide a better understanding of the role played by subsurface drainage in the loading of solutes to the river system and to the processes affecting solute concentrations of tailwater, particularly in the case of Se. Although tile drains prevent mobilization of Se in deeper levels of the aquifer, they also provide a transport pathway that bypasses the organic-rich riparian areas that could remove Se from groundwater by heterotrophic chemical reduction.

Further research is required to determine the actual benefit of tile drains in Se fate and transport. This study was not able to quantify temporal loading from subsurface drainage effluent, nor from tailwater from the entire study region due to difficulties of maintaining flow measurement structures and instruments. Future research would benefit from the installation of a pipe-flow meter near the end of the subsurface drainage system to quantify Se mass loading from subsurface drainage effluent.

## ACKNOWLEDGEMENTS

This work would not have been possible without the collaboration, assistance, and guidance of many people. First, thank you to my advisor Dr. Ryan Bailey, and my co-advisor Dr. Timothy Gates for their patient guidance in the planning of field work and data interpretation. The financial support of the Colorado Agricultural Experiment Station and the US Agency for International Development US-Pakistan Center for Advanced Studies in Water is gratefully acknowledged. Thanks to Jim Valliant for his assistance in the coordination of field work with local farmers. Thanks to the farmers themselves who were very generous in allowing us to conduct our field studies on their land, especially Phillip Chavez of Diamond A Farms and Leon Golden. Thank you to Mike Bartolo and Lane Simmons at the Colorado State University Arkansas Valley Research Center for their generosity in providing lodging and assistance with field work. Thank you to Lorenz Sutherland for sharing his expertise and for his assistance in the collection and handling of water samples. Thank you to my fellow graduate and undergraduate students for their assistance in the many hot, cold and pleasant hours of field work. Finally, thank you to my wife Emily and son Wyatt for their endless love and support.

## TABLE OF CONTENTS

ABSTRACT.....	ii
ACKNOWLEDGEMENTS.....	vi
LIST OF TABLES.....	x
LIST OF FIGURES.....	xi
CHAPTER 1: INTRODUCTION.....	1
1.1 Irrigation Return Flow Pathways and Pollutants.....	1
1.1.1 Salt Pollution.....	1
1.1.2 Selenium Pollution.....	3
1.1.3 Nitrate and Phosphorus Pollution.....	6
1.1.4 Overview of Previous Research of Field-Scale Solute Transport in Irrigated Areas with Subsurface Drainage.....	7
1.2 Overview of Previous Research in the Lower Arkansas River Valley.....	10
1.3 Subsurface Drainage in the Lower Arkansas River Valley.....	13
1.4 Study Objectives.....	14
CHAPTER 2: METHODOLOGY.....	15
2.1 Overview of Fairmont Drainage District.....	15
2.2 Monitoring Network.....	20
2.2.1 Groundwater Measurements.....	20
2.2.2 Tile Drainage Measurements.....	23
2.2.3 Applied Water and Tailwater Measurements.....	25
2.2.4 Rainfall Measurements.....	25
2.2.5 Catlin Canal Water Quality Parameter Measurements.....	26
2.3 Sampling Procedures.....	27
2.3.1 Groundwater Sampling.....	28
2.3.2 Surface Water Sampling.....	30
2.3.3 Tile Drain Sampling.....	30
2.4 Field Scale Mass Balance.....	31
2.4.1 Flume Installation and Maintenance.....	33
2.4.2 Monitoring Irrigation Events.....	35

2.4.3 Sampling for Water Quality .....	40
2.4.4 Pressure Transducer Corrections .....	40
2.4.5 Converting Pressure Transducer Data to Flow Rate .....	41
2.4.6 Detection of Submergence.....	42
2.4.7 Relationship between Measured Conductivity and Total Dissolved Solids.....	43
2.4.8 Relationship between Dissolved Selenium and Total Dissolved Solids .....	46
2.4.9 Mass Balance Calculations.....	48
2.5 Soil Salinity Survey.....	54
2.6 Statistical Methods .....	55
2.6.1 ANOVA Statistics .....	56
2.6.2 Regression Statistics.....	59
CHAPTER 3: RESULTS AND DISCUSSION.....	61
3.1 Analysis of Sample Data from Monitoring Wells, Tile Drains and Surface Sites using ANOVA Statistics .....	61
3.1.1 Comparison of Nitrate Concentration Data .....	61
3.1.2 Comparison of Dissolved Selenium Concentration Data .....	67
3.1.3 Comparison of Total Dissolved Solids Concentration Data.....	73
3.2 Analysis of Relationships between Water Quality Characteristics using Regression Statistical Methods .....	77
3.2.1 Relationship of Dissolved Se and TDS .....	77
3.2.2 Relationship of Dissolved Se and NO <sub>3</sub> .....	84
3.3 Field-Scale Mass Balance of Total Dissolved Solids.....	95
3.3.1 Relationship of Total Dissolved Solids to Electrical Conductivity .....	98
3.3.2 Analysis of Estimated TDS Concentration.....	99
3.3.3 Analysis of TDS Mass .....	103
3.3.4 Analysis of Cumulative TDS Mass .....	108
3.4 Relationship of Soil Salinity and Change in TDS Concentration between Applied Water and Tailwater.....	111
3.5 Field-Scale Mass Balance of Se .....	117
3.5.1 Relationship of Total Dissolved Solids and Dissolved Selenium .....	118
3.5.2 Analysis of Estimates of Dissolved Selenium Concentration .....	119
3.5.3 Analysis of Dissolved Se Mass .....	122

3.5.4 Analysis of Dissolved Selenium Cumulative Mass.....	127
3.6 Analysis of Nitrate Samples from Field-Scale Mass Balance.....	129
CHAPTER 4: CONCLUSIONS AND RECOMMEDATIONS FOR FUTURE RESEARCH .	131
4.1 Key Findings .....	131
4.2 Recommendations for Future Work.....	134
REFERENCES .....	137
APPENDICES .....	142
<i>APPENDIX A: SCATTERPLOTS AND LINEAR REGRESSIONS WITH STATISTICAL     OUTLIERS .....</i>	<i>143</i>
<i>APPENDIX B: CONFIDENCE INTERVALS OF <math>C_{TDS}</math> AND <math>C_{Se}</math> ESTIMATION.....</i>	<i>147</i>
<i>APPENDIX C: STATISTICAL DIAGNOSTIC PLOTS FOR ANOVA STATISTICS .....</i>	<i>154</i>
<i>APPENDIX D: STATISTICAL DIAGNOSTIC PLOTS FOR LINEAR REGRESSIONS .....</i>	<i>158</i>
<i>APPENDIX E: STATISTICAL DIAGNOSTICS FOR ANOVA STATISTICS FOR     COMPARISON OF FIELD-SCALE TDS MASS BALANCE POPULATIONS .....</i>	<i>172</i>
<i>APPENDIX F: STATISTICAL DIAGNOSTICS FOR ANOVA STATISTICS FOR     COMPARISON OF FIELD-SCALE SELENIUM MASS BALANCE POPULATIONS .....</i>	<i>176</i>
<i>APPENDIX G: STATISTICAL DIAGNOSTICS FOR ANOVA STATISTICS AND LINEAR     REGRESSIONS OF SOIL SALINITY SURVEY AND MASS BALANCE .....</i>	<i>181</i>

## LIST OF TABLES

Table 1. Area and proportion of drained fields under each farm in the FDD.....	20
Table 2. Area and proportion of crops on drained fields in the FDD. ....	20
Table 3. Characteristics of Fairmont Drainage District monitoring wells.....	21
Table 4. Tolerances to be met prior to collecting sample. ....	29
Table 5. Characteristics of fields selected for mass balance analysis.....	31
Table 6. Rating equations for flumes.....	42
Table 7. Results of Kruskal-Wallis test and Dunn test for NO <sub>3</sub> -N sample data separated by type of sample.....	62
Table 8. Results of Kruskal-Wallis test and Dunn test for NO <sub>3</sub> -N concentration in applied irrigation water and groundwater samples grouped by presence of drains and depth of monitoring well.....	67
Table 9. Results of one way fit and pairwise comparison of means for C <sub>Se</sub> data grouped by sample type. ....	68
Table 10. Results of Kruskal-Wallis test and Dunn test for C <sub>Se</sub> sample data grouped by type of sample. ....	68
Table 11. Results of Kruskal-Wallis test and Dunn test for C <sub>Se</sub> sample data grouped by presence of drains and depth of monitoring well.....	71
Table 12. Results of Kruskal-Wallis and Dunn tests for C <sub>TDS</sub> sample data grouped by type of sample. ....	74
Table 13. P-values from Kruskal-Wallis test comparing median C <sub>TDS</sub> of applied irrigation water and tailwater for the measured irrigation events on the three fields. ....	102
Table 14. P-values from Kruskal-Wallis test comparing TDS mass loading rate (kg/hr) of applied water and tailwater on fields DA7, Muth2, and Muth9. ....	107
Table 15. Dunn test p-values for the change in C <sub>TDS</sub> between applied water and tailwater (Delta TDS) for each measured irrigation siphon tube sets for field Muth2. ....	112
Table 16. P-values from Kruskal-Wallis test comparing C <sub>Se</sub> of applied irrigation water and tailwater for the measured irrigation events for the three fields. ....	121
Table 17. P-values from Kruskal-Wallis test comparing dissolved Se mass loading rate (g/acre/hr) of applied irrigation water and tailwater for the three fields.....	126
Table 18. Slopes of C <sub>TDS</sub> vs specific conductance for linear regression confidence intervals. ..	150
Table 19. Slopes of C <sub>Se</sub> vs C <sub>TDS</sub> for linear regression confidence intervals for applied water and tailwater.....	150

## LIST OF FIGURES

Figure 1. Diagram showing the relative redox potential of electron acceptors and the product of the redox processes. ....	5
Figure 2. Map of the upstream study region (USR) and downstream study region (DSR) in reference to the state of Colorado and the Arkansas River basin .....	13
Figure 3. Images of an uncovered tile drain within the FDD demonstrating the good structural condition of the drain, (a) minor shifting that occurred over time and (b) reorientation of pipe segments.....	16
Figure 4. Overview of the tile drain lines and monitoring network in the Fairmont Drainage District.....	17
Figure 5. Confluence of central tailwater drainage ditch, tile drain trunk outlet, and Timpas Creek. ....	18
Figure 6. Images of tile drain trunk outlet into the tailwater drainage ditch in the FDD. ....	19
Figure 7. Images of monitoring well drilling and installation process: (a) collection of soil samples from core during drilling process, (b) soil core from top four feet of soil profile, (c) insertion of HOBO pressure transducer into completed monitoring well, and (d) finished well with flush mounting. ....	24
Figure 8. Fields contributing water to the central tailwater ditch and the tile drain. ....	26
Figure 9. Images of sampling from groundwater: monitoring wells (a) well G8, and (b) well G4. ....	29
Figure 10. Sampling from tile drain manhole S3.....	30
Figure 11. Fields selected for mass balance analysis, location of installed flumes for measuring applied water, spillwater, and tailwater; siphon sets (temporal/spatial irrigation divisions); and siphon set intervals from which samples were taken.....	32
Figure 12. Installation practices for trapezoidal flumes used in field mass balance studies: (a)Tarp is folded over and secured to concrete ditch, (b) HOBO water level recorder on upstream side of flume secured in the designated slot, (c) HOBO water level recorder on downstream side of flume, and (d) HOBO water level recorder on downstream side of ramp flume. ....	34
Figure 13. Examples of measured field flows: (a) Spillover flow over a check dam in the head ditch for Muth2 field, (b) Spillover flow under check dam in head ditch for DA7 field, (c) flow through the tailwater flume for field Muth2, and (d) flow through the applied water flume for field Muth2.....	36
Figure 14. Preparation and installation of flow measuring flumes: (a) Cleaning flumes, caulking seams and attaching tarps, (b) securing tarp on upstream side of flume, (c) flume for measuring diverted flow to field DA7, and (d) flume for measuring diverted flow to fields Muth2 and Muth9.....	37

Figure 15. Additional images of flow measuring flumes: (a) Ramp flume leveled with tarp secured, ready to be backfilled, (b) sampling from DA7 tailwater flume, (c) flume for measuring tailwater flow from field Muth9 mixing with spillover water, and (d) flume for measuring tailwater flow from field Muth2. ....	38
Figure 16. Plot of uncorrected, corrected, and flow computed from manual readings for field Muth2.....	41
Figure 17. Correction of SmarTroll specific conductance data for each calibration period for field Muth2.....	44
Figure 18. Sampling locations for past data used for developing specific conductance vs TDS concentration linear regression relationship. ....	45
Figure 19. Fitted linear regression of TDS concentration vs specific conductance for samples taken from Arkansas River and the field scale mass balance. ....	46
Figure 20. Scatterplots and fitted linear regression relationships of dissolved Se vs TDS concentrations for tailwater (top) and diverted water (bottom). ....	47
Figure 21. Plot of flow rate vs time for diverted flow and spillover flow for field Muth2. ....	50
Figure 22. Plot of flow rate vs time for diverted flow and spillover flow for field Muth9. ....	50
Figure 23. Measured and estimated flow rates of diverted, tailwater, and spillover flow for field Muth2.....	52
Figure 24. Measured and estimated flow rates of diverted, tailwater, and spillover flow for field DA7.....	52
Figure 25. Measured and estimated flow rates of diverted, tailwater, and spillover flow for field Muth9.....	53
Figure 26. Example of interpolation of specific conductance values using a cubic spline function in Matlab for field Muth9 tailwater flow. ....	53
Figure 27. Soil salinity contour map of field Muth2 developed from an EM-38 MK-2 survey, with siphon set intervals shown. ....	57
Figure 28. Box plots and bar plots of NO <sub>3</sub> -N concentrations grouped by the type of sample where GW, SW, TD, and TWTD are groundwater, applied irrigation water, tile drain water, and tailwater mixed with tile drain water respectively. ....	62
Figure 29. Diagnostics of NO <sub>3</sub> -N concentrations grouped by sample type: surface water, groundwater, tile drain water, and tile drain mixed with tailwater. ....	63
Figure 30. Box plot and bar plot of NO <sub>3</sub> -N concentration of tailwater mixed with tile drain water grouped by growing season (S) and winter (W). ....	64
Figure 31. Box plot and bar plot of NO <sub>3</sub> -N concentrations from applied irrigation water (SW) and groundwater samples separated by presence of drains and depth of wells. Two letter code: (drained or undrained, deep or shallow). ....	66
Figure 32. Box plot and bar plot of total dissolved Se concentrations grouped by the type of sample where GW, SW, TD, and TWTD refer to groundwater, applied irrigation water, tile drain water, and tailwater mixed with tile drain water.....	68
Figure 33. Box plot and bar plot of C <sub>Se</sub> in tailwater mixed with tile drain water grouped by growing season (S) and winter (W). ....	70

Figure 34. Box plot and bar plot of dissolved Se concentrations from applied irrigation water samples (SW) and groundwater samples grouped by presence of drains and depth of monitoring well. Two letter code: (drained or undrained, deep or shallow). .....	71
Figure 35. Box plot and bar plot of $C_{TDS}$ grouped by type of sample where GW, SW, TD, and TWTD refer to groundwater, applied irrigation water, tile drain water, and tailwater mixed with tile drain water. ....	74
Figure 36. Box plot and bar plot of $C_{TDS}$ of tile drain water water grouped by growing season (S) and winter (W). ....	75
Figure 37. Box plot and bar plot of $C_{TDS}$ of tailwater mixed with tile drain water separated by growing season (S) and winter (W). ....	76
Figure 38. Box plots and bar plots of $C_{TDS}$ from groundwater sample data separated by presence of drains and depth of wells. Two letter code (drained or undrained, deep or shallow).....	77
Figure 39. Scatterplot of dissolved Se and TDS concentrations for all samples. ....	80
Figure 40. Linear regressions of dissolved Se concentration vs TDS concentration. Clockwise from top left: Groundwater samples, Surface Water samples, Tile Drain Water Mixed with Tailwater samples, and Tile Drain Water samples. ....	81
Figure 41. Scatter plots and linear regression of Se concentration vs TDS concentration for surface water samples from the field scale mass balances (August 2016) and the complete FDD study (August 2014 - June 2016). ....	82
Figure 42. Scatter plots of $C_{Se}$ vs $C_{TDS}$ from groundwater samples separated by presence of drains and monitoring well depth with selected outliers removed. Clockwise from top left: Deep GW with tile drains, Shallow GW with tile drains, Shallow GW without tile drains, Deep GW without tile drains. ....	85
Figure 43. Scatter plot of $C_{Se}$ vs $C_N$ for samples from groundwater, surface water, tile drain water, and tailwater mixed with tile drain water. The dashed line represents the threshold $C_N$ above which increases in $C_N$ do not further inhibit reduction of $SeO_4$ . ....	87
Figure 44. Scatter plots and regressions of $C_{Se}$ vs $C_N$ of each sample type. Clockwise from top left: Groundwater, Surface Water, Tailwater mixed with Tile Drain Water, and Tile Drain Water. ....	88
Figure 45. Scatter plot of $\log C_{Se}$ vs $\log C_N$ concentrations for tile drain and groundwater samples. ....	90
Figure 46. Scatter plots of $C_{Se}$ vs $C_N$ from groundwater samples separated by presence of drains or monitoring well depth with outliers omitted. Clockwise from top left: GW with tile drains, GW without tile drains, Shallow GW, and Deep GW. ....	93
Figure 47. Scatter plots and regressions of $C_{Se}$ vs $C_N$ from groundwater samples separated by presence of drains and depth of monitoring wells with outliers omitted. Clockwise from top left: Deep Drained GW, Shallow Drained GW, Shallow Undrained GW, and Deep Drained GW. ...	96
Figure 48. Bar plot of water diverted from the canal, water applied to the field, and tailwater runoff for each field. ....	98
Figure 49. Time series plots of $C_{TDS}$ in applied water and tailwater for the measured irrigation events on the three fields.....	101

Figure 50. Box plots of TDS concentration for applied water (App) and tailwater (TW) for the measured irrigation events on each field. ....	102
Figure 51. Mass loading rate of TDS in applied irrigation water and tailwater for field DA7... ..	104
Figure 52. Mass loading rate of TDS in applied irrigation water and tailwater for field Muth2. ....	105
Figure 53. Mass loading rate of TDS in applied irrigation water and tailwater for field Muth9. ....	106
Figure 54: Box plots of TDS mass loading rate for applied water (App) and tailwater (TW) for the three fields. ....	107
Figure 55. Bar plot of the infiltrated ratio for the volume of water, mass of TDS, and mass of Se for each field. ....	109
Figure 56. Plot of cumulative TDS mass loading for applied water, tailwater, and infiltrated water for field DA7. ....	110
Figure 57. Plot of cumulative TDS mass loading for applied water, tailwater, and infiltrated water for field Muth2. ....	110
Figure 58. Plot of cumulative TDS mass loading for applied water, tailwater, and infiltrated water for field Muth9. ....	111
Figure 59. Boxplot and bar plot of the change in $C_{TDS}$ between applied water and tailwater (Delta TDS) for each measured irrigation siphon tube set for field Muth2. ....	112
Figure 60. Bar plot of the median change in $C_{TDS}$ between applied water and tailwater (Delta TDS) and the average ECe for each measured siphon set on field Muth2. ....	113
Figure 61. Scatter plot and fitted linear regression relationship for the change in $C_{TDS}$ between applied water and tailwater (Delta TDS) and the average soil salinity (ECe) for each measured siphon set for field Muth2. ....	114
Figure 62. Image of cracked soils on field Muth2. ....	114
Figure 63. Image of ponding at the tailwater edge of field Muth9. ....	115
Figure 64. Scatterplot and fitted linear regression relationship for the change in $C_{TDS}$ between applied water and tailwater (Delta TDS) and duration of irrigation for each measured siphon set on field Muth2. ....	116
Figure 65. Scatterplot and fitted linear regression relationship for the change in $C_{TDS}$ between applied water and tailwater (Delta TDS) and volume of applied water for each measured siphon set on field Muth2. ....	116
Figure 66. Scatterplot and fitted linear regression relationship for the change in $C_{TDS}$ between applied water and tailwater (Delta TDS) and volume of tailwater for each measured siphon set on field Muth2. ....	117
Figure 67. Time series plots of $C_{Se}$ in applied water and tailwater for the measured irrigations events. ....	120
Figure 68: Box plots of $C_{Se}$ for applied irrigation water (App) and tailwater (TW) for the measured irrigation events for the three fields. ....	121
Figure 69. Mass loading rate of dissolved Se in applied irrigation water and tailwater for field DA7. ....	123
Figure 70. Mass loading rate of dissolved Se in applied irrigation water and tailwater for field Muth2. ....	124

Figure 71. Mass loading rate of dissolved Se in applied irrigation water and tailwater for field Muth9.....	125
Figure 72. Box plots of dissolved Se mass loading rate for applied irrigation water (App) and tailwater (TW) for the three fields. ....	126
Figure 73. Plot of cumulative dissolved Se mass loading for applied irrigation water, tailwater, and infiltrated water for field DA7. ....	128
Figure 74. Plot of cumulative dissolved Se mass loading for applied irrigation water, tailwater, and infiltrated water for field Muth2. ....	128
Figure 75. Plot of cumulative dissolved Se mass loading for applied irrigation water, tailwater, and infiltrated water for field Muth9. ....	129
Figure 76. Barplot of $C_N$ from applied irrigation water and tailwater samples from field scale mass balance events. ....	130
Figure 77. Scatter plots of $C_{Se}$ vs $C_{TDS}$ from groundwater samples separated by presence of tile drains and by depth of the monitoring well. Clockwise from top left: groundwater with tile drains, groundwater without tile drains, deep groundwater, and shallow groundwater. ....	143
Figure 78. Scatter plots of $C_{Se}$ vs $C_{TDS}$ from groundwater samples separated by presence of drains and depth of monitoring well. Clockwise from top left: Deep GW with tile drains, Shallow GW with tile drains, Shallow GW without tile drains, Deep GW without tile drains..	144
Figure 79. Scatter plots and regressions of $C_{Se}$ vs $C_N$ from groundwater samples separated by presence of tile drains and then by depth of monitoring well. Clockwise from top left: Groundwater with tile drains, Groundwater without tile drains, Shallow Groundwater, Deep Groundwater. ....	145
Figure 80. Scatter plots of $C_{Se}$ vs $C_N$ from groundwater samples separated by presence of drains and depth of monitoring well. Clockwise from top left: Deep Drained GW, Shallow Drained GW, Shallow Undrained GW, and Deep Drained GW. ....	146
Figure 81. $C_{TDS}$ in applied water and tailwater with linear regression confidence intervals plotted for field DA7. Top: Applied Water, Bottom: Tailwater .....	147
Figure 82. $C_{TDS}$ in applied water and tailwater with linear regression confidence intervals plotted for field Muth2. Top: Applied Water, Bottom: Tailwater. ....	148
Figure 83. $C_{TDS}$ in applied water and tailwater with linear regression confidence intervals plotted for field Muth9. Top: Applied Water, Bottom: Tailwater. ....	149
Figure 84. $C_{Se}$ for applied water and tailwater with linear regression confidence intervals for field DA7. Top: Applied Water, Bottom: Tailwater. ....	151
Figure 85. $C_{Se}$ for applied water and tailwater with linear regression confidence intervals for field Muth2. Top: Applied Water, Bottom: Tailwater. ....	152
Figure 86. $C_{Se}$ for applied water and tailwater with linear regression confidence intervals for field Muth9. Top: Applied Water, Bottom: Tailwater. ....	153
Figure 87. Diagnostic plots for $C_N$ for surface water and groundwater samples separated by presence of drains and depth of monitoring well.....	154
Figure 88. Diagnostic plots of $C_{Se}$ samples separated by sample type: GW, SW, TD, TWTD.	155

Figure 89. Diagnostic plots of $C_{Se}$ from groundwater samples separated by presence of drains and depth of monitoring wells. ....	155
Figure 90. Diagnostic plots of $C_{Se}$ from groundwater samples separated by presence of drains and depth of monitoring wells. ....	156
Figure 91. Diagnostic plots of $C_{TDS}$ for each sample type: GW, SW, TD, TWTD. ....	156
Figure 92. Diagnostic plots of $C_{TDS}$ for groundwater samples separated by presence of drains and depth of monitoring wells. ....	157
Figure 93. Diagnostic plots of linear regression for $C_{TDS}$ vs specific conductance. ....	158
Figure 94. Diagnostics of $C_{Se}$ vs $C_{TDS}$ from groundwater samples. ....	159
Figure 95. Diagnostics of $C_{Se}$ vs $C_{TDS}$ from surface water samples. ....	159
Figure 96. Diagnostics of $C_{Se}$ vs $C_{TDS}$ from tile drain water samples. ....	160
Figure 97. Diagnostics of $C_{Se}$ vs $C_{TDS}$ from tile drain water mixed with tailwater samples. ....	160
Figure 98. Diagnostics of $C_{Se}$ vs $C_{TDS}$ from deep and drained groundwater. ....	161
Figure 99. Diagnostics of $C_{Se}$ vs $C_{TDS}$ from shallow and drained groundwater. ....	161
Figure 100. Diagnostics of $C_{Se}$ vs $C_{TDS}$ from deep and undrained groundwater. ....	162
Figure 101. Diagnostics of $C_{Se}$ vs $C_{TDS}$ from shallow and undrained groundwater. ....	162
Figure 102. Diagnostics of $C_{Se}$ vs $C_{TDS}$ from deep and drained groundwater with outliers removed. ....	163
Figure 103. Diagnostics of $C_{Se}$ vs $C_{TDS}$ from shallow and drained groundwater with outliers removed. ....	163
Figure 104. Diagnostics of $C_{Se}$ vs $C_{TDS}$ from deep and undrained groundwater with outliers removed. ....	164
Figure 105. Diagnostics of $C_{Se}$ vs $C_{TDS}$ from shallow and undrained groundwater with outliers removed. ....	164
Figure 106. Diagnostics of $C_{Se}$ vs $C_N$ for groundwater dataset. ....	165
Figure 107. Diagnostics of $C_{Se}$ vs $C_N$ for surface water dataset. ....	165
Figure 108. Diagnostics of $C_{Se}$ vs $C_N$ for tile drain dataset. ....	166
Figure 109. Diagnostics of $C_{Se}$ vs $C_N$ for the mixed tailwater and tile drain water dataset. ....	166
Figure 110. Diagnostics of $C_{Se}$ vs $C_N$ for groundwater with drains present. ....	167
Figure 111. Diagnostics of $C_{Se}$ vs $C_N$ for groundwater with no drains present. ....	167
Figure 112. Diagnostics of $C_{Se}$ vs $C_N$ for deep groundwater. ....	168
Figure 113. Diagnostics of $C_{Se}$ vs $C_N$ for shallow groundwater. ....	168
Figure 114. Diagnostics of $C_{Se}$ vs $C_N$ for deep drained ground water. ....	169
Figure 115. Diagnostics of $C_{Se}$ vs $C_N$ for shallow drained groundwater. ....	169
Figure 116. Diagnostics of $C_{Se}$ vs $C_N$ for deep undrained groundwater. ....	170
Figure 117. Diagnostics of $C_{Se}$ vs $C_N$ for shallow undrained groundwater. ....	170
Figure 118. Diagnostics of $C_{Se}$ vs $C_N$ for deep, drained groundwater with outliers removed. ....	171
Figure 119. Diagnostics of $C_{Se}$ vs $C_N$ for shallow, drained groundwater with outliers removed. ....	171
Figure 120. Diagnostic plots of $C_{TDS}$ for applied water and tailwater for field DA7. ....	172
Figure 121. Diagnostic plots of $C_{TDS}$ for applied water and tailwater for field Muth2. ....	173

Figure 122. Diagnostic plots of $C_{TDS}$ for applied water and tailwater for field Muth9. ....	173
Figure 123. Diagnostic plots of TDS mass loading rate for applied water and tailwater for field DA7. ....	174
Figure 124. Diagnostic plots of TDS mass loading rate for applied water and tailwater for field Muth2. ....	174
Figure 125. Diagnostic plots of TDS mass loading rate for applied water and tailwater for field Muth9. ....	175
Figure 126. Diagnostic plots of $C_{Se}$ vs $C_{TDS}$ linear regression for applied water. ....	176
Figure 127. Diagnostic plots of $C_{Se}$ vs $C_{TDS}$ linear regression for tailwater. ....	177
Figure 128. Diagnostic plots of $C_{Se}$ for applied water and tailwater for field DA7. ....	177
Figure 129. Diagnostic plots of $C_{Se}$ for applied water and tailwater for field Muth2. ....	178
Figure 130. Diagnostic plots of $C_{Se}$ for applied water and tailwater for field Muth9. ....	178
Figure 131. Diagnostic plots of dissolved Se mass loading rate for applied water and tailwater for field DA7. ....	179
Figure 132. Diagnostic plots of dissolved Se mass loading rate for applied water and tailwater for field Muth2. ....	179
Figure 133. Diagnostic plots of dissolved Se mass loading rate for applied water and tailwater for field Muth9. ....	180
Figure 134. Diagnostic plots of the difference between applied water and tailwater $C_{TDS}$ for each siphon interval for field Muth2. ....	181
Figure 135. Diagnostic plots of the difference between applied water and tailwater TDS mass for each siphon interval for field Muth2. ....	182
Figure 136. Diagnostic plots for the linear regression of the average difference of TDS concentration from applied water and tailwater vs average ECe of each siphon interval for field Muth2. ....	182
Figure 137. Diagnostic plots for the linear regression of the average difference of TDS mass from applied water and tailwater vs average ECe of each siphon interval for field Muth2. ....	183
Figure 138. Diagnostic plots for the linear regression of the average difference of TDS mass from applied water and tailwater vs the volume of irrigated water for each siphon interval for field Muth2. ....	183

## CHAPTER 1: INTRODUCTION

### **1.1 Irrigation Return Flow Pathways and Pollutants**

In an irrigated agricultural system with subsurface drainage, irrigation return flows reach the river system in one of three ways: as surface runoff (tailwater), as tile drain effluent, or as groundwater flows. Water in each of these return paths undergoes different processes that alter the chemical makeup and pollutant loads. Pollution from irrigation return flows includes but is not limited to salts, fertilizers, pesticides, and trace nutrients (Novotny, 2002).

For the purposes of this study, surface runoff comprises tailwater runoff (excess water that flows across the field surface and runs off the end) and spillover (water that flows over or around the dam set in the irrigation head ditch to raise the water elevation for flow diversion to the field through siphon tubes). Before it is mixed with tailwater, spillover is of the same quality as the irrigation water. Tailwater runoff quality generally changes in sediment content and associated sorbed contaminants such as pesticides and phosphorous (P) (Isidoro et al., 2006) and can also pick up and transport significant quantities of nitrogen (N) and salts from fields to surface water bodies (Jiao et al. 2012 and Faci et al. 1984). Tile drain effluent can transport substantial amounts of dissolved salts, selenium (Se) and agrochemicals acquired from the root zone and shallow groundwater back to the river system (Isidoro et al. 2006 and Deverel and Fujii, 1988). Groundwater return flows are often the largest source of non-point source pollution to the river system.

#### ***1.1.1 Salt Pollution***

Soil salinization is a major constraint in meeting the world's food demand and is often the most serious water quality problem in arid and semi-arid river basins (El-Ashry et al., 1985). An estimated 20% of the world's irrigated lands are saline (Tanji, 2002). Waterlogged and saline

soils exist naturally in many areas around the world but are often made worse by inefficient irrigation and inadequate drainage (Wichelns, 1999). Water logging has a direct negative effect on plant growth due to the reduced soil aeration which inhibits root respiration, density and depth (Jones and Marshall, 1992). Excess salt in the root zone inhibits plant growth by increasing the osmotic potential of the soil solution which decreases the amount of soil water available to plant roots (Jones and Marshall, 1992; Ayars et al. 2012). The combined impact of waterlogging and soil salinity is more harmful to crop yields when compared to the individual effects (Kahlown and Azam, 2002). Severe declines in agricultural productivity attributed to salinization are seen on 10% of the worlds irrigated land (Wichelns, 1999) and 20 to 25% of irrigated land in the United States experiences crop yield reductions due to salt (El-Ashry et al., 1985).

Soil water salinity increases by a combination of salt loading from irrigation water, dissolution of solid salts present in the soil profile, and concentrating processes. Irrigated water in regions with poor drainage result in high water tables which are prone to upward capillary flow caused by evapotranspiration resulting in evaporative-concentration of salts (Tedeschi et al., 2000; El-Ashry et al., 1985; Deverel and Fuji 1988). Due to evapo-concentration of salts in the upper soil layers, a “leaching fraction” often is added to the applied irrigation water that is in excess of crop consumptive use (El-Ashry et al. 1985; Ayars et al. 2012). In practice, actual leaching fractions often exceed requirements due in part to the high labor costs of achieving uniform water application (Wichelns, 1999) which contributes further to water logging and salinization. Salt concentrations of groundwater continue to increase due to dissolution of naturally-occurring salts in the geologic media (El-Ashry et al. 1985; Ayars et al. 2012). The groundwater containing increased salt concentrations returns to the river via subsurface drainage or baseflow. A study by Skogerboe and Walker (1973) found that irrigation return flows

contribute 37% of the total salt load of the Upper Colorado River Basin. Water in most streams is reused several times for irrigation and downstream users face a compounding problem of increased salinity with each use (Novotny, 2002).

In arid or semi-arid regions, TDS in tailwater typically increases in concentration and decreases in total load when compared to applied water (Faci et al. 1984). This increase in tailwater concentration is an important source of salt loading to the river system and occurs primarily through lateral solute transport processes. As irrigated water flows down furrows, there is typically a “first flush” where the concentration of TDS spikes at the advancing front of applied irrigation water as it picks up salt on the soil surface. The salt load of the water immediately behind the advancing front is similar to the irrigation supply water but as irrigated flow continues tailwater salt concentrations gradually increase due to the dissolution and entrainment of salt from near surface soil layers. Ponding at the edge of fields increases the salt concentration in the surface water but only some of this entrained salt makes its way to tailwater due to low travel velocities (Gilfedder et al. 2000). The increase in tailwater TDS concentration is much greater for soils with extensive cracking (Rhoades et al. 1997).

Subsurface tile drain systems are installed in order to lower the water table, allow freshwater to leach salts from the root-zone, and allow for soil aeration (Saiki, 1987; Christen and Skehan, 2001; Deverel and Fujii, 1988). These engineered systems have the undesired consequence of accelerating the loading pollutants such as salt, Se and N back to the river system (Presser and Ohlendorf, 1985; Johnston et al., 1965; and Hornbuckle et al., 2007).

### ***1.1.2 Selenium Pollution***

After gaining widespread attention from the massive poisoning of aquatic species in the Kesterson National Wildlife Refuge, Se has been viewed as an important environmental

contaminant for the past three decades (Deverel and Fujii, 1988). In 2016 the U.S. Environmental Protection Agency (USEPA) set the chronic criterion for Se concentration in lotic water to 3.1  $\mu\text{g/L}$  for 30-day exposure (USEPA, 2016). Animals accumulate high levels of Se by eating contaminated foods (Saiki, 1987). Studies have shown that Se solute concentrations of 1  $\mu\text{g/L}$  or less have the potential to become toxic to predatory species due to bioaccumulation processes (Lemly, 1992).

There are two major human-related causes of Se mobilization in the environment. The first, which will not be addressed in this study, is from the procurement, processing and combustion of fossil fuels. Within this category, the greatest source is leachate from coal fly-ash. The second cause of Se mobilization is from irrigation of alluvial soils derived from Cretaceous marine shales in arid and semi-arid regions (Lemly, 1992), wherein residual Se is released via autotrophic reduction of oxygenated species such as  $\text{NO}_3$  and dissolved oxygen (DO).

Se exists in four principle forms: selenate ( $\text{SeO}_4$ ), selenite ( $\text{SeO}_3$ ), elemental Se, and selenide ( $\text{Se}^{-2}$ ). For the purposes of this study, we are primarily interested in the soluble forms of Se;  $\text{SeO}_4$  and  $\text{SeO}_3$ . Selenate is a weak sorbent and is the most mobile and most toxic of the four principle forms. Selenite is a strong sorbent and is therefore not as mobile as  $\text{SeO}_4$ . There are four primary processes affecting Se speciation: reduction-oxidation, adsorption/desorption, vegetative uptake and transformation, and microbial mediation (Butler et al. 1996). Volatilization is another process affecting Se speciation. Of these processes, reduction-oxidation (redox) reactions are the principle driving mechanisms transforming Se from one species to another in groundwater. The presence of oxygenated species such as  $\text{O}_2$ ,  $\text{NO}_3$ ,  $\text{SeO}_4$ , and others allow for bacterial respiration to occur. Figure 1 shows the order of redox potential for oxygenated species. Because species such as  $\text{O}_2$  and  $\text{NO}_3$  provide higher quantities of energy for the bacteria than

SeO<sub>4</sub>, their presence prevents the reduction of SeO<sub>4</sub> to SeO<sub>3</sub> (Gates et al. 2009), which would be readily sorbed, leading to more transport of harmful Se species to surface water bodies (Bailey et al., 2012; Wright, 1999, Oremland et al. 1990). A threshold for NO<sub>3</sub> concentration under which SeO<sub>4</sub> reduction begins to occur has been suggested by Oremland et al. (1990) and roughly quantified at 10 mg/L in a regional study of the LARV by Gates et al. (2009). Inefficient irrigation and over-fertilization allow for deep percolation of irrigated water carrying NO<sub>3</sub> and ultimately has the effect of increasing the mobilization rate of Se from marine shale and residuum that contains seleno-pyrite (FeSe<sub>2</sub>) through redox reactions (Bailey et al. 2012). In a study by Deverel and Fujii (1988) it was found that the highest groundwater Se concentrations are the result of evaporative concentration of shallow groundwater.

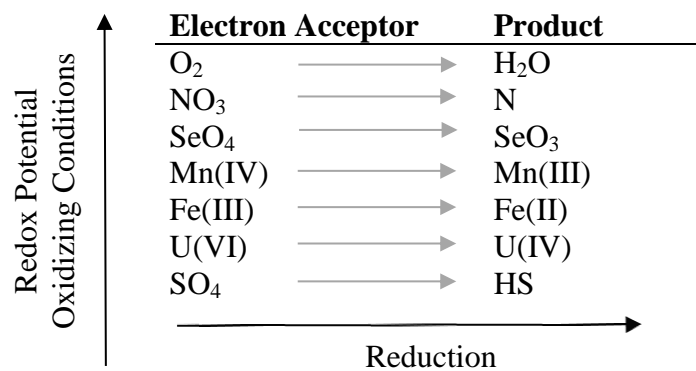


Figure 1. Diagram showing the relative redox potential of electron acceptors and the product of the redox processes.

A correlation has been found to exist between concentrations of Se and salt (Deverel and Fujii, 1988; Donnelly and Gates et al. 2009) and between Se and NO<sub>3</sub> (Wright, 1999; Gates et al. 2009) in tile drain water, surface water and groundwater. Deverel and Fujii, (1988) reported a coefficient of determination ( $R^2$ ) of 0.88 for a log-log linear regression of dissolved Se concentration and electrical conductivity (EC) (an indicator of TDS) of tile drain effluent from three separate fields. Gates et al. (2009) found a statistically significant correlation of linear regression of EC and C<sub>Se</sub> of 0.41 and 0.49 in the upstream study region and downstream study

region of the Lower Arkansas River Valley, respectively. These study regions are defined in section 1.2 of this chapter. While the relationship between TDS and Se is not thought to be causal, the salinity of water is relatively easy to estimate by taking in-situ electrical conductivity readings and these relationships can be used to estimate the concentrations of dissolved Se. As explained, the correlation between  $\text{NO}_3$  and dissolved Se is a causal relationship and can be used to explain the presence or absence of dissolved Se. A log-log linear regression of dissolved Se concentration and  $\text{NO}_3 + \text{NO}_2$  from surface water and groundwater samples had a coefficient of determination of 0.50 (Wright, 1999). Significant non-linear relationships ( $R^2 = 0.37, 0.93$ ) with considerable scatter were found between the concentration of dissolved Se ( $C_{\text{Se}}$ ) and the concentration of  $\text{NO}_3\text{-N}$  ( $C_{\text{N}}$ ) in groundwater for the upstream study region and downstream study region of the Lower Arkansas River Valley by Gates et al. (2016).

### ***1.1.3 Nitrate and Phosphorus Pollution***

N and P are the primary limiting nutrients in aquatic environments, as is also true for surface plants, and are applied abundantly as fertilizer for crop growth. N is applied typically as fertilizer in the form of ammonium salts. The aerated, micro-organism-rich soil leads to nitrification of ammonium to the very stable and mobile N species  $\text{NO}_3$ .  $\text{NO}_3$  is readily transported with both groundwater and surface water. In contrast to  $\text{NO}_3$ , P sorbs readily to soils and sediment and is transported primarily along with suspended sediment in surface waters. Because of this, P typically is the limiting nutrient in downstream nonpoint source pollution problems such as eutrophication and is the nutrient targeted for removal by many best management practices (BMP) such as sedimentation basins (Novotny, 2002).

Excess N and P from diffuse pollution of both agricultural and urban sources lead to eutrophication of surface water bodies causing toxic algal blooms, hypoxic conditions and a loss

of aquatic life and biodiversity (Novotny, 2002 and Carpenter et al. 1998). The most extensive case of excessive nutrient loading to a surface water body is the resulting hypoxic zone in the Gulf of Mexico. An annual cycle of excess nutrients from the Mississippi and Atchafalaya River Basins allow for algal blooms to flourish in the Gulf of Mexico leading to a large hypoxic zone and loss of aquatic life (Alexander et al. 2008).

The presence of P in drinking water is not known to be toxic to humans or animals, but the presence of  $\text{NO}_3$  at high concentrations has been linked to methemoglobinemia in infants and to toxic effects in livestock (Carpenter et al. 1998). For this reason, the USEPA has set a maximum contaminant level for  $\text{NO}_3$  in drinking water of 10 mg/L ( $\text{NO}_3\text{-N}$ ).  $\text{NO}_3$  is the most ubiquitous chemical contaminant in the world's aquifers. In the United States, the highest rates of  $\text{NO}_3$  contamination occur in groundwater in agricultural communities in the Midwest. Approximately 20% of sampled wells in Iowa, Nebraska and Kansas exceeded 10 mg/L in a study by Spalding and Exner (1993). In systems without subsurface drainage, groundwater return flows are the primary pathway for N to surface water bodies and the amount of loading depends in part on fertilizer application, leaching fraction, and spatial extent of riparian zones (Mellander et al. 2012).

This study is primarily focused on the irrigation return flow pathways contributing to salt and Se loading. P loading is not taken into consideration. However,  $\text{NO}_3$  is addressed in this study as it plays an important role in the mobilization of Se, as mentioned earlier.

#### ***1.1.4 Overview of Previous Research of Field-Scale Solute Transport in Irrigated Areas with Subsurface Drainage***

The incidence of massive Se poisoning of aquatic species in the Kesterson National Wildlife Refuge in the western San Joaquin Valley garnered widespread attention and led to extensive research addressing the cause and seeking solutions. Subsurface drainage that replaced

previous source waters of the pond system in the wildlife refuge was determined to be the source of high Se concentrations in surface waters leading to the poisoning incident (Presser and Ohlendorf, 1987). In a study by Deverel and Fujii (1988) of three fields in the western San Joaquin Valley underlain by subsurface drainage where drains were installed 1.5 years, 6 years, and 15 years prior to the study, it was found that newly installed drains export groundwater with high concentrations of salt and Se and the displaced water is replaced with less saline irrigation water with lower Se concentrations. In a separate report of the same field study, Fujii et al. (1988) found salinity and Se concentrations in unsaturated soils were well correlated ( $R^2=0.85$ ) in the field drained for 1.5 years but were not well correlated ( $R^2=0.33$ ) in the fields drained for 6 and 15 years indicating dissolution and precipitation of evaporate minerals containing Se are no longer the dominant factor controlling Se concentrations in unsaturated soils after a long period of irrigation and drainage. The processes of displacement of salt and Se from the root-zone by tile drains is thought to occur over the course of decades (Jury, 1975; Johnston et al. 1965; and Deverel and Fujii, 1988). In the analysis of the field with drains installed 1.5 years prior to the study Fujii and Deverel (1989) found that soluble plus adsorbed Se made up less than 15% of the total Se in the top 3.9 feet (1.19 m) of soil but increased to 80% of total Se at a depth of 8.9 feet (2.71 m) indicating soil leaching with recently installed tile drains contributes large quantities of Se to groundwater. A separate report on the same field study (Gilliom et al. 1988) found that soluble soil Se is leached downward and that it is leached progressively further as more time elapses since the installation of drains. The local geohydrologic conditions and design of a drainage system determine the contributions of water from different depths to tile drain effluent (Gilliom et al. 1988). In the analysis of water samples from monitoring wells located at the field with 15 year old drains, Gilliom et al. (1988) report the highest concentrations of Se in

groundwater were found at the deepest monitoring wells (40 to 50 feet or 12.2 to 5.2 meters deep). These water samples also had the lowest concentrations of tritium indicating their probable origin as irrigation water applied prior to 1952. The author concludes that, after the installation of tile drains, solute concentrations in tile drain effluent become more diluted over time with recently applied irrigation water, but deeper ground water provides a long-term source of water with high Se concentrations.

Installation of tile drains tends to have the effect of reducing the loss of P and organic N and increasing the loss of  $\text{NO}_3$  and soluble salts (Skaggs et al. 1994). Tile drainage salt loads have been found to vary from 0.7 to 11 times greater than those applied by irrigation water, indicating a removal of precipitated and geologic salt (Christen and Skehan, 2001). Johnston et al. (1965) found salt concentrations in tile drain effluent tend to decrease in the summer and increase in the winter due to lagged times in percolated irrigation water causing groundwater discharge to nearby streams. However, Gilliom et al (1988) found water sampling data from the 11 tile drain sumps in the western San Joaquin Valley, CA show no seasonal patterns in salinity or Se concentration despite distinct seasonal patterns in irrigation and drain flow.

The contribution of N to surface water bodies from subsurface drainage is a complex process that cannot be accurately estimated by point measurements of effluent concentrations or by annual N input. This is because the degree to which subsurface drainage accelerates the export of N from an agricultural setting to a river system depends on a number of factors including fertilizer application rate, leaching fractions, rainfall patterns, drain spacing and soil permeability (Jury, 1975; Keller et al. 2008). Assuming constant fertilizer application, high leaching fractions will load more N mass to river systems with lower concentrations whereas irrigation with low leaching fractions exports less N mass with higher concentrations (Devitt et

al., 1976). For this reason practices to prevent excessive nutrient loading may differ depending on if the goal is to protect the surface water body immediately receiving flows which may be more susceptible to high N concentrations, or the entire downstream system which is more susceptible to total N loads.

## **1.2 Overview of Previous Research in the Lower Arkansas River Valley**

The Lower Arkansas River Valley (LARV) is a historically productive agricultural region in southeastern Colorado that has been extensively studied by research groups from Colorado State University and its affiliates from 1998 until the present. The LARV is typically divided into two regions; one upstream of John Martin Reservoir named the upstream study region (USR) and one downstream of the reservoir named the downstream study region (DSR). The USR extends along a 48.5 mile (78.1 km) reach of the Arkansas River from Manzanola to Las Animas encompassing 65,200 acres (26,390 ha) of irrigated land and the DSR extends along a 44.1 mile (71.0 km) reach of the river from Lamar to the Colorado-Kansas border encompassing 81,500 acres (32,980 ha) of irrigated land (Gates et al. 2016). Figure 2 shows the geographic location of the USR and DSR in relation to the state of Colorado and the Arkansas River Basin. Extensive irrigation networks exist to distribute river water within the semi-arid environment. Similar to many irrigated agricultural systems in arid or semi-arid regions, agriculture in the LARV experiences a loss in productivity due to water logging and salinization attributed to irrigation inefficiencies and inadequate drainage (Burkhalter and Gates, 2005; Wichelns, 1999; Gates et al. 2012, Morway and Gates, 2012). TDS concentrations in the Arkansas River increase in the downstream direction averaging 930 mg/L in the USR and 2930 mg/L in the DSR (Gates et al. 2016). A groundwater model created by Morway et al. (2013) from extensive field data collected during the irrigation season from 1999 to 2007 in the USR and 2002 to 2007 in the DSR

estimated the average depth to water during the irrigation season to be 15.3 feet (4.7 m) in the USR and 22.0 feet (6.7 m) in the DSR. The same study found the depth to water for 24% and 21% of cultivated fields in the USR and DSR, respectively, to be less than 6.6 feet (2.0 m). Morway and Gates (2012) found the average soil water extract salinity  $EC_e$  to be 4.1 and 6.2 dS/m in the USR and DSR, respectively, which are high when compared to the regional crop yield thresholds for alfalfa and corn estimated by Gates et al. (2012) of 3 to 5 dS/m. Average crop yield losses due to soil water salinity are estimated to be 6% and 17% in the upstream and downstream study regions of the LARV (Morway and Gates, 2012). If the effects of waterlogging and soil salinization were removed, it is estimated that profits from agriculture could increase by 39% (Houk et al. 2006). High water tables create large hydraulic gradients driving baseflow back to surface water systems with dissolved salts and minerals that are picked up along the way which is a major source of non-point source pollution and a serious concern for downstream agriculture and the aquatic ecosystem (Gates et al. 2009). The large hydraulic gradients from high groundwater tables also drive groundwater under uncultivated land allowing for non-beneficial consumption of irrigated waters leading to more evaporative concentration of groundwater (Niemann et al. 2011). The average TDS concentration in groundwater was found to be 3,242 mg/L in the USR and 4,139 mg/L in the DSR in the analysis of all wells having at least 100 measurements from 1999 to 2011 in the USR and 2002 to 2011 in the DSR (Gates et al. 2016). Regional models developed by Gates et al. (2012) estimate groundwater salt loading to the Arkansas River of 93 and 62 tons (84 and 56 tonnes) per week per mile in the USR and DSR, respectively, which is more than the estimated salt loading to fields from irrigated water indicating a contribution of salts from the underlying geology. Mueller-Price and Gates (2008) found sizeable uncertainty in the results of stochastic models used to perform mass balance

calculations to estimate nonpoint source loading. The average TDS loading values in the USR and DSR were found to be 104 and 139 tons (104 and 126 tonnes) per week per mile. Gates et al. (2016) estimate TDS mass loading to the Arkansas River via groundwater and ungauged tributaries to be 12 tons (11 tonnes) per week per mile in both the USR and DSR. It is important to acknowledge that rising water tables and increasing soil salinity from the present levels are likely to cause proportionally more loss to agricultural production (Houk et al. 2006).

Cretaceous shales and weathered alluvium with high levels of Se underlie large portions of the LARV (Gates et al. 2009). Loading of dissolved Se from both irrigated and non-irrigated land results in high concentrations of dissolved Se within the aquatic habitat often exceeding the chronic toxicity criterion (Divine et al. 2009). The Colorado Department of Public Health and the Environment (CDPHE) has designated all segments of the LARV as impaired according to the U.S. Environmental Protection Agency (USEPA) 1999 aquatic habitat chronic criterion for Se concentration of 4.6  $\mu\text{g/L}$  which is defined as the 85<sup>th</sup> percentile values of a set of samples. In the Arkansas River, average values of dissolved Se concentration were found to be 8.9  $\mu\text{g/L}$  in the USR and 11.1  $\mu\text{g/L}$  in the DSR and the 85<sup>th</sup> percentile values were 3 and 3.3 times greater than the previous, less stringent, USEPA criterion (Gates et al. 2016). The same report found the average dissolved Se concentration in groundwater to be 55.5 and 33.1  $\mu\text{g/L}$  in the USR and DSR, respectively. A solute transport model developed by Bailey et al. (2014, 2015) predicts the spatial and temporal average of selenate ( $\text{SeO}_4$ ) concentration from 2006 to 2009 in the USR to be 53.4  $\mu\text{g/L}$ . Mueller-Price and Gates (2008) found the average loading of the dissolved Se to the Arkansas River in the DSR to be 0.94 pounds per week per mile with sizeable uncertainty. Gates et al. (2016) estimates Se loading to the river via groundwater flow, ungauged tributaries and overland flow to be 0.98 and 1.47 lbs (0.44 and 0.67 kg) per week per mile in the USR and

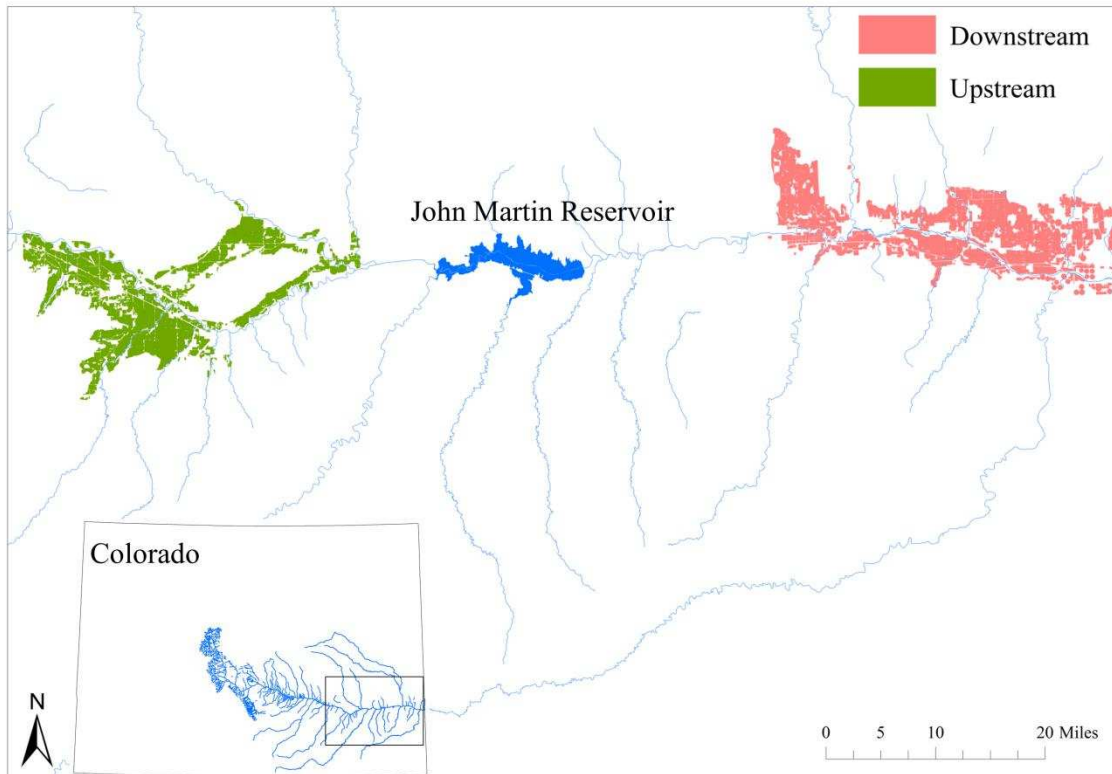


Figure 2. Map of the upstream study region (USR) and downstream study region (DSR) in reference to the state of Colorado and the Arkansas River basin

DSR respectively. A number of studies have been conducted addressing Se impairment of the Arkansas River and methods to alter water management and cultivation practices in order to return the river to compliance (Bailey et al 2014, 2015). Limited work has been done addressing the role that subsurface drainage plays in altering the amount of Se mobilized in groundwater.

### 1.3 Subsurface Drainage in the Lower Arkansas River Valley

Subsurface drainage networks were installed early in the 20<sup>th</sup> century to lower the water table and prevent salinization in select regions of the LARV. There are 25 known tile drain districts in the LARV that were organized between 1911 and 1922 under the Colorado Drainage District Act. The drainage districts vary drastically in the maintenance they have undergone since they were installed, leading to variable operating conditions. The Fairmont Drainage District

(FDD) near Rocky Ford in Otero County, CO has been relatively well maintained and is functioning in good condition. For this reason, the FDD was chosen as the study site for this project. While subsurface drainage is effective at lowering water tables, aerating soils, and improving crop yields, high pollutant concentration in drainage effluent is a concern for aquatic habitat in receiving streams and for diversion to downstream farmers in the LARV.

#### **1.4 Study Objectives**

The goal of this thesis is to better understand the concentrating and loading of salts and Se, as affected by  $\text{NO}_3$ , in irrigation return flows from an irrigated agricultural system underlain by subsurface drains. The study has two parts: the first part analyzes water quality for applied irrigation water, tile drain water, tailwater mixed with tile drain water, and groundwater in the FDD as well as outside the FDD to determine the role played by tile drains in altering solute concentrations in groundwater, and hence the eventual groundwater baseflow pollutant loading to nearby Timpas Creek, a tributary to the Arkansas River, and the export of pollutants to the river system via tile drain effluent. The second part of the study is the analysis of estimated field-scale mass balances of salt and Se for one irrigation event on three fields within the FDD to better understand processes leading to tailwater solute loading.

The remainder of the thesis is organized as follows:

- Chapter 2 provides a detailed description of the monitoring network within the study area and the methods used to collect and interpret data.
- Chapter 3 discusses the results from each part of the study.
- Chapter 4 summarizes important findings from the thesis.

## CHAPTER 2: METHODOLOGY

### 2.1 Overview of Fairmont Drainage District

The Fairmont Drainage District (FDD) is one of 25 drainage districts in the LARV and is located in CSU's USR in Otero County southwest of Swink, Colorado. The subsurface relief drainage system in the district was installed sometime between 1919 and 1928 under the authority of the Colorado Drainage District Act of 1911. The drain lines were constructed with 3 foot sections of straight ceramic pipe. Overall, the pipe seems to have held up well structurally but a few local failures have occurred due to shifting or joint clogging from roots and silt. Compared to the other drainage districts in the LARV, the FDD has been relatively well maintained and operates in good condition. Today, the removal of roots and silt is accomplished with high pressure jets on 1 inch (2.5 cm) hoses that can extend up to 1000 feet (305 m) from tile drain manholes. In the case of shifting due to subsidence, the drain line must be dug up and reoriented or replaced. An exploratory segment of the drain line located just north of Highway 10 and west of Road 24, immediately east of tile drain manhole S3 shown in Figure 4, was uncovered using a backhoe in January 2016. The photos in Figure 3 illustrate the shifting that can occur over time and the remarkably good structural condition of the tile line.

The FDD is made up of a network of field drains that link to a central collector pipe ("trunk"). The field drains are typically 6 inches (15.2 cm) in diameter most of which are buried at a depth of 3 to 5 ft (0.9 to 1.5 m) below ground surface. The trunk is 14 to 15 inches (35.6 to 38.1 cm) in diameter most of which is buried at a depth of about 3 to 5 ft (0.9 to 1.5 m). Depending on local topography, some sections of the drain are as deep as 8 feet (2.4 m). The trunk drains out of a submerged manhole into a large tailwater ditch 2,000 feet upstream of its confluence with Timpas Creek. This location at Timpas Creek is approximately 1.9 miles (3 km)

upstream of its confluence with the Arkansas River. A map of the FDD including the tile drains and monitoring network is shown in Figure 4. Figure 5 and Figure 6 show a map of the tailwater ditch and Timpas Creek and images of the tile drain outlet, respectively.



Figure 3. Images of an uncovered tile drain within the FDD demonstrating the good structural condition of the drain, (a) minor shifting that occurred over time and (b) reorientation of pipe segments.

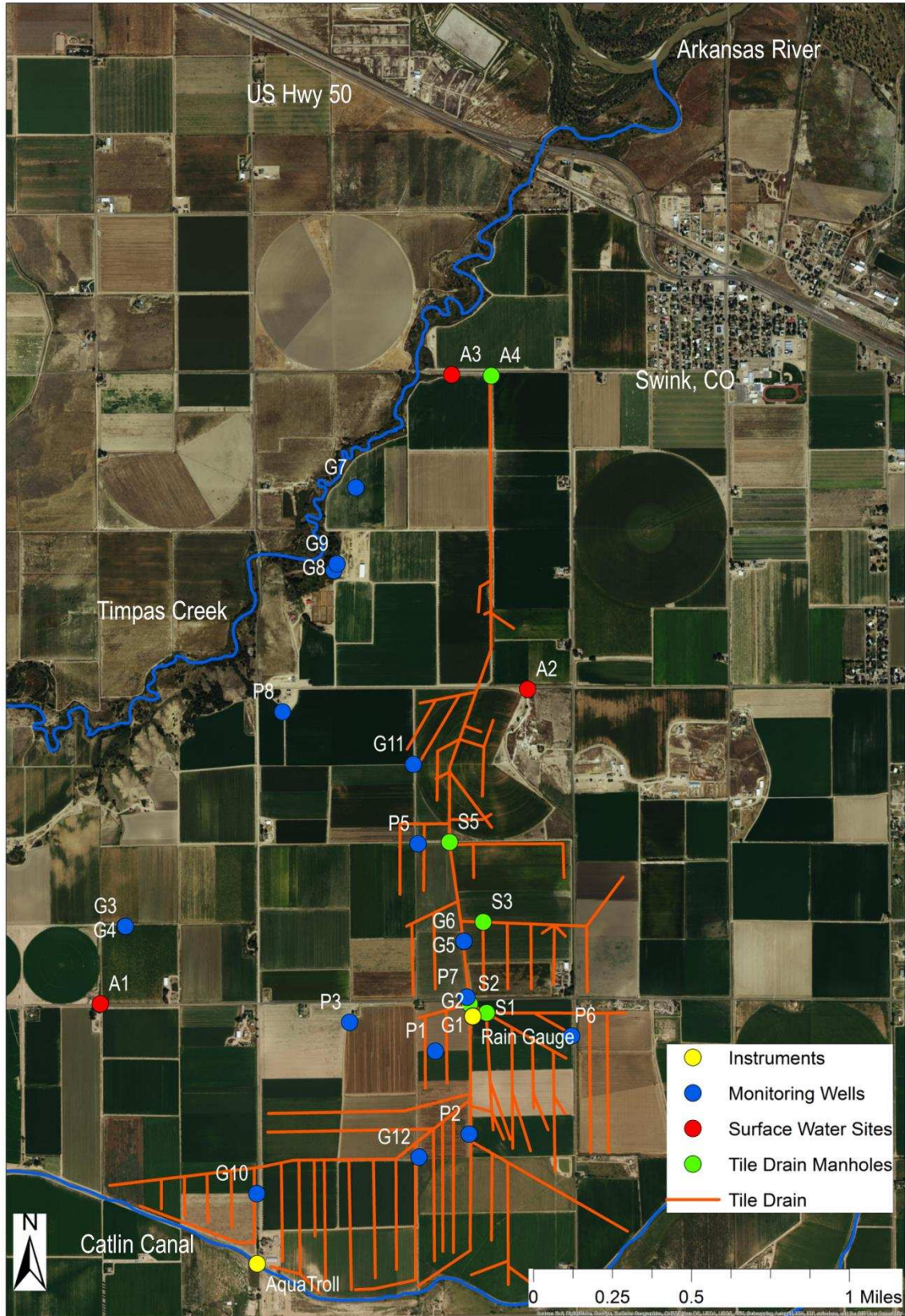


Figure 4. Overview of the tile drain lines and monitoring network in the Fairmont Drainage District.



Figure 5. Confluence of central tailwater drainage ditch, tile drain trunk outlet, and Timpas Creek.

The tile network drains a total area of approximately 950 acres (384 ha). All of the land drained by the FDD is irrigated by diversions from the Catlin Canal. Of the fields drained by the FDD, about 8% of the land is irrigated by center pivot sprinklers and the rest is flood irrigated. There are nine different farmers managing the fields drained by the FDD. The land area of each farm drained by the FDD, along with the proportion, is shown

Table 1. Over 60% of the crops grown on the land drained by FDD are corn and alfalfa. Table 2 shows the acreage and proportional area of crops grown in 2015 and 2016 in the FDD.



Figure 6. Images of tile drain trunk outlet into the tailwater drainage ditch in the FDD

Table 1. Area and proportion of drained fields under each farm in the FDD.

<b>Farm</b>	<b>Area (acres)</b>	<b>Percent of Total</b>
<b>Muth</b>	427.1	39.3
<b>Diamond A</b>	233.7	21.5
<b>Kaess</b>	126.9	11.7
<b>Schlegel</b>	96.0	8.8
<b>Mayhoffer</b>	72.4	6.7
<b>Petramala</b>	52.8	4.9
<b>Grenard</b>	32.6	3.0
<b>Larsen</b>	30.9	2.8
<b>Oliver</b>	14.7	1.4

Table 2. Area and proportion of crops on drained fields in the FDD.

<b>Crop</b>	<b>2015 Acreage</b>	<b>2015 Percent of Total</b>	<b>2016 Acreage</b>	<b>2016 Percent of Total</b>
<b>Alfalfa</b>	359.5	33.1	332.1	30.6
<b>Corn</b>	306.9	28.2	334.3	30.8
<b>Wheat</b>	235.6	21.7	213.3	19.6
<b>Fallow</b>	96.6	8.9	87.9	8.1
<b>Pasture</b>	65.6	6.0	19.3	1.8
<b>Hemp</b>	22.8	2.1	0.0	0.0
<b>Soybean</b>	0.0	0.0	44.7	4.1
<b>Sorghum</b>	0.0	0.0	22.8	2.1

## 2.2 Monitoring Network

### 2.2.1 Groundwater Measurements

There are a total of 20 groundwater observation wells in the study area, six of which are located outside of the area drained by FDD. At the beginning of the study (August 2014), there were nine observation wells (named G1 through G9) in the area. Wells G10, G11 and G12 were installed in March 2016. The remaining wells (P1 through P8) were installed in July 2016 in collaboration with a separate research project. The characteristics (location, depth, approximate ground surface elevation, casing size, and drilling method) for each observation well are summarized in Table 3, and their geographic locations are shown in Figure 4.

Eight of the original nine wells are situated in pairs where one is deep and the other is shallow in order to note differences in groundwater quality based on depth in the aquifer. Of

Table 3. Characteristics of Fairmont Drainage District monitoring wells.

ID	Well Type	UTM Coordinates		Total Depth (ft)	Approximate Ground Surface Elev (ft, MSL)	Casing ID (in)	Drilling Method
G1	Edaphic	619098 E	4204628 N	13.2	4182	2.5	Hydraulic Auger
G2	Aquifer Fill	619099 E	4204630 N	51.3	4182	2.5	Mud Rotary
G3	Edaphic	617329 E	4205088 N	13.6	4191	2.5	Hydraulic Auger
G4	Aquifer Fill	316327 E	4205088 N	39.4	4191	2.5	Mud Rotary
G5	Edaphic	619053 E	4205010 N	13.3	4179	2.5	Hydraulic Auger
G6	Aquifer Fill	619053 E	4205011 N	50.2	4179	2.5	Mud Rotary
G7	Edaphic	618503 E	4207323 N	26.6	4133	2.5	Hydraulic Auger
G8	Edaphic	618391 E	4206900 N	11.4	4147	2.5	Hydraulic Auger
G9	Aquifer Fill	618407 E	4206934 N	23.5	4145	2.5	Mud Rotary
G10	Edaphic	617999 E	4203727 N	14.4	4198	2.5	Hydraulic Auger
G11	Edaphic	618796 E	4205913 N	14.5	4167	2.5	Hydraulic Auger
G12	Edaphic	618825 E	4203912 N	13	4187	2.5	Hydraulic Auger
P1	Edaphic	618907 E	4204452 N	7	4181	2	Hydraulic Auger
P2	Edaphic	619080 E	4204030 N	7.1	4184	2	Hydraulic Auger
P3	Edaphic	618471 E	4204599 N	11.5	4184	2	Hydraulic Auger
P5	Edaphic	618820 E	4205508 N	5.1	4172	2	Hydraulic Auger
P6	Edaphic	619601 E	4204530 N	9.1	4189	2	Hydraulic Auger
P7	Edaphic	619069 E	4204727 N	9.9	4182	2	Hydraulic Auger
P8	Edaphic	618129 E	4206180 N	19.5	4176	2	Hydraulic Auger

these nine wells, four (G1, G2, G5 and G6) are at a centralized location near the trunk of the FDD. The other five original wells are located outside of the drainage network. Wells G3 and G4 are located west of the drainage network in what will be referred to as the upper benchmark. Wells G7, G8 and G9 are also located west of the drainage network in what will be referred to as the lower benchmark. All of the wells are located in or at the edge of agricultural fields with the exception of G8 and G9 which are along the riparian corridor of Timpas Creek. A well at each of these locations (five locations) contains an Onset HOBO pressure transducer in order to log the water table at 15-min intervals in real time. Well G8 contains an additional Onset HOBO pressure transducer for the purpose of logging atmospheric pressure. Beginning in August 2014,

these wells were sampled for major salt ions, including NO<sub>3</sub>, and for dissolved Se every one to three months. In-situ water quality readings of temperature, pH, electrical conductivity, oxidation reduction potential, and dissolved oxygen also were taken during each sampling event using one of three of the following instruments: a QED MP20 multiparameter sonde, an In-Situ smarTroll multiparameter handheld system, or a YSI multiparameter sonde. The instruments were calibrated at least once every 24 hours using a standard pH solutions (4.0, 7.0 and 10.0), a standard conductivity solution (1408.8 μS/cm), and for dissolved oxygen readings. The QED MP20 and YSI multimeter use a membrane DO probe, whereas the In-Situ smarTroll uses an optical DO probe. For a membrane DO probe, the membrane was replaced at least 24 hours prior to a field outing with new electrolyte fluid and the probe was calibrated to the atmospheric pressure for every subsequent 24 hour period. The In-Situ smarTroll was calibrated to 100% saturation and 0% saturation by calibrating with a water-saturated sponge at the bottom of the calibration cup and then with a sodium sulfite solution filled in the calibration cup. Wells G10, G11 and G12 were installed in March 2016 in order to gain a better interpretation of the trends in groundwater movement and quality in the FDD. All three of these wells are equipped with Onset HOBO pressure transducers, recording water pressure every 15 minutes.

Wells P1 through P8 (there is no well named P4) were installed in July 2016 as part of collaboration with a separate research project. Well P8 was installed in order to collect more data on water table elevation and groundwater movement trends in relation to Timpas Creek. Wells P1 through P7 are located in or alongside irrigated fields on which a mass balance was conducted. Wells P1 through P8 were all equipped with Onset HOBO pressure transducers to monitor the water table elevation. Water quality parameters were monitored before, during, and after irrigation events using an In-Situ SmarTroll multiparameter sonde.

A Giddings drill rig, model GSRPS #15-SCS, was used to drill wells P1 - P8 and G10 - G12. The boreholes of wells P1 - P8 were drilled using a 2.5 inch solid core auger bit. Screened sections of 2 inch (5.1 cm) PVC were capped at the bottom, lowered into the well and connected to solid 2 inch PVC that serves as a riser. Wells G10 - G12 were drilled with a 3 inch solid core auger bit. The screened and riser sections are 2.5 inch (6.4 cm) PVC. The width of slots in the screened PVC is 0.01 inches (0.25 mm). Washed sand was poured into the annular space to serve as a filter pack and granular bentonite was used to seal the annular space at the top of the well. Wells G10 - G12 were completed with the PVC riser protruding from the ground and capped. Wells P1 - P8 were completed flush with the ground surface by pouring concrete around 8 inch (20.3 cm) diameter well covers. All of the wells were bailed multiple times in order for proper well development to be achieved.

Images of the well drilling process are presented in Figure 7.

### ***2.2.2 Tile Drainage Measurements***

There were 5 sampling locations within the tile drain network (S1, S2, S3, S5 and A4 in Figure 4). The location originally proposed as S4 is in a branch of the tile drain network that became clogged with debris before the first sampling event. The monitoring locations S2 and S5 are along the main trunk of the tile drain network. Locations S1 and S3 are at manholes where multiple branches of field drains join prior to the confluence with the main trunk. The monitoring location A4 is at the outlet of the trunk and can be seen in Figure 6. Water samples and multiprobe readings were taken on the same schedule as the measurements in wells G1 through G9.



Figure 7. Images of monitoring well drilling and installation process: (a) collection of soil samples from core during drilling process, (b) soil core from top four feet of soil profile, (c) insertion of HOBO pressure transducer into completed monitoring well, and (d) finished well with flush mounting.

### ***2.2.3 Applied Water and Tailwater Measurements***

Water samples were collected from two applied water sites (A1 and A2) and one tailwater site A3. The locations A1 and A2 are in ditches that divert flow from the Catlin Canal at the upstream and downstream reaches of the drainshed, respectively. The tailwater site is located in the main tailwater drainage ditch after the tile drain outlet and prior to its confluence with Timpas Creek. An image of the tile drain trunk outlet and a map of the central tailwater ditch, tile drain outlet and Timpas Creek are shown in Figure 5 and Figure 6. The flow at A3 was comprised of a combination of tailwater from irrigated fields and water from tile drains that varies in proportion, depending on the season and on irrigation practices. A drainshed-scale mass-balance was attempted in this study but was not successful. The measurement of water diverted from the Catlin Canal on to the fields drained by the FDD is very difficult due to the complexity of applied water and tailwater ditches. A discussion of the difficulties involved in measuring a field-scale mass balance is presented in Chapter 4.

The central tailwater ditch carries water that runs off of roughly 1,500 acres (607 ha) of land. Applying a 164-ft (50-m) buffer to the tile network in ArcMap, it was estimated that 80% of the fields that contribute to the central tailwater ditch also are drained by the FDD to some extent. There are 251 acres (102 ha) of fields drained by the FDD that do not contribute to the central tailwater ditch. This is about 17% of the area drained by the FDD (Figure 8).

### ***2.2.4 Rainfall Measurements***

Rainfall was measured using an Onset RG3 Tipping Bucket rain-gauge which was installed between observation well G1 and G2. Its geographic location is shown in Figure 4.

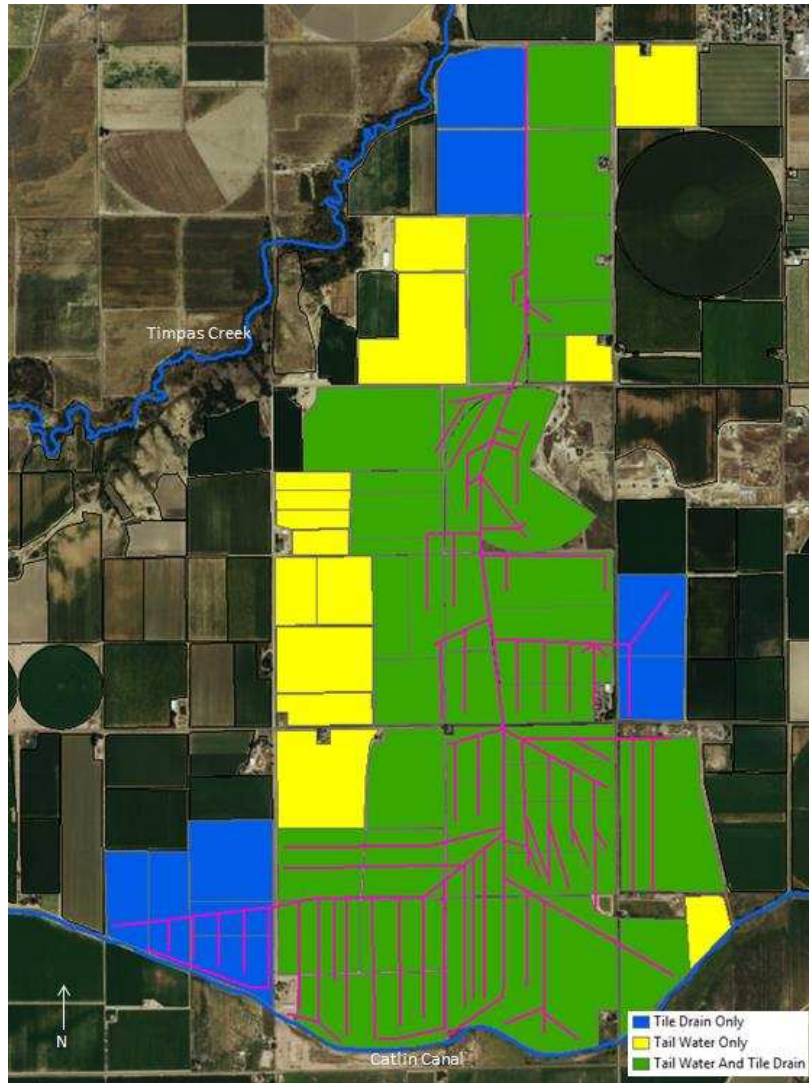


Figure 8. Fields contributing water to the central tailwater ditch and the tile drain.

### ***2.2.5 Catlin Canal Water Quality Parameter Measurements***

A stilling well installed within the Catlin Canal just east of Road 23 was equipped with an In-Situ AquaTroll 200 Multiparameter Sonde to record electrical conductivity and temperature of the applied irrigation water at 10-min intervals in real time. Its geographic location is depicted in Figure 4.

## 2.3 Sampling Procedures

This section explains the methodology for each type of water quality sampling and in-situ readings. Two sets of samples were gathered at each sampling location. One set of samples was sent to Ward Laboratories, Inc. in Kearney, Nebraska for “irrigation water quality” analysis which includes the following parameters and major ion concentrations: (pH, SAR, EC, estimated TDS, and concentration of  $\text{Na}^+$ ,  $\text{Ca}^{2+}$ ,  $\text{Mg}^{2+}$ ,  $\text{K}^+$ ,  $\text{Cl}^-$ ,  $\text{SO}_4^{2-}$ ,  $\text{CO}_3^{2-}$ ,  $\text{HCO}_3^-$ ,  $\text{NO}_3^-$ , and B). A second set of samples was sent to South Dakota Agricultural Laboratories in Brookings, South Dakota for determination of total dissolved Se. Each water sample was directed through the sampling hose into a 0.25 L bottle containing nitric acid as a preservative. The in-situ water quality parameter measurements were taken using one of the following multiparameter sondes: a QED MP20, a YSI multimeter, or an In-Situ smarTroll. The instrument was calibrated at least once every 24 hours using a standard pH solutions (4.0, 7.0 and 10.0), a standard conductivity solution (1408.8  $\mu\text{S}/\text{cm}$ ), and for dissolved oxygen readings. The QED MP20 and YSI multimeter use a membrane DO probe, whereas the In-Situ smarTroll uses an optical DO probe. For a membrane DO probe, the membrane was replaced at least 24 hours prior to a field outing with new electrolyte fluid and the probe was calibrated to the atmospheric pressure for every subsequent 24 hour period. The In-Situ smarTroll was calibrated to 100% saturation and 0% saturation by calibrating with a water-saturated sponge at the bottom of the calibration cup and then with a sodium sulfite solution filled in the calibration cup. For every 10 samples sent to each laboratory, a duplicate sample and a blank sample of distilled water was sent in order to ensure quality laboratory performance and sampling techniques.

### ***2.3.1 Groundwater Sampling***

Groundwater was sampled from the monitoring wells using a low-flow pumping technique. A Sample Pro® Portable MicroPurge Pump was attached to a unique set of tubing for each well that has been washed with a muriatic acid solution, a cation-free detergent solution, and de-ionized water prior to use. It was lowered into the well to a depth of half of the standing water column in the well. The groundwater was pumped through a flow-through cell to which one of the aforementioned multiparameter sondes was attached. The following water quality parameters were measured: electrical conductivity (specific conductance at 25 °C), oxidation-reduction potential (ORP), temperature, pH, and dissolved oxygen (DO). The instruments were calibrated at least every 24 hours as described in the previous section. The pumping rate was adjusted using a QED MicroPurge® Controller MP10 in order to ensure a flow rate of between 100 to 200 mL per minute, low enough to prevent de-watering of the well and entrainment of air. Water quality parameter values were recorded every two minutes using the multiparameter sonde until the change between subsequent recordings was within the tolerances listed in Table 4. Once these tolerances were met, two bottles were filled unfiltered without changing the pump rate. One bottle is for major ion analysis and the other is for dissolved Se analysis. The Se bottle is treated with nitric acid prior to sample collection. The major ion sample and Se sample are stored in the refrigerator and shipped in a cooler with ice packs to Ward Laboratories Inc. and South Dakota Agricultural Laboratories respectively. The sample for dissolved Se is filtered in the lab and the major ion analysis sample is not filtered in the lab. The pump and flow through cell were washed with muriatic acid, detergent and distilled water, between sampling events. See Figure 9 for images of groundwater sampling.

Table 4. Tolerances to be met prior to collecting sample.

<b>pH</b>	<b>Electrical Conductivity (<math>\mu\text{S}/\text{cm}</math>)</b>	<b>DO (mg/L)</b>	<b>ORP (mV)</b>
+/- 0.1	+/- 3%	+/- 10%	+/- 10 mV



Figure 9. Images of sampling from groundwater: monitoring wells (a) well G8, and (b) well G4.

### ***2.3.2 Surface Water Sampling***

The sample for dissolved selenium was filled unfiltered through a tube using a peristaltic pump so as to not lose any of the nitric acid preservative. Because there was no preservative in the major ion sample bottle, it was collected as a grab sample where the clean sample bottle was submerged until it was full. The tubing used in the peristaltic pump was washed by pumping a muriatic acid solution, a cation-free detergent solution and distilled water through it between each sample. In-situ readings were not taken at surface water sampling sites.

### ***2.3.3 Tile Drain Sampling***

Tile drain samples were collected by pumping water up from the bottom of the manhole using a peristaltic pump (Figure 10). The tubing used in the peristaltic pump was washed in between tile drain sampling locations by pumping a muriatic acid solution, a cation-free detergent solution, and distilled water through the tube using the peristaltic pump. For in-situ readings, the YSI, In-Situ, or QED multiparameter sonde was lowered into each manhole and once stable, the water quality characteristics were recorded.

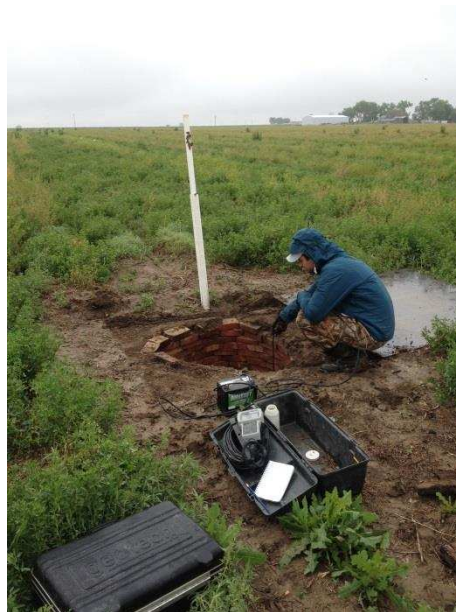


Figure 10. Sampling from tile drain manhole S3.

## 2.4 Field Scale Mass Balance

Three fields were selected to be monitored for mass-balance analysis. They are located within a one square mile central area of the drainshed (Figure 11). The two fields with subsurface drainage are farmed by the same farmer and the control field (DA7), which is not underlain by tile drains, is farmed by a different farmer. Characteristics of each field are summarized in Table 5.

Table 5. Characteristics of fields selected for mass balance analysis.

Field Characteristics			
Field Name	Crop	Tile Drains (y/n)	Area (acres)
Muth2	Corn	y	26.7
Muth9	Alfalfa	y	18.7
DA7	Alfalfa	n	23.7

Equation 1 represents a simplified mass balance for calculating the rate of irrigation water applied to the field segment under analysis:

$$Q_a = Q_d - (Q_s + Q_l + Q_e) + Q_p \quad (1)$$

where  $Q_d$  is the diverted water flow rate,  $Q_s$  is the spillover flow rate,  $Q_l$  is the rate of seepage loss,  $Q_e$  is the evaporation rate, and  $Q_p$  is the precipitation rate. Since the diverted water flows through underground pipes and concrete ditches, we assume  $Q_l$  to be negligible. Similarly, the distance travelled between the trapezoidal flumes measuring flow rate of diverted water and the location where water is applied is short enough that we consider  $Q_e$  to be negligible. There was no precipitation measured by the rain gauge during any of the monitored irrigation events for all three fields, so the precipitation term also was set to zero. The resulting simplified mass balance for applied water is

$$Q_a = Q_d - Q_s \quad (2)$$



Figure 11. Fields selected for mass balance analysis, location of installed flumes for measuring applied water, spillwater, and tailwater; siphon sets (temporal/spatial irrigation divisions); and siphon set intervals from which samples were taken.

A mass balance calculation for the tailwater runoff rate,  $Q_r$  is

$$Q_r = Q_a - (Q_f + Q_e) \quad (3)$$

wherein  $Q_f$  is the field infiltration rate. Inserting Eq. (2) into Eq. (3) and introducing  $Q_{fe} = Q_f + Q_e$  gives

$$Q_r = Q_d - (Q_s + Q_{fe}) \quad (4)$$

#### ***2.4.1 Flume Installation and Maintenance***

In monitoring the irrigation events, two trapezoidal flumes were modified to fit in trapezoidal concrete lined irrigation ditches. One of these flumes measures the diverted water flow rate for field DA7 and the other flume measures the diverted water flow rate for fields Muth2 and Muth9. To prevent water from flowing underneath and around the flume, a tarp was secured to the upstream side of the flume, folded over repeatedly, and secured to the concrete ditch with tap-con screws (Figure 12). The flumes were leveled using cedar shims on the downstream end. An Onset HOBO pressure transducer was placed in the slot on the upstream side of the flume that is designed for such an instrument, as shown in Figure 12. In order to measure submergence, an Onset HOBO pressure transducer was secured to the concrete walls of the ditch on the tailwater side of the flume using tap-con screws and hose clamps (see Figure 12). The pressure transducers were set to take readings either every minute or every five minutes. Tailwater and spillover flow rates were measured using EZ Flow Ramp Flumes™ from Nu-Way Flumes. Spillover is water that flows over, around or under the check dam placed in the applied ditch to raise the water level for siphons. Examples of spillover are shown in Figure 13. The ramp flumes used for field Muth9 tailwater and fields Muth2 and Muth9 spillover have a maximum capacity of 3.5 ft<sup>3</sup>/s (cfs). The flume for Muth9 was installed at the immediate end of the Muth9 field, as shown in Figure 11.



Figure 12. Installation practices for trapezoidal flumes used in field mass balance studies: (a) Tarp is folded over and secured to concrete ditch, (b) HOBO water level recorder on upstream side of flume secured in the designated slot, (c) HOBO water level recorder on downstream side of flume, and (d) HOBO water level recorder on downstream side of ramp flume.

Prior to installation, the ramp flumes were thoroughly cleaned, all the seams were caulked, and tarps were attached to the upstream and downstream ends (Figure 14). The flumes were installed in a portion of the head ditch where the soil has been raised slightly and leveled. Care was taken to maintain a level flume floor (both parallel and perpendicular to flow) while filling and packing soil around the flume. The tarps were pushed into the ditch walls and bed to ensure clean flow through the flume and limit erosion (Figure 15). All of the tailwater flumes were equipped with two Onset HOBO pressure transducers. The pressure transducer on the upstream side of the flume was hung from a cap into the PVC stilling well using static fishing line. The pressure transducer on the downstream side sat in conduit brackets near the outfall of the flume (Figure 12). The pressure transducers were set to take reading every at one minute or five minute intervals.

All of the pressure transducers used were tested in graduated cylinders in the laboratory at 1, 1.5, 2, 3, 6, 12, and 16 inch depths with satisfactory results. While the absolute pressure measured varies between pressure transducers, the change in pressure was measured accurately. The correction applied for the difference in absolute pressure was explained in Section 2.4.4 Pressure Transducer Corrections. Atmospheric pressure was logged by a pressure transducer located in monitoring well G8 located approximately one mile away from the flumes.

#### ***2.4.2 Monitoring Irrigation Events***

During an irrigation event, the diverted water flume, tailwater flume, and spillover flume (if applicable) were visited every two hours during the day and every three hours at night to ensure that no debris was blocking the flume and to take water quality readings. An In-Situ smarTroll was used to take readings of pH, electrical conductivity, temperature, dissolved oxygen, and ORP. The instrument was calibrated at least once every 24 hours. The water level



Figure 13. Examples of measured field flows: (a) Spillover flow over a check dam in the head ditch for Muth2 field, (b) Spillover flow under check dam in head ditch for DA7 field, (c) flow through the tailwater flume for field Muth2, and (d) flow through the applied water flume for field Muth2.



Figure 14. Preparation and installation of flow measuring flumes: (a) Cleaning flumes, caulking seams and attaching tarps, (b) securing tarp on upstream side of flume, (c) flume for measuring diverted flow to field DA7, and (d) flume for measuring diverted flow to fields Muth2 and Muth9.



Figure 15. Additional images of flow measuring flumes: (a) Ramp flume leveled with tarp secured, ready to be backfilled, (b) sampling from DA7 tailwater flume, (c) flume for measuring tailwater flow from field Muth9 mixing with spillover water, and (d) flume for measuring tailwater flow from field Muth2.

on the upstream staff gauge of the flume also was recorded (elevation in cm for the trapezoidal flumes and flow rate in cfs for the ramp flumes). Additionally, the location of the siphon tubes was tracked in order to spatially associate water quality readings with the portion of the field where the irrigation water was applied.

An In-Situ AquaTroll Series 200 was located in a stilling well installed in the Catlin Canal upstream of the head gates which supply water to the three monitored fields. The instrument was set to log electrical conductivity and temperature every 10 minutes. These values were used as a check to ensure that the in-situ measurements of applied water at the fields using the SmarTroll were accurate. The stilling well was located 100 feet (30 m) upstream of the head gate to field DA7. Once water was diverted from the Catlin Canal at the head gate, it traveled in an underground pipe for 3000 feet (910 m) and in a concrete ditch for another 1000 feet (300 m) before it reached the flume where flow rate measurements and in-situ water quality readings were taken. The AquaTroll was located 3000 feet (910 m) upstream of the head gate supplying fields Muth2 and Muth9. The water traveled about 2000 feet (610 m) in an underground pipe prior to surfacing at the flume where in-situ water quality readings were taken. The AquaTroll was calibrated to an electrical conductivity standard of 1408.8  $\mu\text{S}/\text{cm}$  and was deployed in March 2016. After the monitored irrigation events (August 2016), the AquaTroll was tested in electrical conductivity standard solutions of 147  $\mu\text{S}/\text{cm}$  and 1408.8  $\mu\text{S}/\text{cm}$  and reported measurements of 153.3  $\mu\text{S}/\text{cm}$  and 1383.9  $\mu\text{S}/\text{cm}$ , respectively. Using the differences between the electrical conductivity of the solutions and the measured electrical conductivity in August 2016, a regression analysis was conducted to correct the AquaTroll data. All measured electrical conductivity values by the AquaTroll were shifted according to the linear regression. This

correction method assumes that in the six-month period the instrument held a calibration, little change occurred in the last month when the measured irrigation events occurred.

### ***2.4.3 Sampling for Water Quality***

During each irrigation event the diverted water and tailwater were sampled for water quality twice. Figure 15b shows a picture of the sampling technique. The field was broken into quadrants and samples were taken when the siphon tubes are set near the border of the 1<sup>st</sup> and 2<sup>nd</sup> quadrant, and the border of the 3<sup>rd</sup> and 4<sup>th</sup> quadrant (Figure 11). Note that only one set of diverted water and tailwater samples were collected from field DA7. Samples were taken once the in-situ electrical conductivity readings represent a near average value of the electrical conductivity readings taken while the siphon tubes remained at a single location. Three water quality samples were taken. One unfiltered sample was for analysis of major salt ions and NO<sub>3</sub> and was sent to Ward Laboratories in Kearney, NE. A filtered sample and an unfiltered sample were sent to South Dakota Laboratories in Brookings, SD for analysis of total dissolved Se and total recoverable Se, respectively.

### ***2.4.4 Pressure Transducer Corrections***

The pressure transducer logging atmospheric pressure was set to log every 15 minutes. In order to match atmospheric readings with pressure readings taken in each flume, the average pressure reading in flumes for each 15 minute interval was calculated and used. Each pressure transducer used in the flumes has a unique relationship to the pressure transducer logging atmospheric pressure. This difference caused the calculated depth of water to be offset from the true depth of water. Two methods were used to correct for this difference. The pressure transducer readings on the upstream side of the flumes were compared to the staff gauge readings that were periodically recorded. The average difference between the manually recorded

depth and the corresponding value derived from the pressure transducer reading was added back to each pressure transducer value. Figure 16 illustrates this correction technique. The second method was used for the pressure transducers on the downstream side of each flume for which there were no staff gauges to compare calculated flow depths. During periods of no flow, when the downstream pressure transducers were reading atmospheric pressure, the average difference of pressure readings between the pressure transducers on the downstream side of the flume and the atmospheric pressure transducer in well G8 was added back to the flume pressure transducer. This has the same effect of correcting the water elevation.

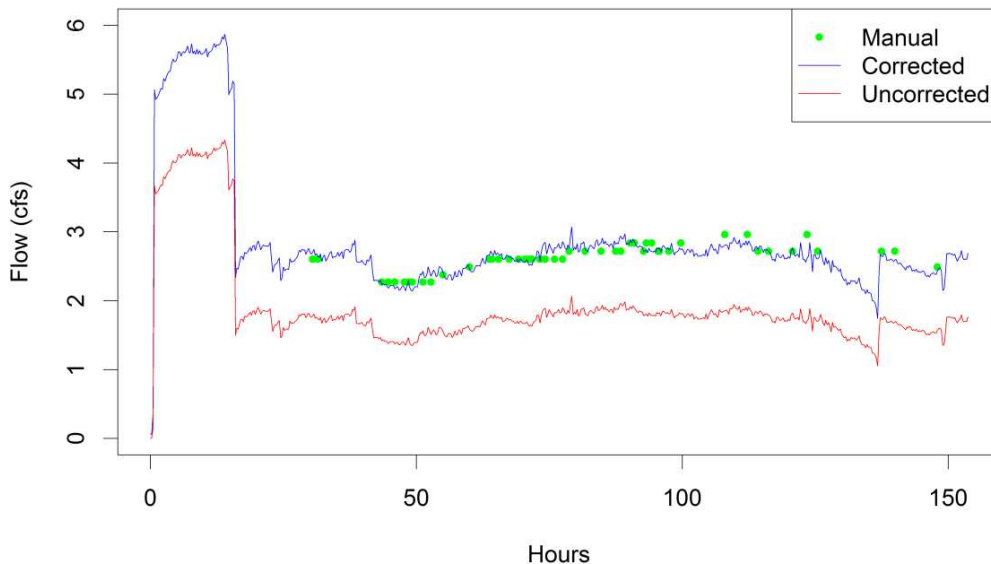


Figure 16. Plot of uncorrected, corrected, and flow computed from manual readings for field Muth2.

#### ***2.4.5 Converting Pressure Transducer Data to Flow Rate***

The flow rating equations for each flume are summarized in Table 6, where  $Q$  is in cfs and  $z$  is the flow depth in feet. In the case of the ramp flumes, the depth is measured from the sill to the water level at the location of the staff gauge. The depth in the trapezoidal flumes, which

have side wall contractions and no bed contraction, is measured from the floor to the water level at the location of the staff gauge.

Table 6. Rating equations for flumes.

Flume	Rating Equation	Accuracy	Submergence Ratio
12" 45° Trapezoidal Open Channel Flow	$Q = 0.05 + 0.063(z^{1.5}) + 3.23(z^{2.5})$	+/- 2-5%	0.80
3.0 cfs Ramp NuWay Flume	$Q = 3.968(z^{1.619})$	+/- 3%	0.85
7.0 cfs Ramp NuWay Flume	$Q = 7.892(z^{1.620})$	+/- 3%	0.85

#### ***2.4.6 Detection of Submergence***

The submergence ratios for the trapezoidal flumes and ramp flumes are 0.80 and 0.85 respectively. This is the ratio of the depth of water on the downstream side of the flume, measured just upstream of the overfall location, to the depth of water on the upstream side of the flume, measured at the location of the staff gauge (Figure 12). The rating equations given in Table 6 are no longer valid when the submergence ratio is exceeded. There were two extended periods of submergence. Flow through the diverted water flume exceeded the submergence ratio during irrigation with the first three siphon setting intervals on field Muth2. This was unavoidable because the applied irrigation water surfaced from an underground pipe at the start of the field. The tailwater flume for DA7 also was submerged for the majority of the last three siphon setting intervals. This potentially could have been prevented by raising the flume floor elevation up by about an inch, but doing so would have risked flooding over the banks of the ditch. Submergence correction factors have not been developed for these flumes; thus, the portion of the irrigation events in which the flumes were submerged are not included in the mass balance analysis.

#### 2.4.7 Relationship between Measured Conductivity and Total Dissolved Solids

Actual electrical conductivity values were converted to specific conductance,  $SC$  ( $\mu\text{S}/\text{cm}$ ), in order to normalize the data to 25 degrees C where  $EC$  is actual conductivity ( $\mu\text{S}/\text{cm}$ ) and  $T$  is temperature ( $^{\circ}\text{C}$ ).

$$SC = \frac{EC}{(1+0.0191(T-25))} \quad (7)$$

The In-Situ SmarTroll uses Eq. (7) (Greenberg et al. 1992) to convert measured  $EC$  and  $T$  values to  $SC$  values. The  $SC$  of the In-Situ SmarTroll at the diverted water flume were compared to the  $SC$  values of the In-Situ AquaTroll which was logging  $EC$  and  $T$  every 10 minutes in the Catlin Canal just upstream of the headgates supplying water to the fields of interest. It was assumed that negligible differences in electrical conductivity exist between the location of the AquaTroll in the Catlin Canal and the flumes measuring diverted water. The SmarTroll electrical conductivity data was found to have a bias associated with the calibration times. In order to have confidence in the SmarTroll tailwater readings, a correction factor for each calibration period was developed. For each calibration period, the data were corrected by adding a correction factor,  $SC_{\text{corr}}$ , to the SmarTroll  $SC$  reading

$$SC_{\text{corr}} = SC_{\text{ST}} + \text{Average}(SC_{\text{AT}} - SC_{\text{ST}}) \quad (8)$$

wherein  $SC_{\text{AT}}$  and  $SC_{\text{ST}}$  are the specific conductivities of the AquaTroll and SmarTroll, respectively. The value of  $SC_{\text{corr}}$  was applied to both the tailwater readings and the diverted water readings that occur within the associated calibration period. Figure 17 depicts the SmarTroll specific conductivity data prior to, and after, correction. Ward Laboratories report the concentration of the following major ions in their irrigation quality analysis: ( $\text{Na}^+$ ,  $\text{Ca}^{2+}$ ,  $\text{Mg}^{2+}$ ,  $\text{K}^+$ ,  $\text{Cl}^-$ ,  $\text{SO}_4^{2-}$ ,  $\text{CO}_3^{2-}$ ,  $\text{HCO}_3^-$ ,  $\text{NO}_3^-$ , B). It is generally assumed that these ions make up the vast

majority of TDS (Tanji and Wallender, 2012). In addition to estimating the relationship of specific conductance with TDS for the samples collected during the mass balance analysis, we estimated a similar relationship for samples collected during June through August for the years 2006 to 2011 from the Arkansas River between the Catlin Canal diversion dam and Swink, CO

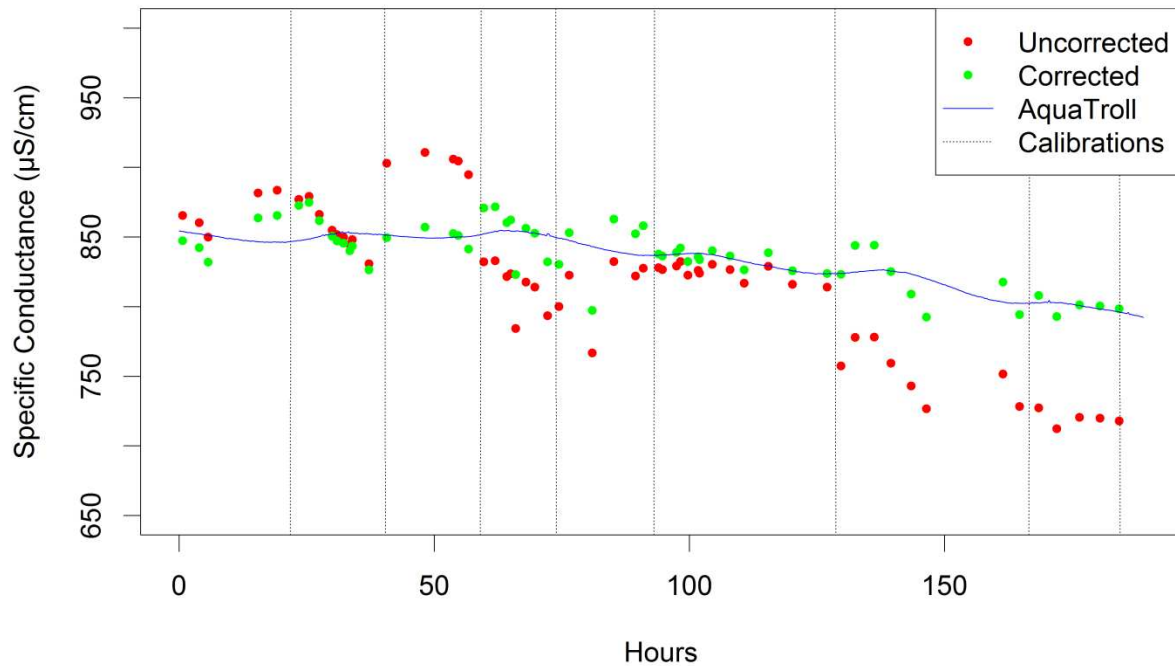


Figure 17. Correction of SmarTroll specific conductance data for each calibration period for field Muth2.

(Figure 18). A scatterplot and fitted linear regression relationship for these data are shown in Figure 19. The regression suggests a statistically significant (alpha level of 0.05) strong ( $R^2 = 0.89$ ) relationship. This linear regression was used to convert the corrected SmarTroll specific conductance values to TDS concentration values as has been done in other studies such as Isidoro et al. (2006).

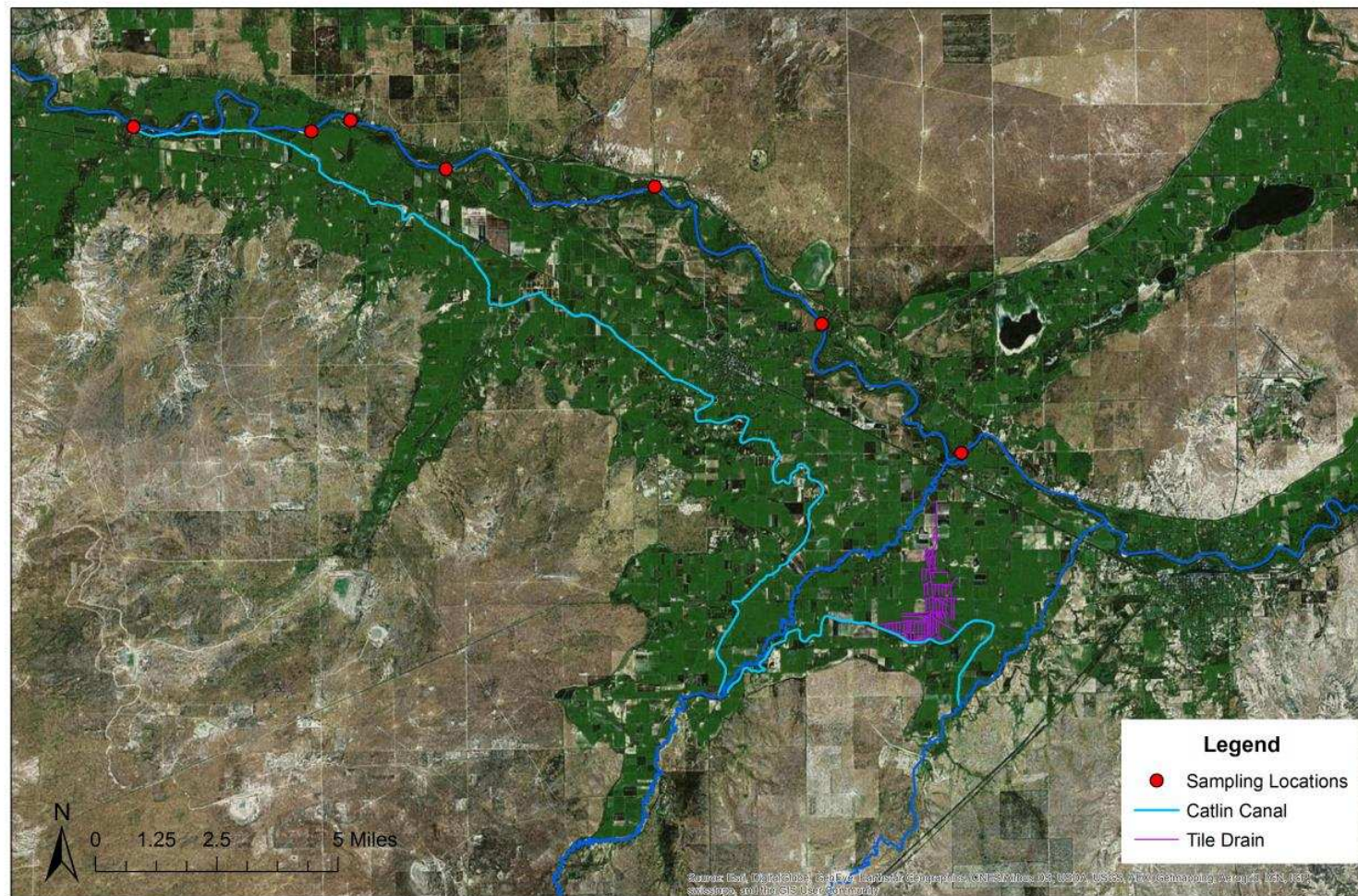


Figure 18. Sampling locations for past data used for developing specific conductance vs TDS concentration linear regression relationship.

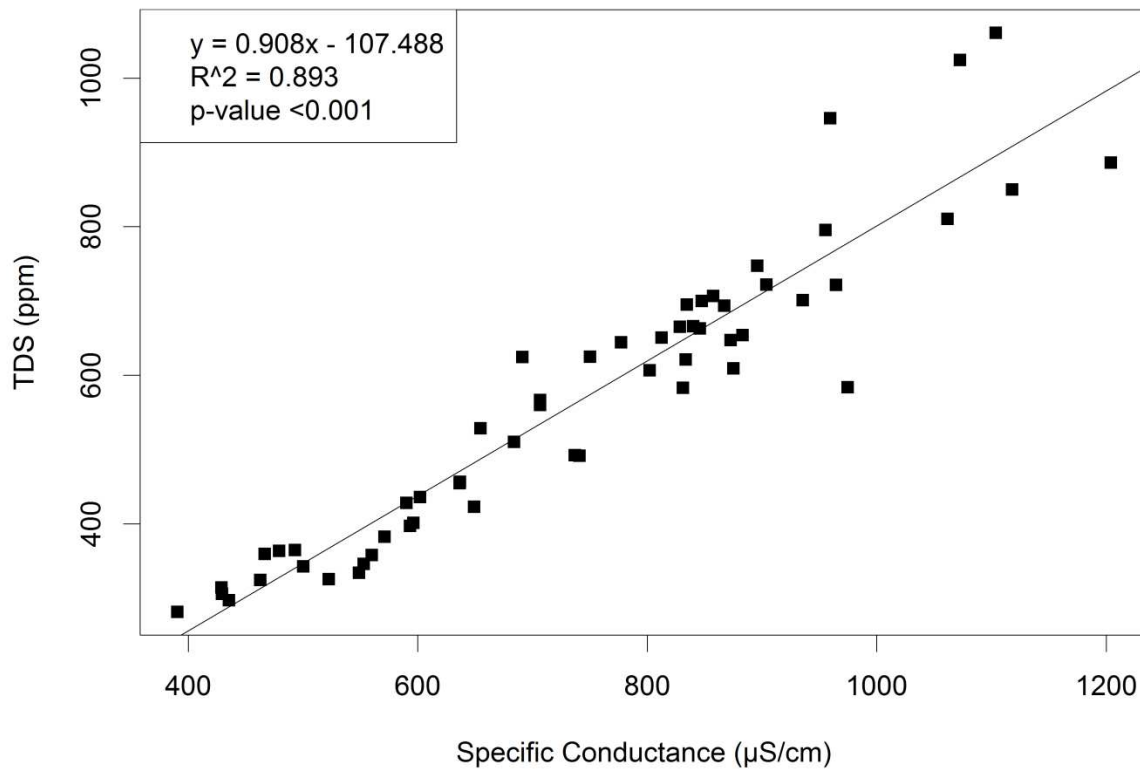


Figure 19. Fitted linear regression of TDS concentration vs specific conductance for samples taken from Arkansas River and the field scale mass balance.

#### ***2.4.8 Relationship between Dissolved Selenium and Total Dissolved Solids***

Analysis of the relationship between dissolved Se and TDS from the mass balance samples indicates the relationship is different for diverted water and tailwater. Separate linear regression relationships were developed and are shown in Figure 20. Both linear regressions are statistically significant ( $p\text{-value} < 0.05$ ). The relationship for the diverted water samples has a higher coefficient of determination ( $R^2 = 0.88$ ) than that for the tailwater samples ( $R^2 = 0.67$ ).

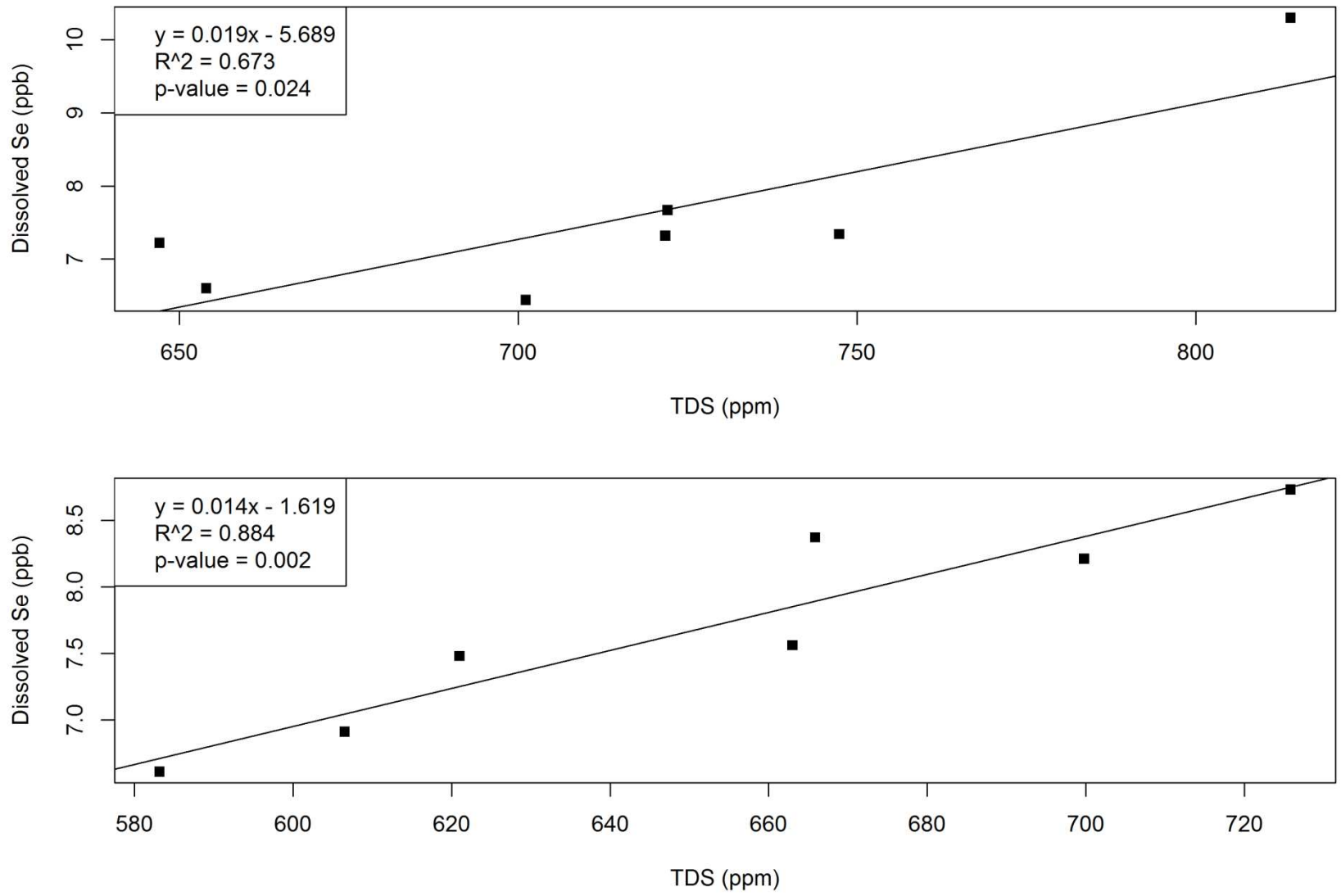


Figure 20. Scatterplots and fitted linear regression relationships of dissolved Se vs TDS concentrations for tailwater (top) and diverted water (bottom).

#### ***2.4.9 Mass Balance Calculations***

There are three properties of interest in the mass balance analysis for each field: flow, TDS, and dissolved Se. The flow mass balance is the most straightforward and the other two mass balances rely on its accuracy.

Each field was divided up into irrigated intervals based on the placement of the siphon tubes (Figure 11). A portion of each of the fields was not included in the mass balance due to submergence of the flumes. In the case of Muth2, the diverted water flume was submerged for the first three irrigation intervals. In the case of DA7, an unexpected large quantity of tailwater caused submergence of the tailwater flume during the last three irrigation intervals. The water flow data from field Muth9 was the most thorough as it only lacked the first siphon set interval which was not logged.

Spillover flow was measured for the entire irrigation event on field Muth9. The spillover for field Muth2 was only measured for the last day of the irrigation event (Figure 21). There was no spillover measured for field DA7 because the ditch carrying spillover water was too wide to install any flumes available in this project. From field observations and photographs taken of the check dam in the head ditch, it is known that the spillover rate was highest for Muth9, second highest for Muth2 and lowest for DA7. While the siphon placement on fields Muth2 and Muth9 allowed water to flow over the crest of the check dam, the siphon placement on DA7 generally only allowed water to flow around the side and bottom edges of the check dam at the beginning of each siphon set (Figure 13). For each siphon placement interval on field Muth9 (with the exception of the 2<sup>nd</sup>), the spillover proportion increases at a rate that can be approximated by a linear slope (Figure 22). The reason for the increase in spillover flow with time for each siphon

interval is thought to be due to irrigation water backing up in the furrows and submerging the siphon tubes.

The portion of the irrigation event on field Muth2 in which spillover flow was measured includes the last 3.25 siphon intervals (Figure 21). The last three intervals show almost no spillover. This is likely because the diverted flow decreased during the same time (possibly due to a lower water level in the Catlin Canal). The latter quarter of the 5<sup>th</sup> interval shown in the plot, shows the end of a trend similar to that seen in the spillover flow for the irrigation event on field Muth9. In order to estimate the spillover flow for the 4.75 siphon placement intervals that were missing from the mass balance, the average slope,  $m$ , of a fitted linear regression ( $m = 0.91$ ) of spillover flow for each siphon placement interval on Muth9 was applied to the 4.75 siphon placement intervals from Muth2 for which data were missing. The  $y$ -intercept was assumed to be 0 at the start of each interval (Figure 23). Due to the high efficiency of the siphon tube setting during the monitored irrigation on field DA7, the slope of the linear regression used to estimate the spillover flow of each siphon interval was assumed to be half of the slope ( $m = 0.46$ ) used to estimate the spillover flow for field Muth2 (Figure 24). Figure 25 includes a plot of the tailwater flow for field Muth9. In order to match water quality data time steps to flow rate time steps an interpolation method was required. Interpolation of specific conductance between measurement points was accomplished using a cubic spline function in Matlab (Figure 26). Cubic splines are advantageous for interpolating between points of a highly-curved data series. They function by forcing the first and second derivatives of piecewise cubic polynomials to be continuous at each known data value (Harrell, 2001). The interpolated and measured specific conductance values ( $\mu\text{S}/\text{cm}$ ) were converted to TDS ( $\text{mg}/\text{L}$ ) using the linear regression relationship shown in Figure 19. Similarly, the linear regression relationships shown in Figure 20 were used to convert the

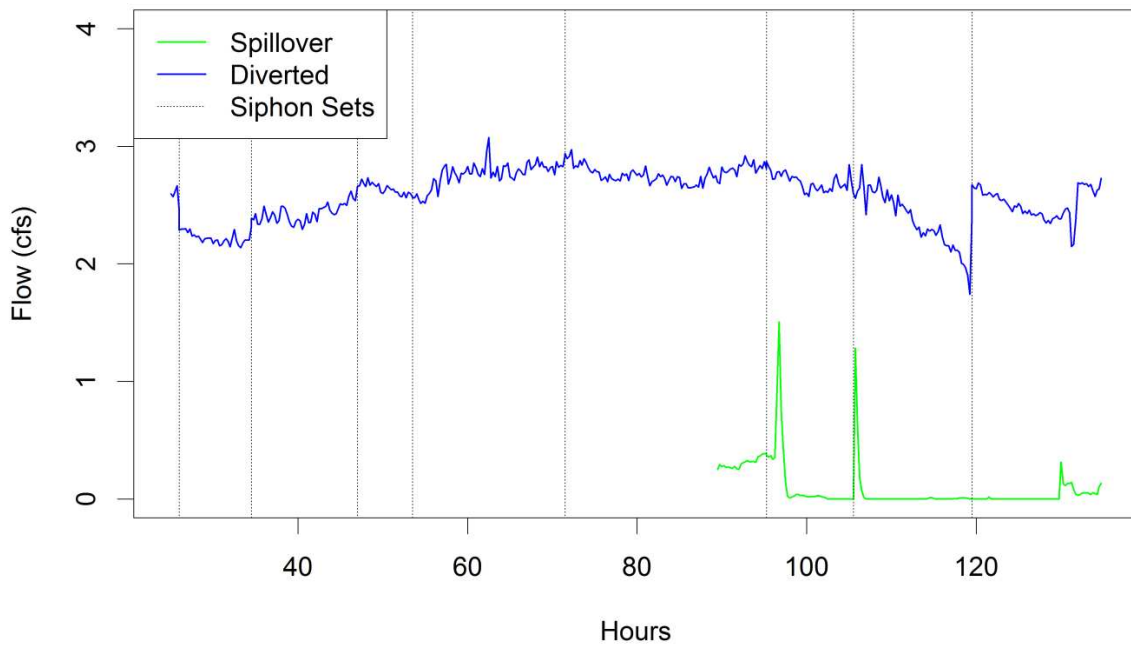


Figure 21. Plot of flow rate vs time for diverted flow and spillover flow for field Muth2.

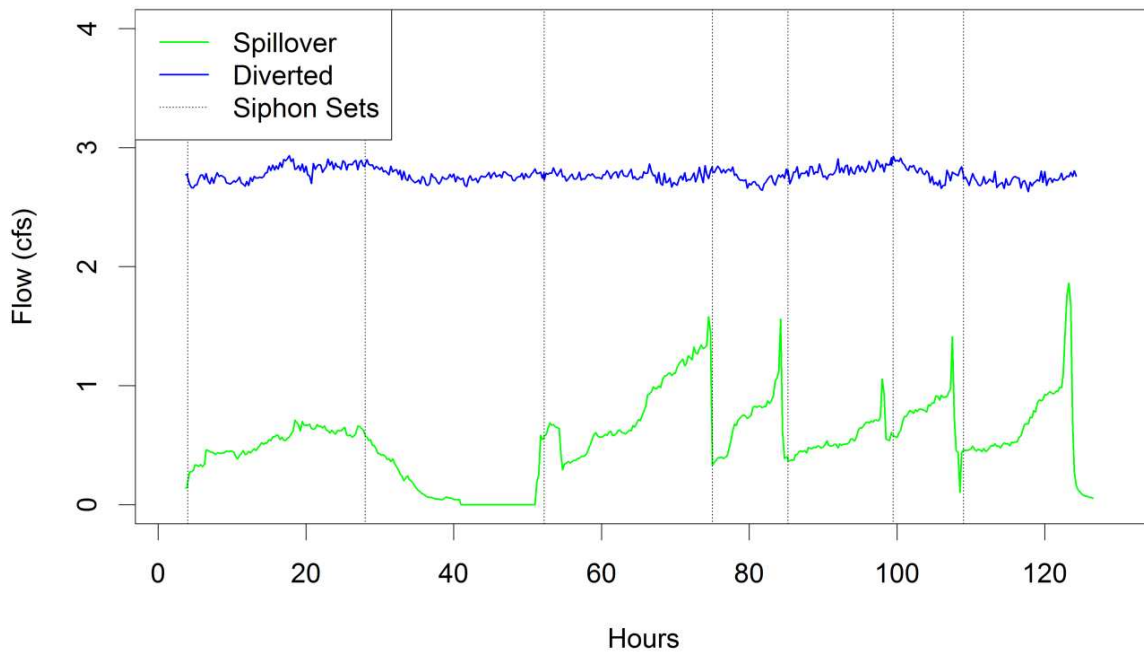


Figure 22. Plot of flow rate vs time for diverted flow and spillover flow for field Muth9.

TDS concentrations (mg/L) to dissolved Se concentrations ( $\mu\text{g/L}$ ). (Note that there are different regression relationships for diverted water and tailwater.)

For the portion of each field incorporated in the mass balance, solute loading of diverted tailwater, and spillover flow was calculated as shown in eq (9)

$$L_i = C_i V_i \quad (9)$$

where, for a given flume,  $L_i$  is the solute load for a 15 minute interval,  $C_i$  is the estimated average solute concentration for a 15 minute interval, and  $V_i$  is the estimated volume of water for a 15 minute interval. Eq (10) gives the total loading ( $L$ ) for an entire irrigation event at a given flume where  $n$  is the total number of 15 minute intervals at each flume during the irrigation event.

$$L = \sum_{i=0}^n L_i \quad (10)$$

Similarly, solute flow rate is calculated as shown in eq (11)

$$Q_{s_i} = C_i Q_i \quad (11)$$

where, for a given flume,  $Q_{s_i}$  is the estimated average solute flow rate for a 15 minute interval and  $Q_i$  is the average measured water flow rate for a 15 minute interval. In-Situ conductivity readings were not taken at the spillover flume and it was assumed that the spillover water has the same TDS and dissolved Se concentrations as the applied water. It was also assumed that the TDS concentration in ppm and the dissolved Se concentration in ppb are equivalent to the concentrations in mg/L and  $\mu\text{g/L}$  respectively (Tanji, 2002).

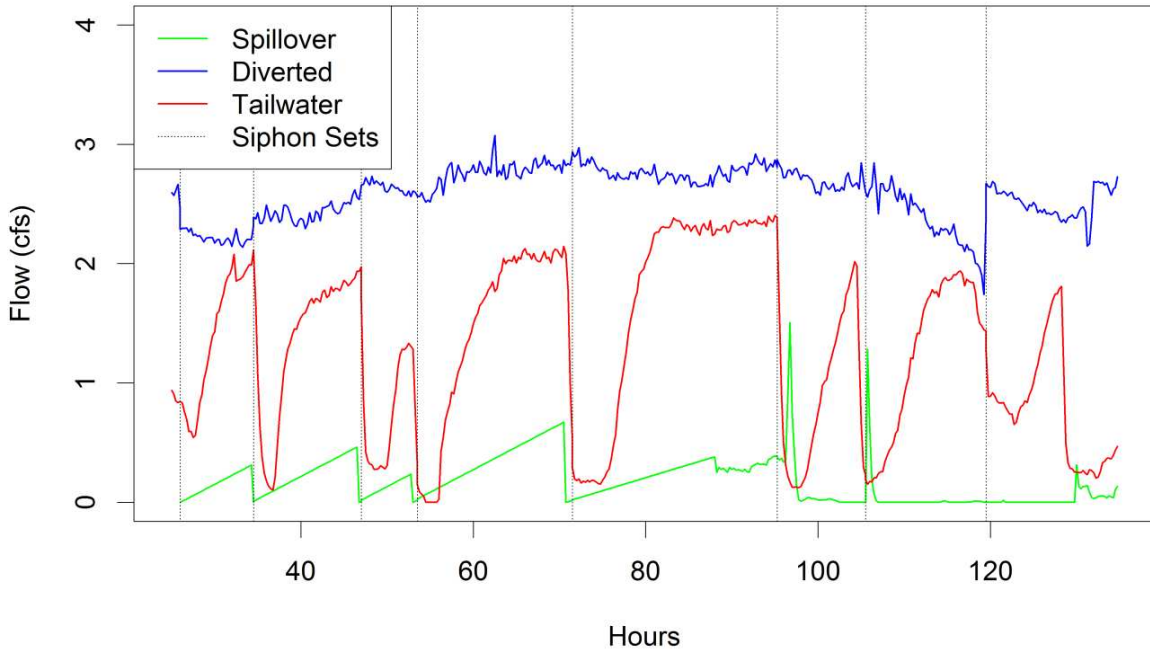


Figure 23. Measured and estimated flow rates of diverted, tailwater, and spillover flow for field Muth2.

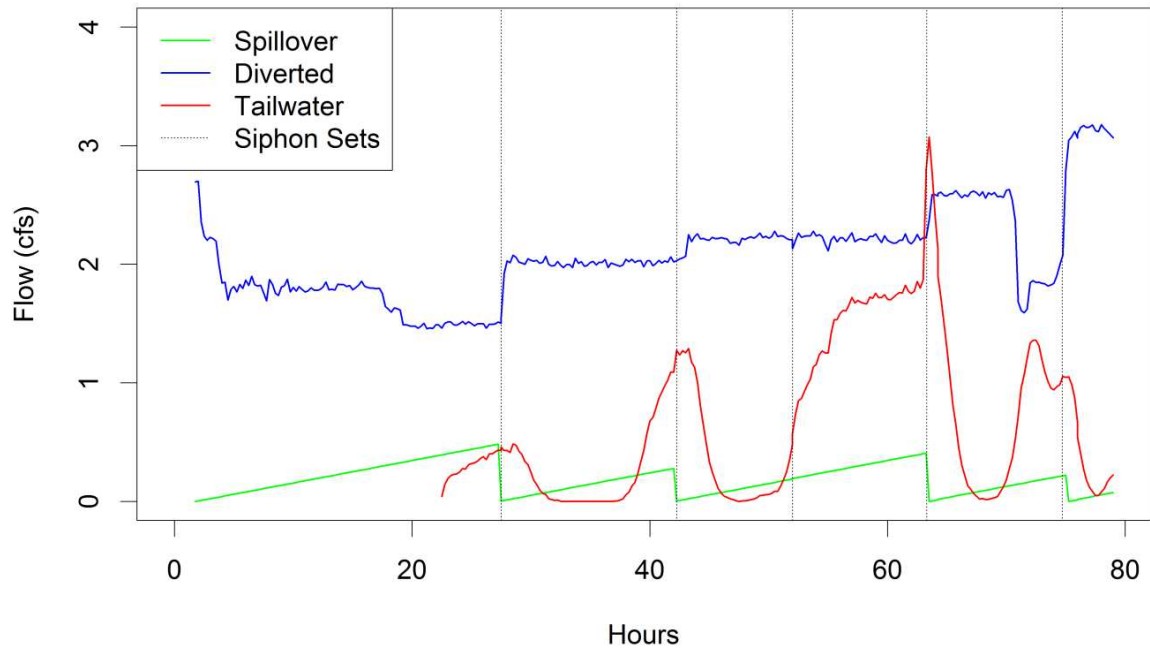


Figure 24. Measured and estimated flow rates of diverted, tailwater, and spillover flow for field DA7.

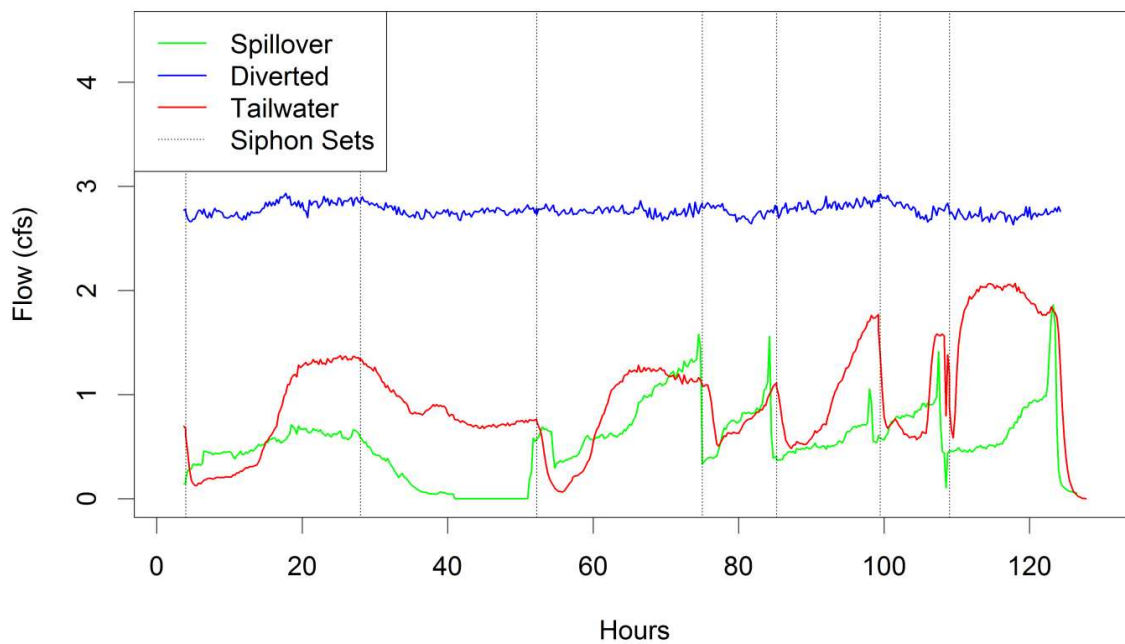


Figure 25. Measured and estimated flow rates of diverted, tailwater, and spillover flow for field Muth9.

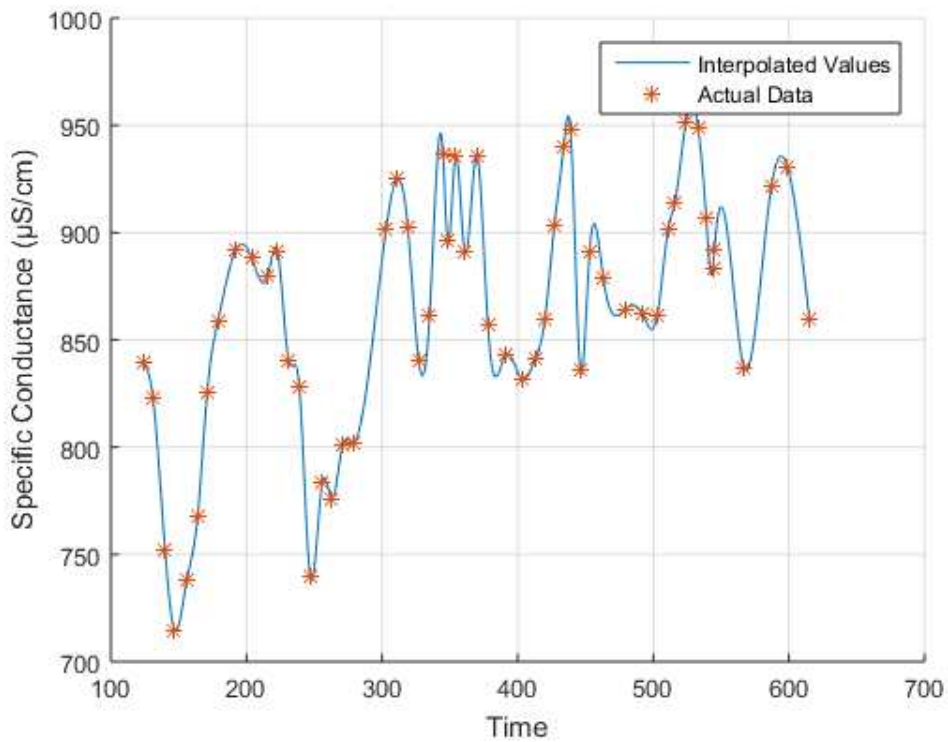


Figure 26. Example of interpolation of specific conductance values using a cubic spline function in Matlab for field Muth9 tailwater flow.

## 2.5 Soil Salinity Survey

A soil salinity survey was conducted for field Muth2 in order to determine the relationship between measured soil salinity and the difference in salinity in the applied irrigation water and the tailwater. The survey was conducted on June 29<sup>th</sup>, 2016 using a Geonics EM-38 MK-2 electromagnetic induction meter that was connected to a Trimble® GPS. The instrument was set to record bulk apparent conductivity ( $EC_a$ ) of the soil to a vertical distance of about 2.5 ft (0.75 m) below the instrument at intervals of one second. The field was paced, carrying the EM-38 MK-2, east to west in rows spaced by approximately 90 feet (27.4 m) with the instrument held about 4 inches (10 cm) above the soil surface, thus reading the average soil  $EC_a$  to a depth of about 2.1 ft (0.65 m) below the ground surface. Boreholes were dug at 5 locations (near the center and four corners of the field) in order to check the soil temperature at 0.5-ft (0.15 m) increments to a depth of 2 ft (0.6 m) and to ensure the soil was not too dry or too wet. The soil would have been determined to be too dry if it fell apart when compressed in one's hand (rather than forming a compressed ball) and too wet if water dripped out of the compressed ball. Bulk apparent soil electrical conductivity ( $EC_a$ ) readings through electromagnetic induction are influenced by soil water salinity, water content, soil texture, bulk density, and temperature. The response of the EM-38 to changes in soil water salinity is greatest at high water contents and least at low water contents and it is recommended that EM38 measurements are taken when soils are below saturation and above 30% available soil moisture (Wittler et al. 2006). Regional calibration equations were developed by Wittler et al. (2006) to convert  $EC_a$  readings to electrical conductivity of a saturated soil paste extract ( $EC_e$ ) for the USR and DSR in the LARV. The  $EC_a$  readings are first corrected for temperature by multiplying  $EC_a$  by the following

temperature correction factor,  $f_{tc}$ , where  $T_s$  is the average soil temperature in degrees C within 2 ft (0.6 m) from the ground surface (Wittler et al 2006):

$$f_{tc} = 1.8509 - 0.0516951(T_s) + 0.000858442(T_s^2) - 0.00000613535(T_s^3) \quad (12)$$

The temperature-corrected value of  $EC_a$  is then converted to  $EC_e$  using the following calibration equation developed by Wittler et al (2006) for the USR:

$$EC_e = 2.31 + 2.29EC_a^{2.3} \quad (13)$$

Eq. (13) was developed with a statistically significant moderate coefficient of determination ( $R^2 = 0.68$ ) for predicting  $EC_e$  in the USR. Because the factors influencing  $EC_a$  readings are highly susceptible to spatially-variable properties that are not incorporated in the univariate calibration equation (soil water content and soil texture) there may be significant error in the estimated  $EC_e$  values. However, the spatial variation of soil water content and soil texture at the time of the survey within field Muth2 was thought to be low, in which case the relative soil salinity estimated within the field was thought to be reasonably accurate.

Using the estimated  $EC_e$  values, a soil salinity contour map was generated using the inverse distance weighting (IDW) function in ArcGIS (Figure 27). Using the Zonal Statistics tool in ArcGIS, the average soil salinity for each siphon set interval was calculated to generate a comparison with the average change in TDS between applied irrigation water and tailwater for each siphon interval.

## 2.6 Statistical Methods

This section describes the statistical methods used for the analysis of water sample data in the search for spatial and temporal trends. All statistical analyses were performed using R software packages (R Development Core Team, 2008) with the probability of making a Type I

error set to 0.05 (significance level). The probability of making a Type I error ( $\alpha$ ) refers to the likelihood that a null hypothesis is rejected which is actually true (Burt and Barber, 1996).

### **2.6.1 ANOVA Statistics**

To determine if sample populations were significantly different, analysis of variance (ANOVA) statistics were conducted. Box and whisker plots and bar plots were used to visually display the sample population characteristics (for an example, see Figure 28). The box and whisker plots contain a box with a central line. The central line represents the median, the upper and lower boundaries of the box represent the 3<sup>rd</sup> and 1<sup>st</sup> quartiles respectively. The whiskers extending from the box represent the “maximum” and “minimum” sample population values. These are in quotations because they exclude the statistical outliers which are defined as the sample population values equivalent to more than 1.5 times the interquartile range above or below the 3<sup>rd</sup> and 1<sup>st</sup> quartiles respectively. The interquartile range is the difference between the 3<sup>rd</sup> quartile and the 1<sup>st</sup> quartile values. The bar plots end at the mean value of the sample population and the error bars extend to the mean value plus or minus the standard error of the sample population.

The standard ANOVA test for testing the equality of means assumes the sample population is normally (Gaussian) distributed and contains homogeneous variances. Sample normality and homogeneity of variances were tested using the Shapiro-Wilk test and Levene’s test, respectively. The null hypothesis of the Shapiro-Wilk test is that the sample is normally distributed and the null hypothesis of the Levene’s test is that the residuals are homogeneously distributed (Shapiro et al. 1965). If the p-value from these tests is less than 0.05 (the specified  $\alpha$  level) it is interpreted that the sample is not normally distributed and/or the sample variances are not homogeneously distributed with statistical significance at a confidence level of 95%, thus



Figure 27. Soil salinity contour map of field Muth2 developed from an EM-38 MK-2 survey, with siphon set intervals shown.

violating the assumptions of the ANOVA equality of means test. Additionally, for each sample population diagnostic plots are analyzed as recommended in Shapiro (1965) (see Figure 29 for an example of a set of diagnostic plots). The upper left panel is a plot of residuals vs predicted values. If the sample population contains homogeneous variance, this plot should show an equal degree of scatter along the full range of the plot (Burt & Barber, 1996). The upper right panel is a Quantile-Quantile plot (Q-Q plot) which is analyzed to assess if the sample residuals are normally distributed. If the sample residuals are normally distributed they will form a nearly straight line along the  $y = x$  line in the Q-Q plot. If the ANOVA test for equality of means assumptions are valid, a One Way Fit test is performed in R using the `aov()` function which tests for the equality of means of all sample populations. Additionally, a pairwise comparison is performed in R using the pairwise method in the `lsmeans` and `multcompView` packages which pairs up each sample population in a test for the equality of means.

In a scenario where the ANOVA test for equality of means assumptions are violated, the Kruskal-Wallis and Dunn's test are performed. These are rank-based tests that are used when the normality of errors are in doubt. They are often interpreted as equality of medians tests. The Kruskal-Wallis test can compare more than two sample populations and determines if all of the samples are similar or not by providing a single p-value (Burt & Barber, 1996). Dunn's test accomplishes pairwise comparisons of two or more sample populations providing a p-value associated with each pair of populations (Kirk, 2013). If the p-values reported are less than 0.05 (the specified  $\alpha$  level) the sample medians are considered statistically different at a confidence level of 95%.

### **2.6.2 Regression Statistics**

Sample populations were analyzed using least-squares linear regressions in order to determine if a statistically significant relationship exists. The following assumptions are made for simple linear regression models: normally-distributed residuals, equal variances, and linear response (Burt & Barber, 1996). The same diagnostic plots are analyzed as for the ANOVA assumptions. If a sample observation demonstrates a linear response, the scatter plot of the dependent vs independent variable shows a linear trend and the residuals vs fitted plot shows equal scatter and no apparent trend of residuals in relation to fitted values. Analysis of the diagnostic plots, and the Shapiro-Wilk and Levene's tests, reveal the degree to which linear regression assumptions are met and should be interpreted as a statistically sound method.

For this study, the `lm()` function in R was used to develop linear regressions of sample populations. The summary of this function provides characteristics of the linear regression including the slope, p-value for the slope, p-value for the intercept, and the coefficient of determination ( $R^2$ ). The  $R^2$  value is a measure of goodness of fit and is interpreted as the proportion of variability in the independent variable that is explained by the dependent variable (Burt & Barber 1996). The p-values associated with the slope and intercept indicate the level of statistical significance attributed to each of the linear regression characteristics. In some instances the 68% and 95% confidence intervals of the slope are incorporated to get a sense of the error associated with the linear regression. The function `confint()` in R was used to generate these confidence intervals. (For examples, see Figure 81 and Figure 84 cited below in Chapter 3).

In order to detect the presence of outliers in a sample set, the `outlierTest()` in R was used. If a p-value of less than 0.05 is reported, it is considered statistically significant with 95%

confidence that there is a statistical outlier in the dataset. The output from the `outlierTest()` includes an index number for the data point which is the same as what is displayed on the diagnostic plots for potential outliers. As an example, see Figure 94 which is cited below in Chapter 3. In these diagnostic plots index point 162 is marked as a potential outlier in all 4 panels of this figure. In this case, if the outlier p-value was below 0.05, the data point should be reviewed for potential errors including those from data entry, sampling, and lab testing in order to determine if the point should be removed. The bottom right panel of the diagnostic plots is the standardized residuals vs leverage plot. The leverage axis indicates the relative influence individual data points have on the linear regression. In Figure 98 cited in Chapter 3, index point 108 has large leverage despite a small standardized residual indicating the importance of analyzing the diagnostic plots as well as performing test statistics because the data point might not be identified as an outlier because it has such great influence on the linear regression (Burt & Barber, 1996).

## CHAPTER 3: RESULTS AND DISCUSSION

### **3.1 Analysis of Sample Data from Monitoring Wells, Tile Drains and Surface Sites using ANOVA Statistics**

Sample data are divided into the following data subsets: groundwater (GW), surface water (SW), tile drain water (TD), and tailwater mixed with tile drain water (TWTD). The surface water sample data were collected from irrigation water in lateral ditches diverted from the Catlin Canal. The locations of SW sampling can be seen in Figure 4 referenced as sites A1 and A2. The groundwater sample data was further divided into the following data subsets: drained and deep (dd), drained and shallow (ds), undrained and deep (ud), undrained and shallow (us). The following subchapters will describe and compare sample populations using these subset categories in order to identify relationships and trends.

#### ***3.1.1 Comparison of Nitrate Concentration Data***

Box plots and bar plots of  $\text{NO}_3\text{-N}$  concentrations ( $C_N$ ) for each sample type are shown in Figure 28. Note that the median and mean groundwater  $C_N$  are substantially different due to the outliers and skewness of the data. The groundwater statistical outlier samples are primarily from wells G7, G8 and G9 (one of the outliers is from well G12), and were collected on different dates, indicating it is unlikely their outlying values are caused by sampling error. The diagnostic plots (Figure 29) indicate the dataset contains unequal variances (due to the unequal scatter in the vertical direction in the upper left panel) and a distribution that is not normal (as indicated by the data not following the line  $y = x$  in the upper right panel). For this reason, a Kruskal-Wallis test and Dunn test are performed to test for equality of medians. The results of these tests are shown in Table 7 along with the sample size. The p-value of the Kruskal-Wallis test is less than 0.05 indicating the median values of all the datasets are not statistically equal with a confidence level

of 95%. The Dunn test p-values show that the median  $C_N$  of GW and SW are not statistically different and that the median  $C_N$  of TD and TWTD are not statistically different. The Dunn test also shows that the median  $C_N$  from the following samples are significantly different: GW and TD, GW and TWTD, SW and TD, SW and TWTD.

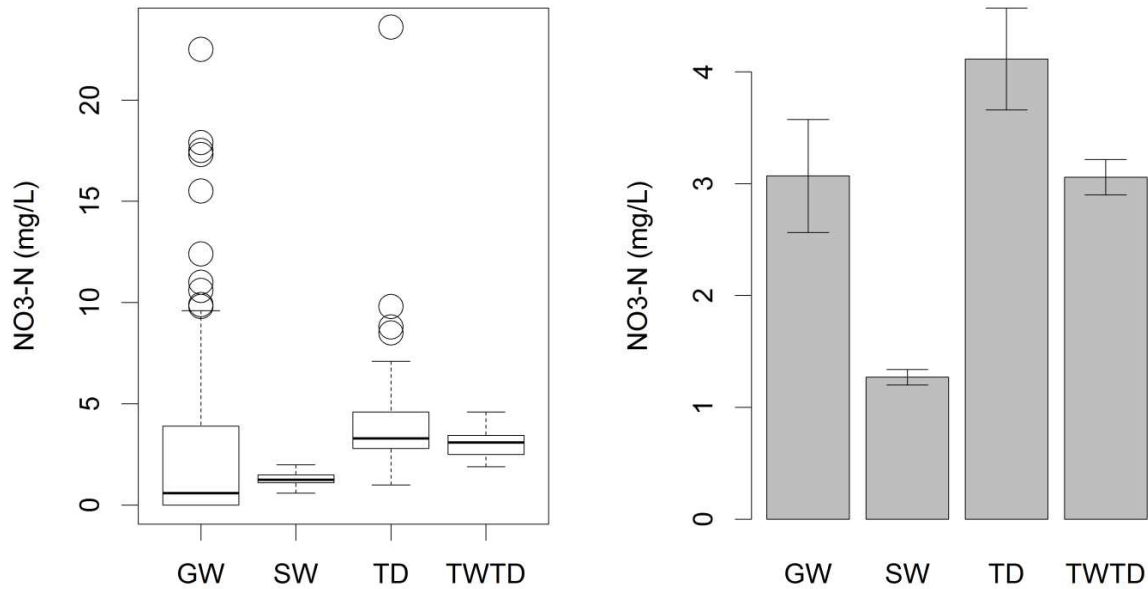


Figure 28. Box plots and bar plots of NO<sub>3</sub>-N concentrations grouped by the type of sample where GW, SW, TD, and TWTD are groundwater, applied irrigation water, tile drain water, and tailwater mixed with tile drain water respectively.

Table 7. Results of Kruskal-Wallis test and Dunn test for NO<sub>3</sub>-N sample data separated by type of sample.

Kruskal-Wallis: <0.001	Groundwater (n=91)	Surface Water (n=30)	Tile Drain Water (n=52)
Surface Water	0.1263		
Tile Drain Water	<0.0001	<0.0001	
Tailwater & Tile Drain (n=23)	0.0005	0.0001	0.2384

These test results suggest that applied surface water picks up NO<sub>3</sub> as it flows through the root-zone and into the tile drain network. Because the relative proportions of tailwater and tile drain water are not known, the  $C_N$  of tailwater is unknown. However, from field observations it

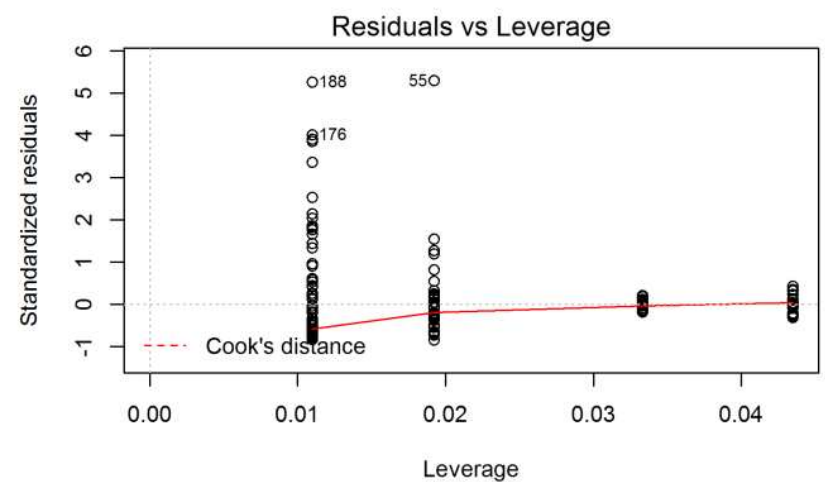
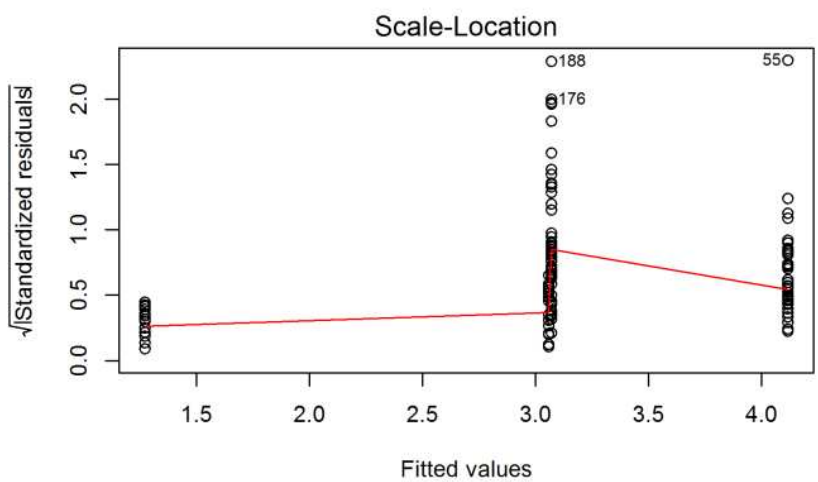
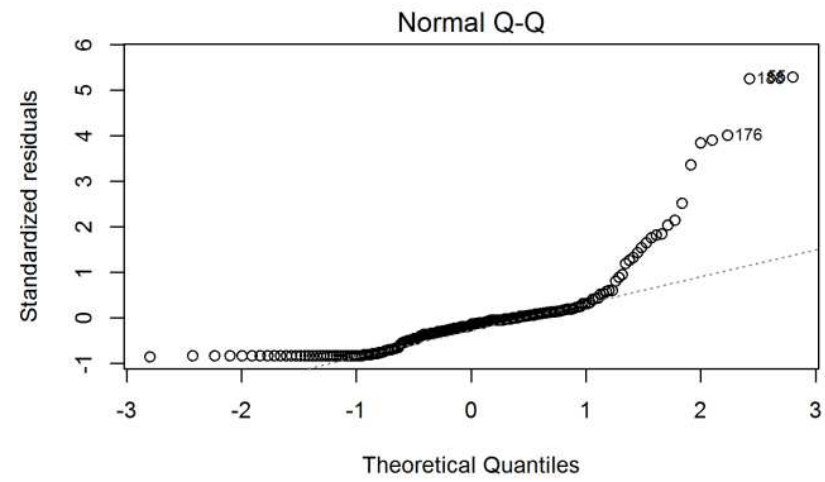
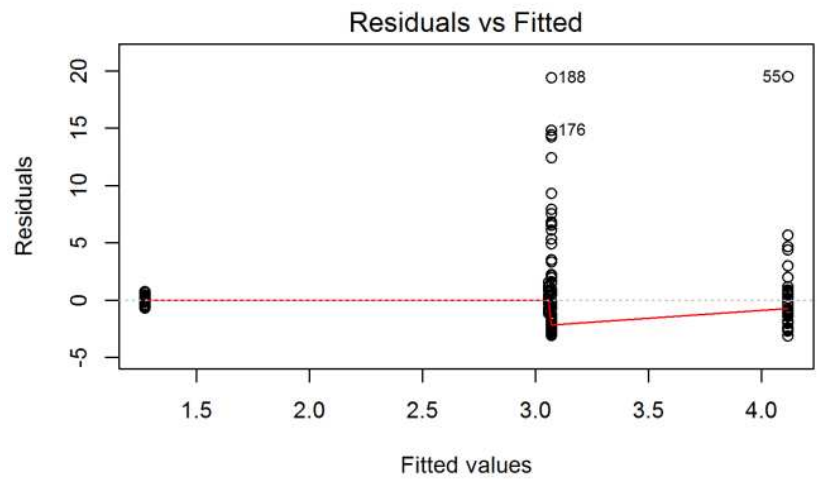


Figure 29. Diagnostics of  $\text{NO}_3\text{-N}$  concentrations grouped by sample type: surface water, groundwater, tile drain water, and tile drain mixed with tailwater.

is known that during the irrigation season the tailwater runoff rate is typically greater than the tile drain effluent rate. Figure 6 is an image of the mixing of tailwater and tile drain effluent during the irrigation season. Because the median  $C_N$  of TD and TWTD are not statistically different it is likely that the  $C_N$  of tailwater is also high relative to SW.

Figure 30 groups  $C_N$  of TWTD samples based on when they were collected: S (growing season), and W (winter). While the population mean and median are not statistically different, the winter  $C_N$  values tend to be higher. This is likely the case because fields are not being irrigated and there is less applied water to dilute the  $C_N$ . The flow rates of Timpas Creek and the Arkansas River are substantially lower in the winter than in the summer and, therefore, are much more susceptible to increases in solute concentration from tributaries with high concentrations of solute loading in the winter.

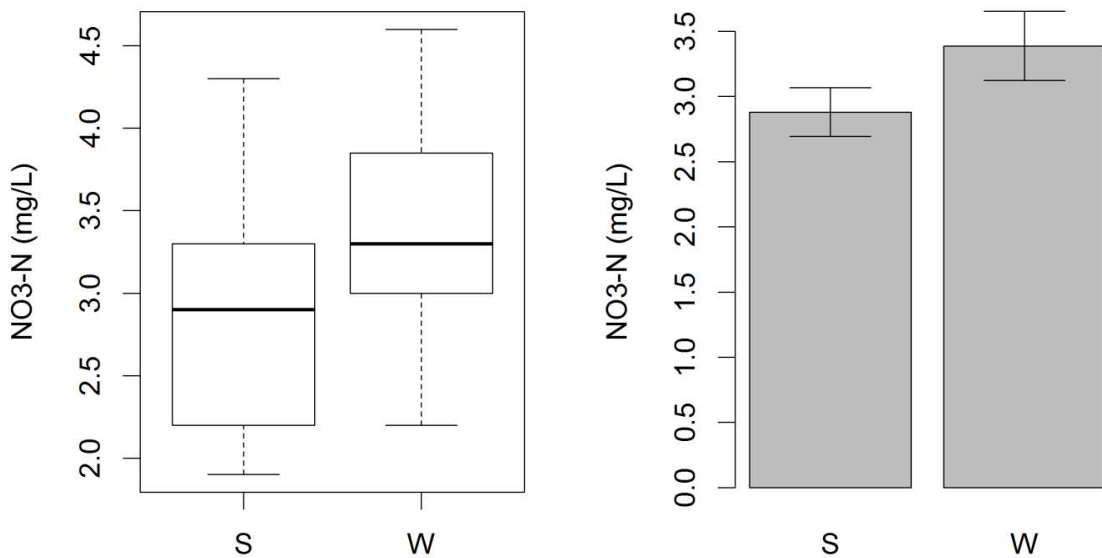


Figure 30. Box plot and bar plot of NO<sub>3</sub>-N concentration of tailwater mixed with tile drain water grouped by growing season (S) and winter (W).

Figure 31 shows box plots and bar plots of  $C_N$  in surface water and groundwater divided into categories based on the presence of drains in the field containing the monitoring well and the depth of the monitoring well. The average depth of deep and shallow groundwater wells in the presence of tile drains is 50.8 and 13.7 feet (16.9 and 4.6 m) respectively. The average depth of deep and shallow groundwater wells in the absence of tile drains is 29.8 and 12.2 feet (9.9 and 4.1 m). Undrained groundwater has greater  $C_N$  than surface water, which itself has greater  $C_N$  than drained groundwater. To determine if these differences are statistically significant an ANOVA test was conducted. The diagnostic test plots (Figure 87 in Appendix C) indicate that the dataset violates the assumptions of equal variance and normal distribution. Given these violations of standard ANOVA assumptions, a Kruskal-Wallis test and a Dunn test were performed, the results of which are shown in Table 8 along with sample sizes. The Kruskal-Wallis test p-value was less than 0.05, indicating that not all of the median values of the  $C_N$  data subsets are equal with statistical confidence of 95%.

The Dunn test results indicate that the median SW  $C_N$  value is significantly different from that of each of the four groundwater sample populations. They also indicate that the median  $C_N$  for both the deep and shallow drained datasets are significantly different from both the deep and shallow undrained datasets. Furthermore, the Dunn test results indicate that the median  $C_N$  for drained deep and drained shallow datasets are not significantly different, and similarly, that the median  $C_N$  for undrained deep and undrained shallow datasets are not significantly different.

These results indicate that the presence of subsurface drainage lowers the  $C_N$  in groundwater to levels less than that in applied SW. This is further enforced by the previous findings which showed the median  $C_N$  value of TD samples is significantly higher than that of

SW samples. It can be inferred from these results that tile drains play a significant role in the export and prevention of the deep percolation of  $\text{NO}_3$ .

While several groundwater and tile drain samples are found to be above the USEPA drinking criterion for  $C_N$  of 10 mg/L, the mean and median  $C_N$  of each sampling type and each groundwater category are well below it. However, the box and whisker plot of undrained shallow groundwater indicates that the 3<sup>rd</sup> quartile is very close to 10 mg/L, meaning that nearly 25% of samples may have values greater than the drinking water criterion. Subsurface drainage appears to be an effective way to maintain local groundwater  $C_N$  significantly below the drinking water maximum contaminant level at this site. However,  $\text{NO}_3$  loading to streams from subsurface drainage is likely to cause compounding downstream effects, as has been shown in other study regions (Isidoro et al. 2006, Alexander et al. 2008).

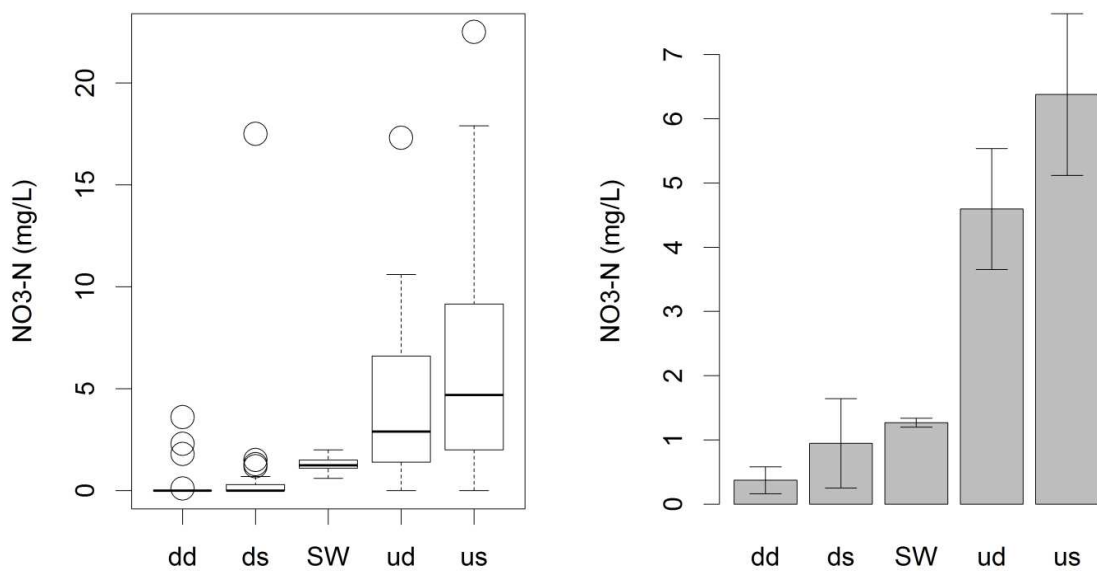


Figure 31. Box plot and bar plot of  $\text{NO}_3\text{-N}$  concentrations from applied irrigation water (SW) and groundwater samples separated by presence of drains and depth of wells. Two letter code: (drained or undrained, deep or shallow).

Table 8. Results of Kruskal-Wallis test and Dunn test for NO<sub>3</sub>-N concentration in applied irrigation water and groundwater samples grouped by presence of drains and depth of monitoring well.

Kruskal-Wallis: <0.001	Drained Deep (n=21)	Drained Shallow (n=25)	Surface Water (n=30)	Undrained Deep (n=22)
Drained Shallow	0.2642			
Surface Water	0.0001	0.0005		
Undrained Deep	<0.0001	<0.0001	0.0286	
Undrained Shallow (n=23)	<0.0001	<0.0001	0.0043	0.2580

### 3.1.2 Comparison of Dissolved Selenium Concentration Data

A box plot and bar plot of total dissolved Se concentration ( $C_{Se}$ ) are shown in Figure 32. Once again, groundwater outliers and the skewness have a large influence on the computed groundwater mean. All three of the outliers were collected either in May or June sampling events of 2016. Two of the three outliers are from monitoring well G6 and the third is from G12. These high  $C_{Se}$  values correspond to high  $C_N$  values, but the cause of an increase in  $C_N$  is not known.

The diagnostic plot (Figure 88 in Appendix C) does not indicate any obvious violations of the assumptions used in the ANOVA test for equality of means. Both the standard ANOVA test for equality of means and the Kruskal-Wallis and Dunn tests for equality of medians were conducted and the resulting p-values are shown in Table 9 and Table 10, respectively. These tests resulted in similar conclusions. The mean and median for each pair of datasets, with the exception of those for surface water and groundwater, are significantly different. There is an increase in the mean and median  $C_{Se}$  values from SW to TD and from SW to TWTD. The mean and median  $C_{Se}$  values for TWTD samples is less than that for TD samples, indicating that tailwater has lower  $C_{Se}$  than tile drain water. This is likely the case because, despite high DO O levels measured in tailwater flow, there is not sufficient time for redox reactions to occur during the period that applied irrigation water flows across and off of fields as tailwater. The increase in  $C_{Se}$  values from SW to TD must be due to the accumulation of dissolved Se while SW percolates through the root zone and is transported via shallow groundwater to the tile drains. This

accumulation can be explained by high levels of DO and NO<sub>3</sub> in the root zone and shallow groundwater that are present due to high DO levels in applied irrigation water and the application of nitrogen fertilizer which allow for the oxidation of elemental Se and the inhibition of the

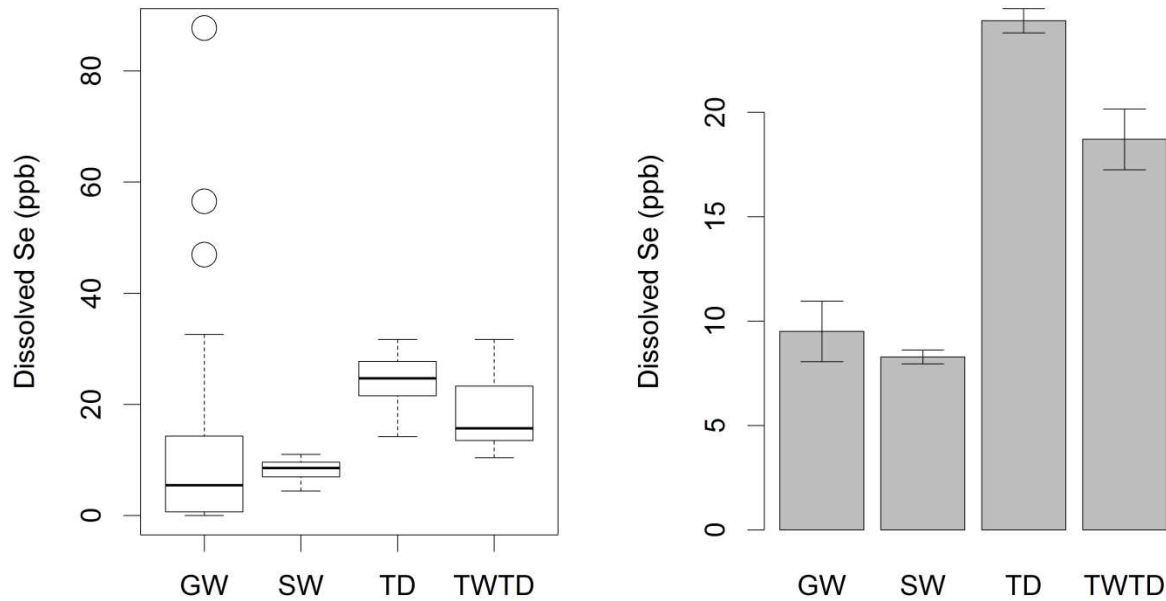


Figure 32. Box plot and bar plot of total dissolved Se concentrations grouped by the type of sample where GW, SW, TD, and TWTD refer to groundwater, applied irrigation water, tile drain water, and tailwater mixed with tile drain water.

Table 9. Results of one way fit and pairwise comparison of means for C<sub>Se</sub> data grouped by sample type.

One Way Fit: <0.001	Groundwater (n=86)	Surface Water (n=28)	Tile Drain Water (n=51)
Surface Water	0.5623		
Tile Drain Water	<0.0001	<0.0001	
Tailwater & Tile Drain (n=22)	0.0001	0.0002	0.0230

Table 10. Results of Kruskal-Wallis test and Dunn test for C<sub>Se</sub> sample data grouped by type of sample.

Kruskal-Wallis: <0.001	Groundwater (n=86)	Surface Water (n=28)	Tile Drain Water (n=51)
Surface Water	0.4458		
Tile Drain Water	<0.0001	<0.0001	
Tailwater & Tile Drain (n=22)	<0.0001	0.0001	0.0227

chemical reduction of  $\text{SeO}_4$  (Gates et al. 2009). Unfortunately, from these samples, we do not know the  $C_{\text{Se}}$  of tailwater and how it changes as compared to applied water. See Section 3.5 Field-Scale Mass Balance of Se for estimates of a field-scale mass-balance of dissolved Se.

The median  $C_{\text{Se}}$  of samples taken from water exported to Timpas Creek (TWTD) is 15.7  $\mu\text{g/L}$ , greater than five times the USEPA chronic criterion of 3.1  $\mu\text{g/L}$ . Because the flow rate of TWTD is not known, it is difficult to state the relative impact that this high  $C_{\text{Se}}$  has on the aquatic system of Timpas Creek or on the Arkansas River. However, it is likely that the Se loading impact is greater in the winter than in the summer growing months (March 15<sup>th</sup> through November 15<sup>th</sup>). Figure 33 shows a box plot and bar plot of  $C_{\text{Se}}$  values in the TWTD water samples collected during the growing season when fields are irrigated and during the winter when the Catlin Canal is not running and fields are not being irrigated. Both the standard ANOVA comparison of means test and the Kruskal-Wallis comparison of medians test resulted in p-values less than 0.05 indicating that the differences in mean and median values are statistically significant. The median winter  $C_{\text{Se}}$  value is 1.8 times greater than the median irrigation season  $C_{\text{Se}}$ . Devitt et al. (1976) found that low leaching fractions export higher  $C_{\text{N}}$  but lower total N loads whereas high leaching fractions export lower  $C_{\text{N}}$  but larger total N loads. There appears to be a similar trend with  $C_{\text{Se}}$  at this site. It was observed that the flow rate of the tile drain network is lower in the winter, so it is likely that the total dissolved Se load is less in the winter than in the summer; nevertheless, the high  $C_{\text{Se}}$  values are a matter of concern. The median  $C_{\text{Se}}$  in the winter is 25.9  $\mu\text{g/L}$ , over eight times the USEPA chronic criterion. Solute concentrations in Timpas Creek and the Arkansas River are more susceptible to change in the winter time due to low flow rates. Because of this, depending on the flow rate of tile drain

effluent, the input of high solute concentration from tile drain effluent may be more problematic in the winter time.

The box plot and bar plot for  $C_{Se}$  from surface water and groundwater samples grouped into categories based on presence of drains in the field containing the monitoring well and depth of the monitoring well are shown in Figure 34. Note that the computed mean values of  $C_{Se}$  for the deep and shallow drained datasets are heavily influenced by outliers. All four of the drained

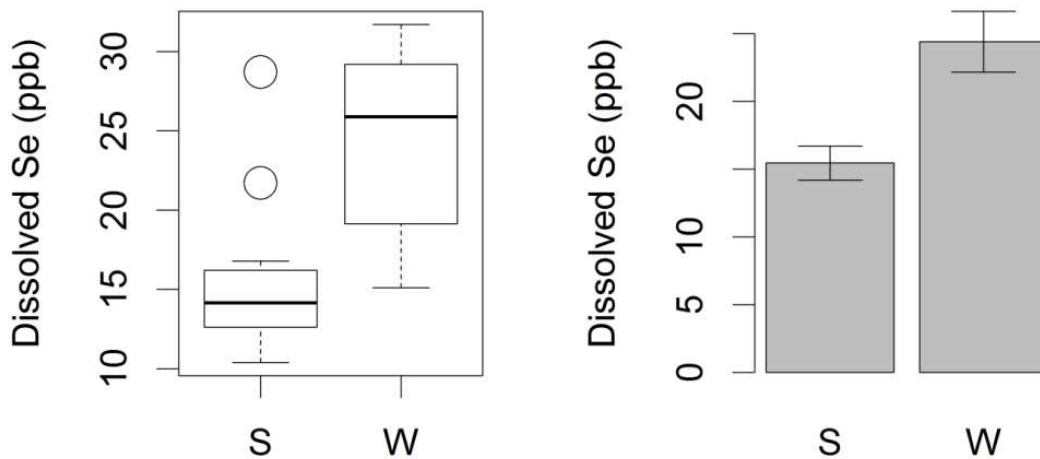


Figure 33. Box plot and bar plot of  $C_{Se}$  in tailwater mixed with tile drain water grouped by growing season (S) and winter (W).

deep outliers are from monitoring well G6 which extends to a depth of 50.2 feet. There are only two drained deep wells and all of the other readings are 0 ppb with the exception of two that are less than 1 ppb. These outliers do not appear to be sampling or lab errors, based on the variation in date of collection and processing. The drained shallow sample outliers are from wells G12 and G10 (depths of 13.0 and 14.4 feet) from which there were only 3 and 2 total samples collected,

respectively. For this reason, trends at these locations cannot be identified. With the exception of the outlier from well G10, all of the other  $C_{Se}$  outliers, from both deep and shallow drained wells, correspond to elevated  $C_N$  values, indicating that surface water contamination is a possible cause of the outliers, and further validating the strong redox relationship between Se and  $NO_3$ . (Surface water contamination is prevented by a layer of bentonite that seals the outside of the well to the

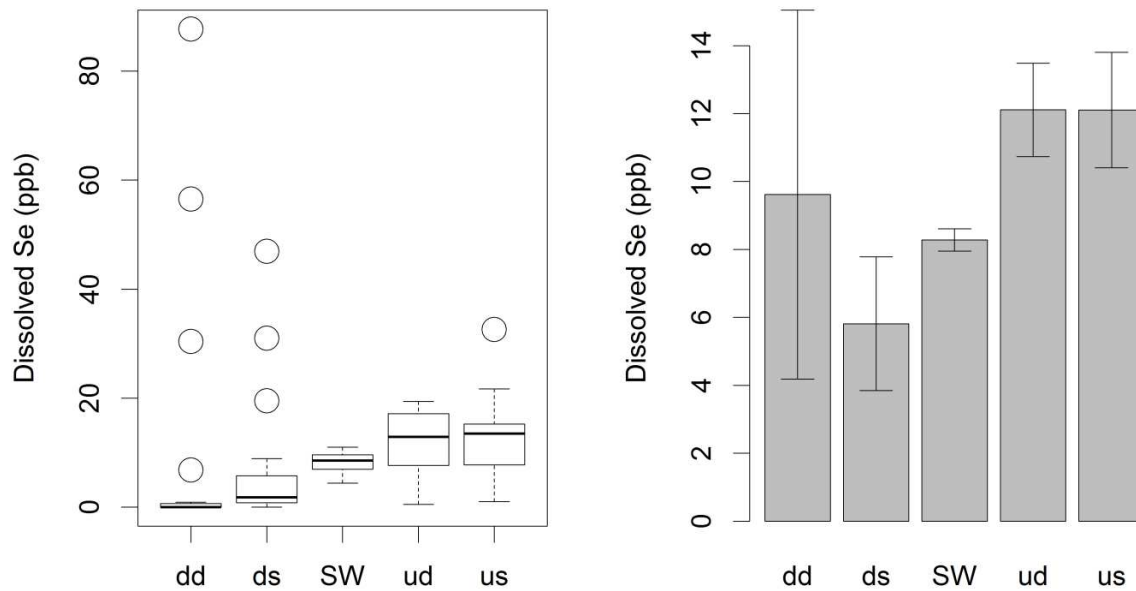


Figure 34. Box plot and bar plot of dissolved Se concentrations from applied irrigation water samples (SW) and groundwater samples grouped by presence of drains and depth of monitoring well. Two letter code: (drained or undrained, deep or shallow).

Table 11. Results of Kruskal-Wallis test and Dunn test for  $C_{Se}$  sample data grouped by presence of drains and depth of monitoring well.

Kruskal-Wallis: <0.001	Drained Deep (n=19)	Drained Shallow (n=28)	Surface Water (n=28)	Undrained Deep (n=20)
Drained Shallow	0.0853			
Surface Water	0.0001	0.0036		
Undrained Deep	<0.0001	<0.0001	0.0688	
Undrained Shallow (n=19)	<0.0001	<0.0001	0.1062	0.4207

surrounding soil. If this bentonite layer fails, surface water can flow down the exterior of the monitoring well and contaminate the groundwater.)

The diagnostic plots shown in Figure 89 in Appendix C indicate that the dataset is not quite normality distributed and shows inequality in variance. For these reasons the Kruskal-Wallis and Dunn test were conducted, with results summarized in Table 11. Similar to the tests performed for  $C_N$  in groundwater, the Dunn test results indicate that the median  $C_{Se}$  values for both the deep and shallow drained datasets are significantly different from both the deep and shallow undrained datasets, suggesting subsurface drainage may have an influence on groundwater  $C_{Se}$ . When comparing deep and shallow monitoring wells that are located in either drained or undrained fields, the median  $C_{Se}$  values are not significantly different, indicating that the depth of groundwater does not have a large influence on  $C_{Se}$ . Surface water median  $C_{Se}$  is significantly different from both deep and shallow drained groundwater median  $C_{Se}$  but is not significantly different from deep and shallow undrained median  $C_{Se}$ , adding to the likelihood that subsurface drainage has influence on groundwater  $C_{Se}$ .

Conclusions from this dataset should be drawn with caution due to the limited spatial variability represented by the data. For example, the drained deep groundwater dataset is comprised of 19 samples taken over two years from only two monitoring wells. These samples directly represent two points in a subsurface drainage system that influences 950 acres. With this in mind, the samples show a statistically significant lower groundwater  $C_{Se}$  in fields with tile drains compared to groundwater  $C_{Se}$  in fields without tile drains as well as a significantly lower  $C_{Se}$  in groundwater with drains when compared to applied irrigation water. The decrease in  $C_{Se}$  in samples from SW in relation to those from GW when subsurface drainage is present most likely is caused by the increased rate of chemical reduction of  $SeO_4$  in the absence of DO and

NO<sub>3</sub> or by the prevention of Se mobilization from marine shale, due to the removal of NO<sub>3</sub> by subsurface drainage as was shown in Section 3.1.1 Comparison of Nitrate Concentration Data.

### ***3.1.3 Comparison of Total Dissolved Solids Concentration Data***

The box plot and bar plot of TDS concentrations ( $C_{TDS}$ ) from samples grouped by sample types are shown in Figure 35. The diagnostic plots (Figure 91 in Appendix C) indicate that the dataset is not normally distributed and contains unequal variances, violating the assumptions of ANOVA statistics. For that reason, the Kruskal-Wallis and Dunn tests are conducted to test for equality of medians among the sample types. Table 12 shows the Dunn test p-value results as well as the sample size for each sample type. The median  $C_{TDS}$  values for the sample types are significantly different from each other. The median  $C_{TDS}$  of TWTD is nearly half the median  $C_{TDS}$  of TD suggesting the tailwater has substantially lower  $C_{TDS}$  in comparison with water from the tile drains. It is expected for tile drain effluent to have high  $C_{TDS}$  due to evapo-concentration that occurs in the root zone and dissolution processes that occur as the applied water infiltrates and flows through the root towards the tile drain (El-Ashry et al. 1985). Both the median and mean values for TD  $C_{TDS}$  are 4.8 times larger than those for SW  $C_{TDS}$ . Because the applied water and tile drain flow rates are not known, it is not possible to determine the change in salt load between applied water and subsurface drainage effluent.

A box plot and bar plot of  $C_{TDS}$  from tile drains in the growing season and winter are shown in Figure 36. There were far fewer tile drain samples for  $C_{TDS}$  collected in the winter (n=6) compared with the growing season (n=21) which is not an ideal scenario for ANOVA statistics. With that in mind, the Kruskal Wallis comparison of median test was used, resulting in a p-value of 0.05 indicating the median  $C_{TDS}$  values are significantly different. Tile drain effluent  $C_{TDS}$  decreases in the summer and increases in the winter.

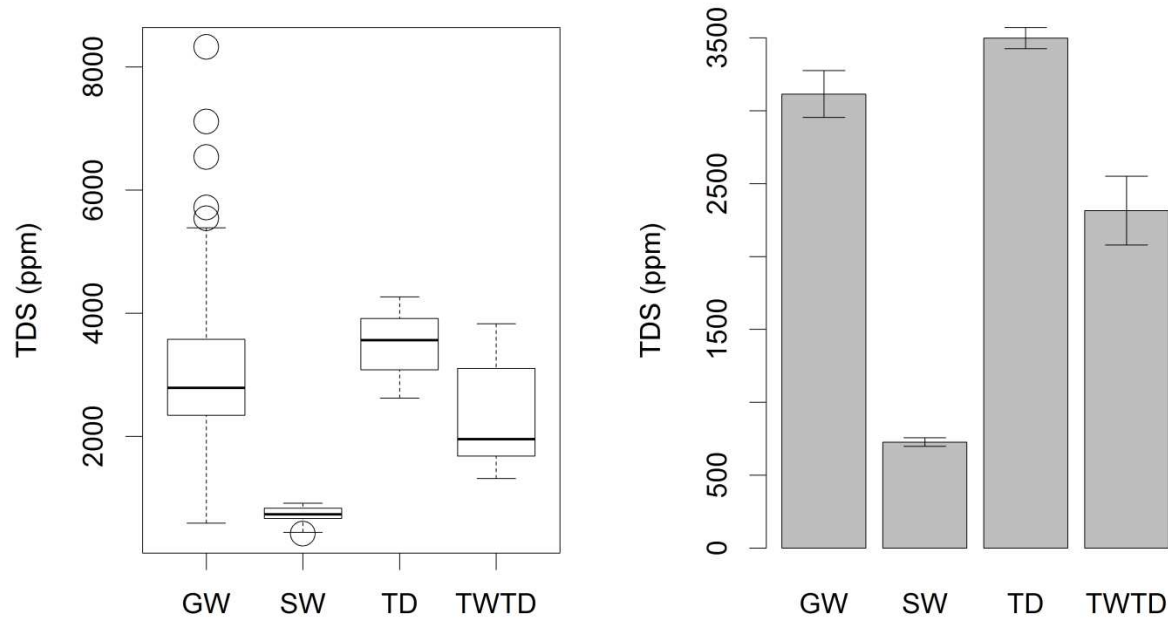


Figure 35. Box plot and bar plot of  $C_{TDS}$  grouped by type of sample where GW, SW, TD, and TWTD refer to groundwater, applied irrigation water, tile drain water, and tailwater mixed with tile drain water.

Table 12. Results of Kruskal-Wallis and Dunn tests for  $C_{TDS}$  sample data grouped by type of sample.

Kruskal-Wallis: <0.001	Groundwater (n=76)	Surface Water (n=21)	Tile Drain Water (n=40)
Surface Water	<0.0001		
Tile Drain Water	0.0008	<0.0001	
Tailwater & Tile Drain (n=15)	0.0367	0.0008	0.0001

The box plot and bar plot shown in Figure 37 is of  $C_{TDS}$  in TWTD samples in the winter and growing season. The Kruskal-Wallis test resulted in a p-value of 0.044 indicating the median values are significantly different. The median  $C_{TDS}$  in samples from TWTD flowing to Timpas Creek in the winter is twice what it is in the summer. As mentioned previously, Timpas Creek and the Arkansas River may be more susceptible to changes in solute concentrations in the winter time when stream flow rates are lower.

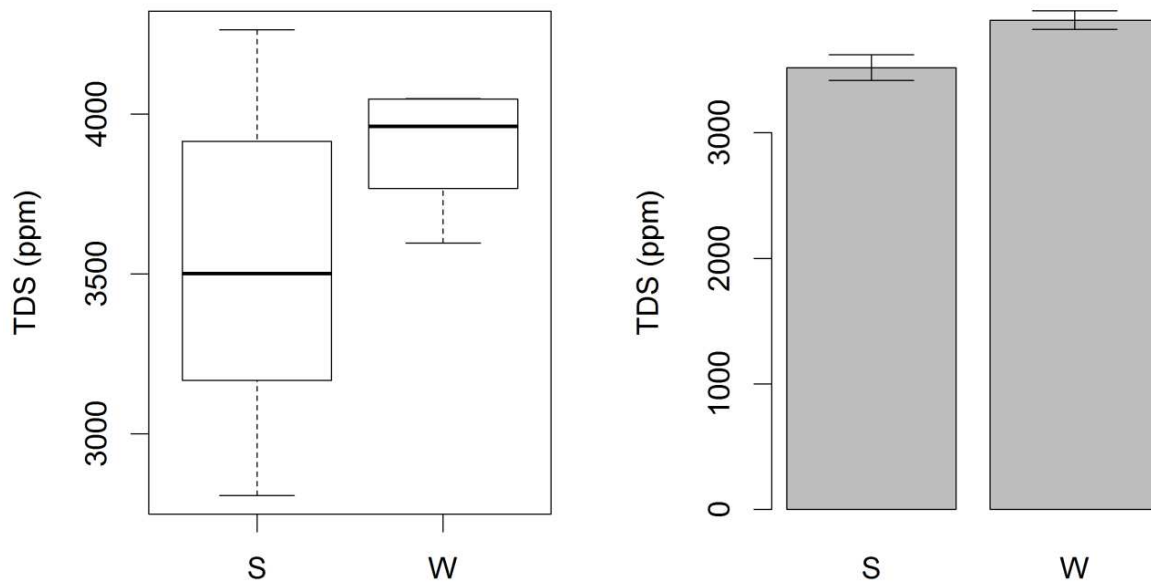


Figure 36. Box plot and bar plot of  $C_{TDS}$  of tile drain water water grouped by growing season (S) and winter (W).

The box plots and bar plots of  $C_{TDS}$  of groundwater samples grouped into datasets based on presence of tile drains and depth of monitoring wells is shown in Figure 38. The diagnostic plots shown in Figure 92. Diagnostic plots of  $C_{TDS}$  for groundwater in Appendix C indicate the dataset contains unequal variance. The p-value of the Kruskal-Wallis test was 0.21 indicating that the median values of each data set are not significantly different from one another. The presence of drains and the depth of groundwater do not appear to have a statistically significant influence on the groundwater  $C_{TDS}$ .

Assuming that most of the water exported by the tile drain would contribute to groundwater baseflow in the absence of tile drains, and that this contribution does not affect the  $C_{TDS}$  as shown, the significantly higher levels of  $C_{TDS}$  in samples from TD water are an

additional source of TDS loading to the river system that would not occur in the absence of subsurface drainage. However, this assumes that the preexisting conditions of the drained and

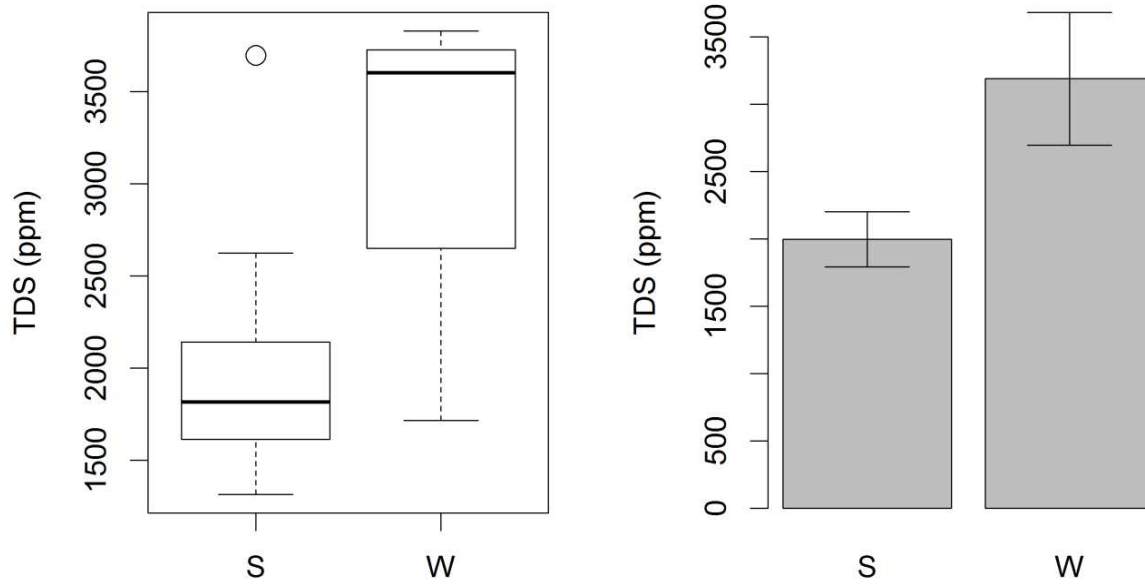


Figure 37. Box plot and bar plot of  $C_{TDS}$  of tailwater mixed with tile drain water separated by growing season (S) and winter (W).

undrained land are the same which is probably not true since the location in which tile drains are installed was probably more salinized than the remaining lands. It is possible that in the absence of tile drains, evaporative-concentration of salts would increase sufficiently to increase the  $C_{TDS}$  of deeper GW through deep percolation and solute transport of TDS via baseflow would make up for the increased transport of TDS via subsurface drainage. Subsurface drainage accelerates the transport of salts to the river system in comparison to baseflow which travels at relatively slow rates.

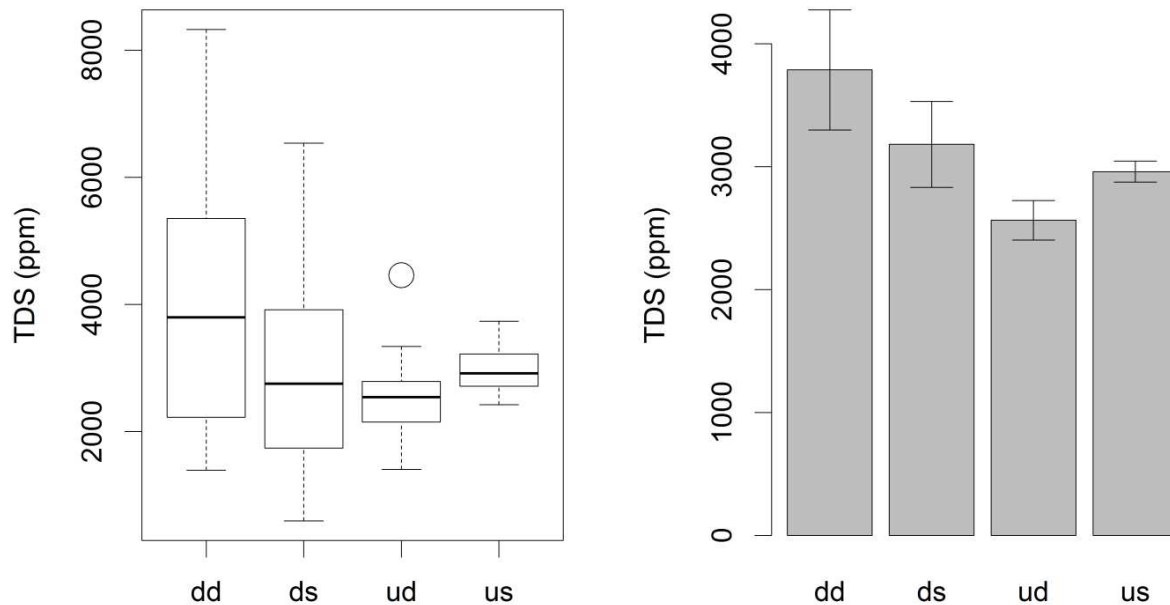


Figure 38. Box plots and bar plots of  $C_{TDS}$  from groundwater sample data separated by presence of drains and depth of wells. Two letter code (drained or undrained, deep or shallow)

### 3.2 Analysis of Relationships between Water Quality Characteristics using Regression Statistical Methods

#### 3.2.1 Relationship of Dissolved Se and TDS

A scatterplot of  $C_{Se}$  vs  $C_{TDS}$  for all sample types is presented in Figure 39. Tile drain water tends to have the highest  $C_{TDS}$  and  $C_{Se}$  values and the applied surface water tends to have the lowest  $C_{TDS}$  and  $C_{Se}$ . Figure 40 shows scatter plots with fitted linear relationships between  $C_{Se}$  vs  $C_{TDS}$  for each type of sample (GW, SW, TD, and TWTD) along with the corresponding  $R^2$  value and p-value of the slope. The coefficient of determination is significant and high for both the SW and TWTD samples ( $R^2 = 0.87, 0.97$ ). The slopes of the linear regressions are significant to a 95% confidence level for all sample types with the exception of GW. The diagnostic plots for the linear regressions for the SW, TD, and TWTD samples are shown in Figure 95, Figure 96,

and Figure 97 in Appendix C. The residuals vs fitted plots for these three datasets show no trend and relatively uniform scatter, indicating that the datasets satisfy the regression assumptions of linear response and equal variance. The QQ plots from these same datasets are nearly straight lines, indicating the data satisfies the regression assumption of normal distribution.

For SW, the relationship between  $C_{TDS}$  and  $C_{Se}$  is very similar to that found from the field scale mass balance samples of applied surface water ( $R^2 = 0.87$  and  $0.88$ , see Figure 20). However, the linear regressions are notably different (see Figure 41). For the field-scale mass balance, the  $C_{Se}$  value tended to be higher for a given value of  $C_{TDS}$ . The cause of these differences is not known, but a larger sample size might result in a linear regression with a slope between the two regressions shown. Despite a larger sample size for the samples collected for the complete FDD study, the linear regression of the samples collected from the field-scale mass balance is used for the mass balance because it is reflective of the relationship between  $C_{TDS}$  and  $C_{Se}$  that existed at the time of the mass balance.

The coefficient of determination for the fitted linear relationship between  $C_{TDS}$  and  $C_{Se}$  for TD samples ( $R^2 = 0.42$ ) suggests that  $C_{TDS}$  explains much less of the variance in  $C_{Se}$  than it did in the case of SW. This is likely due to the variable redox conditions present in the root zone and groundwater near the water table, as affected by the presence of  $NO_3$  and DO. Since the conditions for TDS dissolution are relatively constant spatially and redox conditions vary spatially, the amount of Se mobilized is not as reflective of  $C_{TDS}$  as it is where redox conditions are more homogeneous and there is sufficient time for redox reactions to take place, such as occurs at deeper levels in the aquifer.

As shown in Figure 20,  $C_{TDS}$  explains less of the variation in  $C_{Se}$  for tailwater ( $R^2 = 0.67$ ) than it did for applied water ( $R^2 = 0.88$ ) in the field-scale mass balance. The limited number of

samples from the mass balance events and the lack of tailwater sampling data from the entire FDD study prevent confident interpretation of the processes occurring that change solute concentrations as water flows across a field. Despite the weaker relationship for tailwater samples from the field scale mass balance samples, the linear relationship between  $C_{Se}$  and  $C_{TDS}$  is best ( $R^2 = 0.97$ ) for TWTD samples. The reason for this is not known.

The diagnostic plot of the linear relationship between  $C_{Se}$  and  $C_{TDS}$  for groundwater samples is shown in Figure 93 in Appendix C. The groundwater dataset shows a “megaphone” trend and unequal scatter in the residuals vs fitted plot and the QQ plot is not linear, indicating the dataset does not satisfy any of the regression assumptions mentioned above. The results of the outlier test indicate that, with 95% confidence, the only dataset in Figure 40 containing outliers is that for the groundwater samples. While the outliers could be identified and omitted, it does not appear that this would substantially improve the fit of the linear regression. With all the groundwater samples in the same dataset, the  $C_{TDS}$  does not appear to explain any variance in the  $C_{Se}$  values.

In order to investigate further the relationship between  $C_{Se}$  and  $C_{TDS}$  in groundwater, the groundwater dataset is divided into different categories. Figure 77 in Appendix A contains scatter plots and linear regressions of  $C_{Se}$  vs  $C_{TDS}$  from groundwater samples that are grouped based on monitoring well depth and by presence of subsurface drains in the field containing the monitoring well. Splitting the groundwater data into the subsets shown does not appear to improve the strength of any linear regression trends. The coefficient of determination for each linear regression relationship is less than 0.1 and the p-value for each dataset is greater than 0.05, indicating no statistical significance. Each dataset contains outliers according to the outlier test, but the outliers do not appear to be skewing any obvious linear trend. This indicates that,

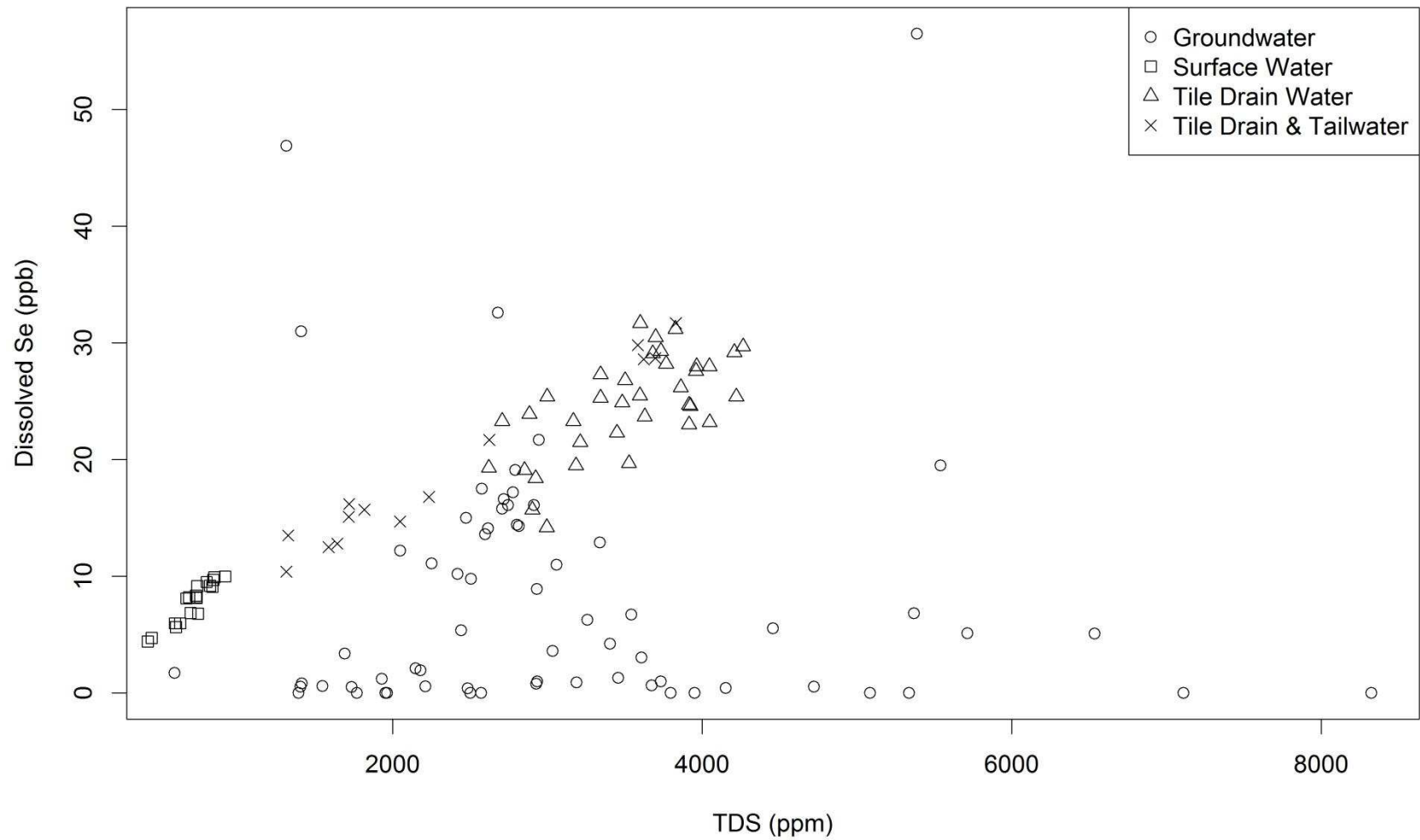


Figure 39. Scatterplot of dissolved Se and TDS concentrations for all samples.

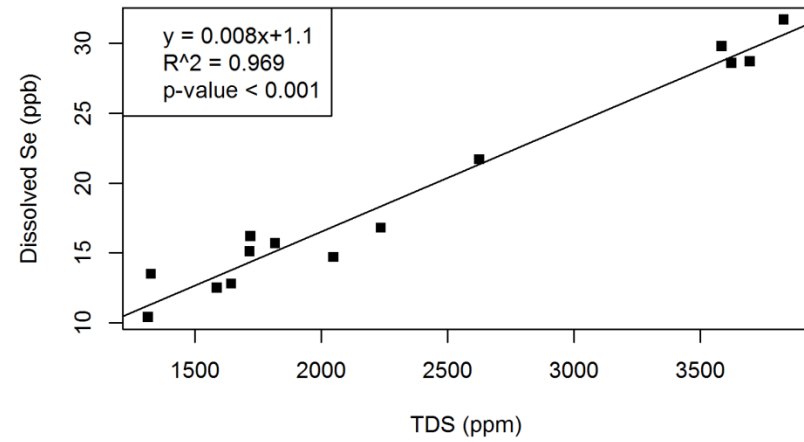
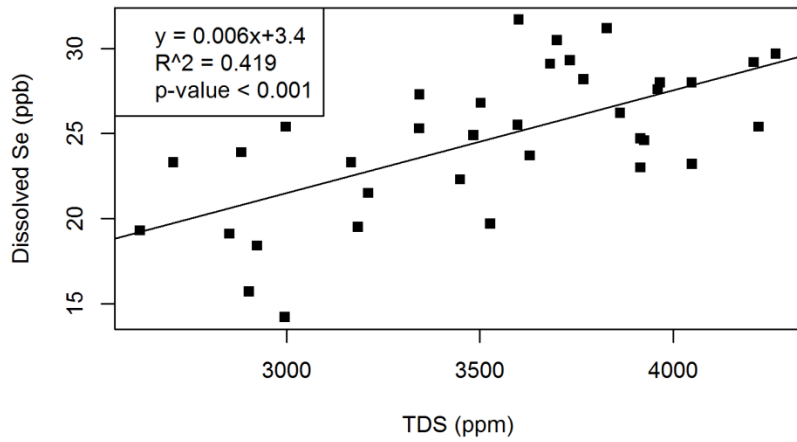
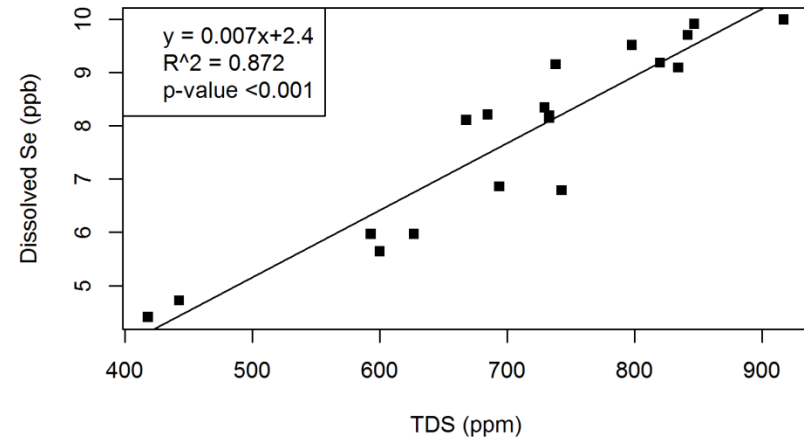
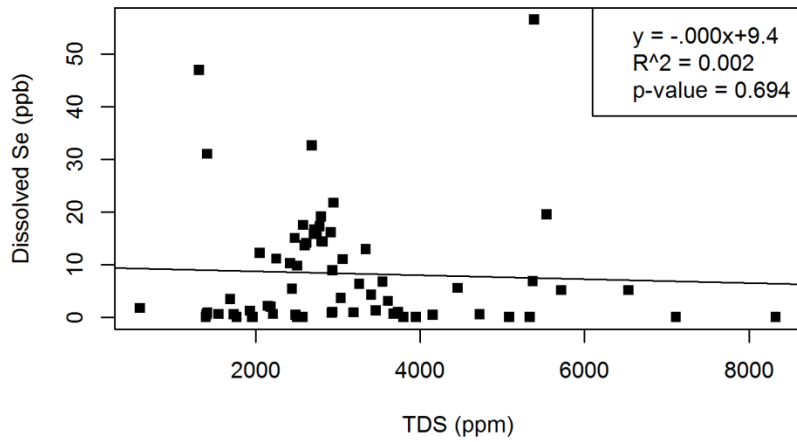


Figure 40. Linear regressions of dissolved Se concentration vs TDS concentration. Clockwise from top left: Groundwater samples, Surface Water samples, Tile Drain Water Mixed with Tailwater samples, and Tile Drain Water samples.

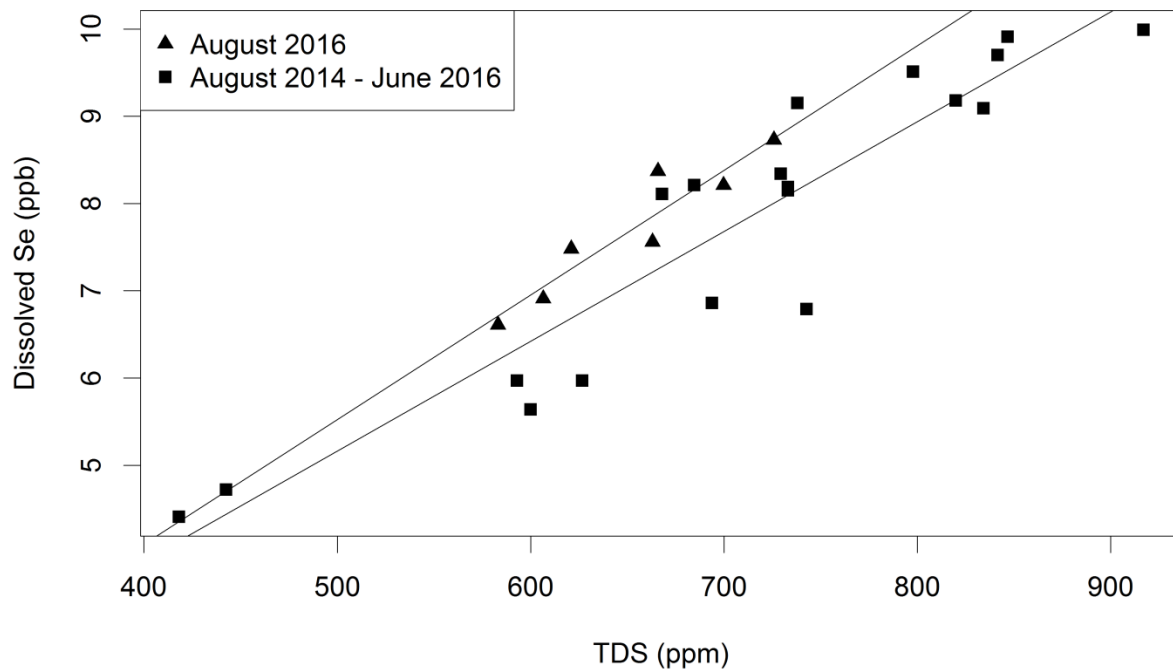


Figure 41. Scatter plots and linear regression of Se concentration vs TDS concentration for surface water samples from the field scale mass balances (August 2016) and the complete FDD study (August 2014 - June 2016).

when isolated, the presence of subsurface drains and the depth of groundwater do not significantly influence the relationship between  $C_{Se}$  and  $C_{TDS}$ .

Figure 78 in Appendix A contains  $C_{Se}$  vs  $C_{TDS}$  scatter plots and fitted linear relationships for groundwater sample data grouped based on presence of tile drains *and* depth of the monitoring wells. The outlier test p-value is less than 0.05 for each linear regression indicating statistical significance. In order to determine if any statistically significant linear trend exists, the outliers were identified and removed from each data set. The following data points, represented by index points in the diagnostic plots generated in R, were removed from the dataset: 131, 188, 102, 101, 108, and 162. Diagnostic plots before and after removal of the detected outliers are

shown in Figure 98, Figure 99, Figure 100, and Figure 101 in Appendix D and in Figure 102, Figure 103, Figure 104, and Figure 105 in Appendix D, respectively.

The two outlier points from the shallow drained dataset are both from monitoring well G12 (depth of 13.0 feet). One of these outliers was identified in the boxplots of  $C_N$  and  $C_{Se}$  in Figure 28 and Figure 32. Similarly, both of the outlier points from the deep drained dataset were from monitoring well G6 (depth of 50.2 feet) and one of them was identified as an outlier in Figure 28 and Figure 32. All of these outliers are suspected to be the result of surface water contamination caused by a failure of bentonite to seal the annular space of the monitoring wells. The outlier removed from the deep undrained dataset is from well G4 (depth of 39.4 feet) and the outlier removed from the shallow undrained dataset is from well G8 (depth of 11.4 feet). The cause of these outliers is suspected to be either lab analysis or field data collection error.

Figure 42 shows scatter plots of each dataset with the aforementioned outliers removed. The  $R^2$  value and slope p-value improved for each linear regression with the exception of that for the samples from deep groundwater with tile drains. The  $C_{Se}$  vs  $C_{TDS}$  linear regressions for the deep and shallow undrained samples are a much better fit than those for the drained samples. This indicates that subsurface drainage appears to have an influence on the relationship between  $C_{Se}$  and  $C_{TDS}$ . The diagnostic plots show a trend and unequal scatter in the residuals vs fitted plots for the deep and shallow drained linear regressions meaning that the regression assumptions were violated. The diagnostic plots for the deep and shallow undrained linear regressions raise no suspicion and appear to meet the regression assumptions.

These plots reaffirm what was shown previously regarding the impact that tile drains appear to have on groundwater solutes: drains do not influence groundwater  $C_{TDS}$ , but substantially influence groundwater  $C_{Se}$ . The correlation of  $C_{TDS}$  with  $C_{Se}$  likely is not due to a

causal relationship, whereas the relationship between  $C_N$  and  $C_{Se}$  is likely causal, as will be shown in the next section.

All six points in the lower right hand corner of the shallow undrained scatter plots in Figure 42 are from samples of well G8 (depth of 11.4 feet), and are what cause the linear regression to have a negative slope. This trend does not exist in the neighboring deep monitoring well G9 (depth of 23.5 feet). Monitoring well G8 is located within the riparian zone and monitoring well G9 is located along the riparian zone of Timpas Creek. It is possible that riparian vegetation uptakes and transforms dissolved Se species to organic species (Butler et al. 1996) thereby decreasing concentrations in the shallow groundwater sampled from well G8. The  $C_{TDS}$  most likely would not be significantly impacted by these processes as most of the ions that make up TDS are relatively conservative. The deep groundwater of well G9 would be less affected by these processes as there are few plant roots at that depth and fewer deep plant roots along the edge of the riparian zone. The degree of plant Se uptake near well G8 cannot be determined since plant sampling was not part of this study.

### ***3.2.2 Relationship of Dissolved Se and $NO_3$***

A log-log scatter plot of  $C_{Se}$  vs  $C_N$  for all water samples (GW, SW, TD and TWTD) is shown in Figure 43, where  $C_{Se}$  and  $C_N$  have 1 added to them (e.g.  $\log(C_N+1)$ ) to allow for the plotting of zero values. It is apparent that the GW dataset contains the largest range of  $C_{Se}$  and  $C_N$  values while SW appears to have the smallest range. There also appears to be a log-log linear relationship between  $C_{Se}$  and  $C_N$  up to a certain point (approximately 4 mg/L  $NO_3-N$ ) when the correlation becomes weak.

To identify trends within each sample type, scatter plots of  $C_{Se}$  vs  $C_N$  from GW, SW, TD and TWTD samples are shown in Figure 44. They are plotted similarly as mentioned above.

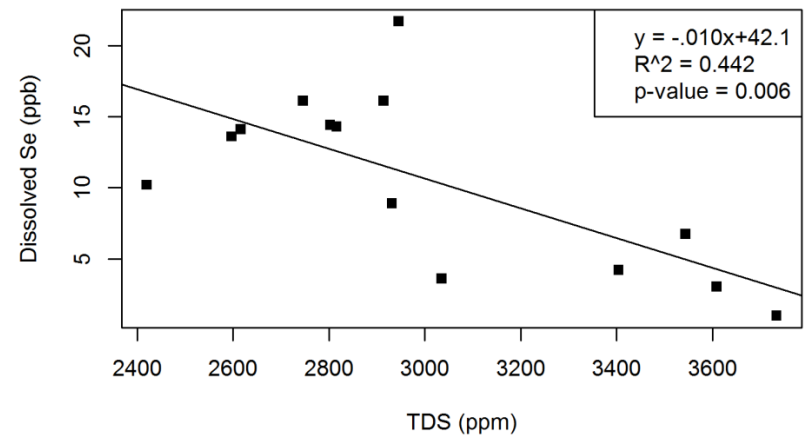
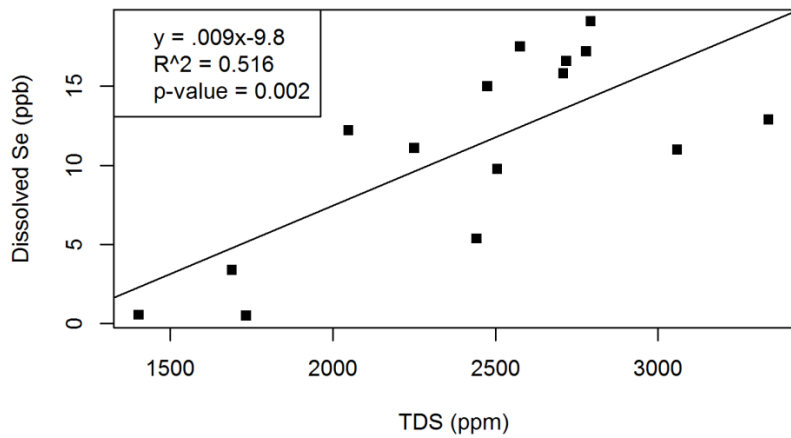
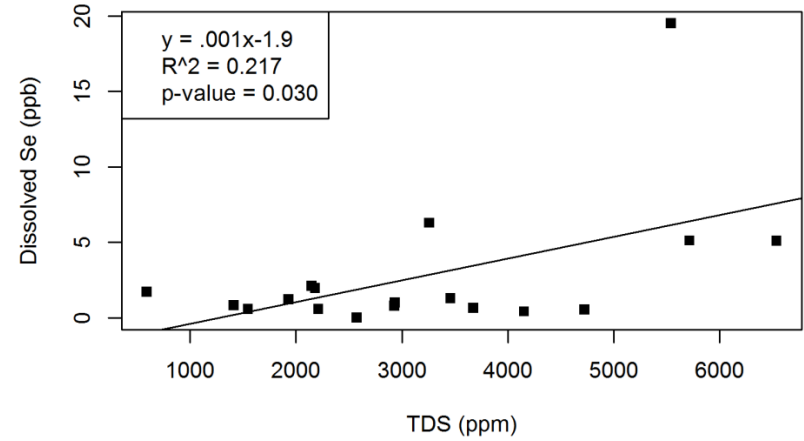
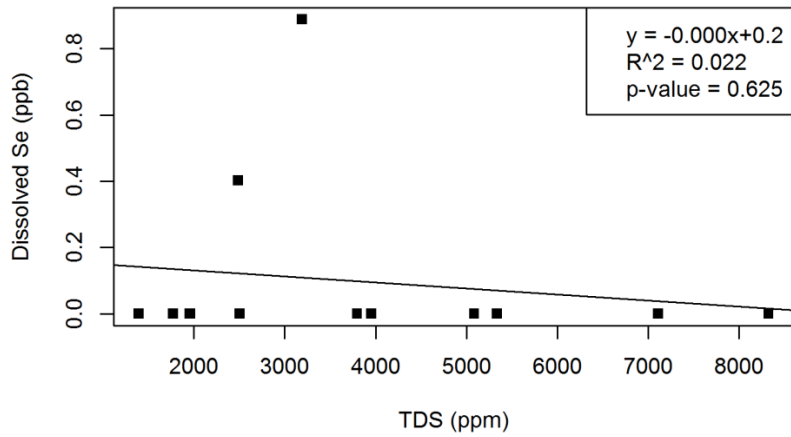


Figure 42. Scatter plots of  $C_{Se}$  vs  $C_{TDS}$  from groundwater samples separated by presence of drains and monitoring well depth with selected outliers removed. Clockwise from top left: Deep GW with tile drains, Shallow GW with tile drains, Shallow GW without tile drains, Deep GW without tile drains.

Diagnostic plots (Figure 106, Figure 107, Figure 108, and Figure 109 in Appendix D) reveal that all four of the linear regressions do not contain normally-distributed residuals and that the GW, SW and TD data sets do not display homogeneous variance. Therefore, the assumptions of linear regression are violated. Outlier tests conducted for each linear regression found no statistically significant outliers and analysis of the diagnostic plots did not reveal any suspected outliers.

The  $C_{Se}$  and  $C_N$  for GW and SW have moderate coefficient of determination values ( $R^2 = 0.67$ ,  $0.60$ ) that are statistically significant to a confidence level of 95%. The log-log linear regression appears to be continuous for all SW samples. In the case of GW samples, the scatterplot shows that above  $C_N \approx 4$  mg/L (denoted by the red dashed line) changes in  $C_N$  explain much less of the variance in  $C_{Se}$ . This may indicate that in this geochemical environment  $NO_3$  plays an important role in the inhibition of  $SeO_4$  reduction at  $C_N$  below approximately 4 mg/L. When the  $C_N$  exceeds this threshold value, the reduction of both  $NO_3$  and  $SeO_4$  can occur simultaneously. A threshold  $C_N$  value, above which the reduction of  $SeO_4$  is no longer inhibited, was suggested to be roughly 10 mg/L by Gates et al. (2009) in the LARV region. Oremland et al. (1999) also suggested such a threshold exists but did not provide a value for the threshold concentration. Variations in the value of this threshold may be due to differences in geologic Se sources and other factors influencing the reduction environment such as presence of certain bacteria.

The scatterplot and regression analysis of the TD dataset indicate that there is essentially no correlation between  $C_N$  and  $C_{Se}$ . The cause of this lack of correlation might include variance in spatial and temporal application of fertilizer and irrigation water, spatial variation in geological Se sources, spatial variation in the presence of reducing bacteria, and disparity in other chemical and physical conditions such as temperature, DO, pH, etc. as mentioned by Gates et al. (2009) in respect to groundwater  $C_N$  and  $C_{Se}$  correlation. In comparison with GW samples,

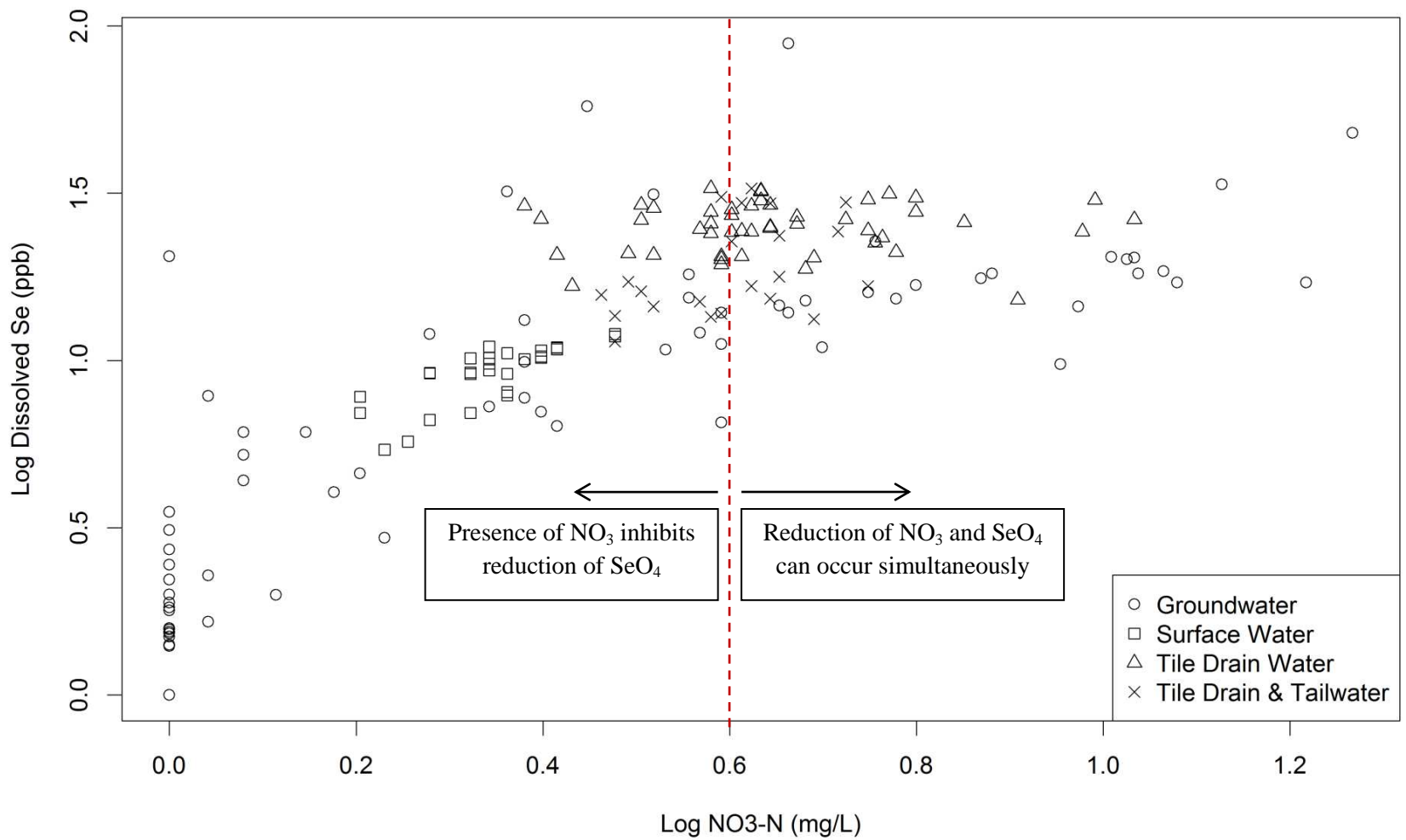


Figure 43. Scatter plot of  $C_{Se}$  vs  $C_N$  for samples from groundwater, surface water, tile drain water, and tailwater mixed with tile drain water. The dashed line represents the threshold  $C_N$  above which increases in  $C_N$  do not further inhibit reduction of  $SeO_4$ .

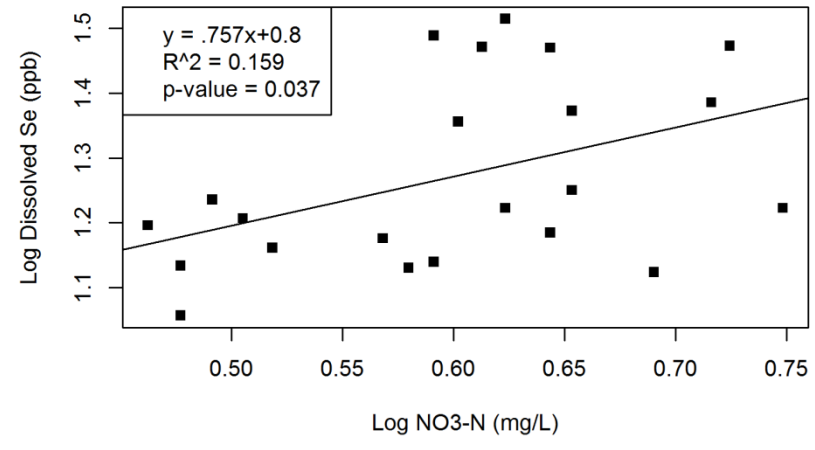
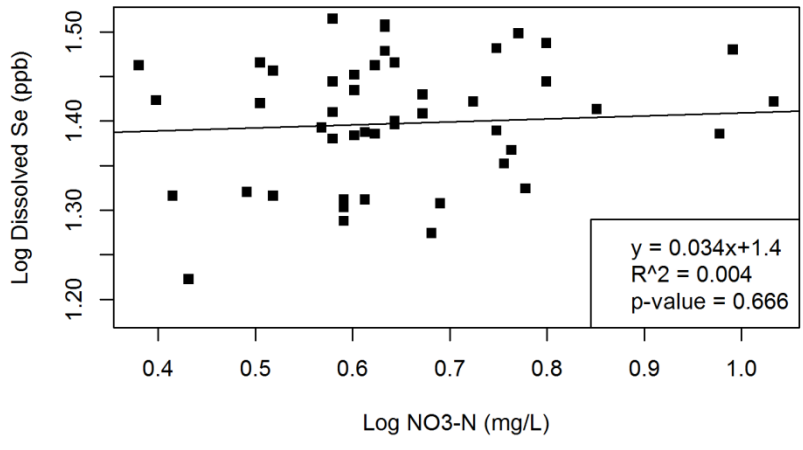
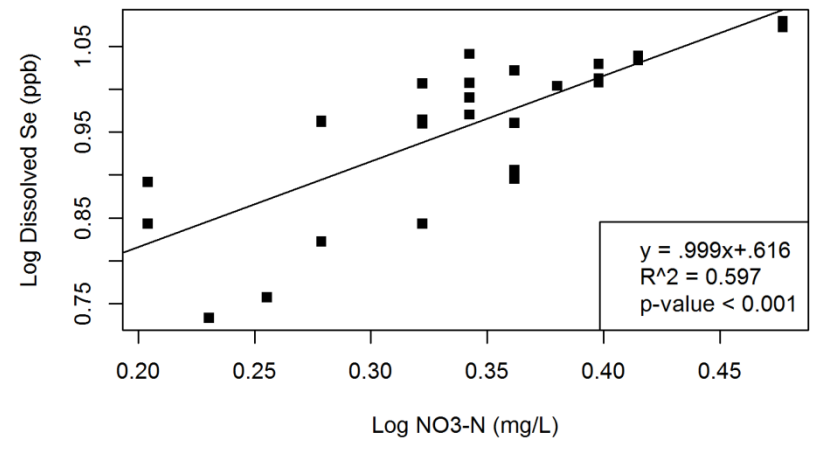
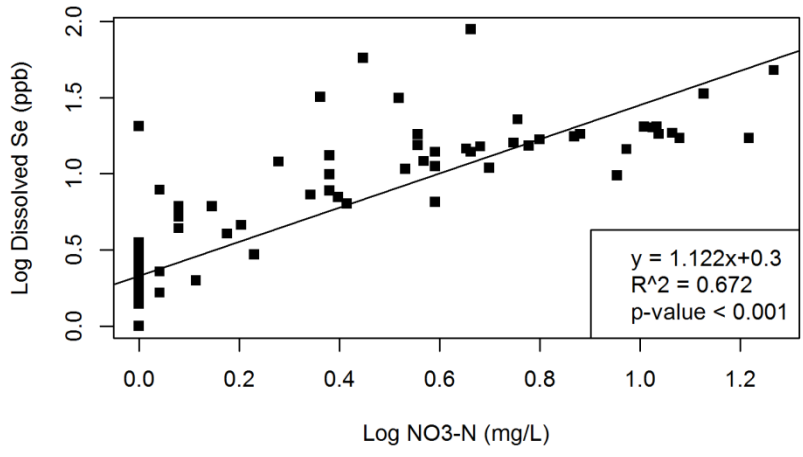


Figure 44. Scatter plots and regressions of  $C_{Se}$  vs  $C_N$  of each sample type. Clockwise from top left: Groundwater, Surface Water, Tailwater mixed with Tile Drain Water, and Tile Drain Water.

the  $C_{Se}$  tends to be higher for a given  $C_N$  (Figure 43). This is likely reflective of a difference in redox conditions in the upper alluvium compared with the lower alluvium but could also be due to spatial variation with depth of geologic Se sources. Since soil sampling was not a part of this study, no evidence can be provided regarding variation in geologic Se sources. Dissolved oxygen in the root zone and upper groundwater table is much higher than it is deeper in the aquifer due to aeration of the unsaturated zone and application of irrigation water with high levels of DO. Oxygen is preferentially consumed (over  $NO_3$ ) for bacterial respiration because it provides the highest quantities of energy (Butler, 1996). The presence of  $O_2$  inhibits the reduction of  $SeO_4$ , and allows for the oxidation of elemental Se to  $SeO_3$  and  $SeO_4$ . This is the most likely explanation for the high  $C_{Se}$  to  $C_N$  ratio in tile drain water and for the lack of correlation because  $C_N$  is not the principle factor driving redox reactions in the root zone and upper groundwater levels.

The log-log linear regression of  $C_{Se}$  vs  $C_N$  for the TWTD dataset results in a weak, yet statistically significant, coefficient of determination ( $R^2 = 0.16$ ). The stronger relationship (compared to the TD dataset) is most likely due to the addition of tailwater which is more similar to applied surface water. Even though tailwater has high levels of  $O_2$ , there is not sufficient time for redox reactions to take place as they are inherently slow. Mixing of tailwater and tile drain water leads to the dilution of  $C_{Se}$  in the tile drain water.

Figure 79 in Appendix A contains  $C_{Se}$  vs  $C_N$  scatter plots and linear regressions of the groundwater dataset grouped into 4 data subsets: groundwater with tile drains present, groundwater without tile drains present, groundwater from deep wells, and groundwater from shallow wells. Outlier tests indicate that there are statistically significant outliers for the datasets

of groundwater with drains and shallow groundwater and the diagnostic plots (Figure 110, Figure 111,

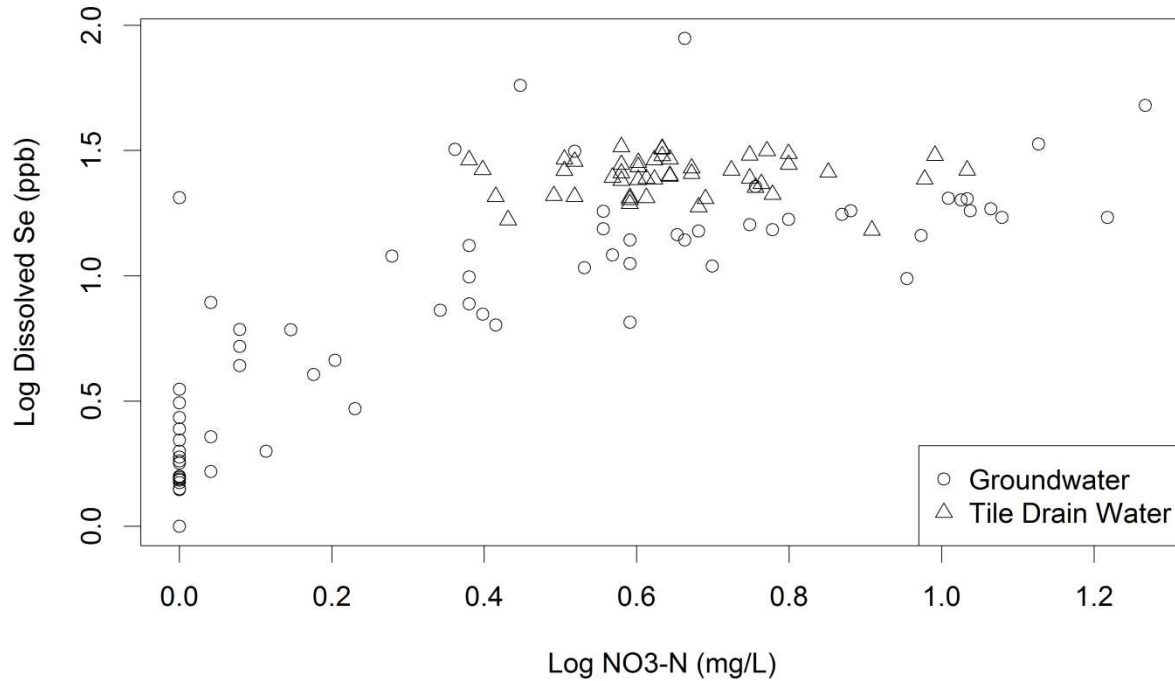


Figure 45. Scatter plot of  $\log C_{Se}$  vs  $\log C_N$  concentrations for tile drain and groundwater samples.

Figure 112, and Figure 113 in Appendix D) confirm that index points 46, 45, and 38 are outliers. Index point 46 is a sample from monitoring well G12 (depth of 13.0 feet) that has been noted previously as an outlier (Figure 28, Figure 32, and Figure 34) and index point 45 is a separate sample from G12 that has not been previously indicated as an outlier. Index point 38 is from monitoring well G10 (depth of 14.4 feet). Similar to G12, it is difficult to detect water quality trends in samples from well G10 because only two sampling events contain data for both  $C_N$  and  $C_{Se}$ . The diagnostic plots reveal that regression assumptions are violated for all three plots other than for shallow groundwater. Once the outliers are removed, the shallow groundwater dataset satisfies the regression analysis assumptions in consideration of the diagnostic plots.

Figure 46 shows scatter plots and linear regressions of  $C_{Se}$  vs  $C_N$  with the aforementioned outliers removed. Omitting outliers improved the coefficient of determination in both cases. All four regression relationships are strong ( $0.7 < R^2 < 0.8$ ) and are statistically significant with 95% confidence, indicating that  $C_N$  explains a lot of the variance of  $C_{Se}$ . This is expected to be the case in groundwater because DO levels are low, allowing  $NO_3$  to be the principal reactant in redox reactions (Butler, 1996).

It is noted that at negligible  $C_N$  values the  $C_{Se}$  is not explained by the linear regression trend. The scatter plot of concentrations in drained groundwater samples shows that when the  $C_N$  is equal to 0 mg/L,  $C_{Se}$  ranges between 0 and 4 mg/L. The cause of this may be the presence of other oxidizing species, such as  $SO_4$ , which are not preferred for bacterial respiration due to the lower level of energy gained, but which become more prevalent in redox reactions in the absence of  $O_2$  and  $NO_3$ .

The trend seen previously, in Figure 42 of low  $C_{Se}$  to  $C_{TDS}$  ratios for monitoring well G8 (depth of 11.4 feet) does not exist in the regression relationship of  $C_{Se}$  vs  $C_N$  shown in Figure 46. The log-log linear regression of shallow, undrained groundwater has a moderate to strong coefficient of determination ( $R^2 = 0.71$ ) and a positive slope. This indicates that whatever processes led to the decreased  $C_{Se}$  to  $C_{TDS}$  ratio did not affect the  $C_{Se}$  to  $C_N$  relationship. If low  $C_{Se}$  were caused by plant uptake, it is likely there was also plant uptake of  $NO_3$  since riparian zones have been shown to be effective removing nutrient contaminants such as  $NO_3$  from groundwater (Cooper, 1990).

Scatter plots and linear regressions of  $C_{Se}$  vs  $C_N$  for groundwater samples grouped by presence of subsurface drainage and depth of monitoring well are shown in Figure 80 in Appendix A. The high coefficient of determination ( $R^2=0.90$ ) for the deep drained groundwater

dataset is thought to be due to the presence of outliers strongly influencing the regression. Recall the box plots of  $C_N$  and  $C_{Se}$  (Figure 31, and Figure 34) which show the median values of deep drained

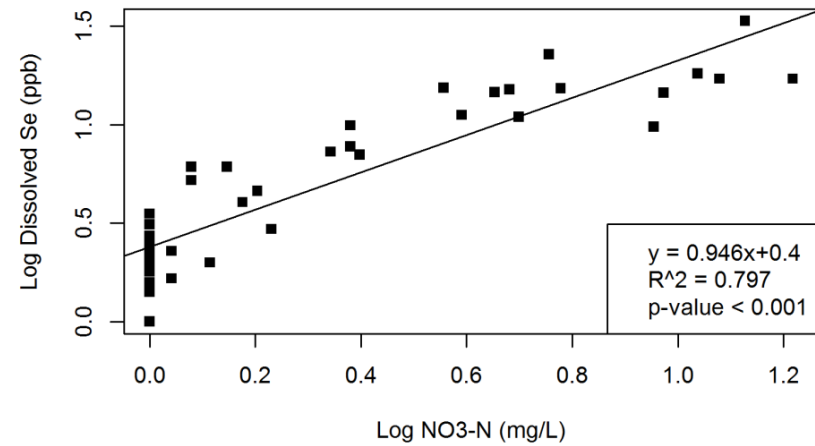
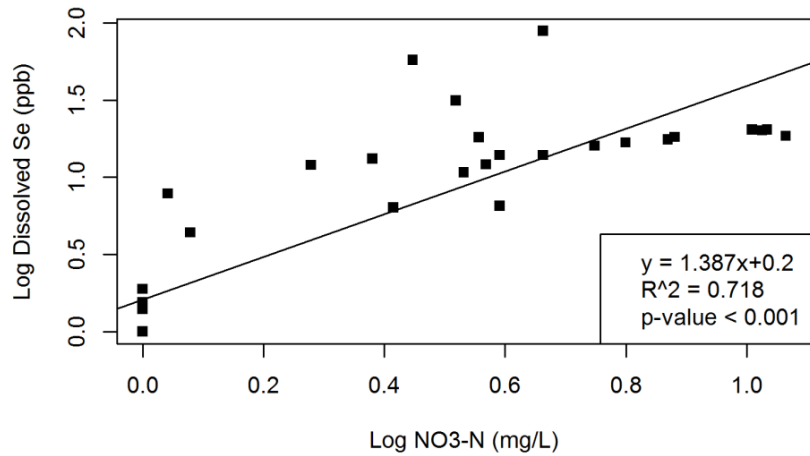
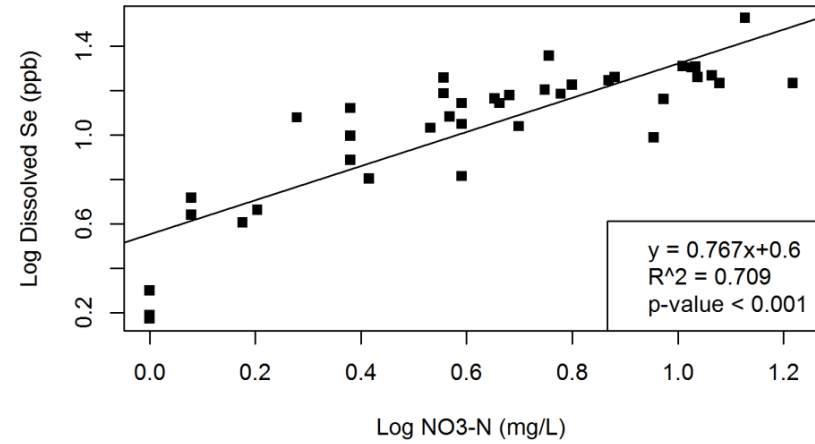
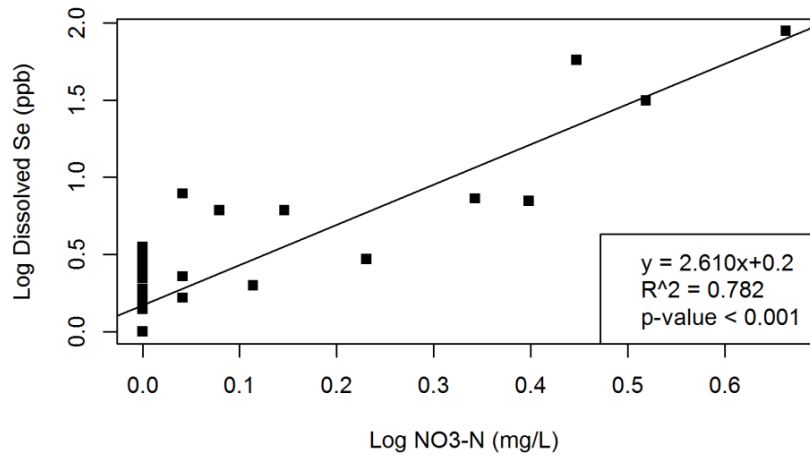


Figure 46. Scatter plots of  $C_{Se}$  vs  $C_N$  from groundwater samples separated by presence of drains or monitoring well depth with outliers omitted. Clockwise from top left: GW with tile drains, GW without tile drains, Shallow GW, and Deep GW.

samples to be 0 mg/L and 0 µg/L, respectively, and all other values to be outliers. While the cause of these outliers is unknown, the  $C_N$  values are well correlated with the  $C_{Se}$  values whether the concentrations are very low or very high. The box plot of the  $C_{Se}$  values (Figure 31) also shows 3 outliers for shallow wells in the presence of drains, one of which heavily influences the linear regression.

The dataset from shallow, undrained conditions does not violate any regression assumptions as can be seen in the diagnostic plot (Figure 117 in Appendix D). The deep, undrained dataset shows a slight trend in the residuals vs fitted graph (Figure 116 in Appendix D), which is a violation of the regression assumptions. The diagnostic plots (Figure 114, and Figure 115 in Appendix D) also show three potential outliers for the deep drained regression analysis, one of which possesses very large leverage and a large standardized residual, and two potential outliers for the shallow drained regression, one of which has large leverage and standardized residual. Leverage is a measure of the separation of the independent variable of an observation from the independent variable of other observations within the same sample population. An observation with large leverage and a large residual is likely to have large influence on the regression analysis (Chatterjee and Hadi, 1986). Thus, the diagnostic plots reveal the potential influence of certain potential outliers in the regression analysis. Outlier tests performed on these two regression analyses suggest that statistical outliers exist with 95% confidence. These five outliers (index points 13, 23, 19, 38, and 46) are omitted from the dataset used to develop scatter plots and linear regressions shown in Figure 47.

Despite a high  $R^2$  value and low slope p-value, the regression analysis of the samples from the deep drained groundwater conditions can be disregarded due to the high influence of one data point. The scatter plot essentially shows barely any  $NO_3$  or dissolved Se present in deep

groundwater, at an average depth of 50.8 feet, where subsurface drainage is present. This reaffirms the indication that subsurface drainage inhibits the transport of  $\text{NO}_3$  to the underlying groundwater system, and the causal role that dissolved  $\text{NO}_3$  plays in the mobilization of Se.

In the case of the linear regression analysis of the samples from the shallow drained groundwater conditions (average depth of 13.7 feet), removal of outliers increased the coefficient of determination ( $R^2 = 0.60$ ). The slope is roughly three times steeper as it is in the case of samples from undrained groundwater conditions, indicating a higher  $C_{\text{Se}}$  to  $C_{\text{N}}$  ratio. The cause of this is unknown. The majority of data points are at  $C_{\text{N}} = 0$  mg/L with varying levels of  $C_{\text{Se}}$ . As mentioned previously, the unexplained variance in  $C_{\text{Se}}$  while  $C_{\text{N}} = 0$  mg/L is likely due to the presence of other redox reactive species.

The presence of subsurface tile drains appears to limit the vertical transport of  $\text{NO}_3$  in groundwater. With tile drains present, there are some instances of  $\text{NO}_3$  presence in shallow groundwater, but only up to concentrations of about 1.5 mg/L. There was essentially no  $\text{NO}_3$  detected in deep groundwater where tile drains are present (with the exception of outlier scenarios where surface contamination is suspected). The strong correlation between  $C_{\text{Se}}$  and  $C_{\text{N}}$ , along with the absence of DO, suggests that the interception and export of  $\text{NO}_3$  by subsurface drainage has the effect of inhibiting the oxidation of Se and allowing for the reduction of  $\text{SeO}_3$  and  $\text{SeO}_4$  thereby reducing the quantity of mobile Se in groundwater.

### **3.3 Field-Scale Mass Balance of Total Dissolved Solids**

The quantities of diverted water, applied water, and tailwater expressed as depth of water (total volume / irrigated area) for each field are shown in Figure 48. The depth of applied water is 5.9, 9.6, and 14.2 inches for fields DA7, Muth2, and Muth9 respectively. Applied irrigation depth for Muth9 is high when compared to the findings of Gates et al. (2012) which found that

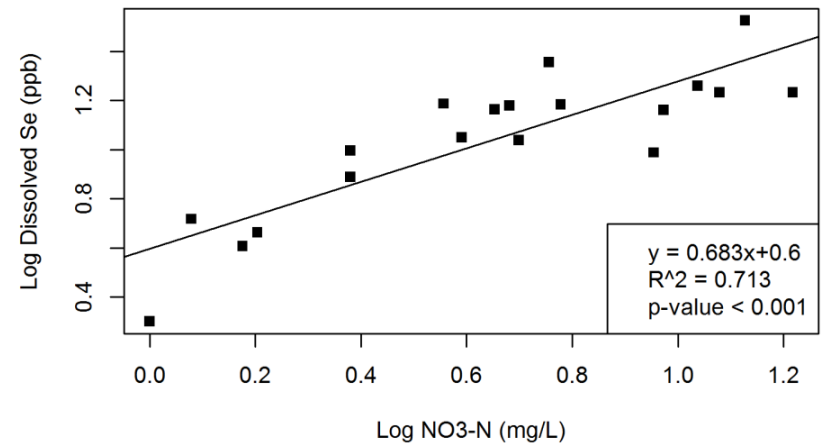
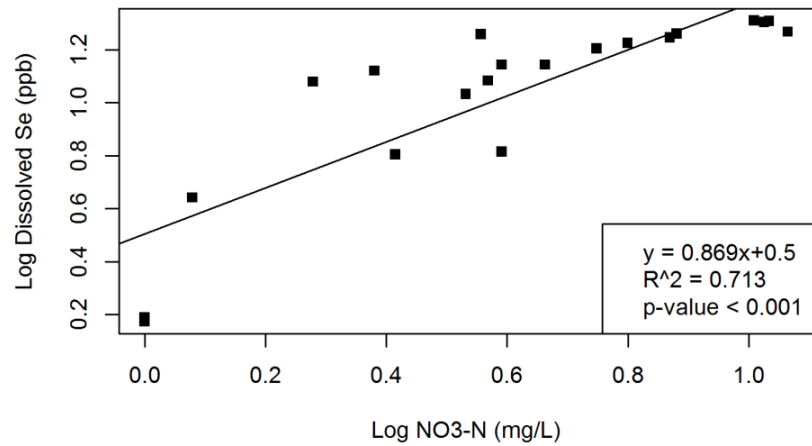
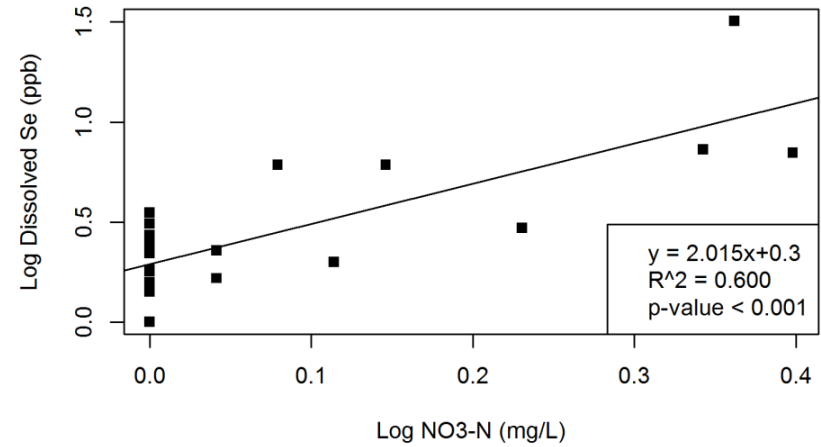
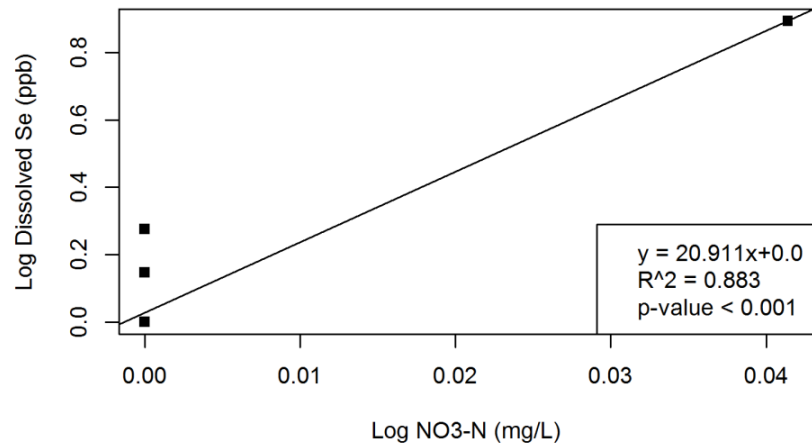


Figure 47. Scatter plots and regressions of  $C_{Se}$  vs  $C_N$  from groundwater samples separated by presence of drains and depth of monitoring wells with outliers omitted. Clockwise from top left: Deep Drained GW, Shallow Drained GW, Shallow Undrained GW, and Deep Drained GW.

the applied irrigation depth measured for 90% of the 229 surface irrigation events monitored in the USR and DSR in the LARV ranged from 4.0 inches to 13.41 inches, averaging 8.2 inches. The difference between diverted water and applied water should be interpreted as spillover, and the difference between applied water and tailwater should be interpreted as infiltrated water, assuming that evaporation as water flows across the fields is negligible. The spillover proportion is 9%, 6.7% and 19.8% for fields DA7, Muth2 and Muth9 respectively. The tailwater fraction for each of the fields is very high: 35%, 54%, and 48% for fields DA7, Muth2, and Muth9 respectively. Gates et al (2012) reported tailwater fractions ranging from 0 to 69% and averaging 8% for measured surface-irrigation events in the USR and DSR of the LARV. At the time of the study there was a large amount of water available in the Catlin Canal which may have played a role in irrigation decisions leading to the high tailwater fractions. Part of the reason the tailwater fraction for field DA7 is lower is because it is the only field for which the first siphon set is incorporated into the mass balance. The first siphon set tended to have a lower fraction of tailwater runoff due to the dry conditions on both sides of the set interval. For example, all of the set intervals on field DA7 were roughly 12 hours in duration with the exception of the first interval which was roughly 24 hours because there was no tailwater flow for the first 20 hours. This has a large impact on the tailwater fraction since there were only 5 siphon sets incorporated in the mass balance for field DA7. Given that the tailwater fractions observed in this study seem high in relation to average irrigation practices in the LARV as a whole, the results regarding tailwater solute loading should not be extrapolated to represent a larger region.

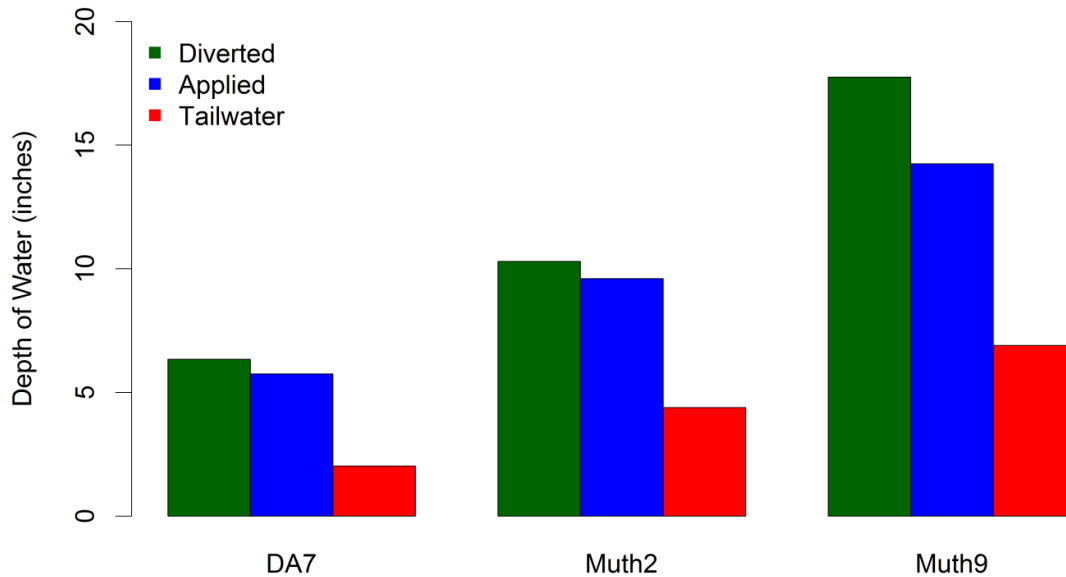


Figure 48. Bar plot of water diverted from the canal, water applied to the field, and tailwater runoff for each field.

### 3.3.1 Relationship of Total Dissolved Solids to Electrical Conductivity

To relate in-situ electrical conductivity readings to TDS concentration values, a linear regression was developed from samples collected from applied water and tailwater during the field-scale mass balance events as well as from samples collected in a separate study from the Arkansas River (see Figure 18 for geographic locations of sampling points in the Arkansas River). A plot and characteristics of the fitted linear regression can be seen in Figure 19 which reveals a statistically significant high coefficient of determination ( $R^2 = 0.89$ ). Figure 93 in Appendix D shows the diagnostic plots for the linear regression. The QQ plot shows that with the exception of a few data points on the high end, the data are normally distributed. The residuals vs fitted plot shows relatively equal scatter and little trend indicating no violation of the linear regression assumptions of equal variance and linear response. The regression fits both

applied water and tailwater samples well, and is used to convert measured electrical conductivity readings to  $C_{TDS}$  for both.

### ***3.3.2 Analysis of Estimated TDS Concentration***

The estimated  $C_{TDS}$  of applied water and tailwater plotted as a function of time for the irrigation events of fields DA7, Muth2, and Muth9 are shown in Figure 81, Figure 82, and Figure 83 in Appendix B. The plotted confidence intervals plotted correspond to the statistical confidence of the linear regression slope. The slope corresponding to each confidence level is shown in Table 18 in Appendix B. The plots show that there is an error range of roughly 75 mg/L and 150 mg/L in the estimation of TDS for the 67% and 95% confidence intervals. The confidence intervals do not represent any additional uncertainty beyond that of the estimated linear regression and are included simply to give an idea of a portion of the statistical uncertainty involved with findings from the mass balance portion of this study. Additional uncertainty, that is not quantified herein, is derived from sampling error, laboratory analysis error, instrument error, etc.

Figure 49 clearly indicates that tailwater tends to have a higher TDS concentration than applied water. This tendency was statistically confirmed using the Kruskal - Wallis test to compare the median  $C_{TDS}$  of applied water to tailwater at 15 minute intervals for each field (see Figure 50). The diagnostic plots of the applied water and tailwater datasets for each field show that none of the fields satisfy all of the assumptions of the ANOVA comparison of means test. The QQ plot reveals the DA7 dataset is not normally distributed (see Figure 120 in Appendix E). The residuals vs fitted plot for the Muth2 data show that the dataset violates assumptions of homogenous variances (see Figure 121 in Appendix E). The Muth9 dataset violates assumptions of homogenous variances and normal distribution (see Figure 122 in Appendix E). Due to the

violation of ANOVA comparison of means test assumptions, the Kruskal-Wallis test was used to compare the median values of  $C_{TDS}$  from applied water and tailwater for each field. The results from these tests, shown in Table 13, indicate that for each field, the median estimated  $C_{TDS}$  of applied water and tailwater are significantly different. For each field, the median tailwater  $C_{TDS}$  is significantly higher than the median applied water  $C_{TDS}$ , confirming what has been shown in other studies (Gilfedder et al. 2000, Rhoades et al. 1997).

The median applied water  $C_{TDS}$  for fields DA7, Muth2, and Muth9 is 698, 649 and 636 mg/L, respectively. These values are substantially higher than the average  $C_{TDS}$  (532 ppm) found by Gates et al. 2012 in mass balance studies of 130 surface irrigation events in the USR. However, in that study, the average  $C_{TDS}$  varied substantially from year to year with a minimum average of 305 ppm and a maximum average of 795 ppm. Therefore, the applied irrigation  $C_{TDS}$  in this study are well within range of what is expected.

Trends in measured  $C_{TDS}$  in tailwater do not appear to correspond directly to the siphon sets nor with the measured  $C_{TDS}$  in applied water, indicating the possible influence of other variables. If  $C_{TDS}$  were monitored in real time, it would be expected that at the start of each siphon set there would be a pulse of high  $C_{TDS}$  in the tailwater flow that first emerges from the field, a sudden fall in values, and then a slow increase over time, as observed by Gilfedder et al. (2000). The high  $C_{TDS}$  pulses at the start of each siphon set are restricted to the leading edge of tailwater and occur over a short period of time (Gilfedder et al. 2000). It is likely that the majority of leading edge pulses were missed in this study since in-situ readings were taken roughly every two hours. The relationship of soil salinity and the difference between median  $C_{TDS}$  in tailwater and applied water is analyzed in section 3.4 for field Muth2.

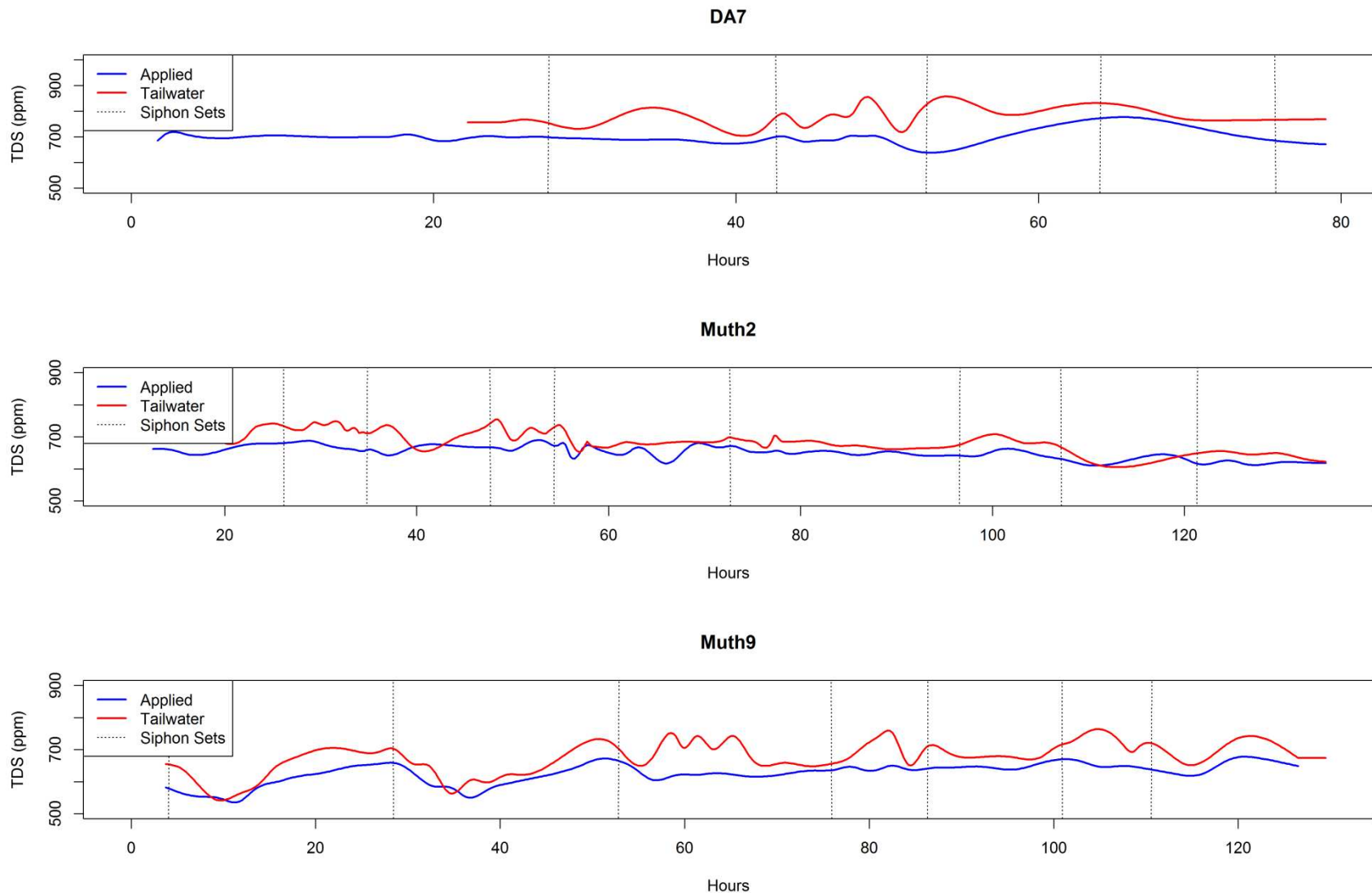


Figure 49. Time series plots of  $C_{TDS}$  in applied water and tailwater for the measured irrigation events on the three fields.

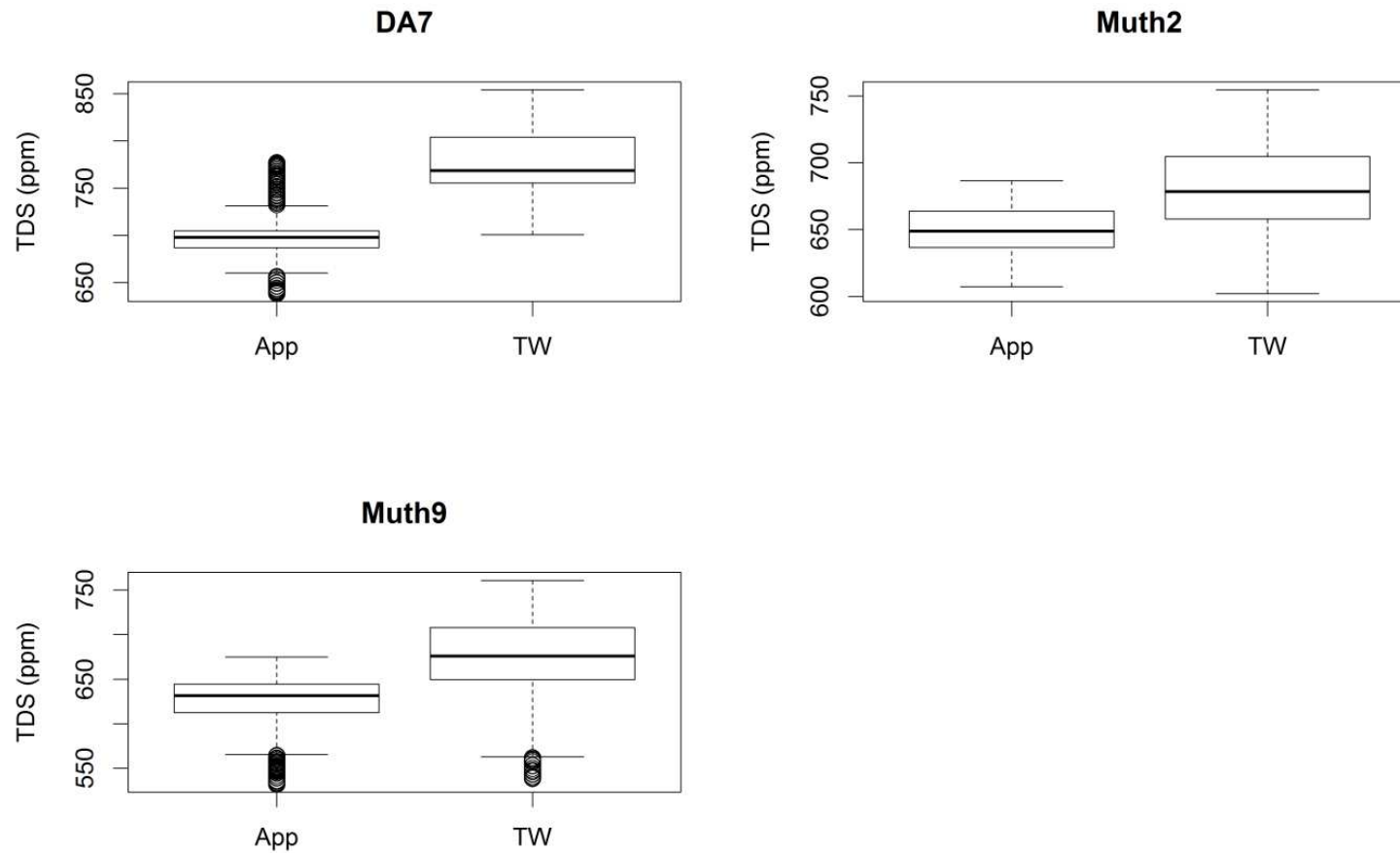


Figure 50. Box plots of TDS concentration for applied water (App) and tailwater (TW) for the measured irrigation events on each field.

Table 13. P-values from Kruskal-Wallis test comparing median  $C_{TDS}$  of applied irrigation water and tailwater for the measured irrigation events on the three fields.

	DA7	Muth2	Muth9
Shapiro p-value	<0.001	<0.001	<0.001
Levene p-value	<0.001	<0.001	<0.001
Kruskal-Wallis p-value	<0.001	<0.001	<0.001

### 3.3.3 Analysis of TDS Mass

The mass loading rate of TDS (kg/acre/hr) is plotted vs time for each field in Figure 51, Figure 52, and Figure 53. The vertical dotted gray lines represent changes in siphon sets. Tailwater mass loading rate varies in cyclical trends with respect to siphon sets and shows trends similar to those for the tailwater flows rates shown in Figure 23, Figure 24, and Figure 25 whereas tailwater  $C_{TDS}$  does not show similar trends (see Figure 81, Figure 82, and Figure 83 in Appendix B). Thus, the cyclical trend in tailwater TDS mass flow rate that is related to siphon sets appears to be caused predominantly by changes in the tailwater flow rate rather than in the tailwater  $C_{TDS}$ .

With few exceptions, the TDS mass loading rate remains higher for applied water than it is for tailwater for each field. Box plots of applied water vs tailwater TDS loading rates are shown in Figure 54. Diagnostic plots (Figure 123, Figure 124, and Figure 125 in Appendix E) show that the dataset for each field is not normally distributed and that the datasets for fields Muth2 and Muth9 have unequal variances. These violations of assumptions are confirmed by the Shapiro-Wilks Test and Levene's test which resulted in p-values less than 0.05 for each field data set. Since the datasets violate the assumptions of ANOVA comparison of means tests, the Kruskal-Wallis test for equality of medians was conducted. The p-values from the Kruskal-Wallis tests (shown in Table 14) indicate that the median TDS mass loading rate in applied water and tailwater are significantly different for each field. For each field, the median TDS mass loading rate in applied water is higher than that of the tailwater, indicating a greater amount of salt mass applied by irrigation water than is removed by tailwater.

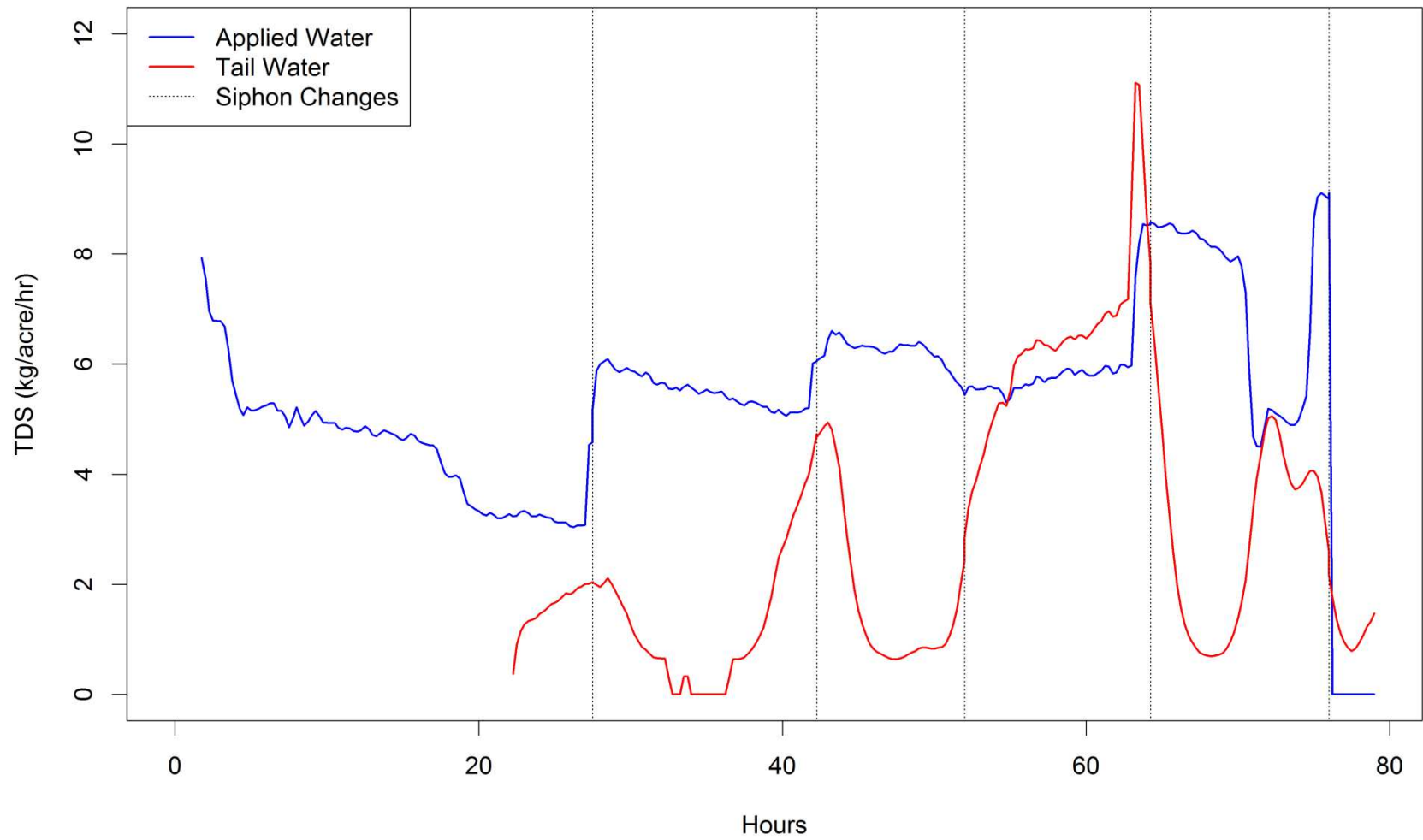


Figure 51. Mass loading rate of TDS in applied irrigation water and tailwater for field DA7.

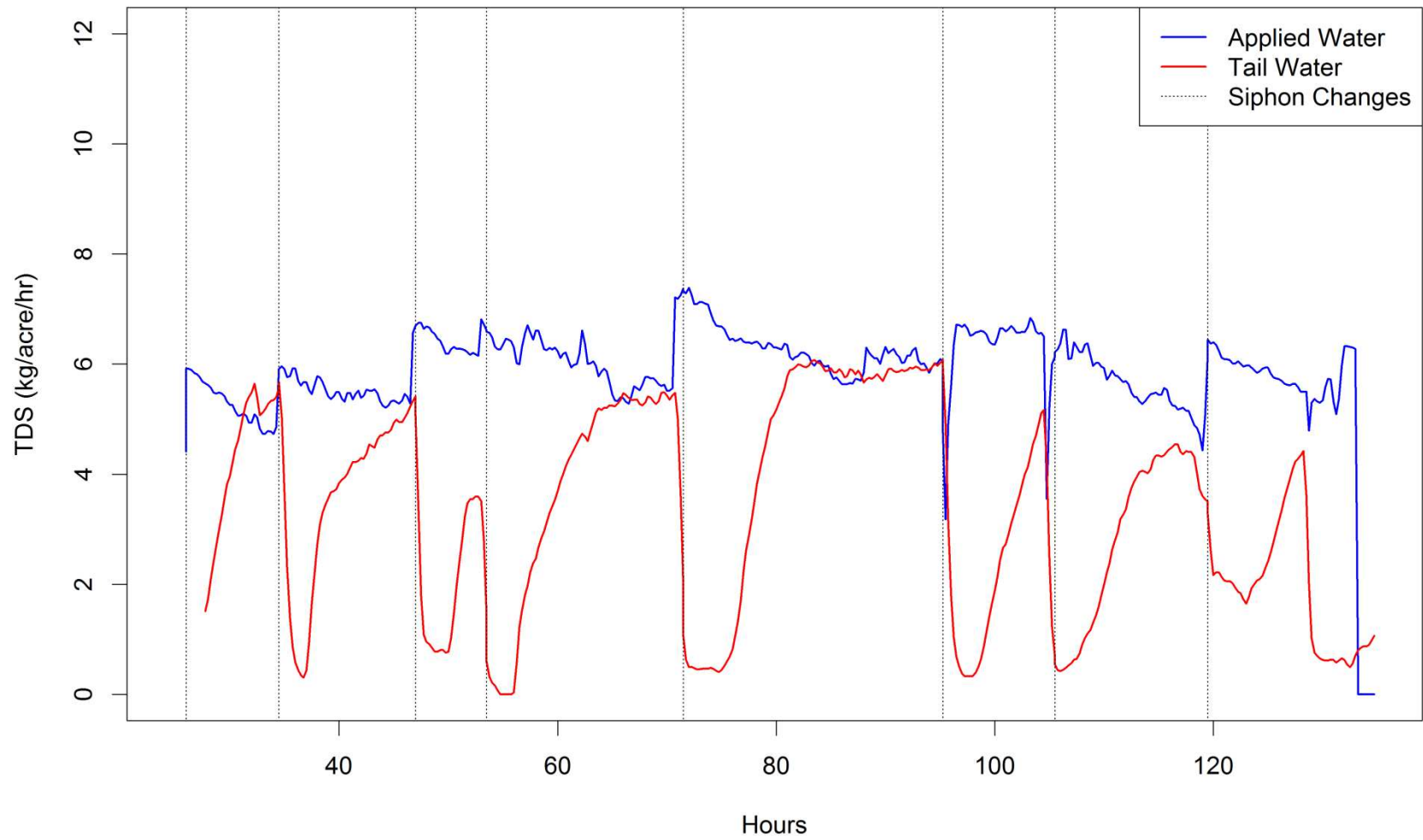


Figure 52. Mass loading rate of TDS in applied irrigation water and tailwater for field Muth2.

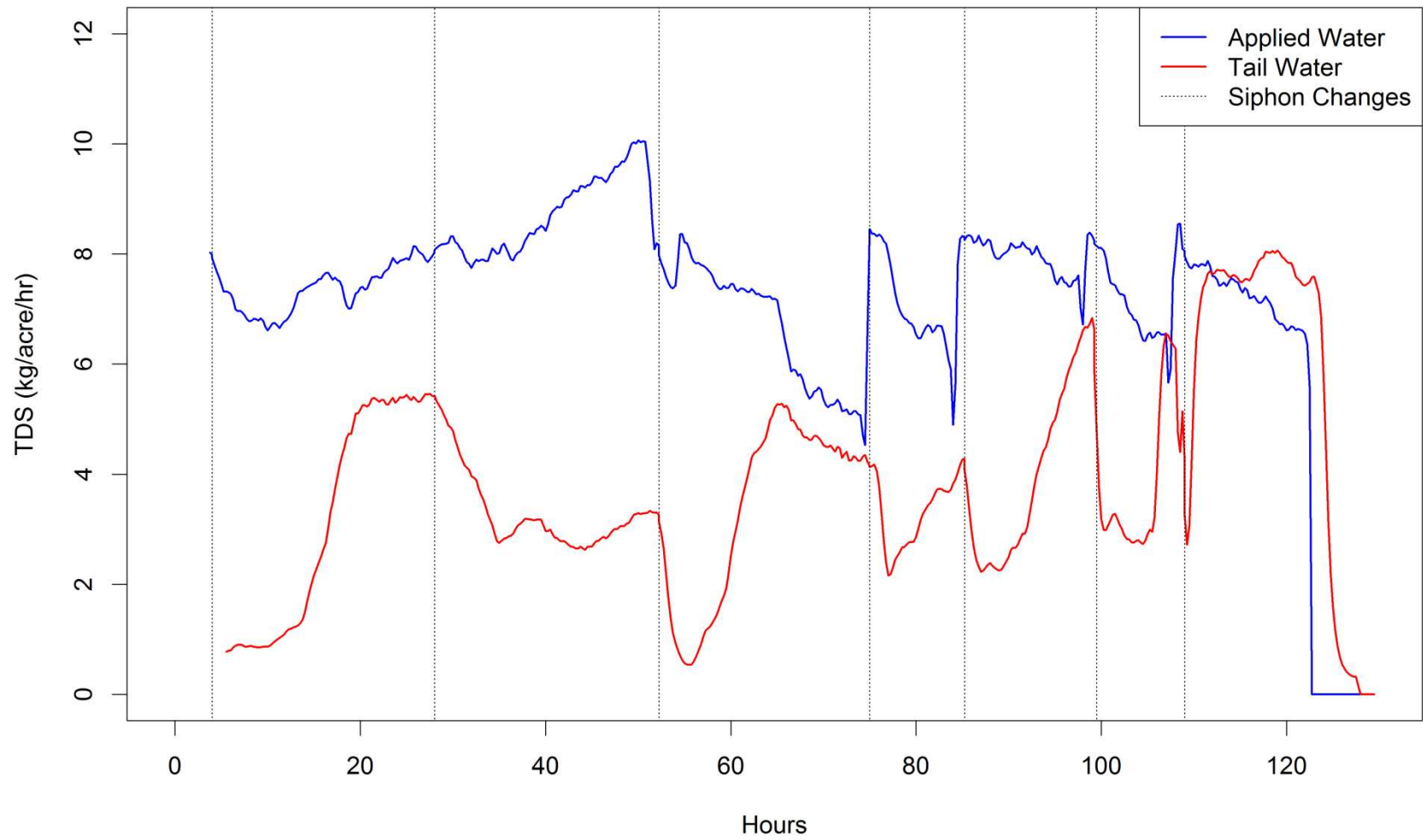


Figure 53. Mass loading rate of TDS in applied irrigation water and tailwater for field Muth9.

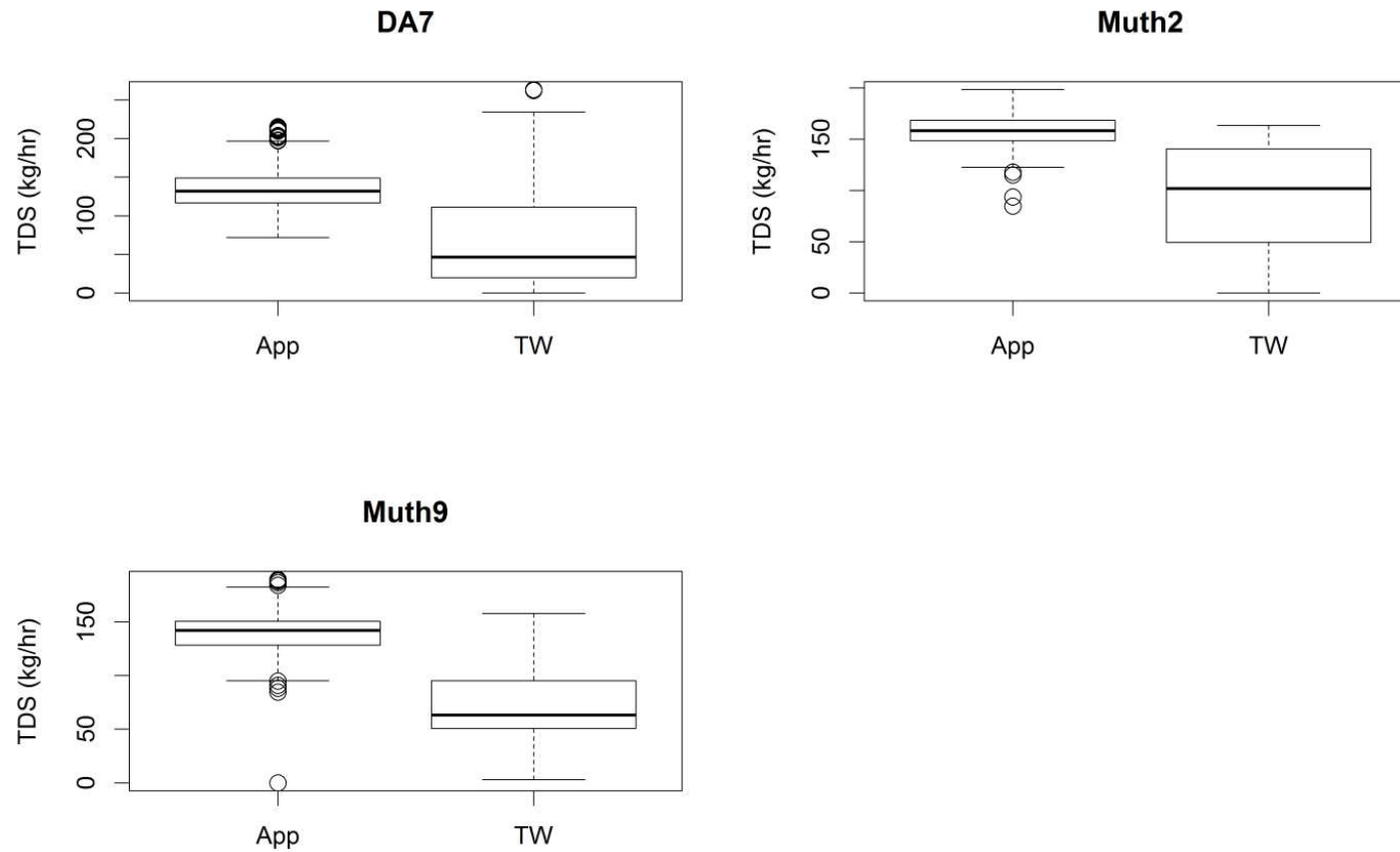


Figure 54: Box plots of TDS mass loading rate for applied water (App) and tailwater (TW) for the three fields.

Table 14. P-values from Kruskal-Wallis test comparing TDS mass loading rate (kg/hr) of applied water and tailwater on fields DA7, Muth2, and Muth9.

	DA7	Muth2	Muth9
Shapiro p-value	<0.001	<0.001	<0.001
Levene p-value	<0.001	<0.001	<0.001
Kruskal-Wallis p-value	<0.001	<0.001	<0.001

### **3.3.4 Analysis of Cumulative TDS Mass**

The bar plot shown in Figure 55 shows the infiltrated ratio ((applied amount – tailwater runoff amount) / applied amount) for the volume of water, mass of TDS, and mass of Se for each field. For water volume, this ratio is interpreted as the proportion of applied irrigation water that was infiltrated (neglecting evaporation). For TDS and Se, this ratio is interpreted as the proportion of TDS or Se mass that was infiltrated or left on the surface of the field. The ratio is less for TDS than it is for water for each field which is attributed to the higher  $C_{TDS}$  values in tailwater than in applied water, as shown in Section 3.1.3. The cause of this disparity is likely due to the pick-up of salts on and near the soil surface and to evaporation as irrigation water runs down the field. See Section 3.4 for an analysis of the relationship between soil salinity and the change in  $C_{TDS}$  between applied water and tailwater. This ratio is larger for field DA7, likely due in part to the incorporation of the first siphon set.

The cumulative mass of TDS per area (kg/acre) in applied water and in tailwater, and the difference between the two for each field, are shown in Figure 56, Figure 57, and Figure 58. These plots show that the cumulative mass of TDS applied is greater than the cumulative mass of TDS removed via tailwater for each field. The cumulative mass of TDS infiltrated is greater than the cumulative mass of TDS in tailwater for field DA7, but not for fields Muth2 and Muth9, which is likely attributed to the incorporation of the first siphon set in the DA7 mass balance. The mass of TDS applied was 425, 650, and 910 kg/acre for fields DA7, Muth2, and Muth9, respectively. Gates et al. (2012) reported average applied salt loading of 452 kg/acre for surface irrigated fields in the USR of the LARV. The salt loading to fields Muth2 and Muth9 are substantially higher than the average loading reported by Gates et al. (2012) due to large amounts of applied irrigation water (9.6 and 14.2 inches compared with 8.2 inches) and the relatively high

$C_{TDS}$  of applied irrigation water. The salt loading to DA7 is smaller due to the small amount of applied water (5.9 inches) despite relatively high  $C_{TDS}$ . For fields DA7, Muth2, and Muth9, tailwater carries an estimated 166, 361 and 479 kg/acre. As mentioned previously, due to the abnormally large amounts of water applied to fields Muth2 and Muth9, as well as the abnormally high tailwater fractions on each field, the solute loading results from this study likely are not representative of the region and should not be applied in regional models.

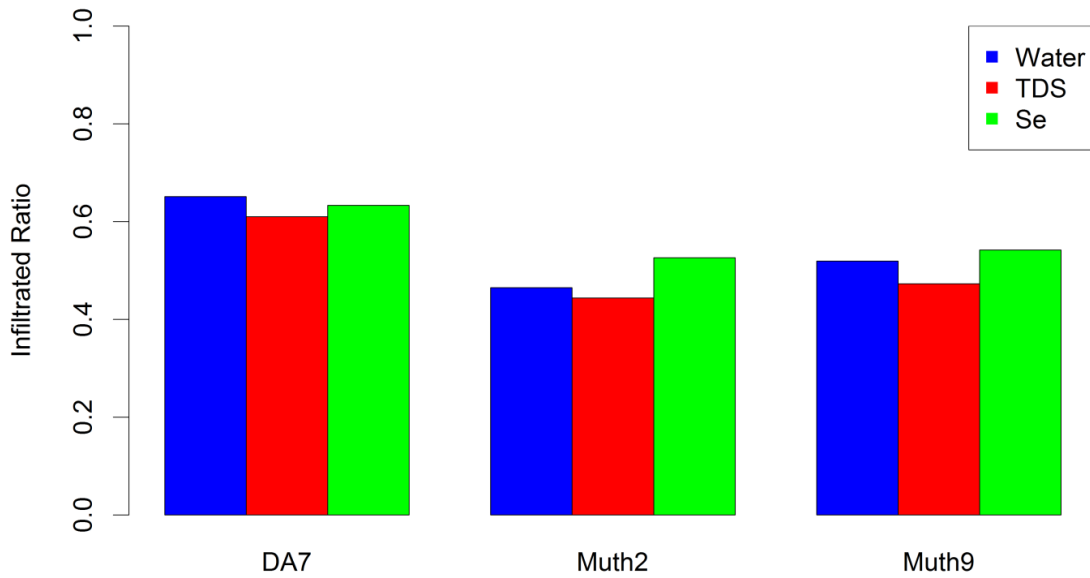


Figure 55. Bar plot of the infiltrated ratio for the volume of water, mass of TDS, and mass of Se for each field.

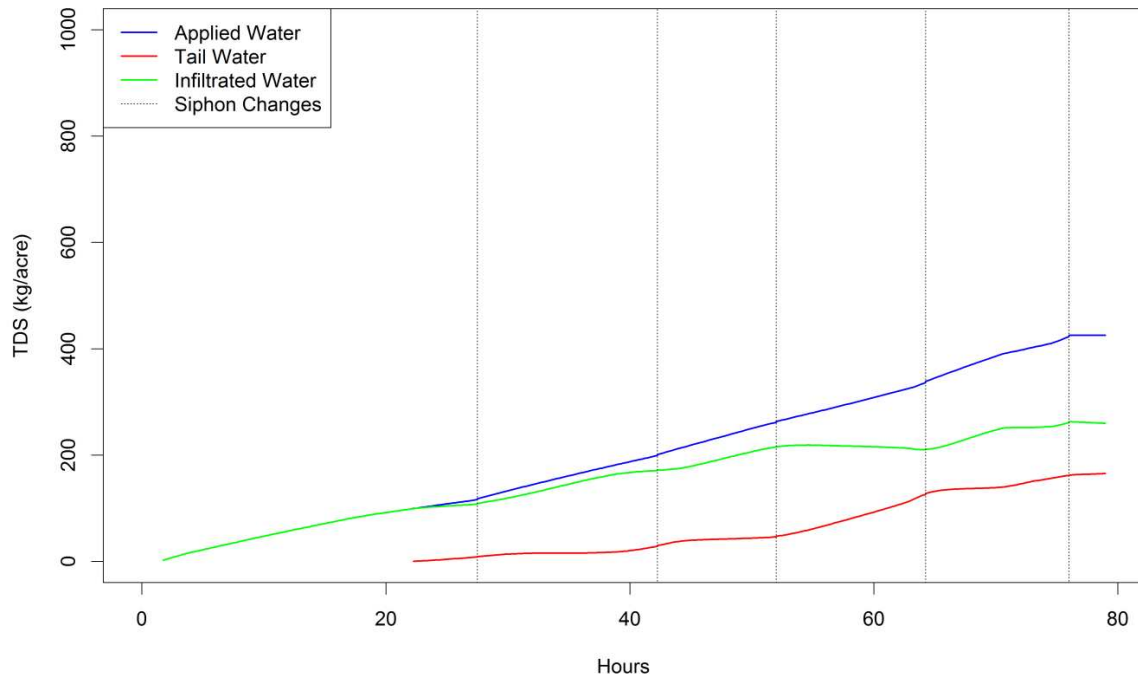


Figure 56. Plot of cumulative TDS mass loading for applied water, tailwater, and infiltrated water for field DA7.

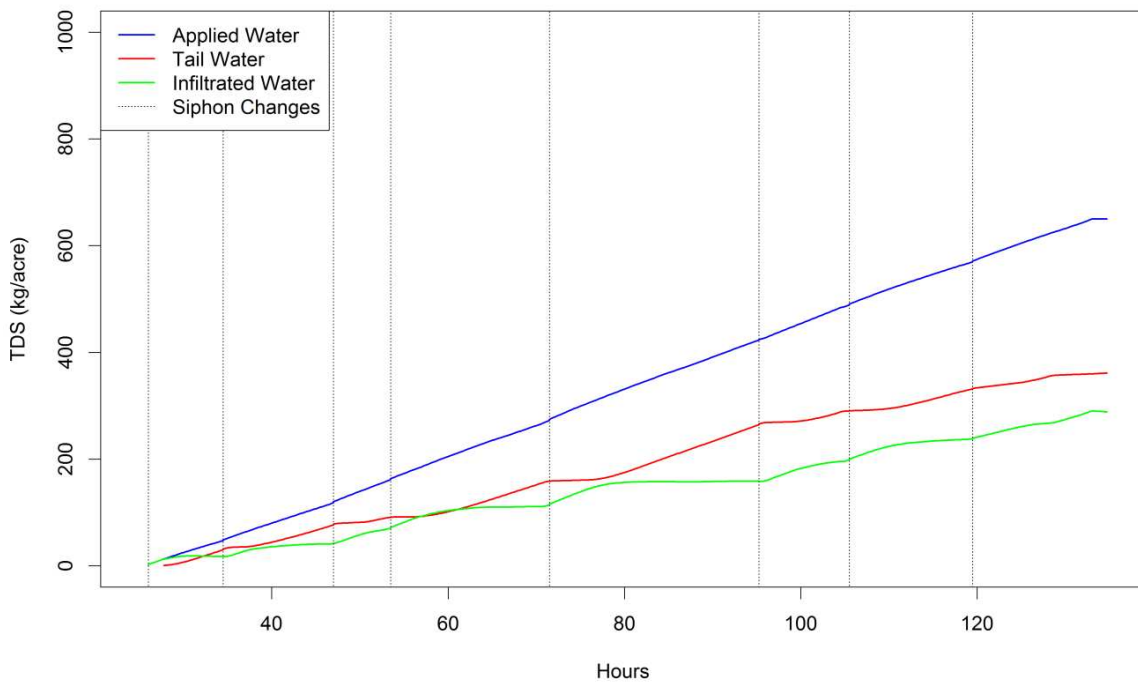


Figure 57. Plot of cumulative TDS mass loading for applied water, tailwater, and infiltrated water for field Muth2.

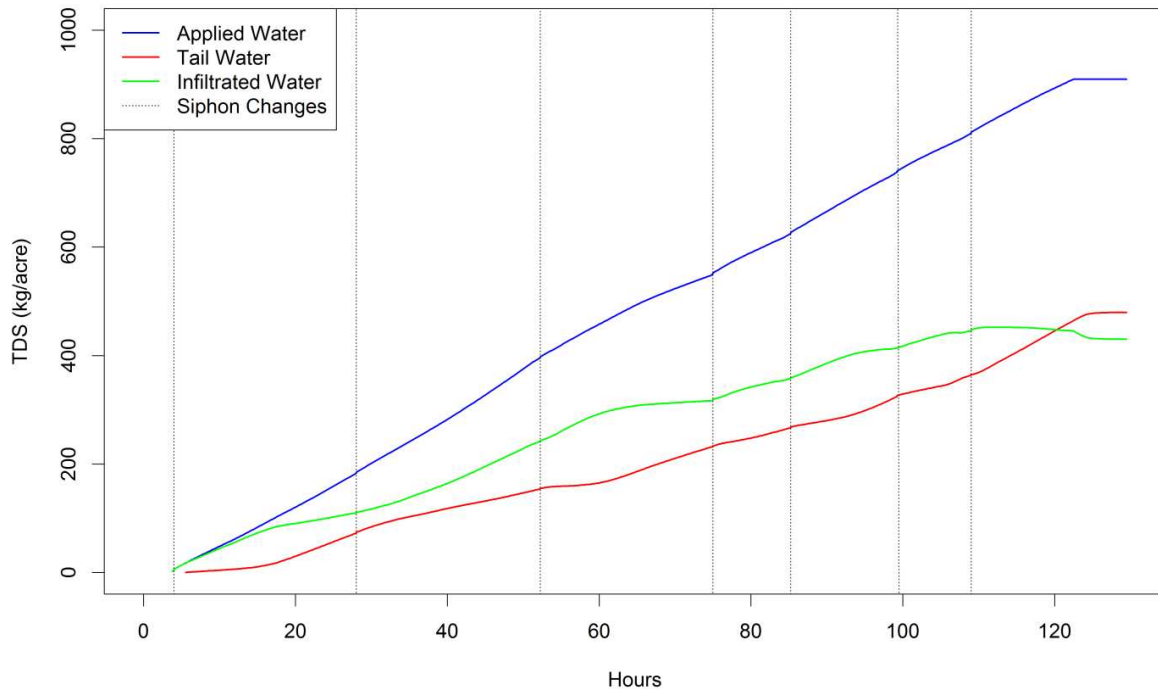


Figure 58. Plot of cumulative TDS mass loading for applied water, tailwater, and infiltrated water for field Muth9

### 3.4 Relationship of Soil Salinity and Change in TDS Concentration between Applied Water and Tailwater

In this section, the relationship of soil salinity and change in TDS concentration between applied irrigation water and tailwater ( $\Delta C_{TDS}$ ) is analyzed for the measured irrigation event on field Muth2. A boxplot and bar plot of  $\Delta C_{TDS}$  between applied water and tailwater at 15 minute intervals for each siphon set incorporated in the mass balance is shown in Figure 59. Diagnostic plots (shown in Figure 134 in Appendix G) indicate that the sample populations are close to normally distributed but contain unequal variances. For this reason, Dunn's test is performed to test the equality of medians. The resulting p-values are shown in Table 15 which indicates that most, but not all, of the sample population medians are significantly different.

A bar plot comparing the median  $\Delta C_{TDS}$  with the average soil salinity  $E_{Ce}$  estimated from the EM-38 survey for each siphon set is shown in Figure 60. Additionally, a scatter plot and

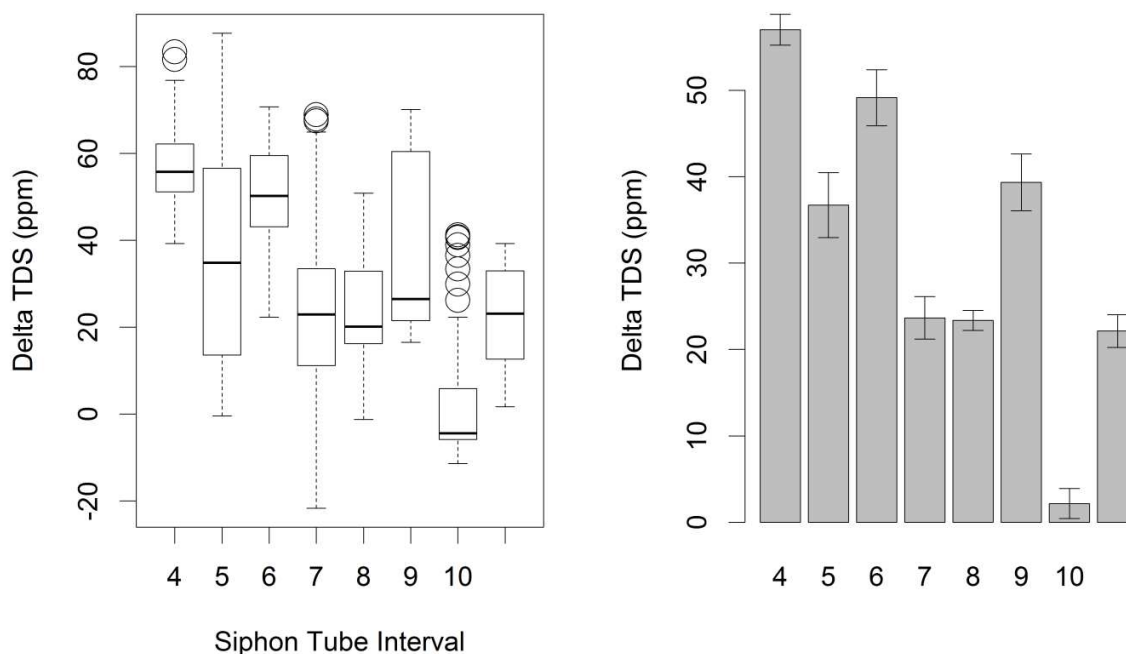


Figure 59. Boxplot and bar plot of the change in  $C_{TDS}$  between applied water and tailwater (Delta TDS) for each measured irrigation siphon tube set for field Muth2.

Table 15. Dunn test p-values for the change in  $C_{TDS}$  between applied water and tailwater (Delta TDS) for each measured irrigation siphon tube sets for field Muth2.

Siphon Tube Sets	4	5	6	7	8	9
5	<0.0001					
6	0.1695	0.0066				
7	<0.0001	0.0063	<0.0001			
8	<0.0001	0.0032	<0.0001	0.4598		
9	0.0009	0.1875	0.0456	0.0006	0.0002	
10	<0.0001	<0.0001	<0.0001	<0.0001	<0.0001	<0.0001
11	<0.0001	<0.0001	<0.0001	0.4404	0.4704	0.0014

linear regression of the same two variables is shown in Figure 61. The linear regression has a weak to moderate  $R^2 = 0.39$  that is not statistically significant. It is expected that soil salinity would not explain all of the variance in the median change in delta  $C_{TDS}$  because of the influence of other important factors such as soil cracking (Rhoades et al. 1997), duration of irrigation flow, and amount of ponding (Gilfedder et al. 2000).

Scatterplots and linear regressions of delta  $C_{TDS}$  with the duration of the siphon set, volume of applied water, and volume of tailwater are shown in Figure 64, Figure 65, and Figure 66 respectively. The linear regressions have low  $R^2$  values that are not statistically significant. The fitted linear regressions have negative slopes indicating greater application of water is related to a lower delta  $C_{TDS}$ . Some of the variation in delta  $C_{TDS}$  may be due to spatial variability in the degree of soil cracking (see Figure 62) and to a variable amount of ponding at the tailwater edge of the field (see Figure 63) between siphon sets, however such variations were not observed on the intra-field scale.

Low Delta  $C_{TDS}$  values from the 10<sup>th</sup> measured siphon set is the anomaly in the data set and are not explained by irrigation duration. A negative delta  $C_{TDS}$  could be due to a precipitation event. Field notes indicate that a thunderstorm occurred during the night that the 10<sup>th</sup> siphon set

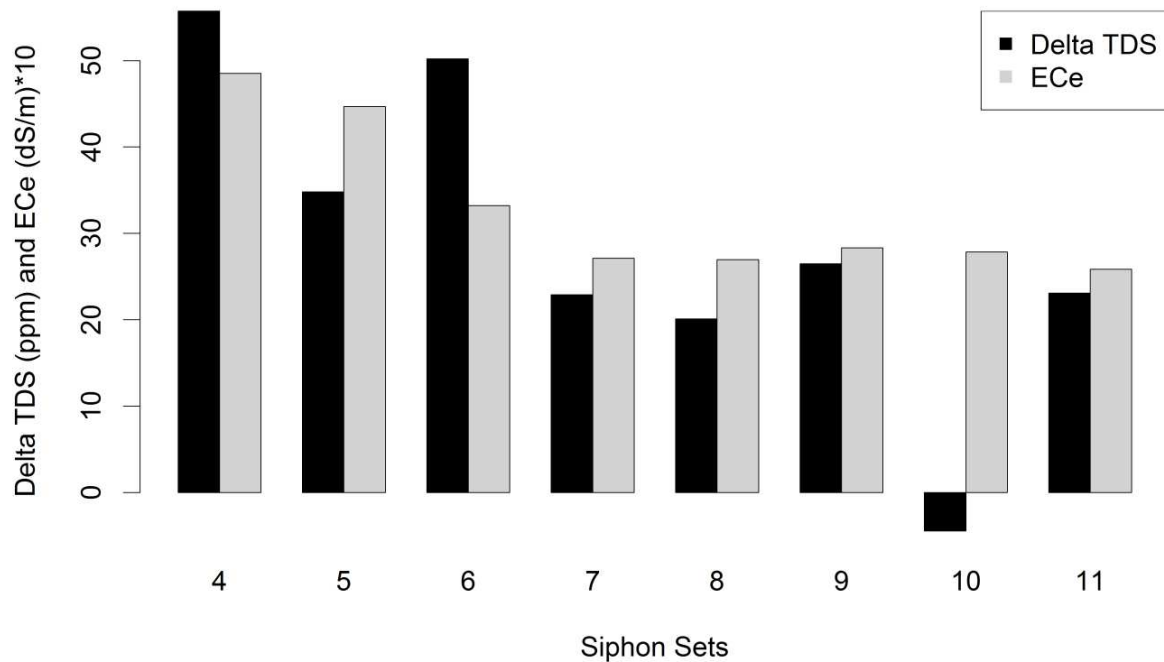


Figure 60. Bar plot of the median change in  $C_{TDS}$  between applied water and tailwater (Delta TDS) and the average ECe for each measured siphon set on field Muth2.

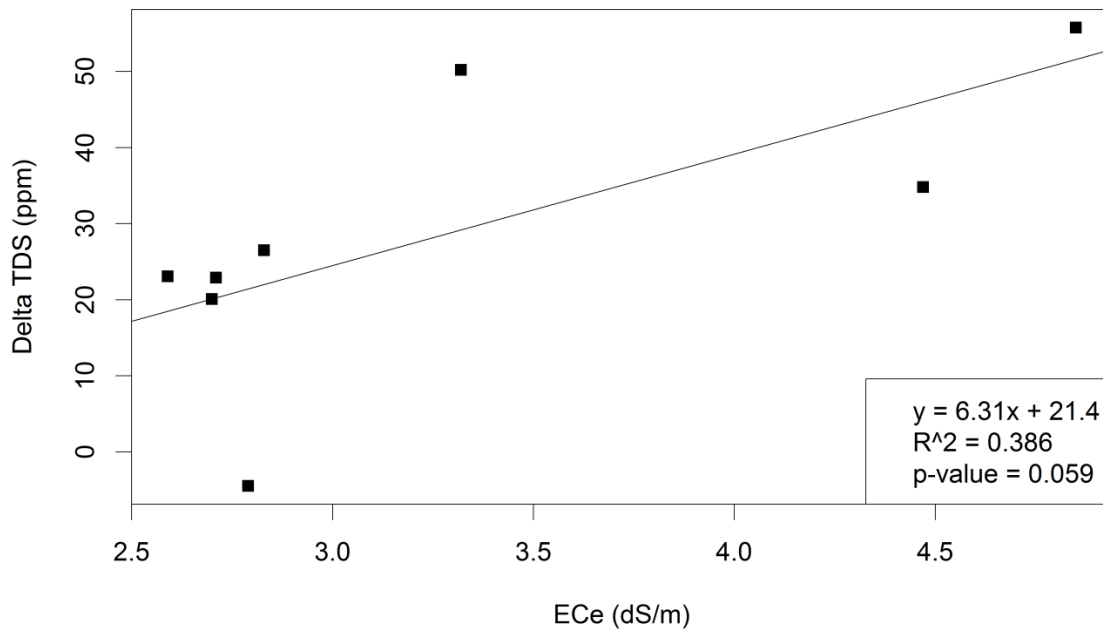


Figure 61. Scatter plot and fitted linear regression relationship for the change in  $C_{TDS}$  between applied water and tailwater (Delta TDS) and the average soil salinity (ECe) for each measured siphon set for field Muth2.



Figure 62. Image of cracked soils on field Muth2



Figure 63. Image of ponding at the tailwater edge of field Muth9.

occurred; however, the rain gauge (located adjacent to the field) did not log any precipitation for the entire irrigation event. As shown in Figure 23, the tailwater flow rate was not abnormally high, which would be expected in the case of a rain event. It is possible that a light precipitation event occurred that was sufficient to decrease the tailwater  $C_{TDS}$  yet was not logged by the rain gauge due to an equipment malfunction.

The average soil salinity to a depth of 2.1 ft (0.65 m) explains a portion of the variance in delta  $C_{TDS}$ . Since salt is entrained into surface water from near-surface soil layers through lateral solute transport processes, it is likely that the average soil salinity to a depth of less than 2.1 ft (0.65 m) would explain more of the variance in delta  $C_{TDS}$ .

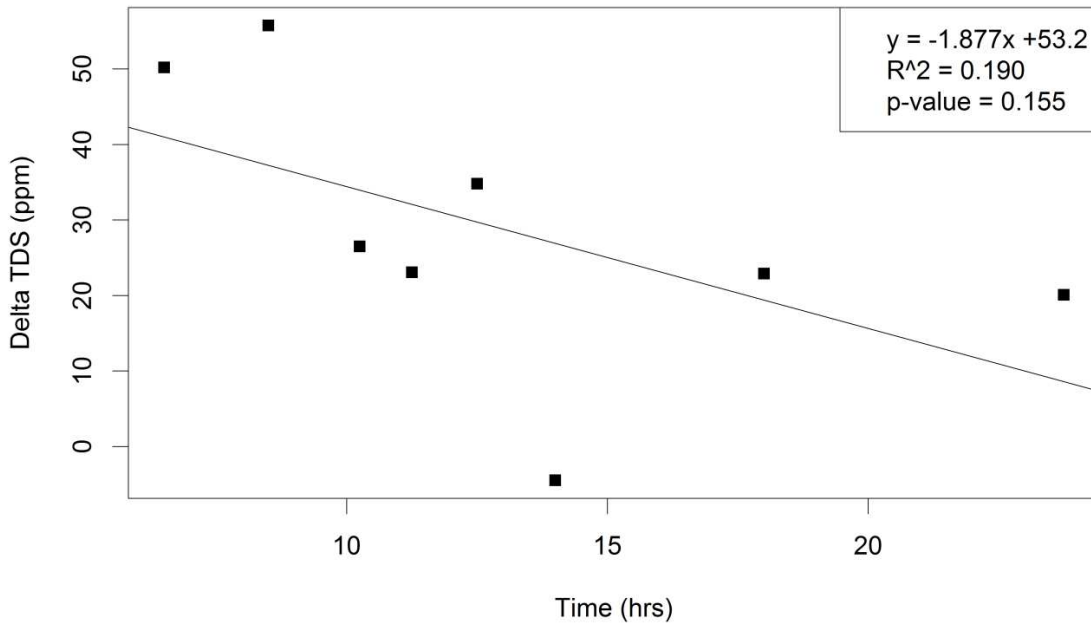


Figure 64. Scatterplot and fitted linear regression relationship for the change in  $C_{TDS}$  between applied water and tailwater (Delta TDS) and duration of irrigation for each measured siphon set on field Muth2.

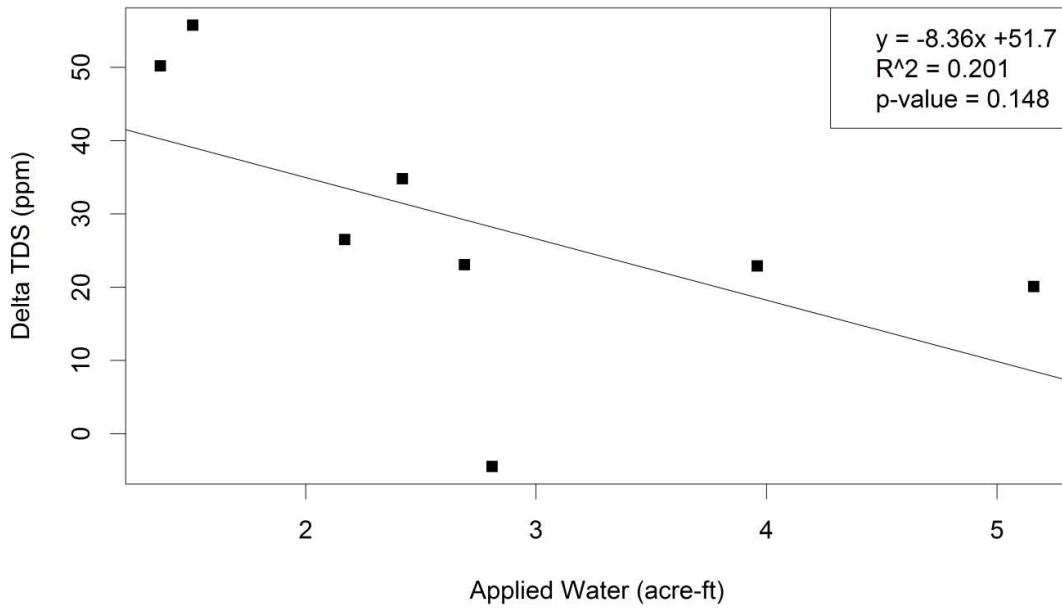


Figure 65. Scatterplot and fitted linear regression relationship for the change in  $C_{TDS}$  between applied water and tailwater (Delta TDS) and volume of applied water for each measured siphon set on field Muth2.

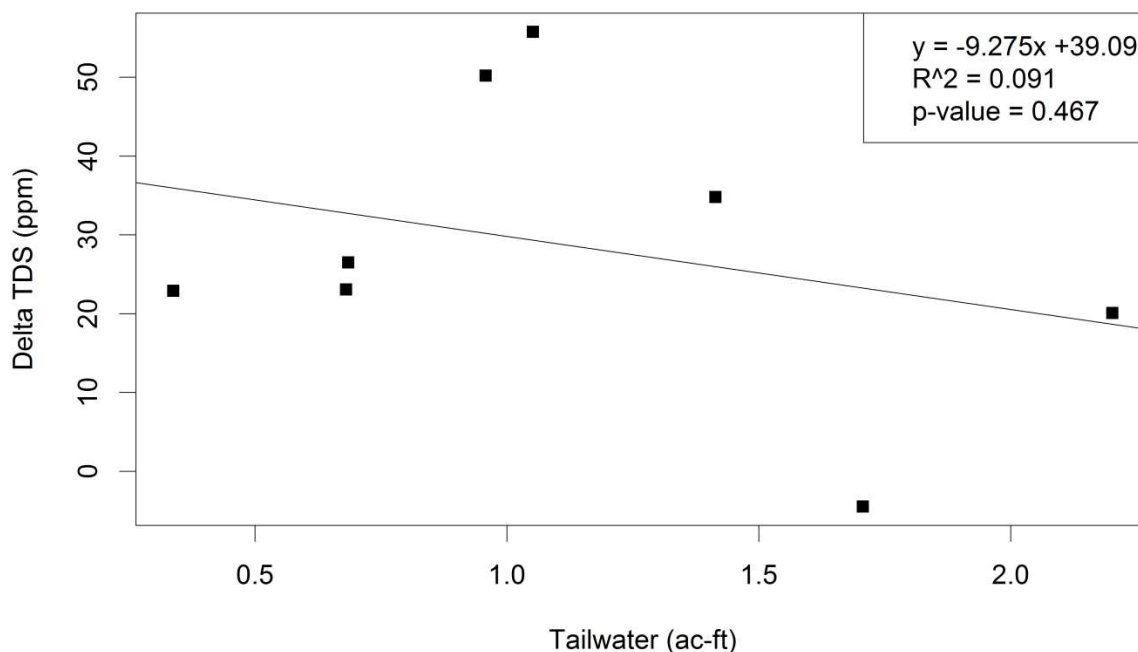


Figure 66. Scatterplot and fitted linear regression relationship for the change in  $C_{TDS}$  between applied water and tailwater (Delta TDS) and volume of tailwater for each measured siphon set on field Muth2.

### 3.5 Field-Scale Mass Balance of Se

As described in the methodology section, the field-scale mass balance of dissolved Se is accomplished similarly as with TDS with the additional step of converting  $C_{TDS}$  estimates to  $C_{Se}$  estimates. Water samples collected from applied irrigation water and tailwater were analyzed for total recoverable Se in addition to total dissolved Se. For fields DA7 and Muth9, the total recoverable Se of tailwater was less than that of applied irrigation water and the reverse was true for field Muth2. It was observed in the field that Muth9 and DA7 had more ponding at the tailwater edge than Muth2 which can allow sufficient time for suspended particles to settle. For field Muth9, the tailwater was clear compared to the applied irrigation water indicating the presence of less suspended solids. Figure 15 shows a side by side comparison of tailwater from

field Muth2, DA7 and Muth9. It would be foolish to draw firm conclusions from such small sample sizes, but it appears that an increase of ponding decreases total recoverable Se concentrations in tailwater.

### ***3.5.1 Relationship of Total Dissolved Solids and Dissolved Selenium***

Scatter plots and linear regressions of dissolved Se vs TDS from applied water and tailwater are shown in Figure 20. The linear regression of the applied water has a statistically significant high coefficient of determination ( $R^2 = 0.88$ ), whereas the linear regression of the tailwater has a statistically significant moderate correlation ( $R^2 = 0.67$ ). The diagnostic plots (Figure 126 and Figure 127 in Appendix F) show the data are nearly normally distributed and variances are nearly homogenous. However, the standardized residuals vs leverage plot for tailwater shows there is a point with a large standardized residual and large leverage indicating it is pulling the slope towards it. This point is the highest in  $C_{TDS}$  and  $C_{Se}$  and appears to cause the slope for the tailwater regression to be greater than the slope for the applied irrigation water regression. While it is possible this point would be an outlier from a larger set of samples, the outlier test p-values were substantially greater than 0.05 and upon review of the data collection, data entry, and lab testing; nothing warranted its omission. It should be noted that a sample size of seven is very small for developing a linear regression and the confidence intervals shown in Table 19 and plotted in Figure 84, Figure 85 and Figure 86 in Appendix B reveal the uncertainty associated with it. The confidence intervals plotted correspond to the statistical confidence of the linear regression slope of  $C_{TDS}$  vs  $C_{Se}$ . The plots show that there is an error range of roughly 3.5 and 8  $\mu\text{g/L}$  in the estimation of  $C_{Se}$  for the 67% and 95% confidence intervals for applied irrigation water. The error range for tailwater is 8 and 20  $\mu\text{g/L}$  for the 67% and 95% confidence intervals. The confidence intervals do not represent any additional uncertainty beyond that of the

estimated linear regression of  $C_{TDS}$  vs  $C_{Se}$  and are included simply to give an idea of a portion of the statistical uncertainty involved with any of the findings from the Se mass balance portion of this study. Additional uncertainty, that is not quantified herein, is derived from the linear regression of  $C_{TDS}$  vs  $EC_W$ , sampling error, lab error, instrument error, etc.

### ***3.5.2 Analysis of Estimates of Dissolved Selenium Concentration***

Plots of  $C_{Se}$  vs time for applied water and tailwater for each field are shown in Figure 67. Because these plots are based on linear regressions of  $C_{Se}$  vs  $C_{TDS}$ , they display similar trends with time. However, because there are separate linear regressions for the applied water and tailwater, the relative trends between applied water and tailwater are different. At lower  $C_{TDS}$ , values the  $C_{Se}$  tends to be lower than the  $C_{Se}$  for applied water and the opposite is true for higher  $C_{TDS}$  values.

Box plots and bar plots of each dataset of estimated  $C_{Se}$  at 15 minute intervals are shown in Figure 68. Each dataset fails the Shapiro test and the Levene test with p-values less than 0.05 indicating the datasets are not normally distributed and contain variances that are not homogeneous with statistical significance to a confidence level of 95%. For this reason, and also based on analysis of the diagnostic plots (Figure 128, Figure 129, and Figure 130 in Appendix F) the ANOVA assumptions are violated and the Kruskal-Wallis test of equal medians was conducted. The results of these tests indicate that the median  $C_{Se}$  for applied water and tailwater are statistically different for each field with a confidence level of 95%. The difference between medians of applied water and tailwater  $C_{Se}$  are not consistent across the three fields. For fields Muth2 and Muth9, the  $C_{Se}$  of tailwater is lower than that of applied water, whereas the reverse is true for DA7. This discrepancy can be attributed to the higher  $C_{TDS}$  values of DA7 tailwater.

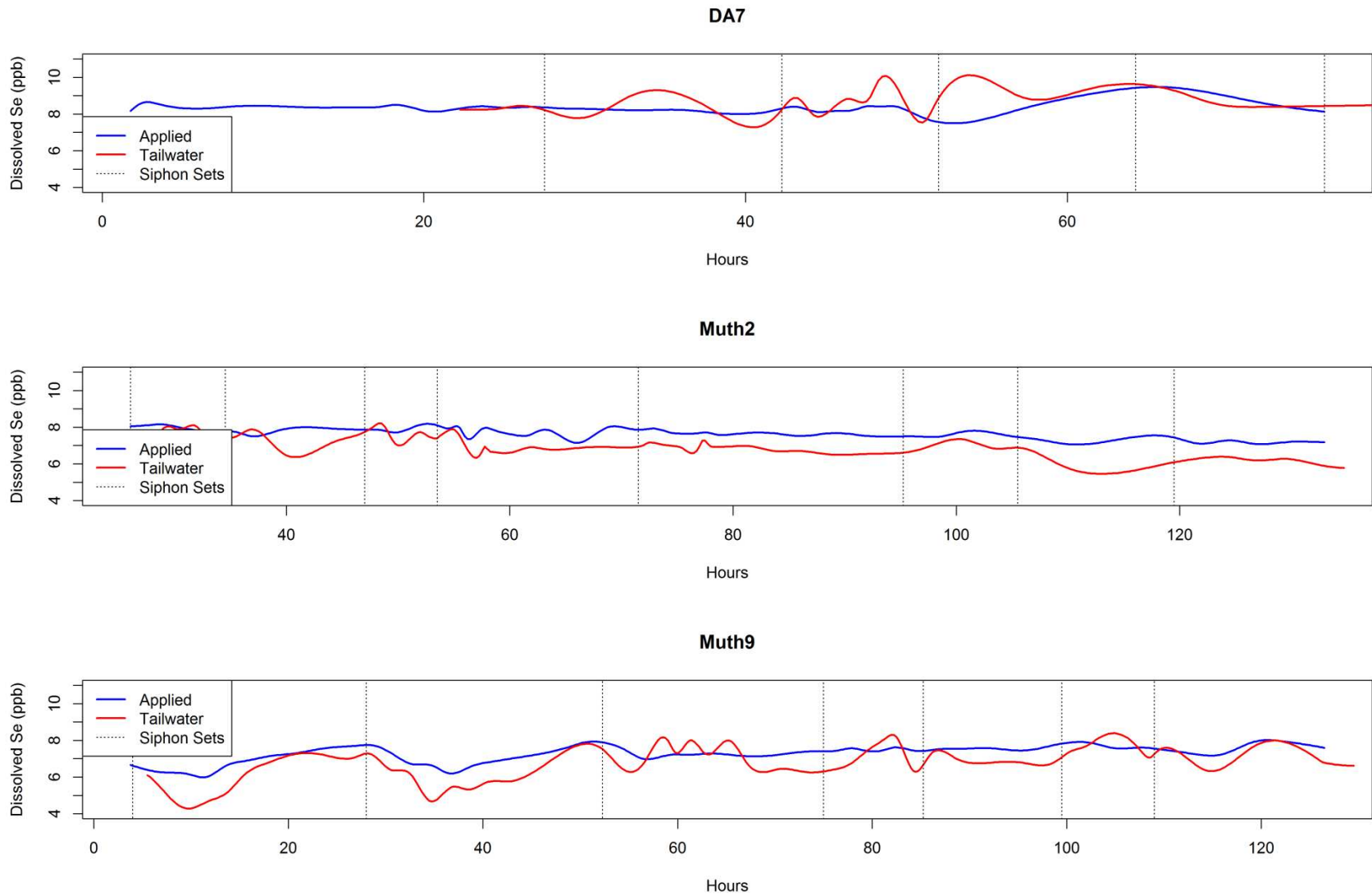


Figure 67. Time series plots of  $C_{Se}$  in applied water and tailwater for the measured irrigations events.

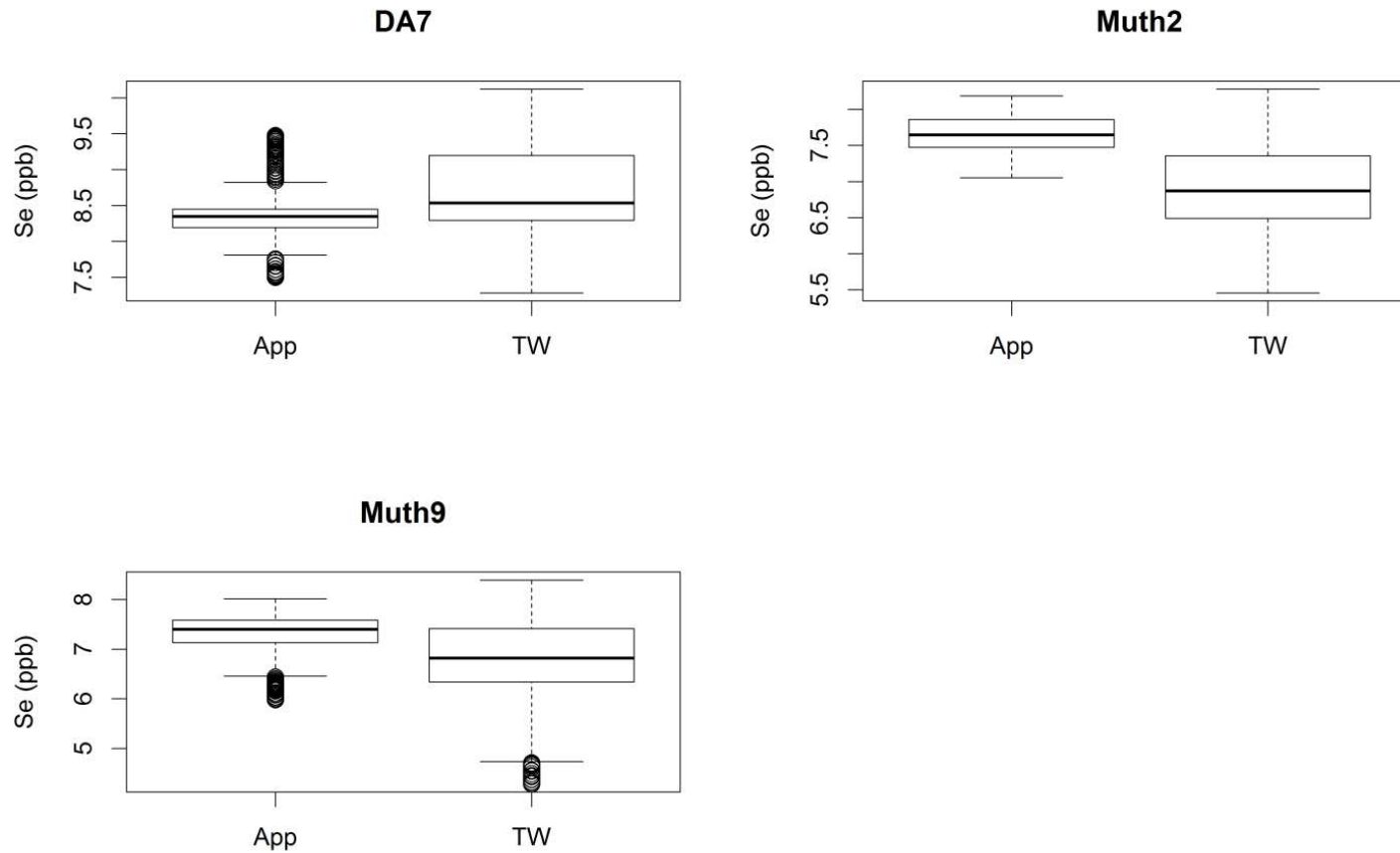


Figure 68: Box plots of  $C_{Se}$  for applied irrigation water (App) and tailwater (TW) for the measured irrigation events for the three fields.

Table 16. P-values from Kruskal-Wallis test comparing  $C_{Se}$  of applied irrigation water and tailwater for the measured irrigation events for the three fields.

	DA7	Muth2	Muth9
Shapiro p-value	<0.001	<0.001	<0.001
Levene p-value	<0.001	<0.001	<0.001
Kruskal-Wallis p-value	<0.001	<0.001	<0.001

The relationship between  $C_{TDS}$  and  $C_{Se}$  in groundwater and rivers that are dependent on groundwater baseflow has proven to be highly correlated in this study and many others. However, it is possible that  $C_{TDS}$  of tailwater is not a good predictor of the  $C_{Se}$  of tailwater. The vast majority of ions that make up TDS are conservative relative to Se which is more susceptible to redox reactions and adsorption/desorption processes. The process of dissolving salts is fast, especially in comparison with redox reactions which, over the course of an irrigation event, may not have sufficient time to take place as they would in a groundwater setting. That said, Figure 40 reveals a statistically significant high coefficient of determination ( $R^2 = 0.97$ ) for the linear regression of  $C_{Se}$  vs  $C_{TDS}$  for tailwater mixed with tile drain water. Future research involving more sampling from tailwater is necessary in order to better determine the relationship between tailwater  $C_{TDS}$  and  $C_{Se}$ .

### ***3.5.3 Analysis of Dissolved Se Mass***

Plots of dissolved Se mass loading rate (g/acre/hr) of applied water and tailwater for each field are shown in Figure 69, Figure 70, and Figure 71. The vertical dotted gray lines represent times when the siphon tube sets were changed. These plots also resemble the trends seen in TDS mass flow rate plots because they are calculated using the same flow rates and estimated  $C_{Se}$  from linear regressions of  $C_{TDS}$  for applied water and tailwater. Because the applied water and tailwater linear regressions are different, there are differences in the relative change of mass flow rate between applied water and tailwater in comparison to the TDS mass flow rate plots.

The box and whisker plots of dissolved Se mass flow rate (Figure 72) demonstrate a clear trend where the applied mass flow rate is higher than the tailwater mass flow rate. The results of a Kruskal-Wallis test confirm this trend as being statistically significant (see Table 17). The Kruskal-Wallis test of equality of medians was conducted due to violation of the assumptions for

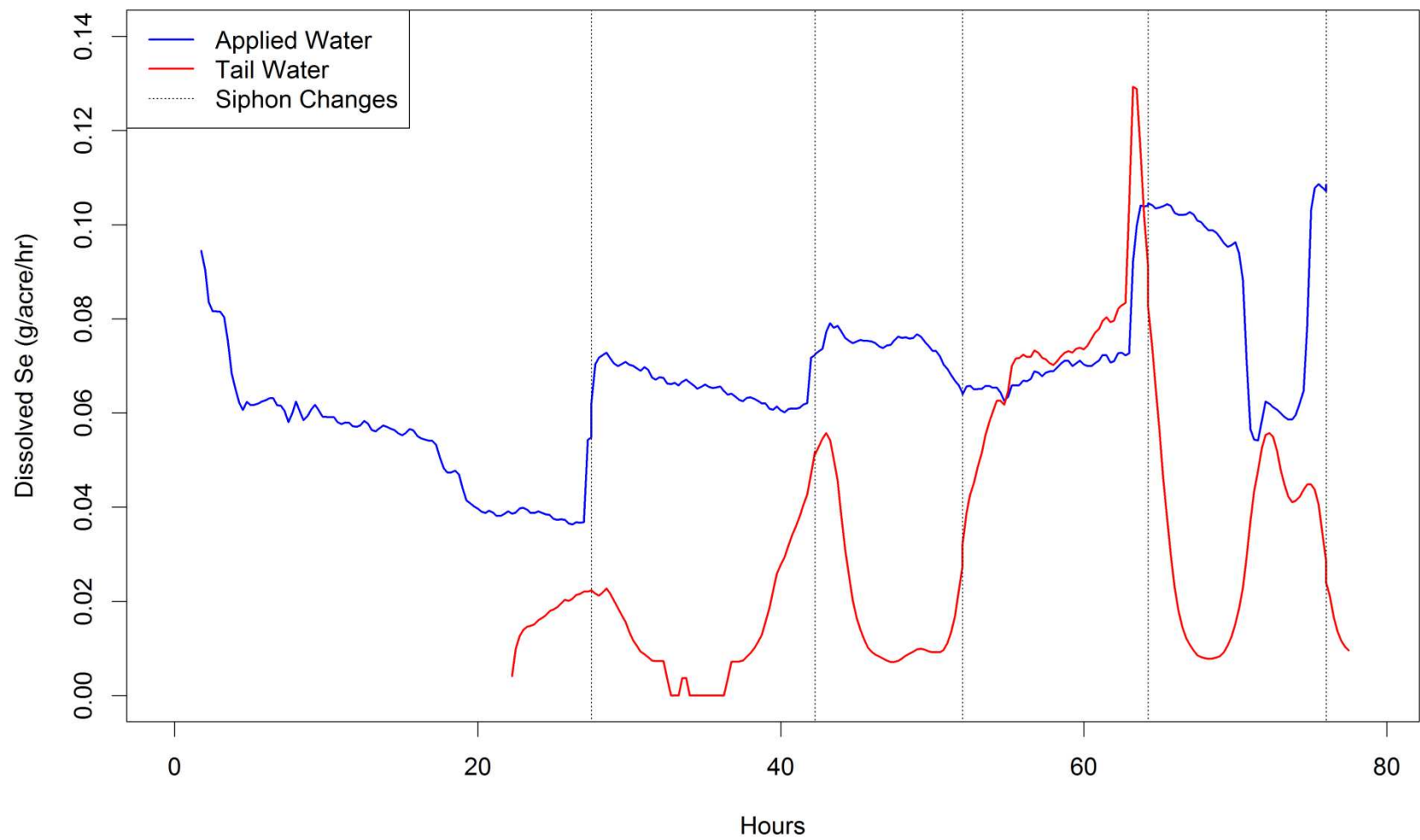


Figure 69. Mass loading rate of dissolved Se in applied irrigation water and tailwater for field DA7.

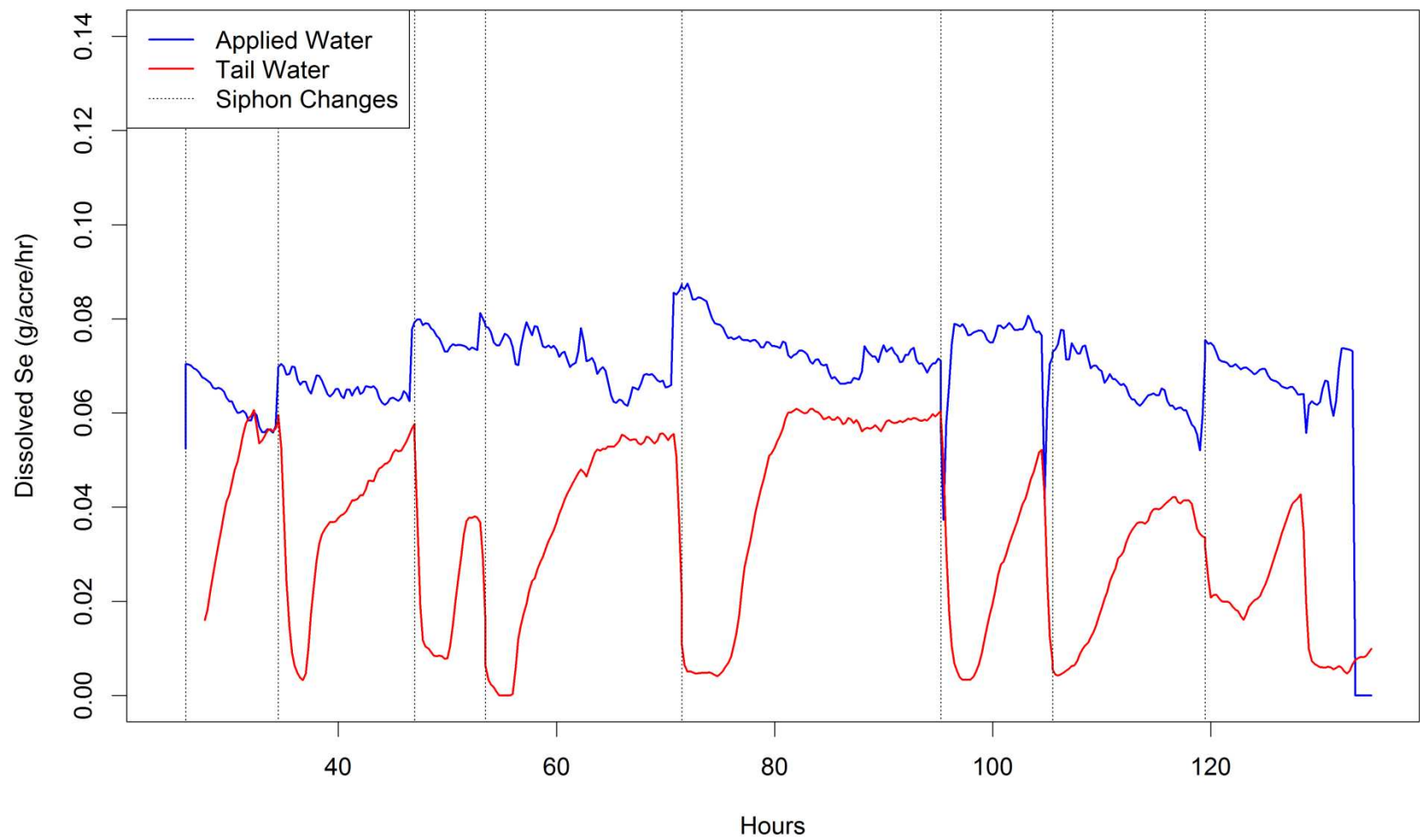


Figure 70. Mass loading rate of dissolved Se in applied irrigation water and tailwater for field Muth2.

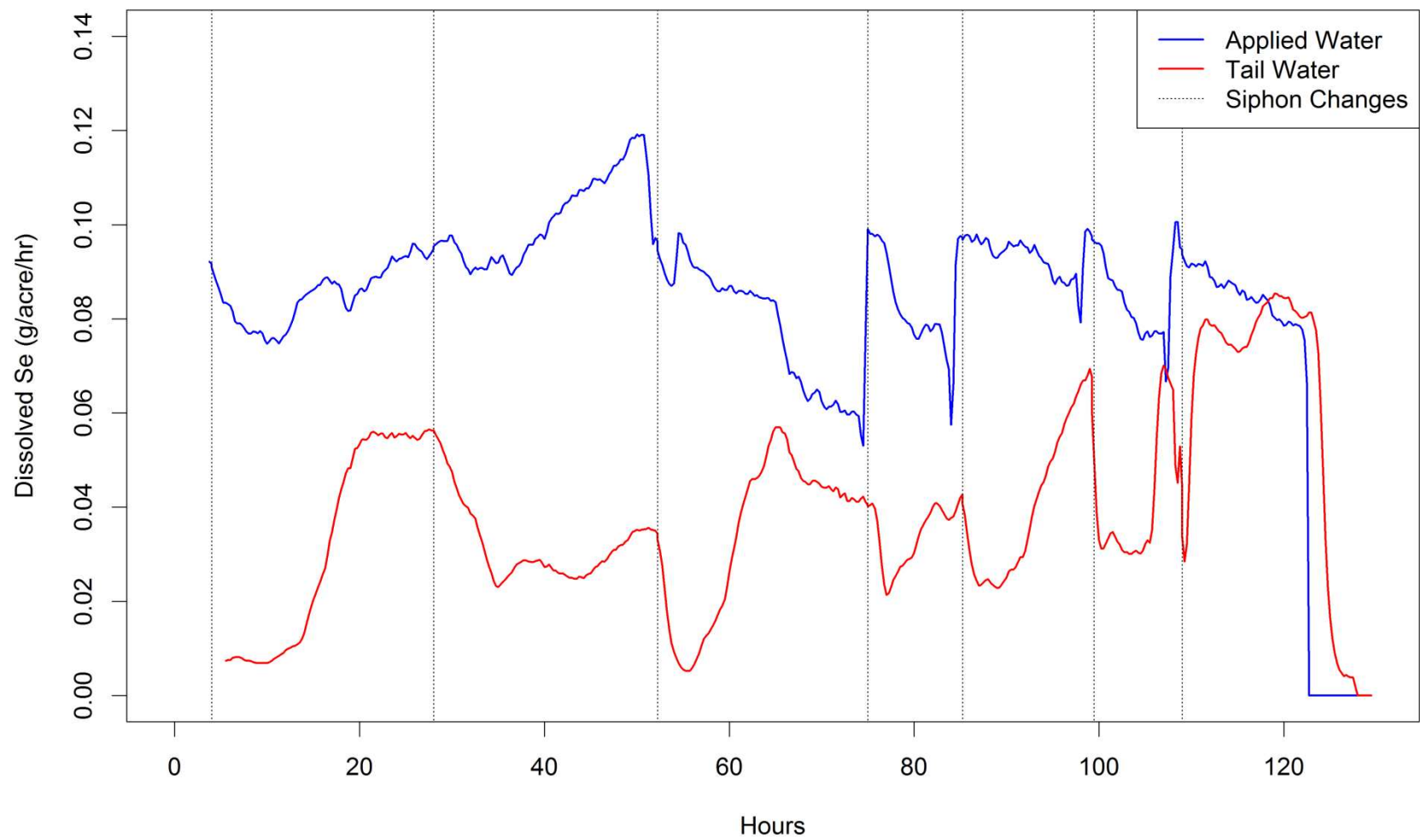


Figure 71. Mass loading rate of dissolved Se in applied irrigation water and tailwater for field Muth9.

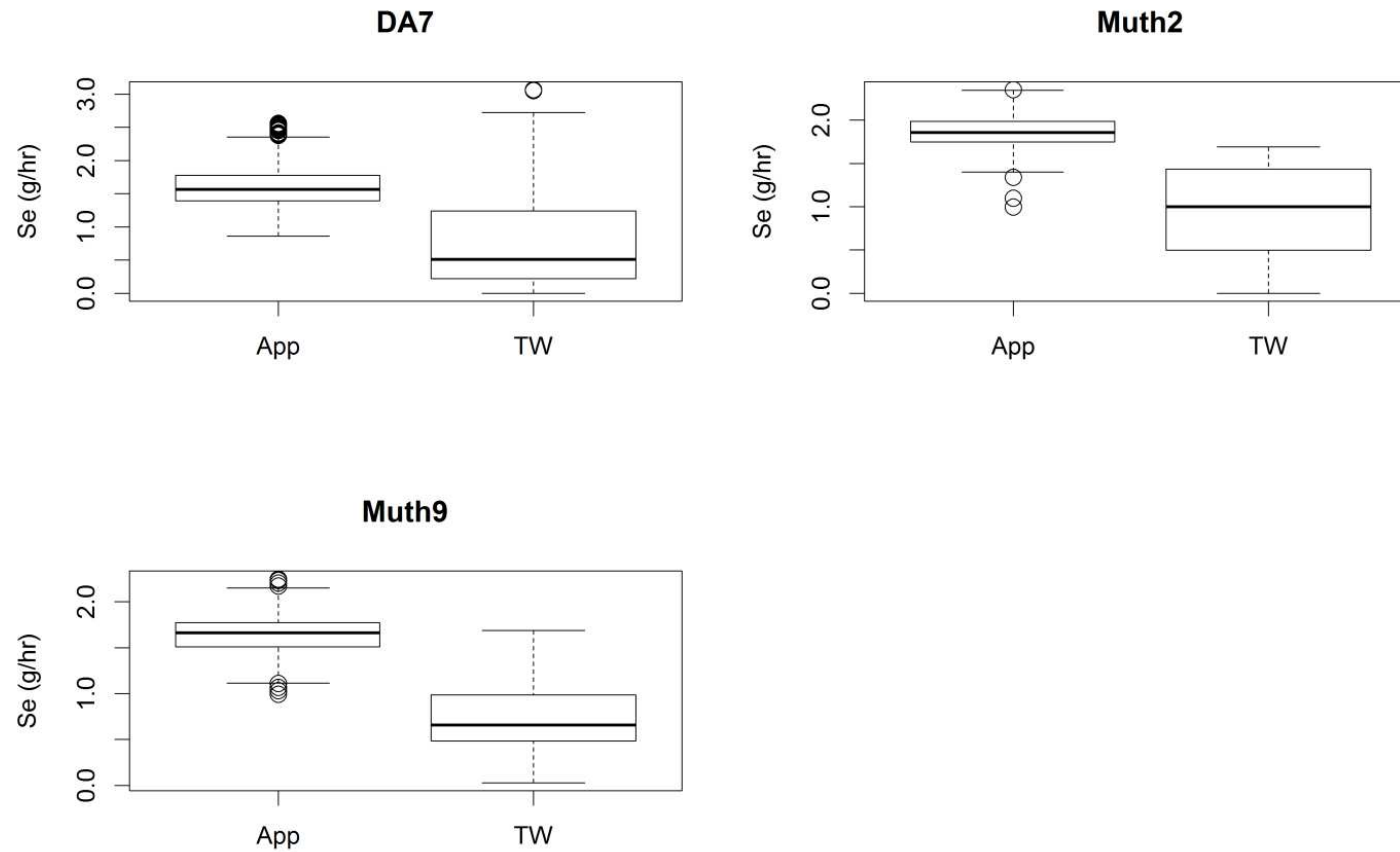


Figure 72. Box plots of dissolved Se mass loading rate for applied irrigation water (App) and tailwater (TW) for the three fields.

Table 17. P-values from Kruskal-Wallis test comparing dissolved Se mass loading rate (g/acre/hr) of applied irrigation water and tailwater for the three fields

	DA7	Muth2	Muth9
Shapiro p-value	<0.001	<0.001	<0.001
Levene p-value	<0.001	<0.001	<0.001
Kruskal-Wallis p-value	<0.001	<0.001	<0.001

ANOVA equality of means tests. The diagnostic plots can be seen in Figure 132, and Figure 133 in Appendix F. This is the same trend seen when comparing the tailwater and applied water TDS mass flow rates and is due to the large differences in applied water and tailwater flow rates.

#### ***3.5.4 Analysis of Dissolved Selenium Cumulative Mass***

Plots of the cumulative mass of dissolved Se from applied water, tailwater and infiltrated water for each field are shown in Figure 73, Figure 74, and Figure 75. There is 5.1, 7.7 and 10.6 g/acre applied to fields DA7, Muth2 and Muth9 respectively. There is more dissolved Se infiltrating than there is running off as tailwater for all three fields, though the two values are close for field Muth2. For fields DA7, Muth2 and Muth9 tailwater carries an estimated 3.2, 3.6 and 4.9 g/acre. Figure 55 shows that for each field there is a higher infiltration ratio (and thus a lower tailwater fraction) for dissolved Se than there is for TDS. This difference is more pronounced for fields Muth2 and Muth9 than it is for field DA7 which can be attributed to the high tailwater  $C_{TDS}$  of DA7 for which the tailwater linear regression predicts higher  $C_{Se}$ . Lower tailwater fractions for Se in comparison to TDS may be due to 1) dissolved Se undergoing sorption or reduction processes as irrigation water flows across the field, 2) a greater proportional mass of TDS picked up through lateral solute transport processes, 3) or a combination of the two. Sediment sample analysis before and after irrigation events would be required in order to determine which scenario plays a larger role. Once again, these findings are based off of linear regressions of seven samples from applied water and tailwater and should be interpreted with caution.

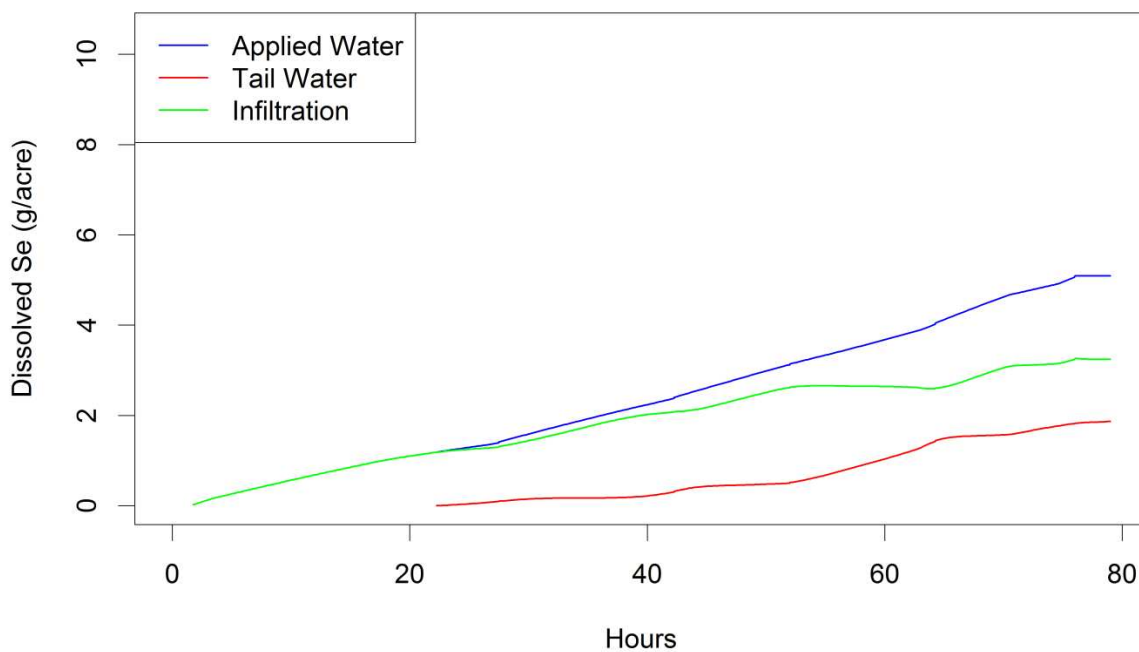


Figure 73. Plot of cumulative dissolved Se mass loading for applied irrigation water, tailwater, and infiltrated water for field DA7.

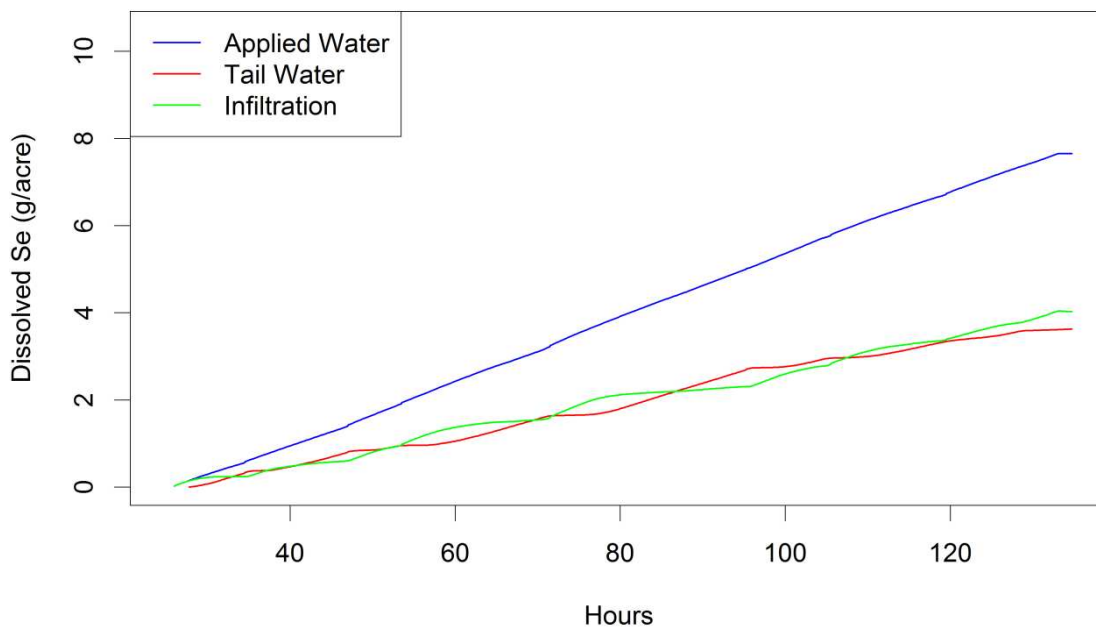


Figure 74. Plot of cumulative dissolved Se mass loading for applied irrigation water, tailwater, and infiltrated water for field Muth2.

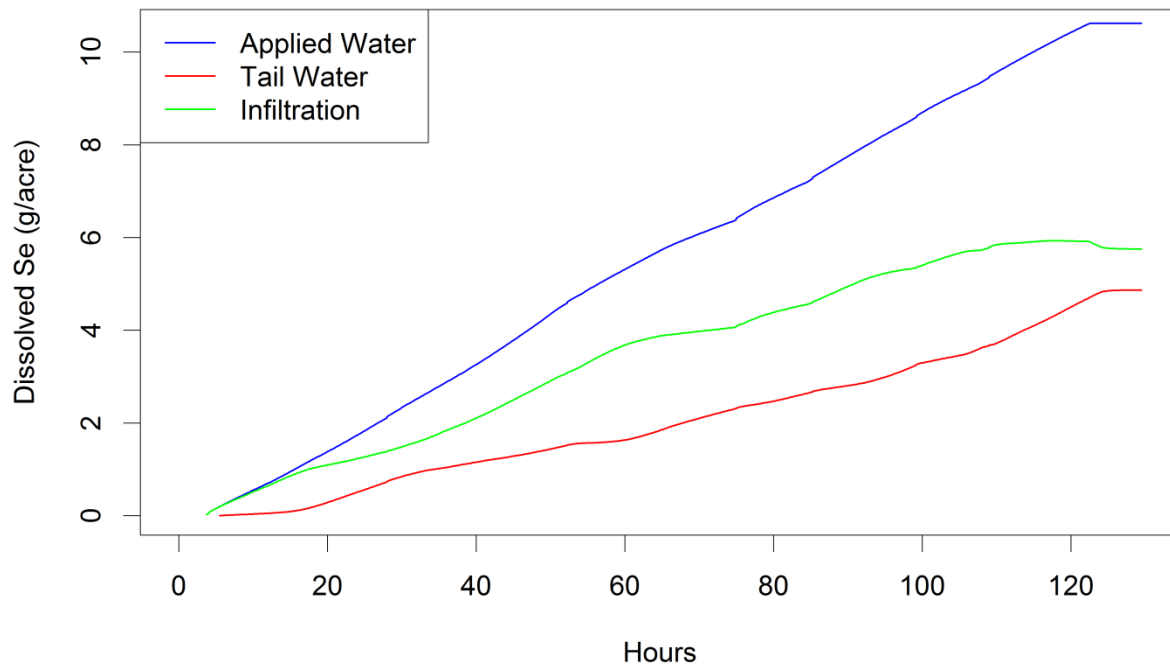


Figure 75. Plot of cumulative dissolved Se mass loading for applied irrigation water, tailwater, and infiltrated water for field Muth9.

### 3.6 Analysis of Nitrate Samples from Field-Scale Mass Balance

Figure 76 is a barplot of  $C_N$  of sequentially collected applied irrigation water and tailwater samples from the field scale mass balances. The three sets of samples on the right side of the bar plot are all from field Muth2. The other four samples are from fields DA7 and Muth9. The  $C_N$  decreases from applied irrigation water to tailwater for fields DA7 and Muth9 whereas it increases substantially for field Muth2 implying substantial spatial and temporal variation. The low sample size and spatial variation of the field scale mass balances prevent statistically significant interpretation of the results. Since the samples are collected sequentially, it is possible the tailwater sample is not representative of the applied water sample as it takes a considerable amount of time for the water to flow across the field. It is also possible that the samples from these fields are representative of the entire FDD system where, depending on fertilizer

application practices and timing, the  $C_N$  of tailwater is lower than applied water on some fields and drastically higher than applied water on other fields leading to a median tailwater  $C_N$  that is statistically higher than applied water. As shown in Section 3.1.1, it is likely that the  $C_N$  of tailwater in the central tailwater ditch is high relative to SW because the median  $C_N$  of TD and TWTD are not statistically different from each other and are both significantly greater than  $C_N$  of SW. In order to identify statistically significant trends there is a need for a greater sample size for each irrigation event. In order to identify temporal and spatial trends there is a need for sampling from multiple irrigation events on multiple fields.

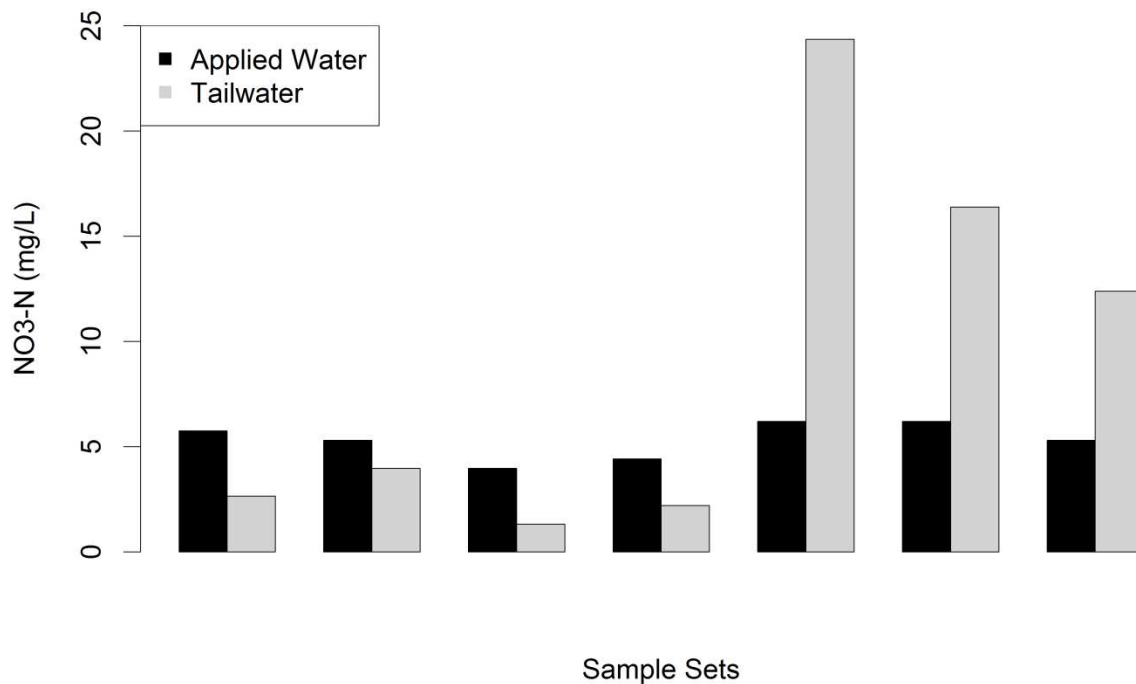


Figure 76. Barplot of  $C_N$  from applied irrigation water and tailwater samples from field scale mass balance events.

## CHAPTER 4: CONCLUSIONS AND RECOMMENDATIONS FOR FUTURE RESEARCH

Through the flow measurement and collection and analysis of water samples in applied irrigation water, tile drain water, and tailwater runoff mixed with tile drain water, and from monitoring wells within and outside of the FDD, it was found that subsurface drainage has a significant influence on salinity, Se and  $\text{NO}_3$  in underlying groundwater and in transport to the river system. These findings are summarized in this chapter along with recommendations for future research. Groundwater samples tend to be a good representation of temporal variability; however, they lack representation of spatial variability. For this reason, conclusions regarding the influence that subsurface drainage has on groundwater chemistry should be interpreted with caution.

### 4.1 Key Findings

- Subsurface tile drains seem to prevent deep percolation of  $\text{NO}_3$  by intercepting and exporting out of the groundwater flow system, thereby reducing the redox capacity of the deep groundwater environment. This likely decreases the rate of Se mobilization in deep groundwater by lowering the potential for the oxidation of elemental Se and by increasing the rate of  $\text{SeO}_4$  reduction. Thus, evidence is provided that the presence of tile drains decreases the contribution of dissolved Se to rivers via groundwater baseflow.
- The median  $C_{\text{Se}}$  of tile drain water and tailwater mixed with tile drain water were 2.9 and 1.8 times greater than the median  $C_{\text{Se}}$  of applied irrigation water. The median  $C_{\text{Se}}$  exported to the river system via tailwater mixed with tile drain water was 15.7 mg/L over the entire year and was 25.9 mg/L in the winter; roughly 5 times and 8 times greater than the USEPA criterion

for aquatic life. This study was not able to determine the total loading of Se from tailwater or tile drains, but the impact may be greater in the winter when river flows are lower.

- Subsurface drainage also appears to be an effective way of maintaining  $C_N$  of groundwater in this area at levels well below the USEPA drinking water standard of 10 mg/L as the median  $C_N$  of groundwater below drains was found to be close to 0 mg/L.
- The high  $C_{Se}$  in tile drain water was not explained by the  $C_N$  values, indicating the likely presence of other high energy redox species such as  $O_2$ .
- Sampled tailwater had lower  $C_{Se}$  than sampled tile drain water despite an environment of high DO levels, indicating either a lack of elemental Se or selenide at the surface or insufficient time for redox reactions to take place.
- Riparian zones appeared to be effective at removing Se and  $NO_3$  from shallow groundwater.
- The median  $C_{TDS}$  of tile drain water and tailwater mixed with tile drain water were nearly 5 and 2.7 times greater than the median  $C_{TDS}$  of applied irrigation water, indicating tailwater had substantially lower  $C_{TDS}$  than tile drain water in the area.  $C_{TDS}$  in tailwater mixed with tile drain water were higher in the winter than they were in the summer.
- Sampling data show the tile drains have no influence on the  $C_{TDS}$  in the underlying groundwater. However, this conclusion assumes no spatial variance in the alluvial aquifer properties between the drained and undrained areas in the study area which might cause higher  $C_{TDS}$  in the underlying groundwater in the absence of tile drains. It is likely, however, that there is indeed a difference in the underlying alluvial properties that influenced selection of the sites for installation of the tile drains. It is impossible to test what the deep groundwater  $C_{TDS}$  would be in the absence of tile drains. It is thought, though, that (if the fields were irrigated in the same manner) the  $C_{TDS}$  of deep groundwater would be

substantially higher due to leaching of accumulated salts from the root zone, leading to higher  $C_{TDS}$  in groundwater baseflow. That is to say, (assuming equal irrigation with or without tile drains) the additional loading of salts to the river system through subsurface drainage may be equivalent to the additional loading of salts via groundwater baseflow in the absence of drains. This hypothesis could be further investigated through the application of a local-scale groundwater flow and reactive solute transport model.

- Tailwater salt mass loading results from the mass balance analysis should be interpreted with caution due to the abnormally high tailwater fractions. The average increase between median applied irrigation water and median tailwater  $C_{TDS}$  was 4%, 7% and 10% for fields DA7, Muth2 and Muth9, respectively, and the respective tailwater mass loading for the same fields was 166, 361 and 479 kg/acre. The amount of salt that infiltrated or remained on the surface was 259, 289 and 431 kg/acre for fields DA7, Muth2, and Muth9. Decreasing tailwater fractions would substantially reduce the amount of salt loaded to the river system via tailwater and would reduce the amount of salts loaded to the fields.
- The linear regression relationship between  $C_{Se}$  and  $C_{TDS}$  in applied irrigation water was stronger than that in tailwater. This may be due to spatially or temporally inconsistent sorption or redox reactions of dissolved Se as water flows across the field, causing a net removal of dissolved Se. Since the estimated field-scale mass balance of dissolved Se relied on the  $C_{Se}$  vs  $C_{TDS}$  linear regressions of applied water and tailwater developed from small sample sizes, the results should be interpreted with caution.
- The relationship between the change in  $C_{TDS}$  between applied irrigation water and tailwater and the average soil salinity to a depth of 0.65 m was weak ( $R^2=0.39$ ) and not quite

statistically significant. Additional variation may result from degree of cracking, duration of irrigation, volume of tailwater, and the amount of ponding at the tailwater edge of the field.

- There appears to be a relationship between increased ponding at the tailwater edge of the field and decreased total recoverable Se concentrations, which may be due to the settling of suspended particles.

#### **4.2 Recommendations for Future Work**

Based on results from this thesis, the following recommendations are made for providing further understanding of salinity and Se fate and transport in this and similar irrigated, tile-drained groundwater systems:

- Enhance and expand field-scale monitoring to better characterize parameters and processes of flow and reactive transport:
  - In order to better ensure that submergence of measuring flumes does not occur, a staff gauge should be added to the downstream side of each flume to permit periodic manual readings of downstream flow depths for use in calibrating the downstream pressure transducer readings;
  - A trapezoidal flume should be installed at the end of the head ditch for field DA7 in order to monitor spillover water from DA7;
  - The bed of the tailwater flume for DA7 should be raised approximately one inch to inhibit submergence;
  - More tailwater samples for dissolved Se should be collected in concert with in-situ electrical conductivity readings and analyzed to explore the development of a significant and sufficiently strong relationship from which a field scale Se mass balance can be estimated using in-situ electrical conductivity readings;

- All monitoring wells should be re-sealed with bentonite on a periodic basis to prevent contamination from surface water;
- A pipe flow meter should be carefully installed in the main trunk of the tile drain near the outlet in order to measure flow rate in real time and estimate solute loading to the river system; and
- An effort should be made to measure the total flow diverted from the Catlin Canal onto all of the fields drained by the FDD along with the associated surface drainage. This will prove very difficult due to the complexity and extent of the water distribution and drainage network serving the area. There are check dams conveniently located in the Catlin Canal in the vicinity of the upstream and downstream ends of the FDD that would facilitate an estimate of total diverted flow using mass balance calculations if canal seepage losses also can be adequately estimated. However, between these check dams there are two offtake gates that irrigate fields to the south of the canal and at least two drainage channels that discharge water into the Catlin from fields irrigated by the Otero canal. These flows would need to be measured. Furthermore, the two offtake gates with the largest diverted flows along this reach of the Catlin Canal supply the majority of their diverted water to fields outside of the FDD. Accurately monitoring of water and solute loads applied to all fields within the FDD from the Catlin Canal would require many flow measurement and sampling devices, along with extensive labor, but would supply valuable spatiotemporal data about the nature of irrigation return flows and loads in irrigated areas underlain by subsurface drainage.
- Develop a local-scale groundwater flow and reactive solute transport model to use field data in simulating alternative BMP scenarios including:

- Improved subsurface drain configurations (size, material, depth, spacing, filter packs),
- Improved irrigation application efficiency,
- Improved fertilizer application timing and efficiency, and
- Buffered riparian corridors.

## REFERENCES

- Alexander, R. B., Smith, R. A., Schwarz, G. E.; Boyer, E. W., Nolan, J. V., and Brakebill, J. W. (2008). "Differences in phosphorus and N delivery to the Gulf of Mexico from the Mississippi River Basin." *Environmental Science and Technology*, 42, 822-830.
- Ayars, J.E., Hoffman, G.J., and Corwin, D.L. (2012). *Agricultural salinity assessment and management: Leaching and rootzone salinity control*, 2<sup>nd</sup> Ed. American Society of Civil Engineers. 371-402.
- Bailey, R. T., Hunter, W. J., and Gates, T. K. (2012). "The influence of NO<sub>3</sub><sup>-</sup> on selenium in irrigated agricultural groundwater systems." *Journal of Environmental Quality*, 41, 783-792.
- Bailey, R.T., Gates, T.K., and Ahmadi, M. (2014). "Simulating reactive transport of selenium coupled with nitrogen in a regional-scale irrigated groundwater system." *Journal of Hydrology*, 515(16) 29-46.
- Bailey, R.T., Romero, E.C., and Gates, T.K. (2015). "Assessing best management practices for remediation of selenium loading in groundwater to streams in an irrigated region." *Journal of Hydrology*, 521, 341-359.
- Burkhalter, J.P., and Gates, T.K. (2005). "Agroecological impacts from salinization and waterlogging in an irrigated river valley." *Journal of Irrigation Drainage Engineering*, 131, 197-209.
- Burt J.E., and Barber G.M. (1996). *Elementary statistics for geographers* 2<sup>nd</sup> ed. The Guilford Press New York, NY.
- Butler, D.L, Wright, W. G., Stewart K.C., Osmundson B.C., Krueger R. P., and Crabtree D.W. (1996). *Detailed study of selenium and other constituents in water, bottom sediment, soil, alfalfa, and biota associated with irrigation drainage in the Uncompahgre Project area and in the Grand Valley, west-central Colorado, 1991-1993*. Water Resources Investigations (U.S. Geological Survey) Report 96-4138.
- Carpenter, S. R., Caraco, N. F., Correll, D. L., Howarth, R. W., and Sharpley, A. N. (1998). "Nonpoint pollution of surface waters with phosphorus and N." *Ecological Applications*, 559-568.
- Chatterjee, S., and Hadi, A.S. (1986). "Influential observations, high leverage points, and outliers in linear regression." *Statistical Science*, 1(3)379-416.
- Christen, E., and Skehan, D. (2001). "Design and management of subsurface horizontal drainage to reduce salt loads." *Journal of Irrigation and Drainage Engineering*. 127, 148-155.

- Cooper, A. B. (1990). "NO<sub>3</sub><sup>-</sup> depletion in the riparian zone and stream channel of a small headwater catchment." *Hydrobiologia*, 202, 13-26.
- Deverel, S.J., and Fujii, R. (1988). "Processes affecting the distribution of selenium in shallow groundwater of agricultural areas, Western San Joaquin Valley, California." *Water Resources Research*, 24(4), 516-524.
- Devitt, D., Letey, J., Lund, L.J., and Blair, J.W. (1976). "Nitrate-nitrogen movement through soil as affected by soil profile characteristics." *Journal of Environmental Quality*, 5(3), 283-288
- Divine, C. E., Gates, T.K., Keller, N., and Michael, G. Y. (2009). "Evaluation of selenium loading to the Arkansas River near Pueblo, Colorado." *Journal of Environmental Hydrology*, 17(26), 1-20.
- Donnelly, J. P., and Gates, T.K. (2005). "Assessing irrigation induced selenium and iron in the Lower Arkansas River Valley in Colorado." *Environmental and Water Resources Institute: Impacts of Global Climate Change Conference*, ASCE
- El-Ashry, M.T., van Schilfgaarde, J., and Schiffman, S. (1985). "Salinity pollution from irrigated agriculture." *Journal of Soil and Water Conservation*, 40, 48-52.
- Faci, J., Aragues, R., Alberto, F., Quilez, D., Machin, J., and Arrue, J.L. (1985). "Water and salt balance in an irrigated area of the Ebro River Basin (Spain)." *Irrigation Science*, 6, 29-37.
- Fujii, R., Deverel, S.J., and Hatfield, D.B. (1987). "Distribution of selenium in soils of agricultural fields, western San Joaquin Valley, California." *Soil Science Society of America*, 52(5), 1274-1283.
- Fujii, R., and S. J. Deverel (1989). *Mobility and Distribution of Selenium and Salinity in Ground-water and Soil of Drained Agricultural Fields, Western San Joaquin Valley of California*. In: *Selenium in Agriculture and the Environment*. W. L. Jacobs. SSSA Spec. Publ. 23. SSSA and ASA, Madison, WI. p. 195-212.
- Gates, T.K., Cody, B.M., Donnelly, J.P., Herting, A.W., Bailey, R.T., and Mueller Price, J. (2009). "Assessing selenium contamination in the irrigated stream-aquifer system of the Arkansas River, Colorado." *Journal of Environmental Quality*, 38. 2344-2356.
- Gates, T.K., Garcia, L.A., Hemphill, R.A., Morway, E.D., and Elhaddad, A. (2012). *Irrigation practices, water consumption, and return flows in Colorado's Lower Arkansas River Valley*. Colorado Water Institute Report No. 221.
- Gates, T. K., Steed, G. H., Niemann, J. D., and Labadie, J. W. (2016). *Data for improved water management in Colorado's Arkansas River Basin: Hydrological and water quality studies*. Special Report No. 24, Colorado Water Institute, Fort Collins, CO.

- Gilfedder, M., Mein, R.G., and Connell, L.D. (2000). "Border irrigation field experiment. II: Salt transport." *Journal of Irrigation and Drainage Engineering*, 126(2), 92-97
- Gilliom, R.J. (1989). *Preliminary assessment of sources, distribution, and mobility of selenium in the San Joaquin Valley, California*. USGS Water Resources Investigations Report 88-4186.
- Greenberg, A.E., Clesceri, L.S., Eaton, A.D., and Franson, M.A. (1992). *Standard Methods 2510: for the examination of water and wastewater*. American Public Health Association, American Water Works Association, Water Environment Federation.
- Harrell F.E. Jr. (2001). *Regression modeling strategies: with applications to linear models, logistic regression, and survival analysis*. Springer-Verlag, New York.
- Hornbuckle, J.W., Christen, E.W., and Faulkner, R.D. (2007). "Evaluating a multi-level subsurface drainage system for improved drainage water quality." *Agricultural Water Management*, 89, 208-216.
- Houk, E., Frasier, F., and Schuck, E. (2006). "The agricultural impacts of irrigation induced waterlogging and soil salinity in the Arkansas Basin." *Agricultural Water Management*, 85, 175-183.
- Isidoro D., Quilez D., and Aragues R. (2006). "Environmental impact of irrigation in La Violada District (Spain): I. Salt Export Patterns." *Journal of Environmental Quality*, 35, 766-775
- Jiao, P., Xu, D., Wang, S., Wang, Y., Lin, K., and Tang, G. (2012). "Nitrogen loss by surface runoff from different cropping systems." *Soil Research*, 50, 58-66.
- Johnston, W.R., Ittihadieh, F., Daum, R.M., and Pillsbury, A. F. (1965). *Nitrogen and phosphorus in tile drainage effluent*. Division S-6: Soil and Water Management and Conservation.
- Jones R., and Marshall G. (1992). "Land salinization, waterlogging and the agricultural benefits of a surface drainage scheme in Benerembah Irrigation District." *Review of Marketing and Agricultural Economics*, 60(2), 173-189.
- Jury, W.A. (1975). "Solute travel-time estimates for tile-drained fields: I. Theory." *Soil Science Society of America Journal*, 39, 1020-1024.
- Kahlowan, M. A., and Azam, M. (2002). "Individual and combined effect of waterlogging and salinity on crop yields in the Indus basin." *Irrigation and Drainage*, 51, 329-338.
- Keller, C. K., Butcher, C. N., Smith, J. L., and Allen-King, R. M. (2008). "Nitrate in tile drainage of the semi-arid Palouse Basin." *Journal of Environmental Quality*, 37, 353-361.
- Kirk R.E. (2013). *Experimental design: procedures for the behavioral sciences*. 4<sup>th</sup> ed. Sage Publications inc. Thousand Oaks, CA

- Lemly, A.D. (1992). "Guidelines for evaluating selenium data from aquatic monitoring and assessment studies." *Environmental Monitoring Assessment*, 28, 83-100.
- Mellander, P.-E., Melland, A. R., Jordan, P., Wall, D. P., Murphy, P. N., and Shortle, G. (2012). "Quantifying nutrient transfer pathways in agricultural catchments using high temporal resolution data." *Environmental Science and Policy*, 24, 44-57.
- Morway, E.D, and Gates T.K. (2012). "Regional assessment of soil water salinity across an intensively irrigated river valley." *Journal of Irrigation and Drainage Engineering*, 138(5), 393-405.
- Morway, E.D., Gates, T.K., and Niswonger, R.G. (2013). "Appraising options to reduce shallow groundwater tables and enhance flow conditions over regional scales in an irrigated alluvial aquifer system." *Journal of Hydrology*, 495(12) 216-237.
- Mueller, D. K., Hamilton, P. A., Helsel, D. R., Hitt, K. J., and Ruddy, B. C. (1992). "Nutrients in ground water and surface water of the United States-an analysis of data through 1992." USGS Water-Resources Investigations Report 95-4031.
- Mueller-Price, J.M., and Gates, T.K. (2008). "Assessing uncertainty in mass balance calculation of river nonpoint source loads." *Journal of Environmental Engineering*, 134(4) 247-258.
- Niemann, J. D., Lehman, B. M., Gates, T. K., and Hallberg, N. U. (2011). "Impact of shallow groundwater on evapotranspiration losses from uncultivated land in an irrigated river valley." *Journal of Irrigation and Drainage Engineering*, 137(8), 501–512.
- Novotny, V. (2002). *Water quality: Diffuse pollution and watershed management*. 2<sup>nd</sup> ed. John Wiley and Sons, Inc. Hoboken, NJ.
- Oremland, R.S., Steinberg N.A., Maest A.S., Miller L.G., and Hollibaugh, J.T. (1990). "Measurement of in situ rates of selenate removal by dissimilatory bacterial reduction in sediments." *Environmental Science and Technology*, 24, 1157–1164.
- Presser, T. S., and Ohlendorf, H.M. (1987). "Biogeochemical cycling of selenium in the San Joaquin Valley, California, USA." *Environmental Management*, 11(6), 805-821.
- R Development Core Team (2008). R: A language and environment for statistical computing. R Foundation for Statistical Computing, Vienna, Austria. ISBN 3-900051-07-0, URL <http://www.R-project.org>.
- Rhoades, J.D., Lesch, S.M., Burch, S.L., Letey, J., LeMert, R. D., Shouse, P.J., Oster, J.D., and O'Halloran, T. (1997). "Salt distributions in cracking soils and salt pickup by runoff waters." *Journal of Irrigation and Drainage Engineering*, 123(5), 323-328.

- Saiki, M.K., and Lowe, T.P. (1987). "Selenium in aquatic organisms from subsurface agricultural drainage water, San Joaquin Valley, California." *Archives of Environmental Contamination and Toxicology*, 16, 657-670.
- Shapiro S.S. and Wilk M.B., (1965). "An analysis of variance test for normality." *Biometrika*, 52, 591-611.
- Skaggs, R W., Breve M. A., and Gilliam, J.W. (1994). "Hydrologic and water quality impacts of agricultural drainage". *Critical Reviews in Environmental Science and Technology*. 24(1), 1-32.
- Skogerboe, G.V. and Walker, W.R. (1973). "Salt Pickup form agricultural lands in the Grand Valley of Colorado." *Journal of Environmental Quality*, 2, 377-382.
- Spalding, R. F. and Exner, M. E. (1993). "Occurrence of nitrate in groundwater - a review." *Journal of Environmental Quality*, 22, 392-402.
- Tanji K.K. (2002). *Salinity in the Soil Environment. In: Salinity: Environment - Plants - Molecules*. Springer, Netherlands. pp 21-51
- Tanji, K.K., and Wallender, W. W. (2012). "Agricultural Salinity Assessment and Management: Nature and extent of agricultural salinity and sodicity." American Society of Civil Engineers. 1-24.
- Tedeschi, A., Beltran, A., and Aragues, R. (2000). "Irrigation management and hydrosalinity balance in a semi-arid area of the middle Ebro river basin (Spain)." *Journal of Agricultural Water Management*, 49, 31-50.
- United States Environmental Protection Agency (USEPA). (2016). Federal Register. 81(134), 45285-45287.
- Wichelns, D. (1999). "An economic model of waterlogging and salinization in arid regions." *Journal of Ecological Economics*, 30, 475-491.
- Wittler, J.M., Cardon, E.C., Gates, T.K., Cooper, C.A., and Sutherland, P.L. (2006). "Calibration of electromagnetic induction for regional assessment of soil water salinity in an irrigated valley." *Journal of Irrigation and Drainage Engineering*, 132, 436-444.
- Wright, W.G. (1999). "Oxidation and mobilization of selenium by nitrate in irrigation drainage." *Journal of Environmental Quality*, 28, 1182-1187.

## APPENDICES

APPENDIX A: SCATTERPLOTS AND LINEAR REGRESSIONS WITH STATISTICAL OUTLIERS

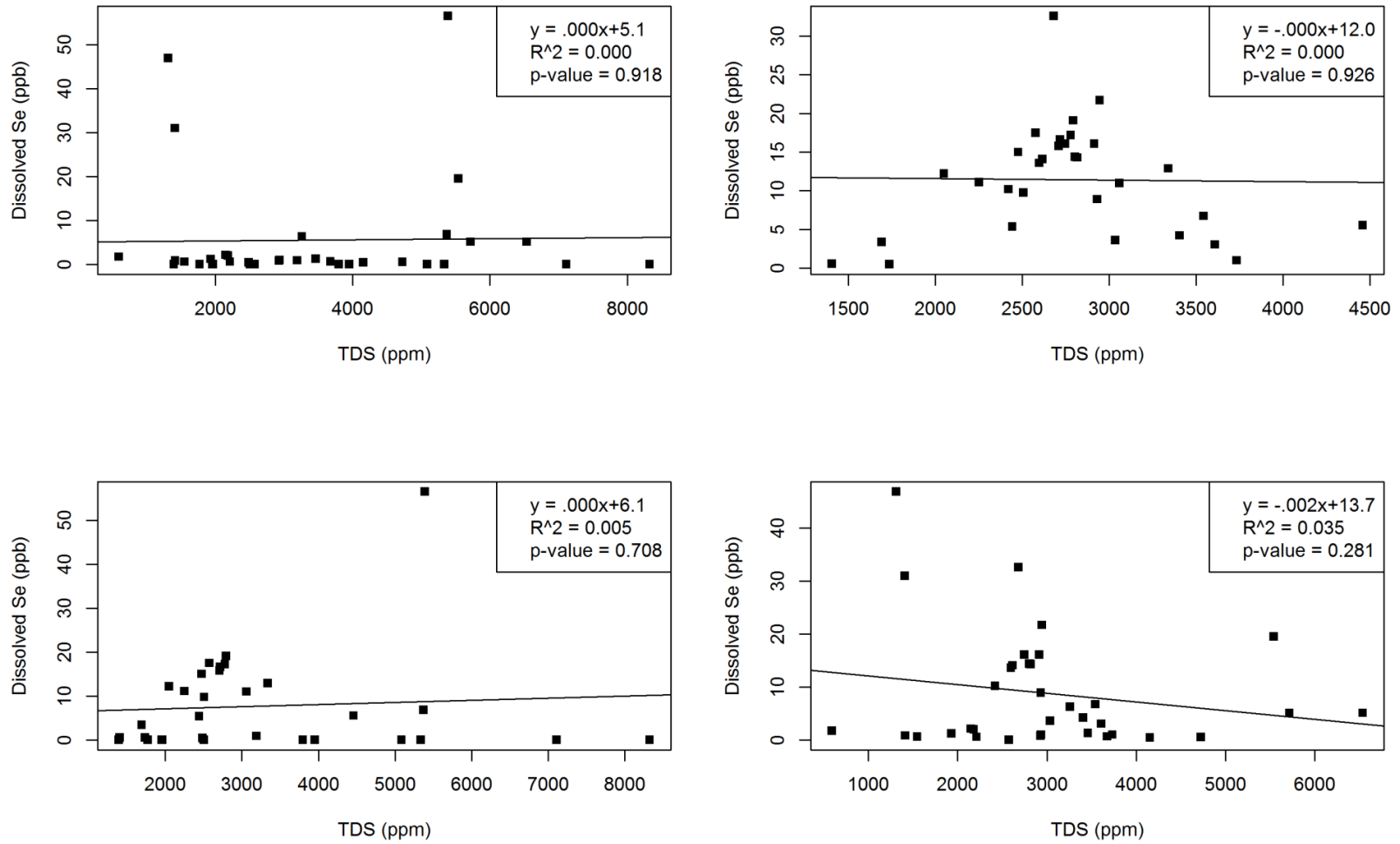


Figure 77. Scatter plots of  $C_{Se}$  vs  $C_{TDS}$  from groundwater samples separated by presence of tile drains and by depth of the monitoring well. Clockwise from top left: groundwater with tile drains, groundwater without tile drains, deep groundwater, and shallow groundwater.

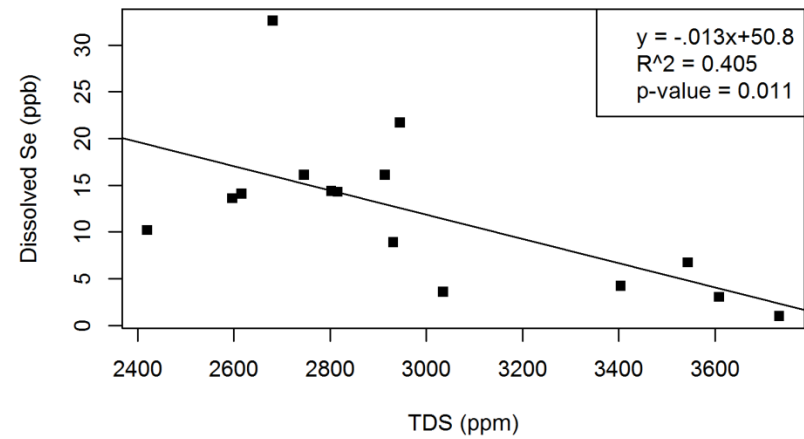
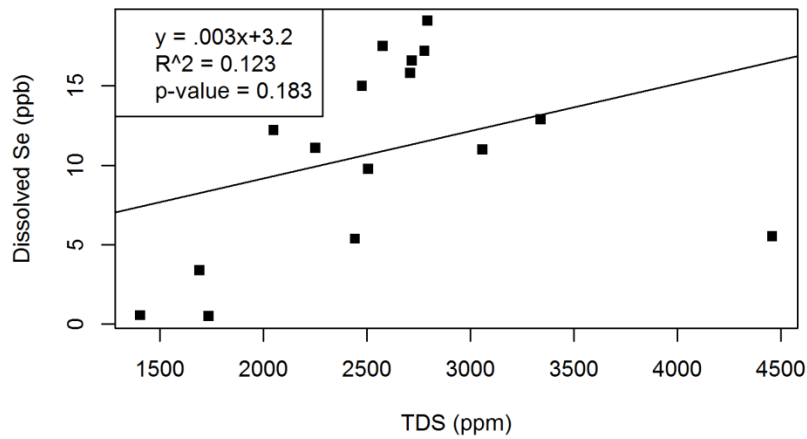
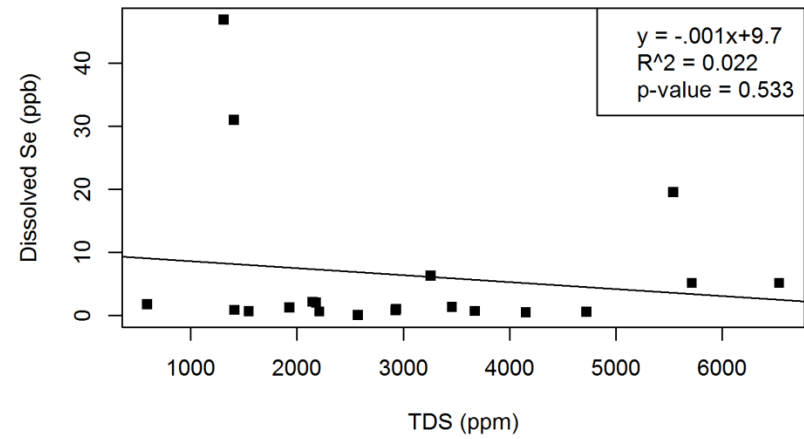
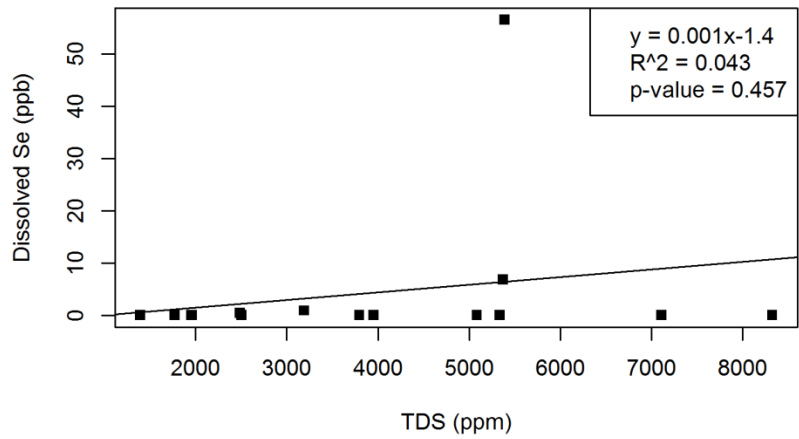


Figure 78. Scatter plots of  $C_{Se}$  vs  $C_{TDS}$  from groundwater samples separated by presence of drains and depth of monitoring well. Clockwise from top left: Deep GW with tile drains, Shallow GW with tile drains, Shallow GW without tile drains, Deep GW without tile drains.

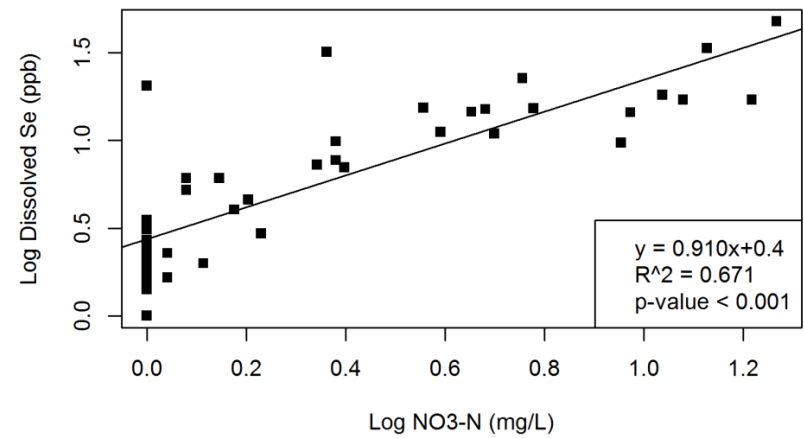
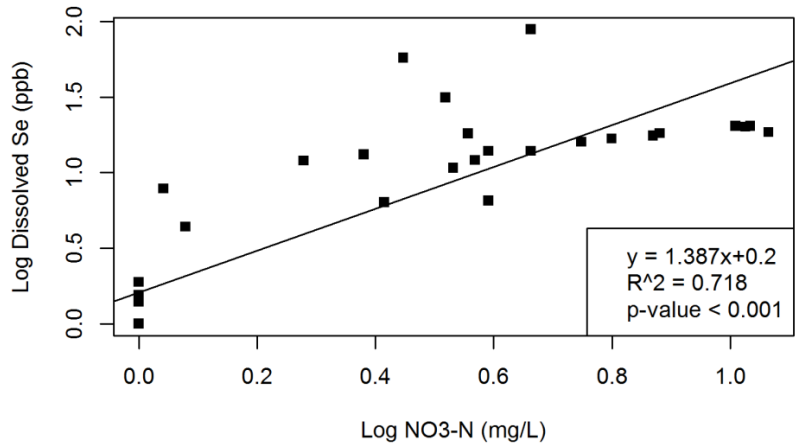
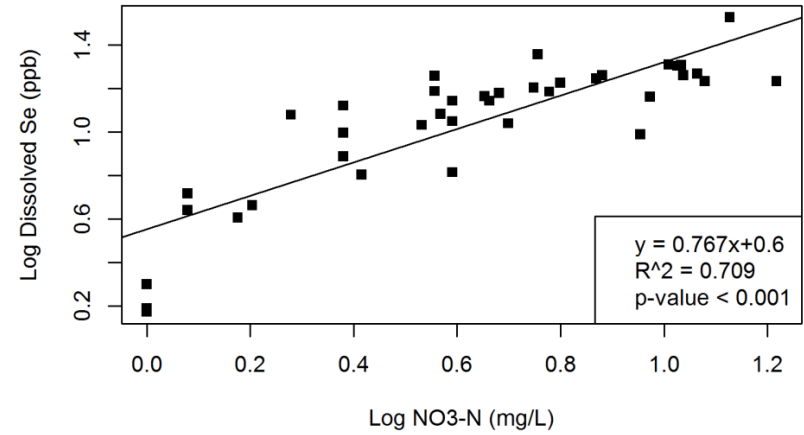
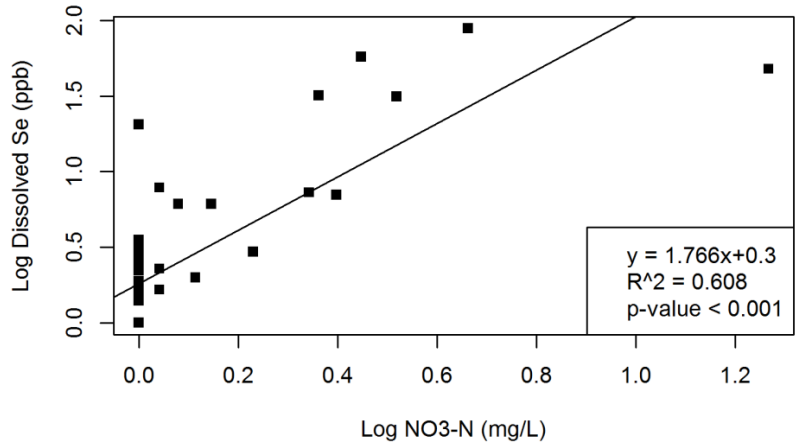


Figure 79. Scatter plots and regressions of  $C_{Se}$  vs  $C_N$  from groundwater samples separated by presence of tile drains and then by depth of monitoring well. Clockwise from top left: Groundwater with tile drains, Groundwater without tile drains, Shallow Groundwater, Deep Groundwater.

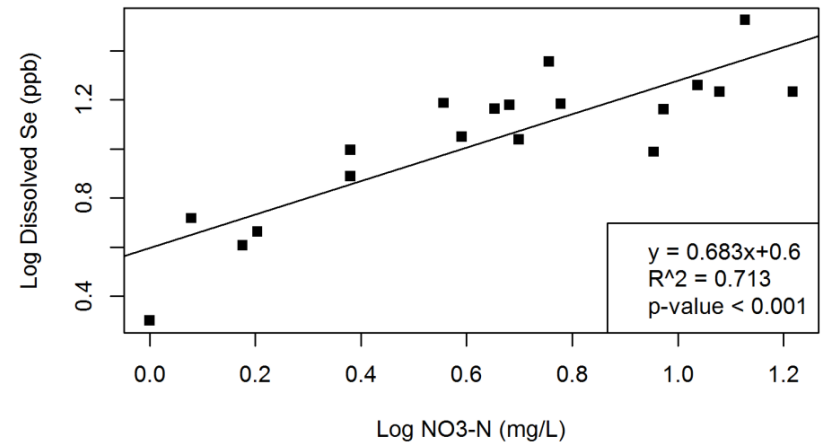
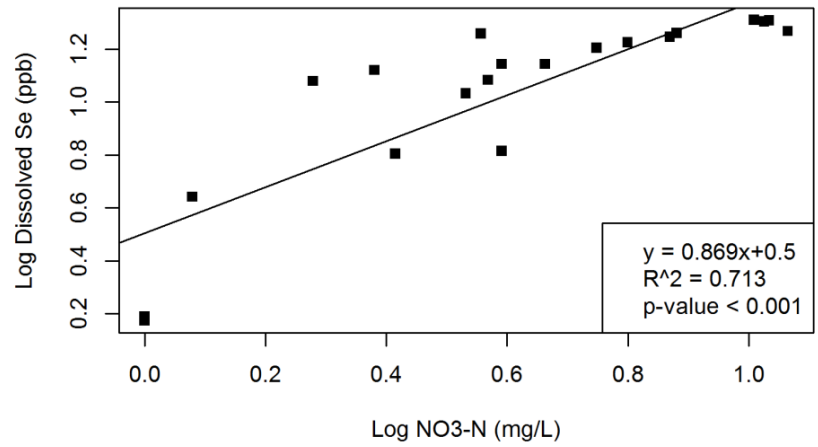
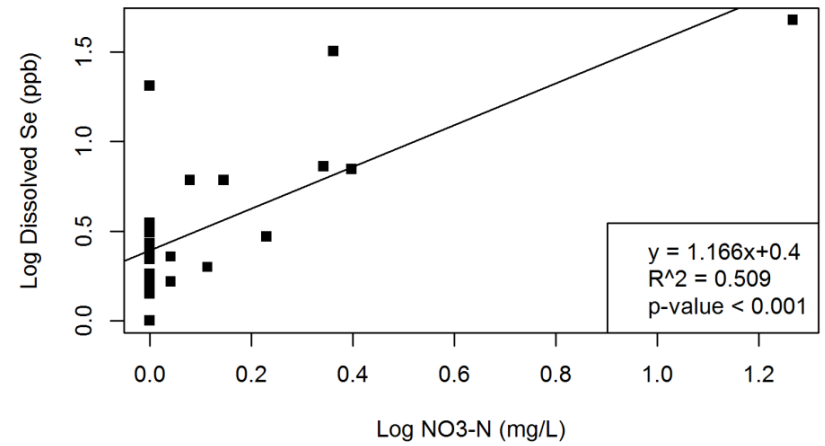
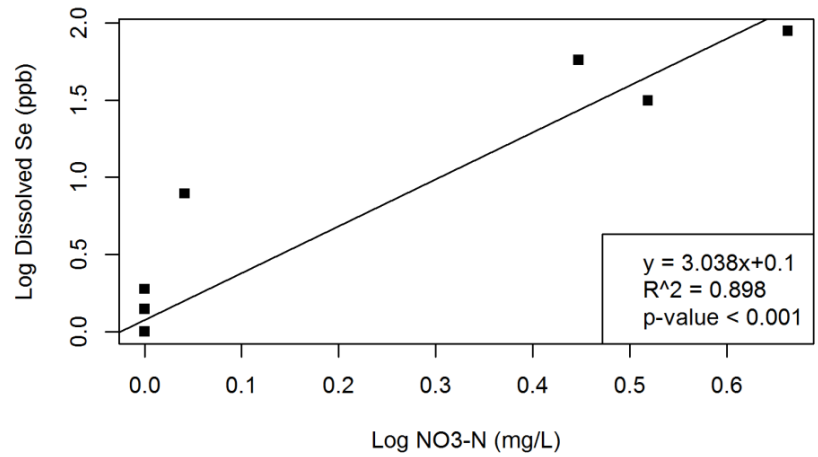


Figure 80. Scatter plots of  $C_{Se}$  vs  $C_N$  from groundwater samples separated by presence of drains and depth of monitoring well. Clockwise from top left: Deep Drained GW, Shallow Drained GW, Shallow Undrained GW, and Deep Drained GW.

APPENDIX B: CONFIDENCE INTERVALS OF  $C_{TDS}$  AND  $C_{Se}$  ESTIMATION

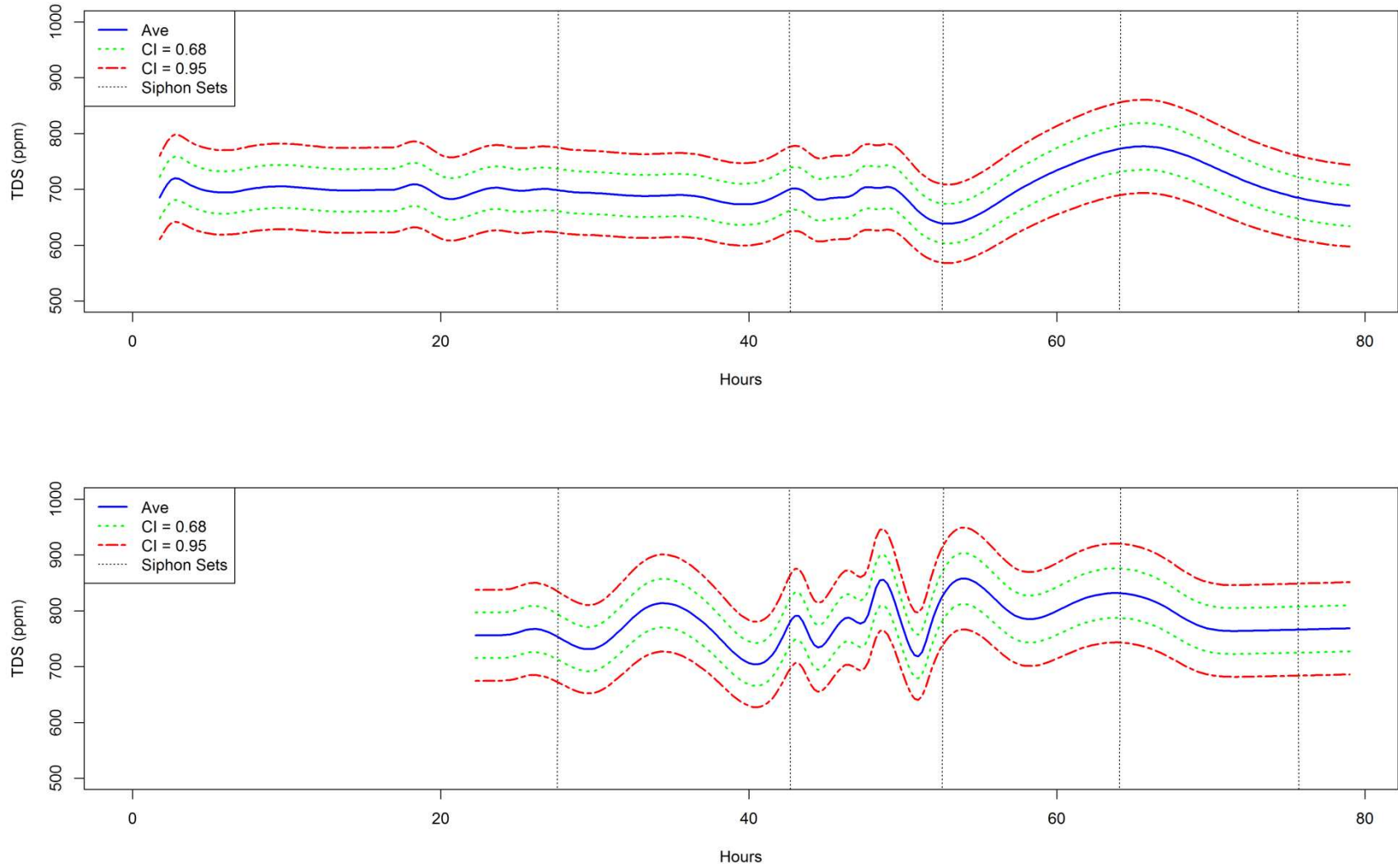


Figure 81.  $C_{TDS}$  in applied water and tailwater with linear regression confidence intervals plotted for field DA7. Top: Applied Water, Bottom: Tailwater

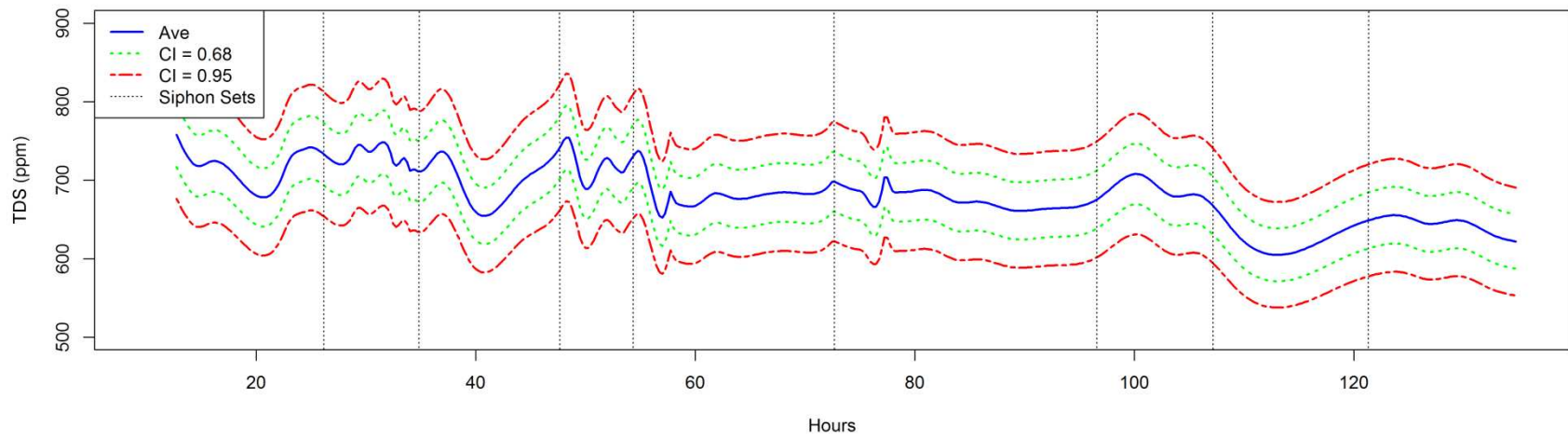
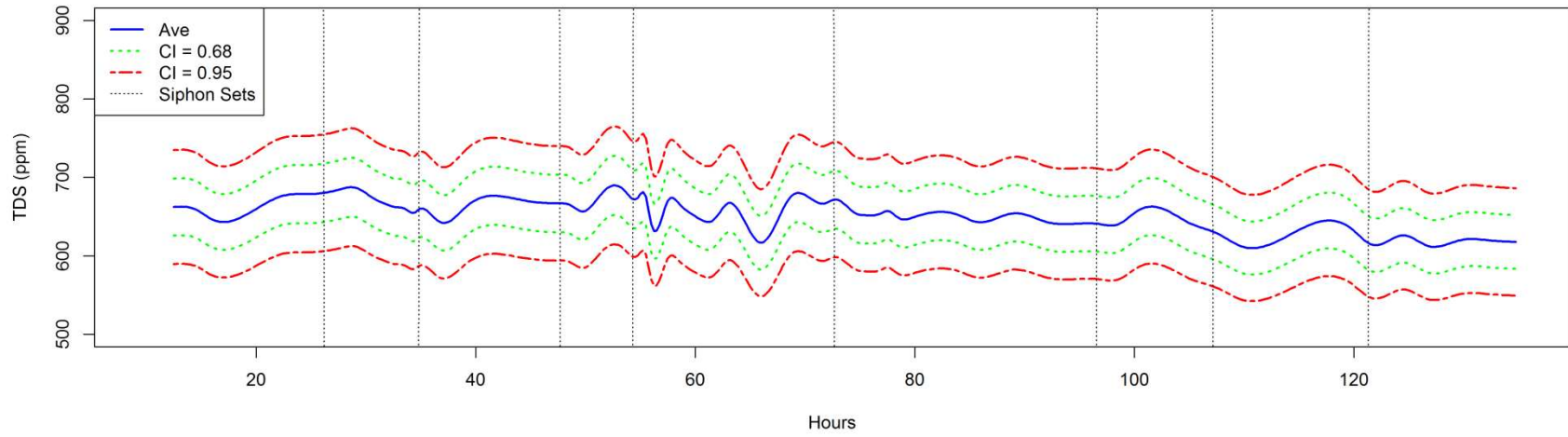


Figure 82.  $C_{TDS}$  in applied water and tailwater with linear regression confidence intervals plotted for field Muth2. Top: Applied Water, Bottom: Tailwater.

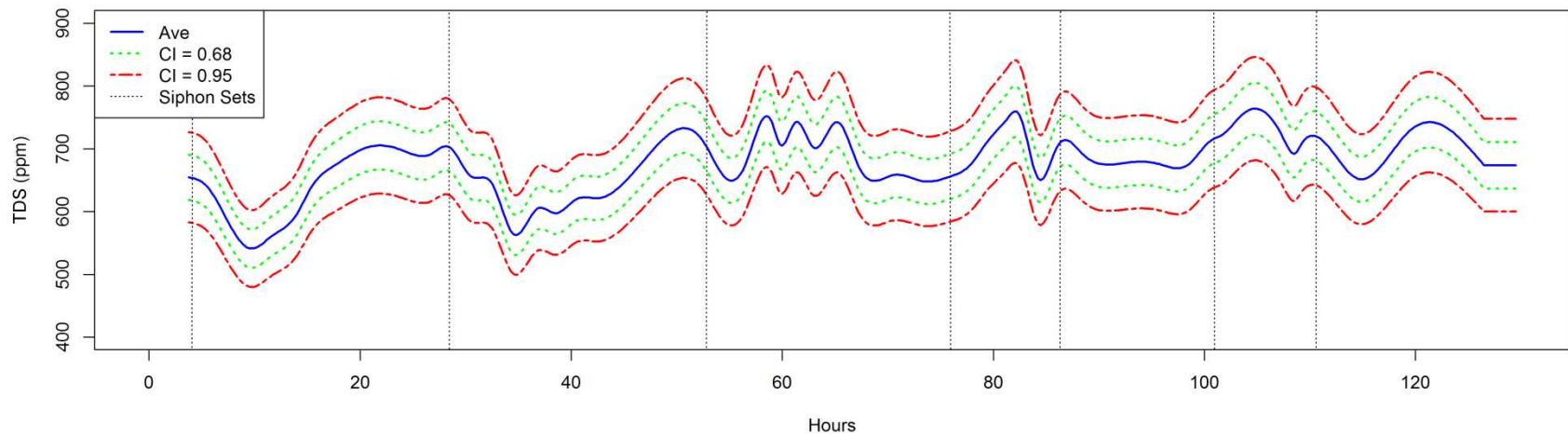
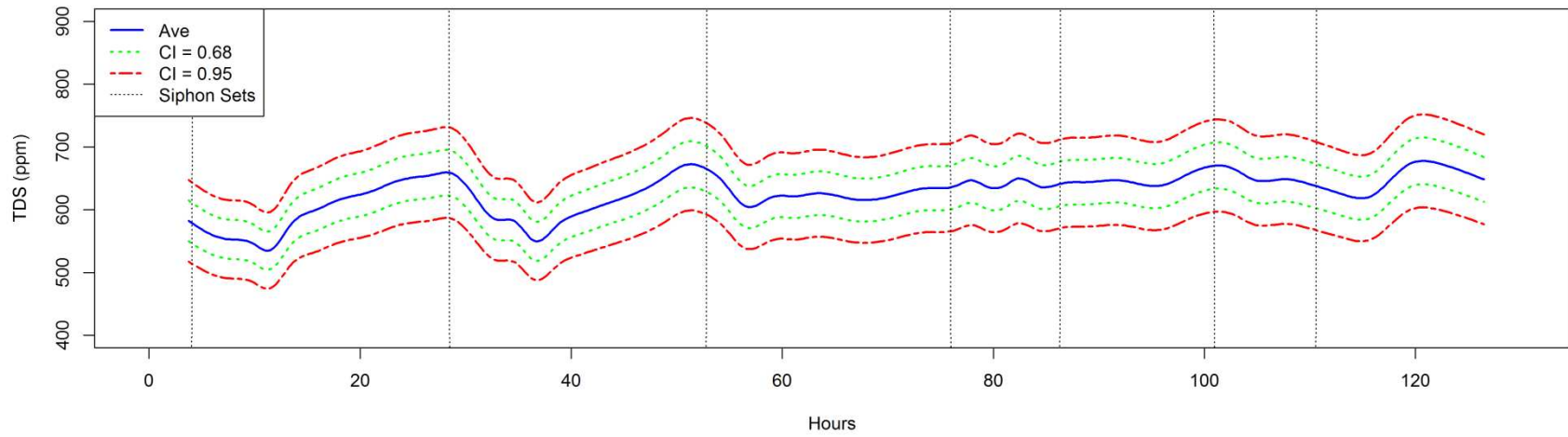


Figure 83.  $C_{TDS}$  in applied water and tailwater with linear regression confidence intervals plotted for field Muth9. Top: Applied Water, Bottom: Tailwater.

Table 18. Slopes of  $C_{TDS}$  vs specific conductance for linear regression confidence intervals.

<b>Confidence Level</b>	<b>2.5%</b>	<b>97.5%</b>	<b>16%</b>	<b>84%</b>
<b>Slope</b>	0.8228	0.9941	0.8655	0.9513

Table 19. Slopes of  $C_{Se}$  vs  $C_{TDS}$  for linear regression confidence intervals for applied water and tailwater.

<b>Confidence Level</b>	<b>2.5%</b>	<b>97.5%</b>	<b>16%</b>	<b>84%</b>
<b>Slope for App</b>	0.0083	0.0202	0.0117	0.0168
<b>Slope for TW</b>	0.0037	0.0334	0.0121	0.0249

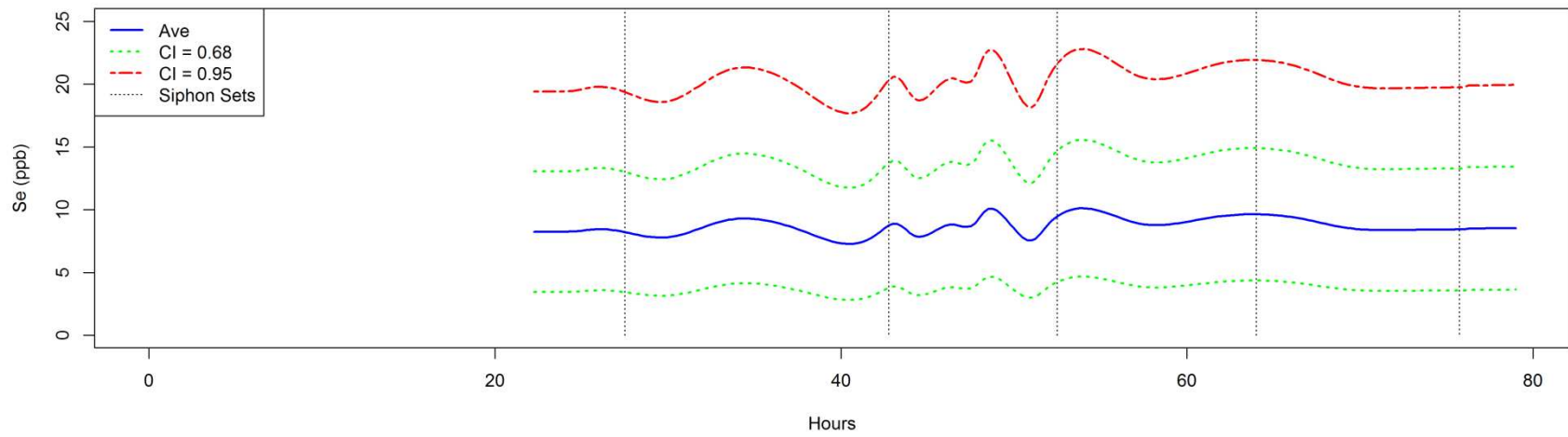
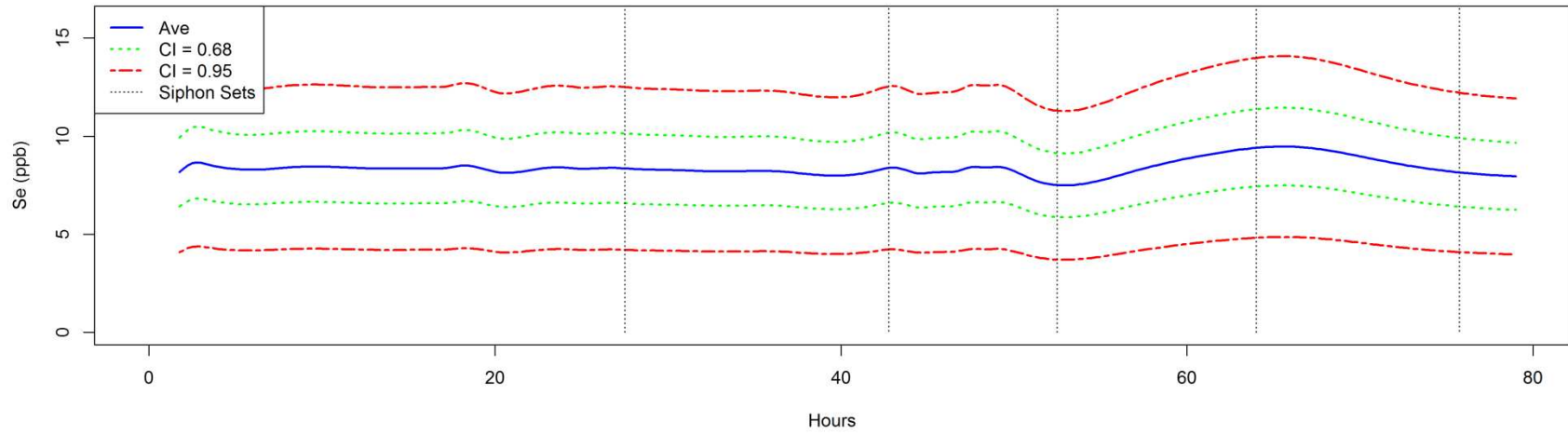


Figure 84.  $C_{Se}$  for applied water and tailwater with linear regression confidence intervals for field DA7. Top: Applied Water, Bottom: Tailwater.

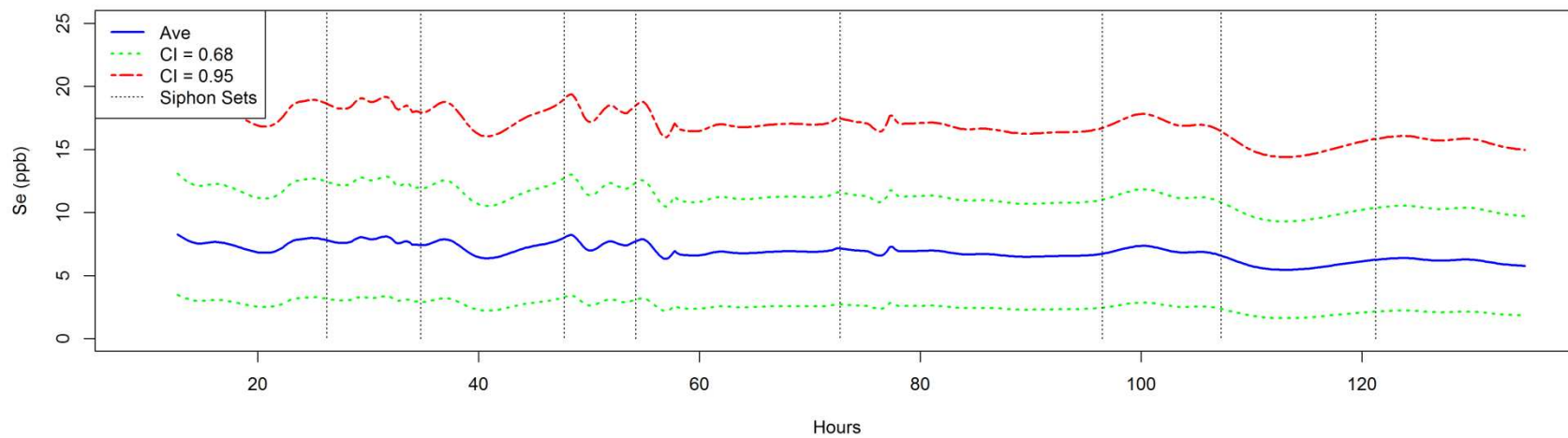
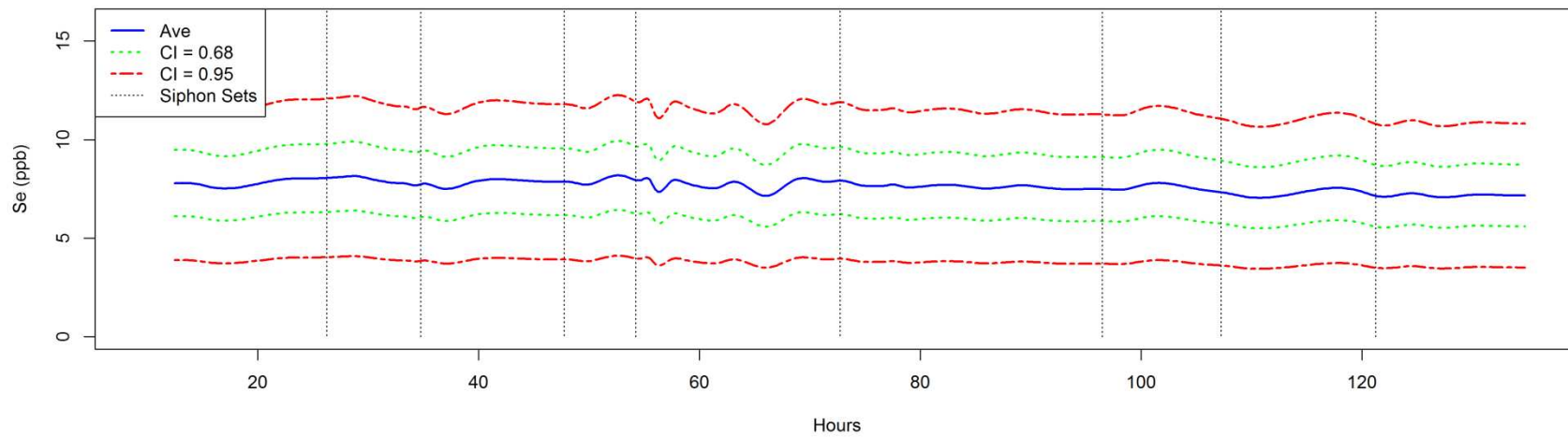


Figure 85.  $C_{Se}$  for applied water and tailwater with linear regression confidence intervals for field Muth2. Top: Applied Water, Bottom: Tailwater.

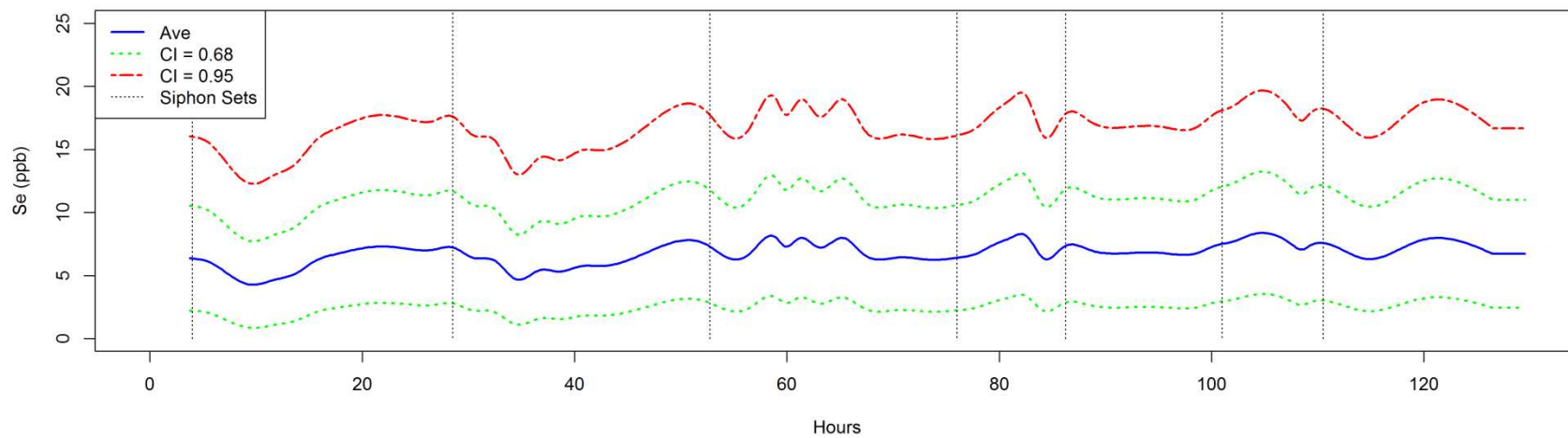
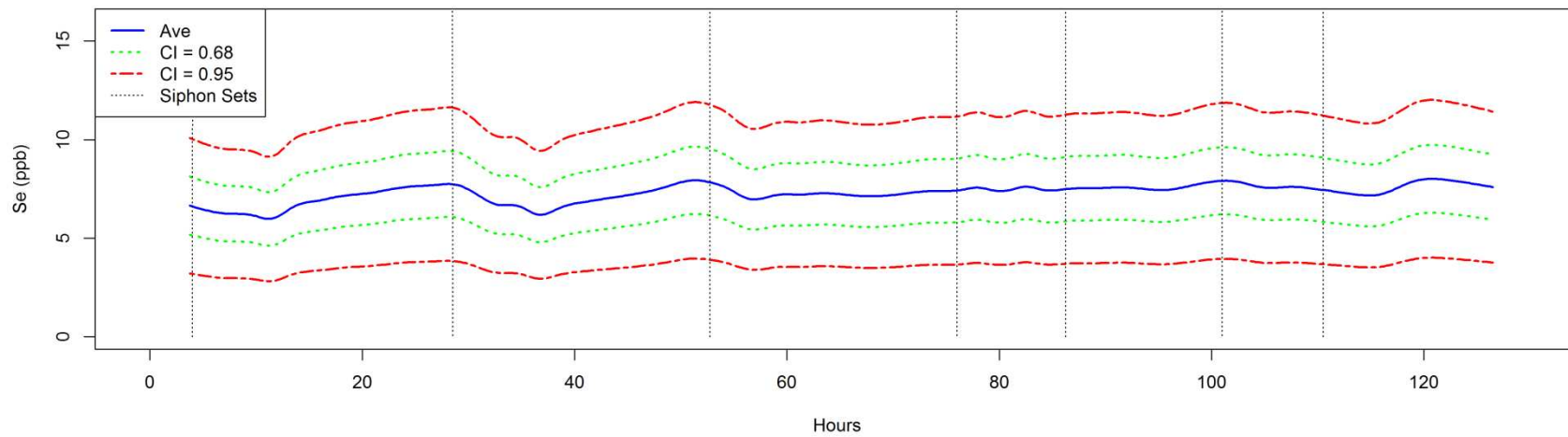


Figure 86.  $C_{Se}$  for applied water and tailwater with linear regression confidence intervals for field Muth9. Top: Applied Water, Bottom: Tailwater.

APPENDIX C: STATISTICAL DIAGNOSTIC PLOTS FOR ANOVA STATISTICS

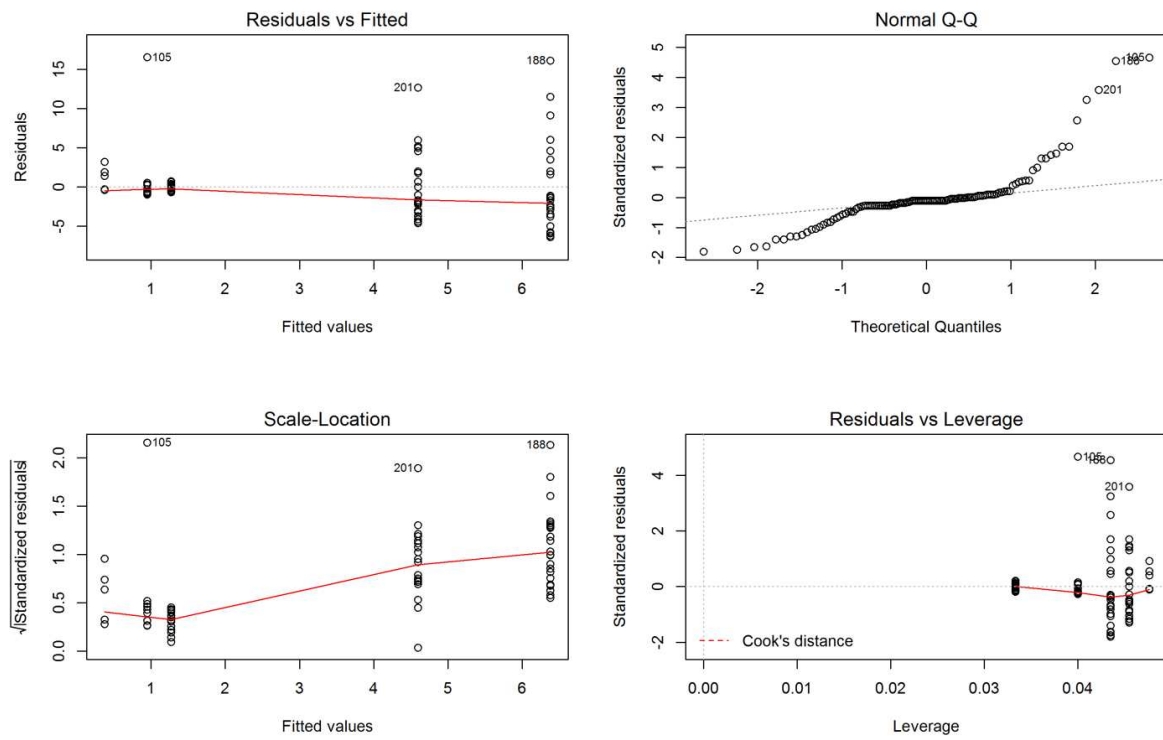


Figure 87. Diagnostic plots for  $C_N$  for surface water and groundwater samples separated by presence of drains and depth of monitoring well.

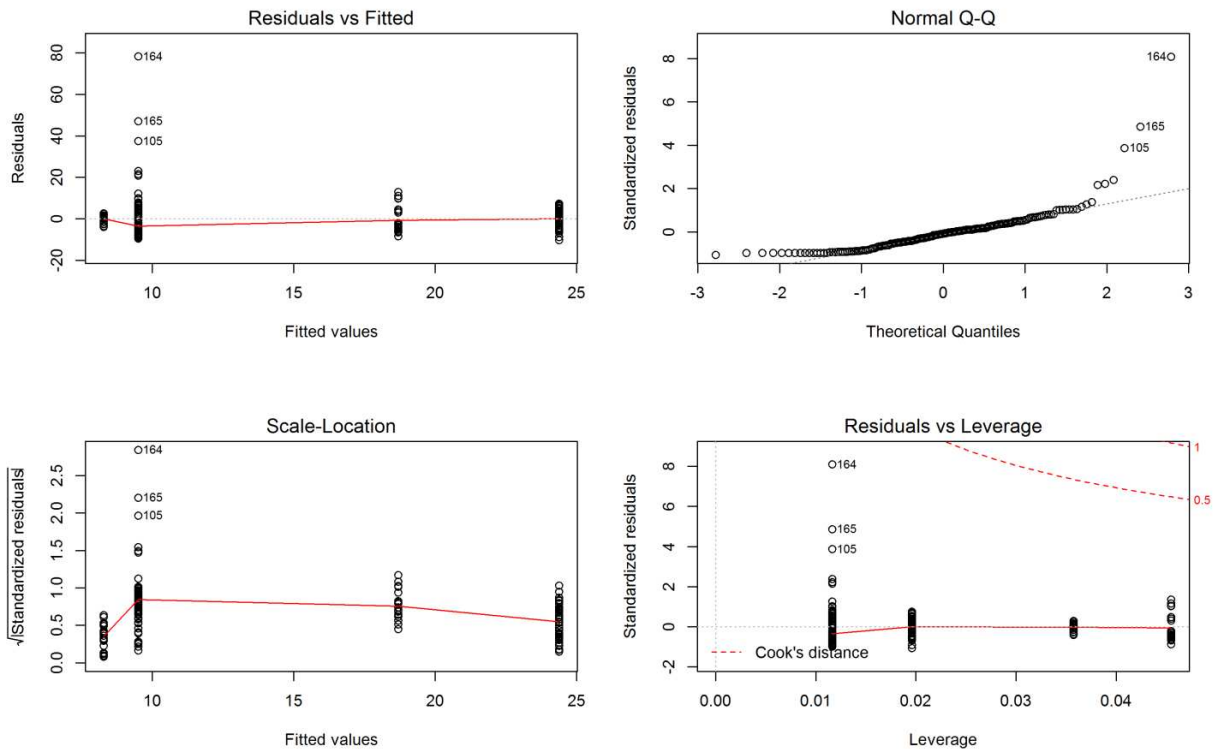


Figure 88. Diagnostic plots of  $C_{se}$  samples separated by sample type: GW, SW, TD, TWTD.

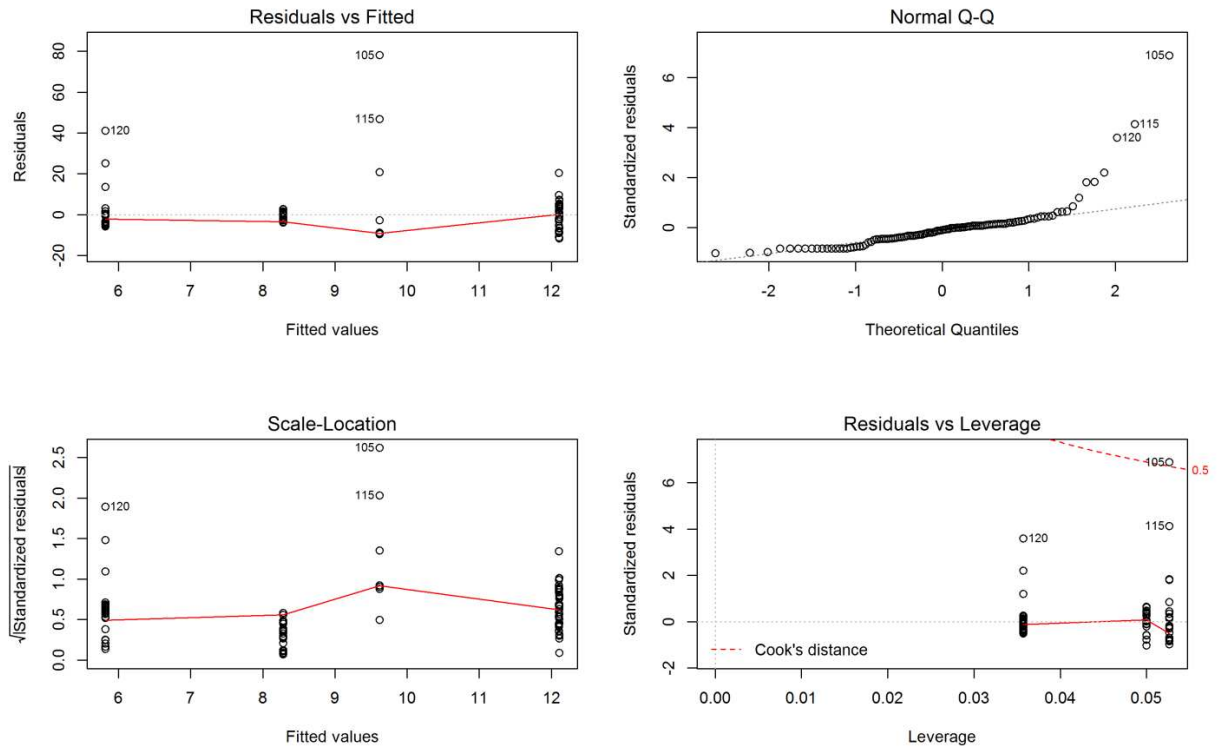


Figure 89. Diagnostic plots of  $C_{se}$  from groundwater samples separated by presence of drains and depth of monitoring wells.

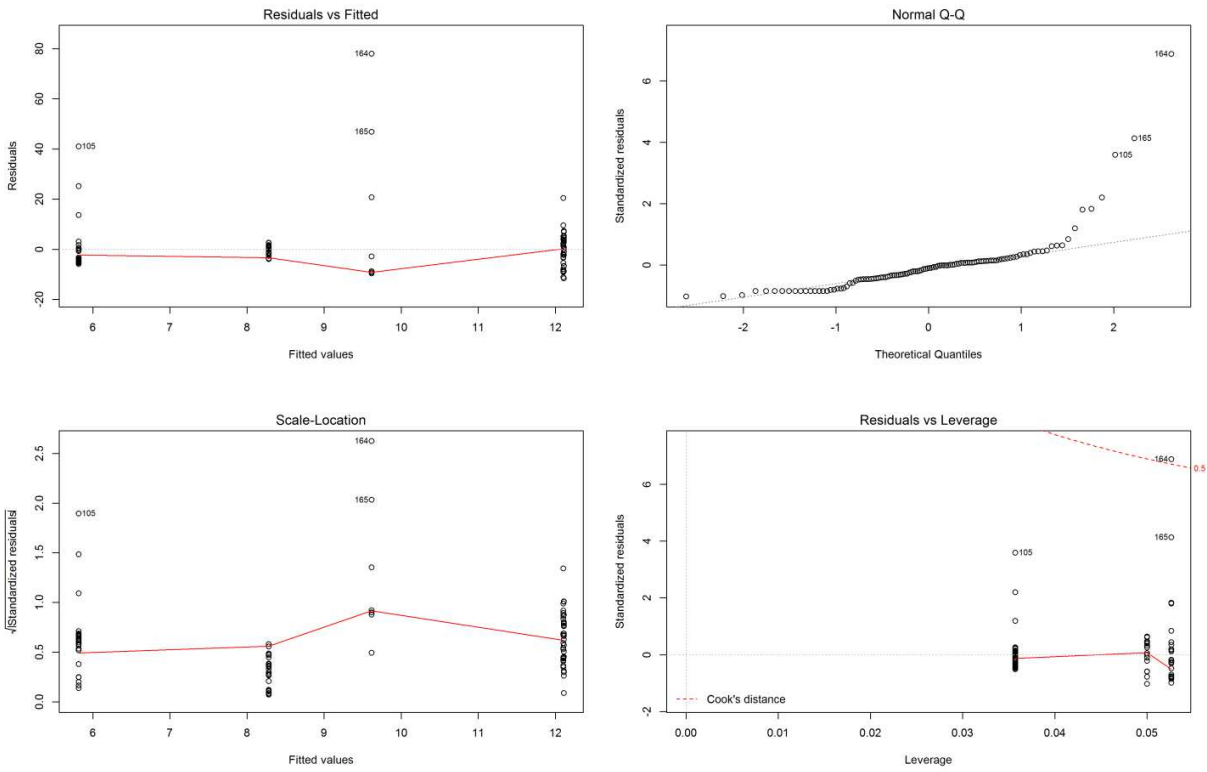


Figure 90. Diagnostic plots of  $C_{Se}$  from groundwater samples separated by presence of drains and depth of monitoring wells.

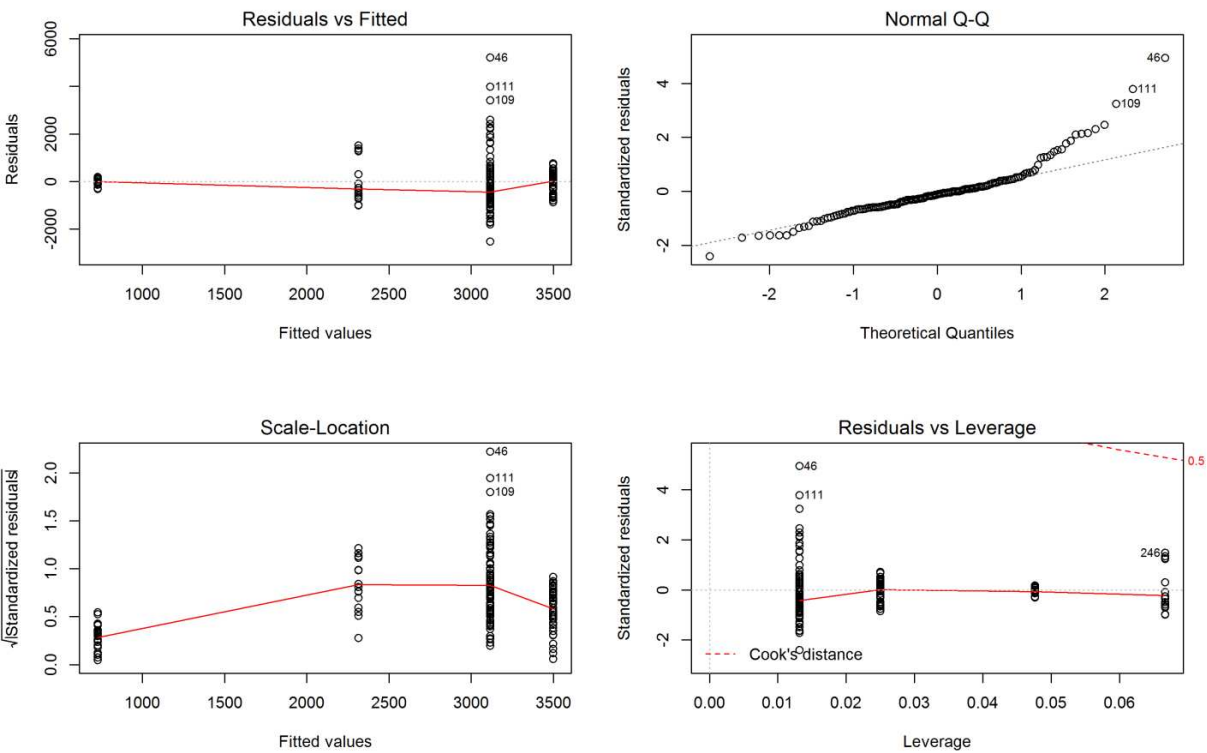


Figure 91. Diagnostic plots of  $C_{TDS}$  for each sample type: GW, SW, TD, TWTD.

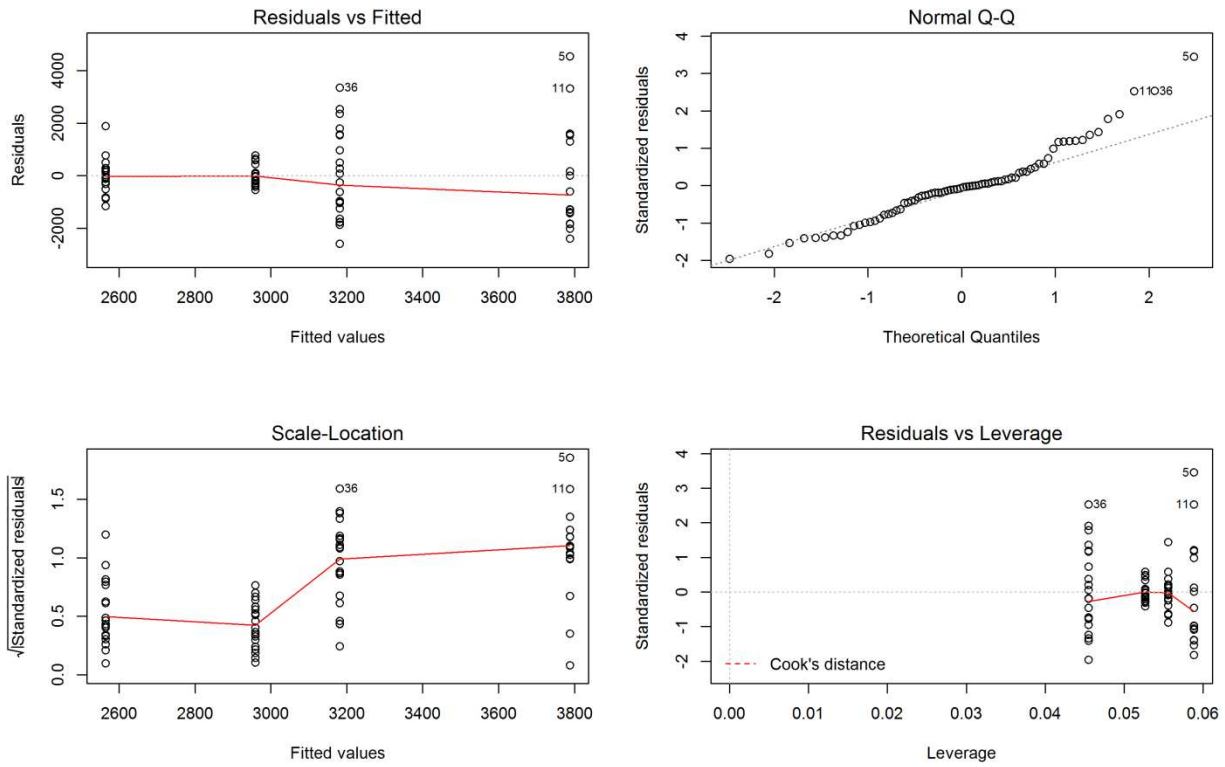


Figure 92. Diagnostic plots of  $C_{TDS}$  for groundwater samples separated by presence of drains and depth of monitoring wells.

APPENDIX D: STATISTICAL DIAGNOSTIC PLOTS FOR LINEAR REGRESSIONS

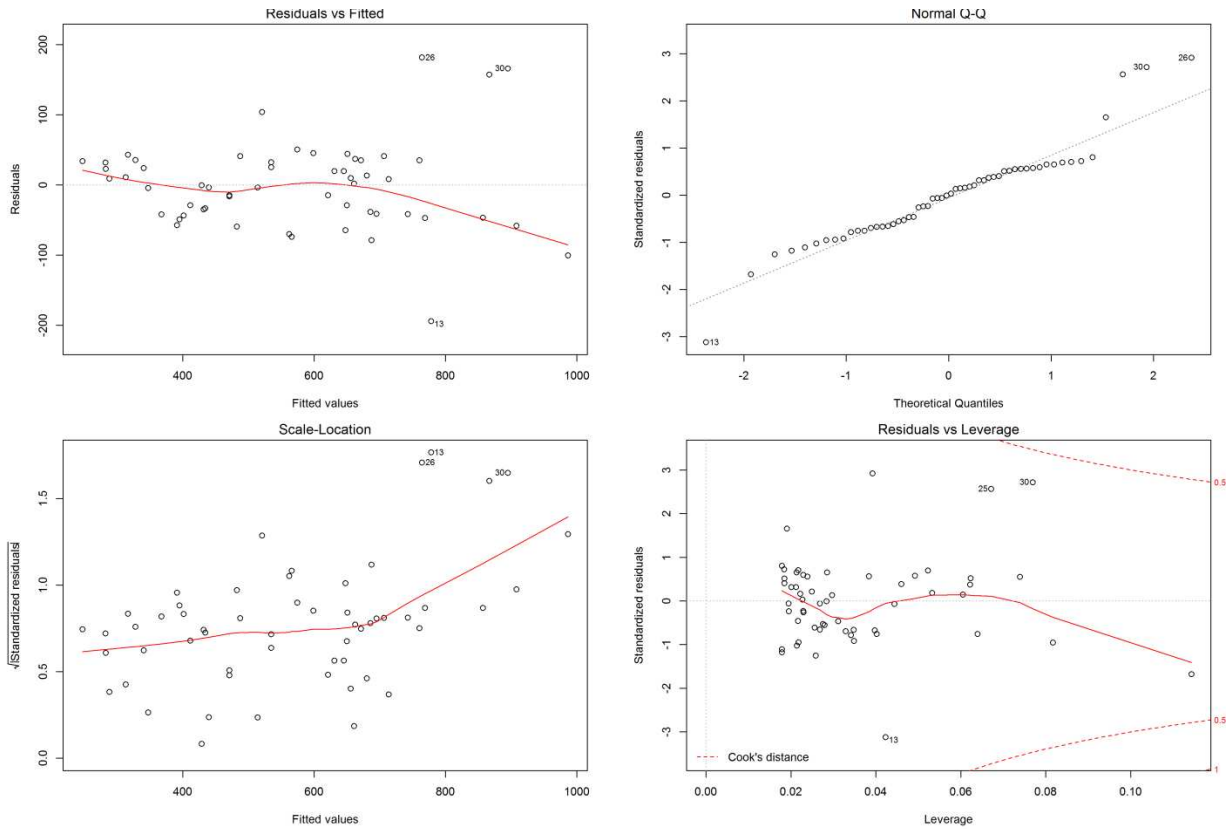


Figure 93. Diagnostic plots of linear regression for  $C_{TDS}$  vs specific conductance.

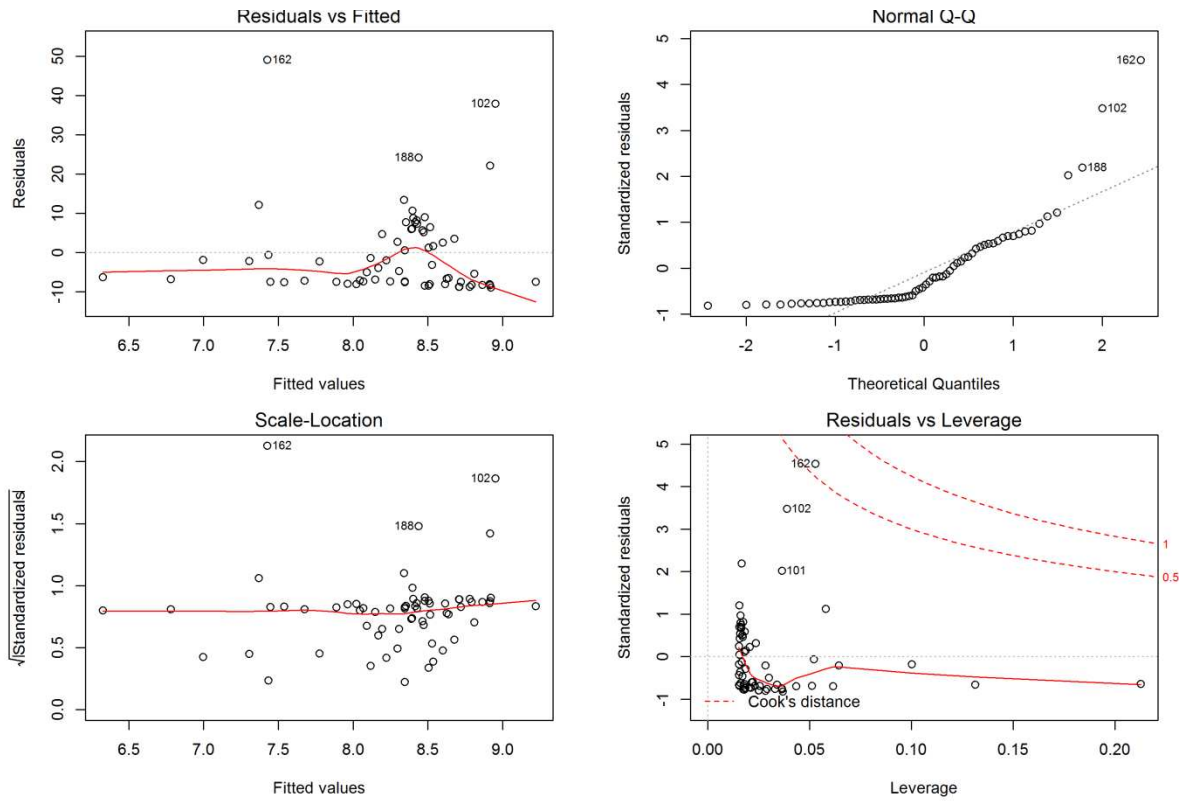


Figure 94. Diagnostics of  $C_{Se}$  vs  $C_{TDS}$  from groundwater samples.

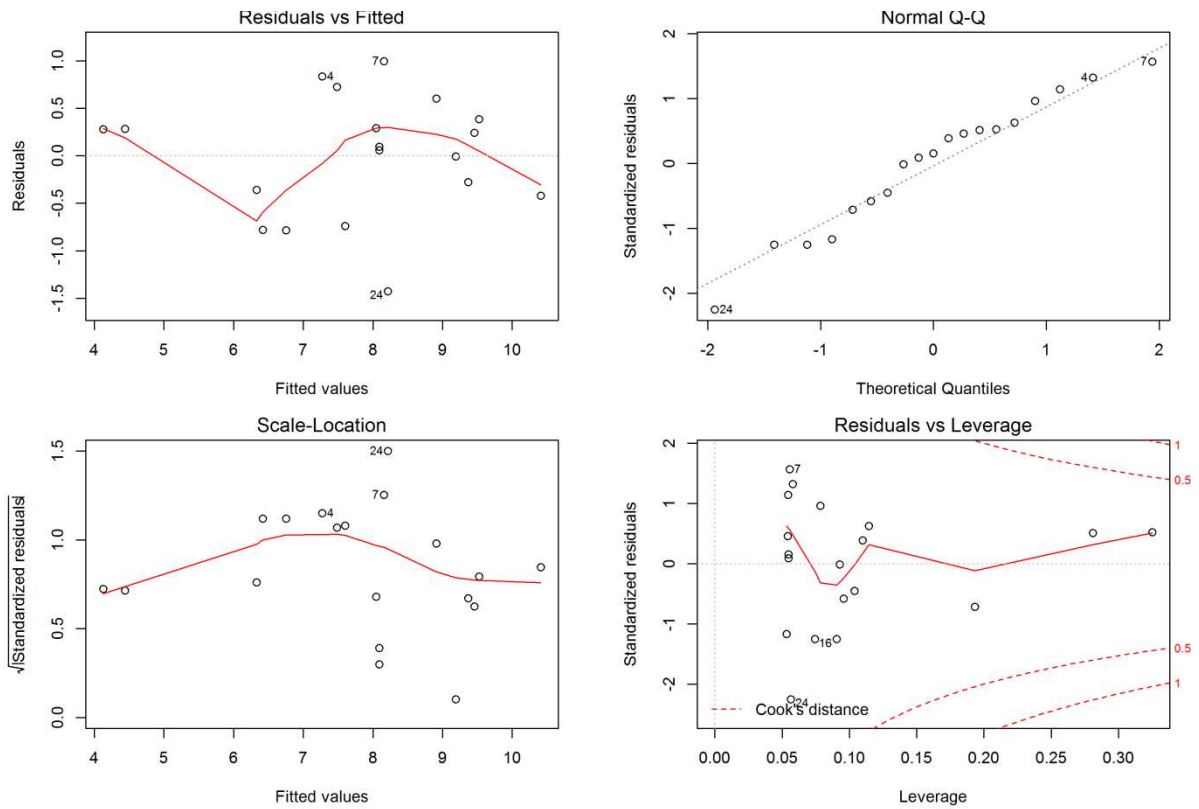


Figure 95. Diagnostics of  $C_{Se}$  vs  $C_{TDS}$  from surface water samples.

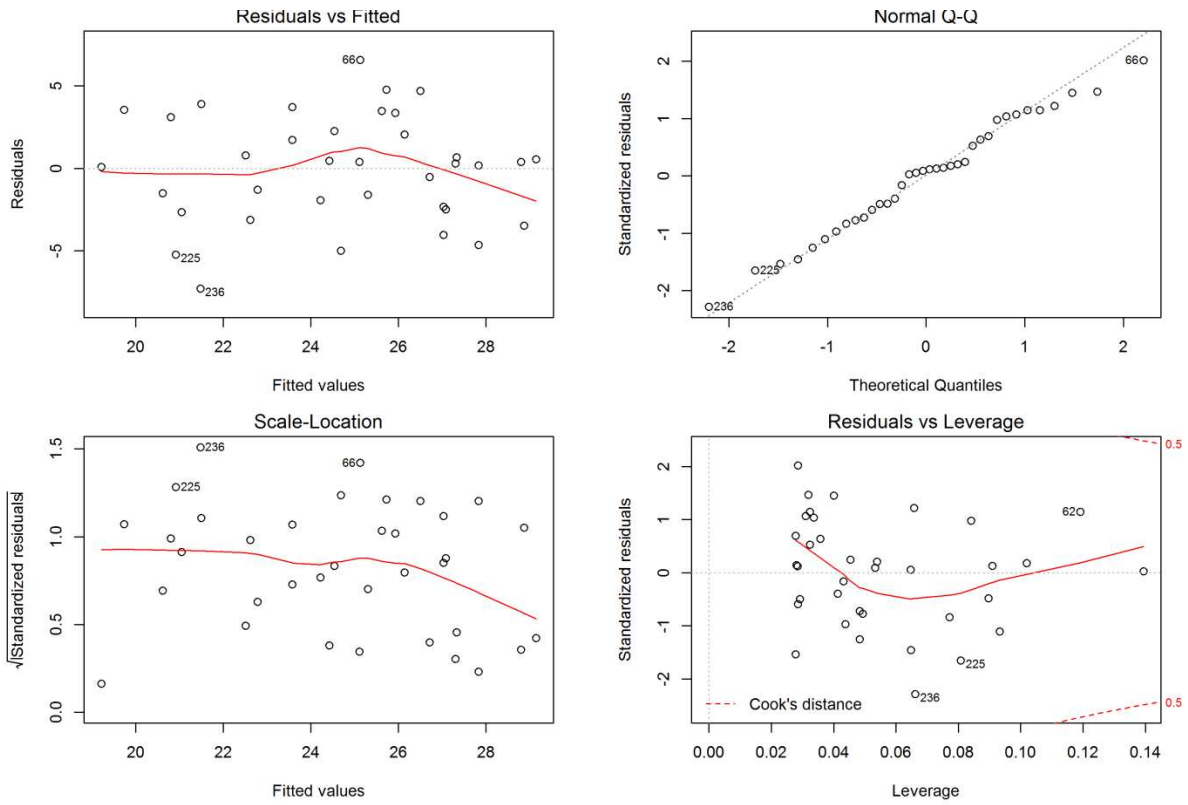


Figure 96. Diagnostics of  $C_{Se}$  vs  $C_{TDS}$  from tile drain water samples.

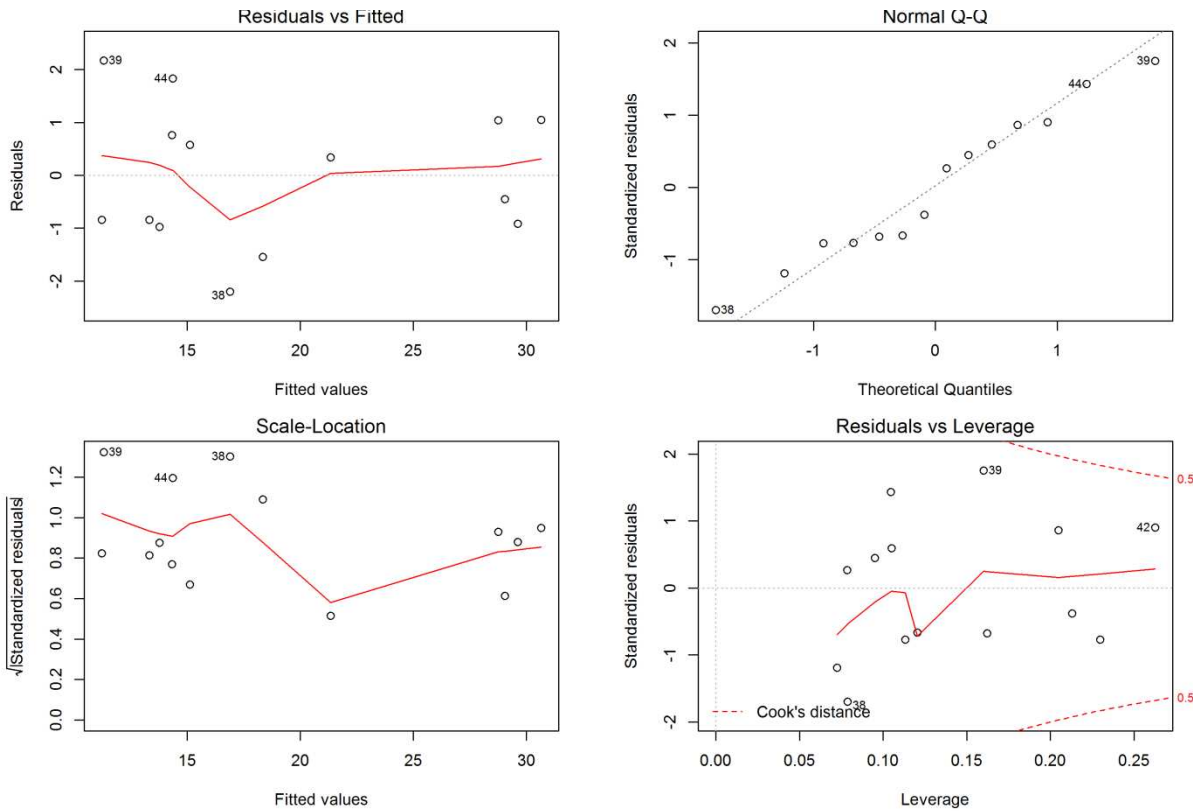


Figure 97. Diagnostics of  $C_{Se}$  vs  $C_{TDS}$  from tile drain water mixed with tailwater samples.

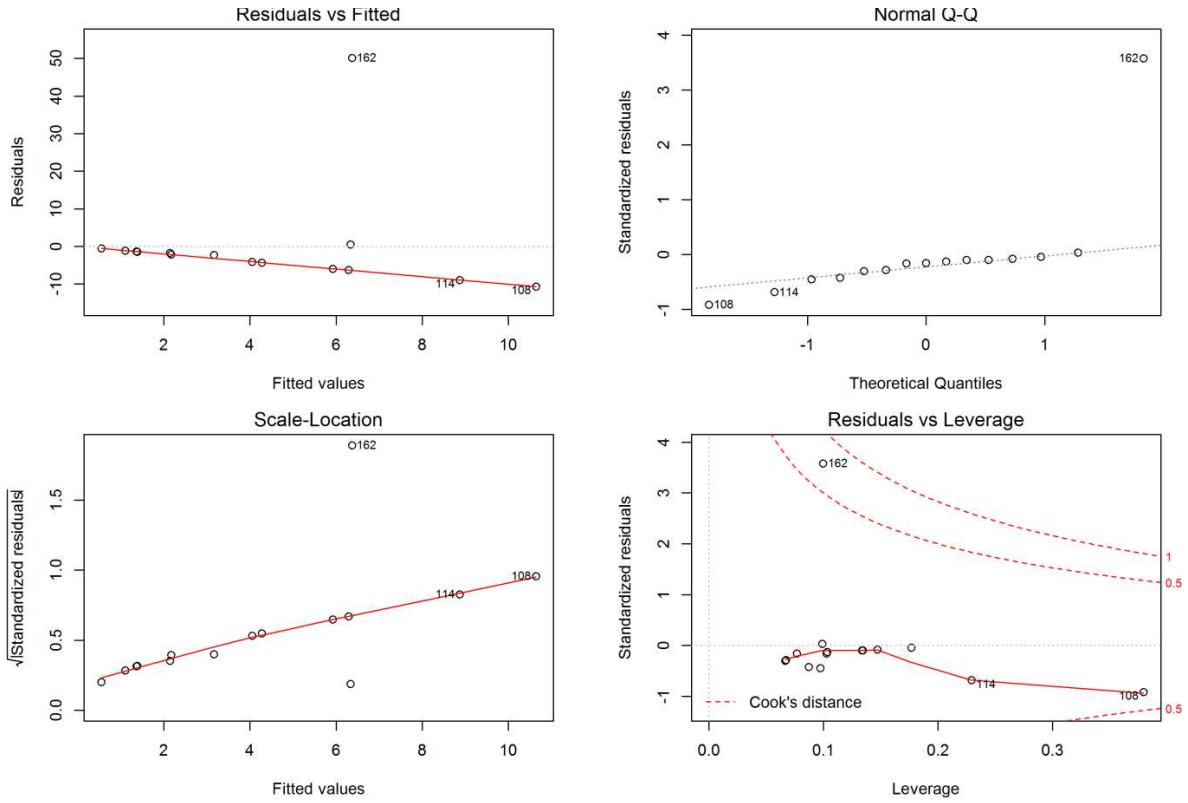


Figure 98. Diagnostics of  $C_{Se}$  vs  $C_{TDS}$  from deep and drained groundwater.

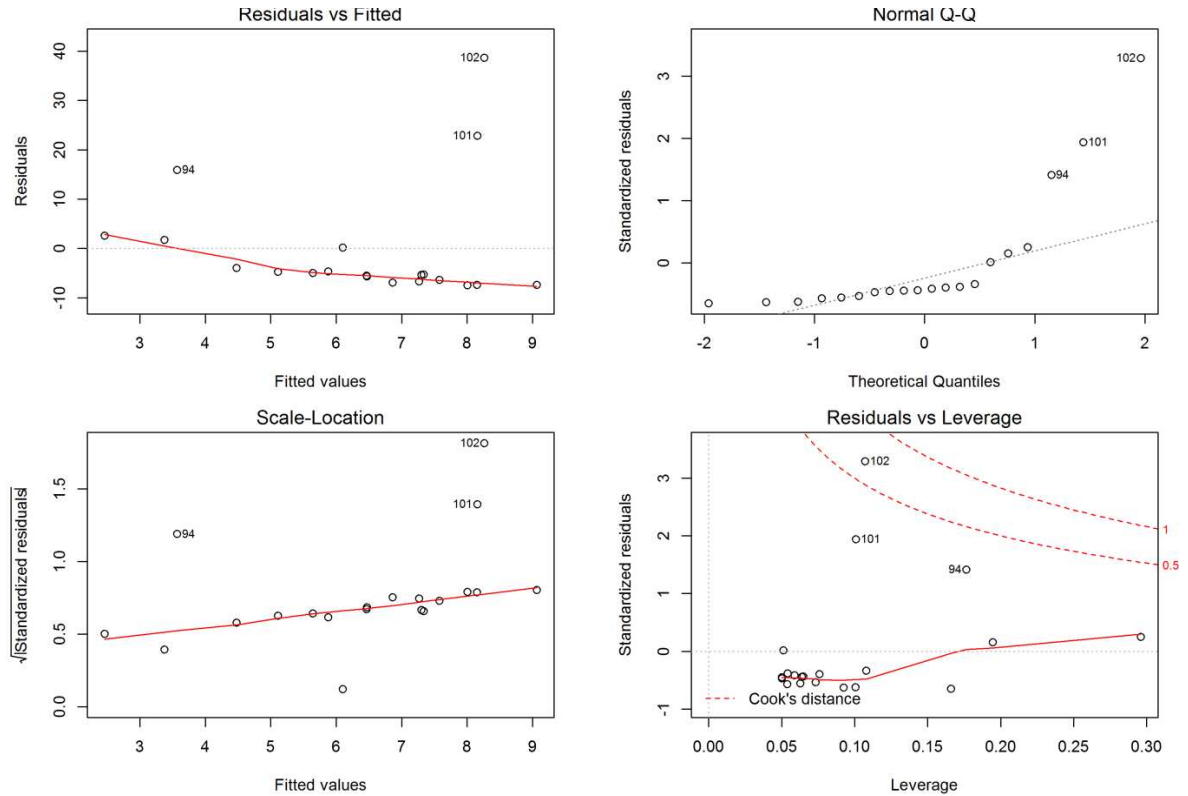


Figure 99. Diagnostics of  $C_{Se}$  vs  $C_{TDS}$  from shallow and drained groundwater.

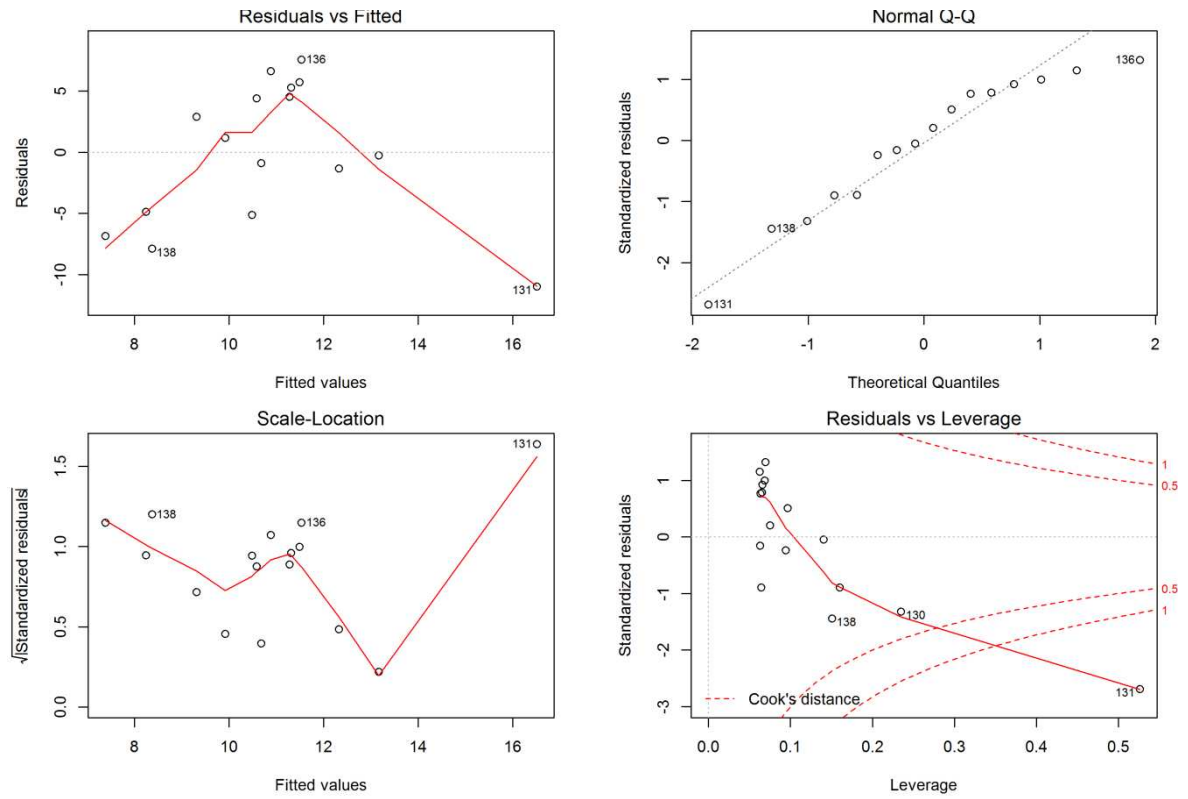


Figure 100. Diagnostics of  $C_{Se}$  vs  $C_{TDS}$  from deep and undrained groundwater.

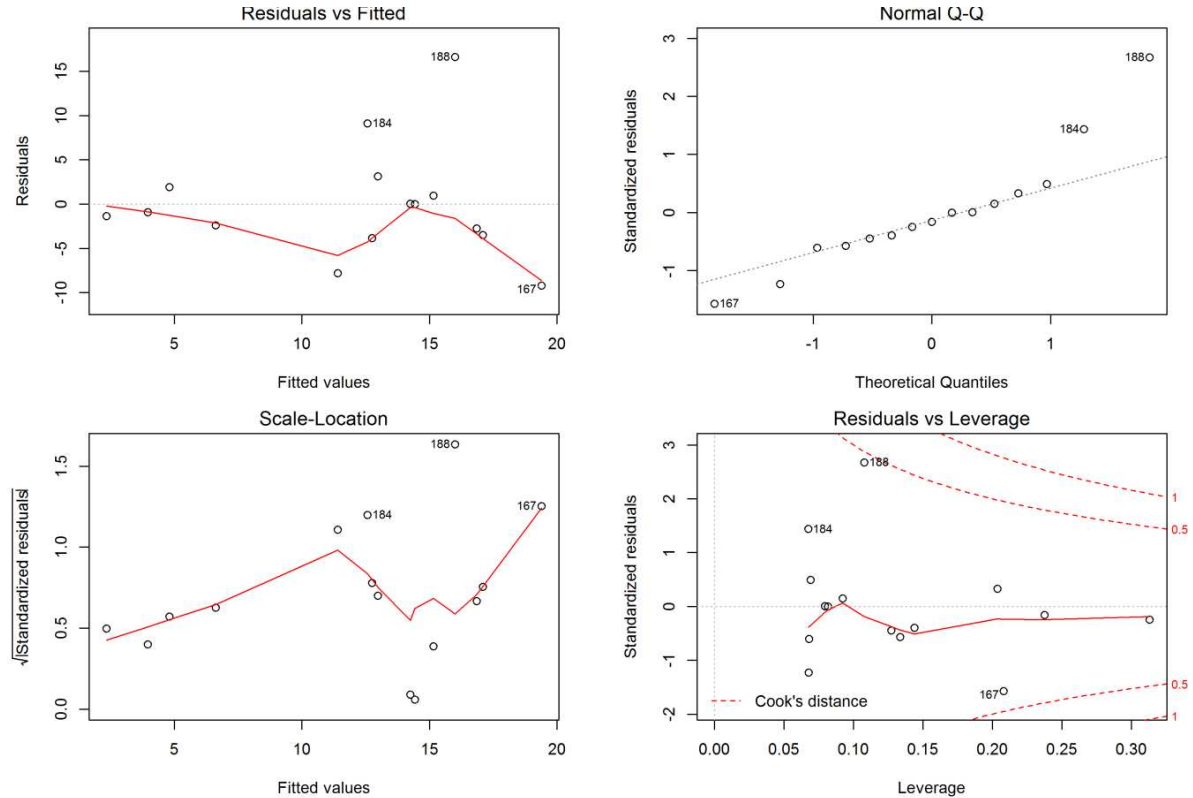


Figure 101. Diagnostics of  $C_{Se}$  vs  $C_{TDS}$  from shallow and undrained groundwater.

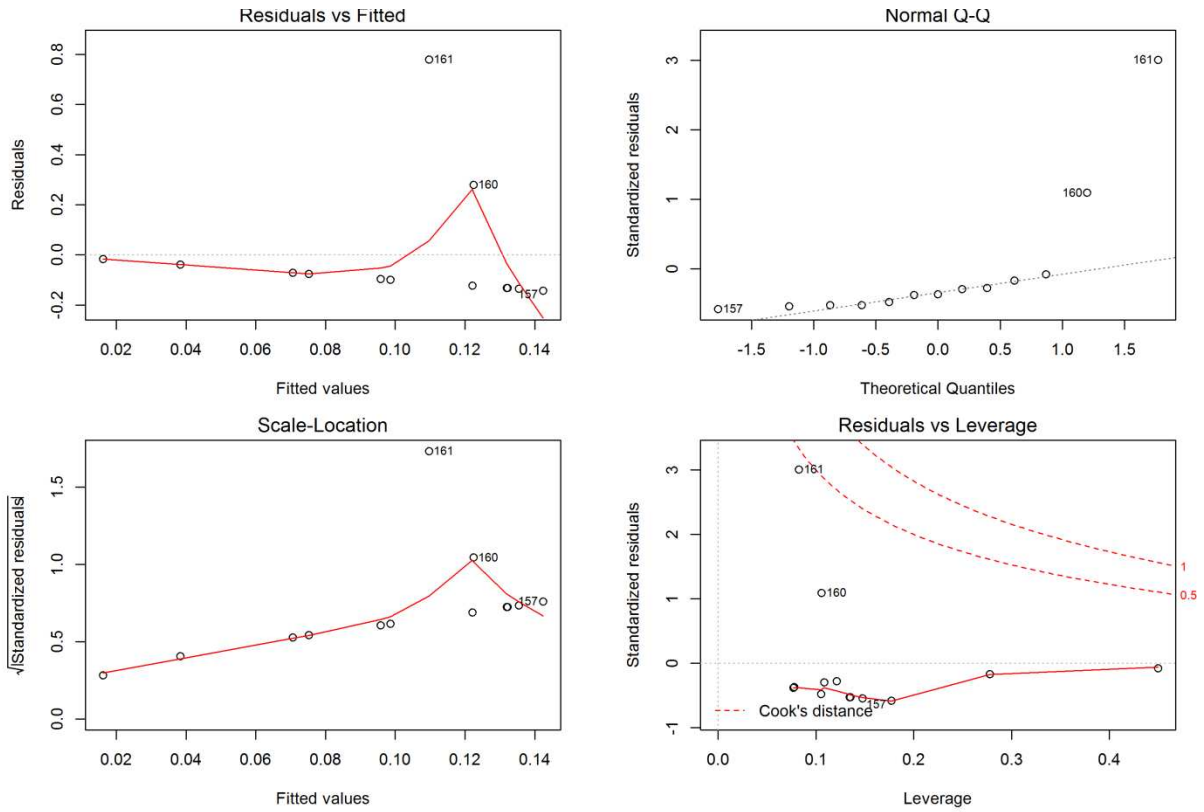


Figure 102. Diagnostics of  $C_{Se}$  vs  $C_{TDS}$  from deep and drained groundwater with outliers removed.

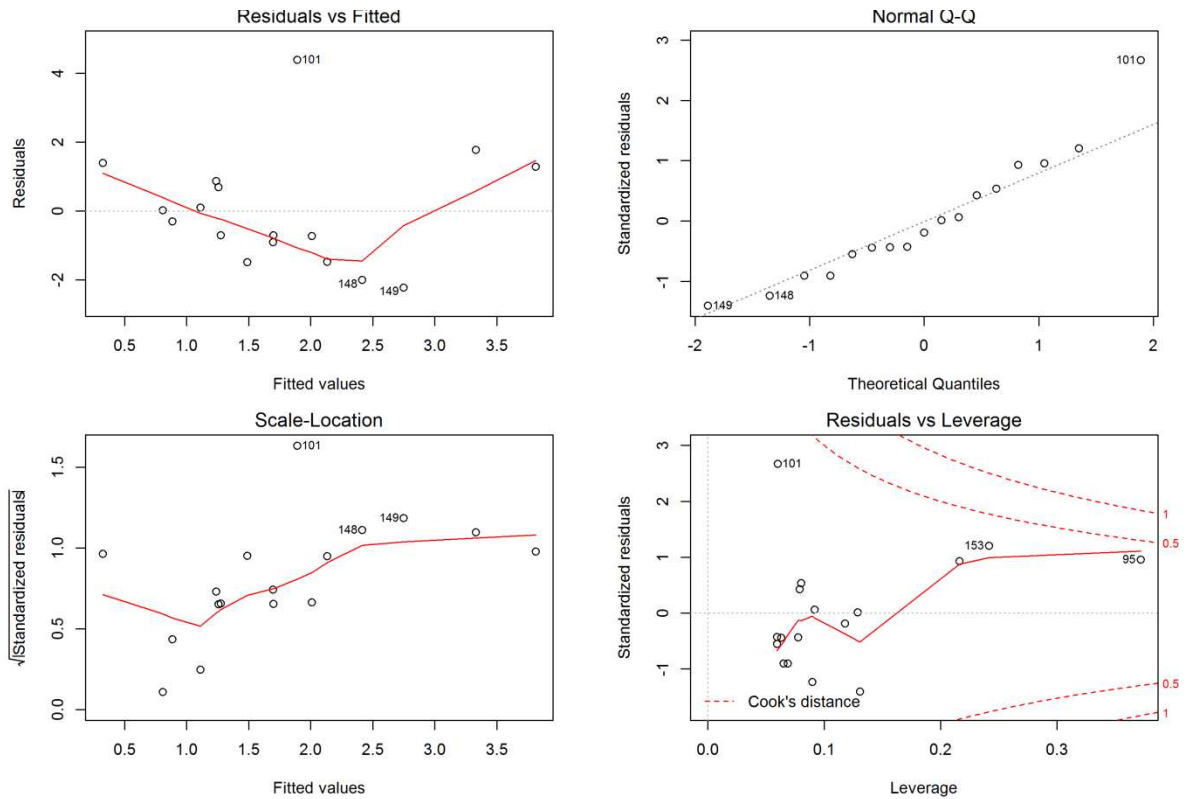


Figure 103. Diagnostics of  $C_{Se}$  vs  $C_{TDS}$  from shallow and drained groundwater with outliers removed.

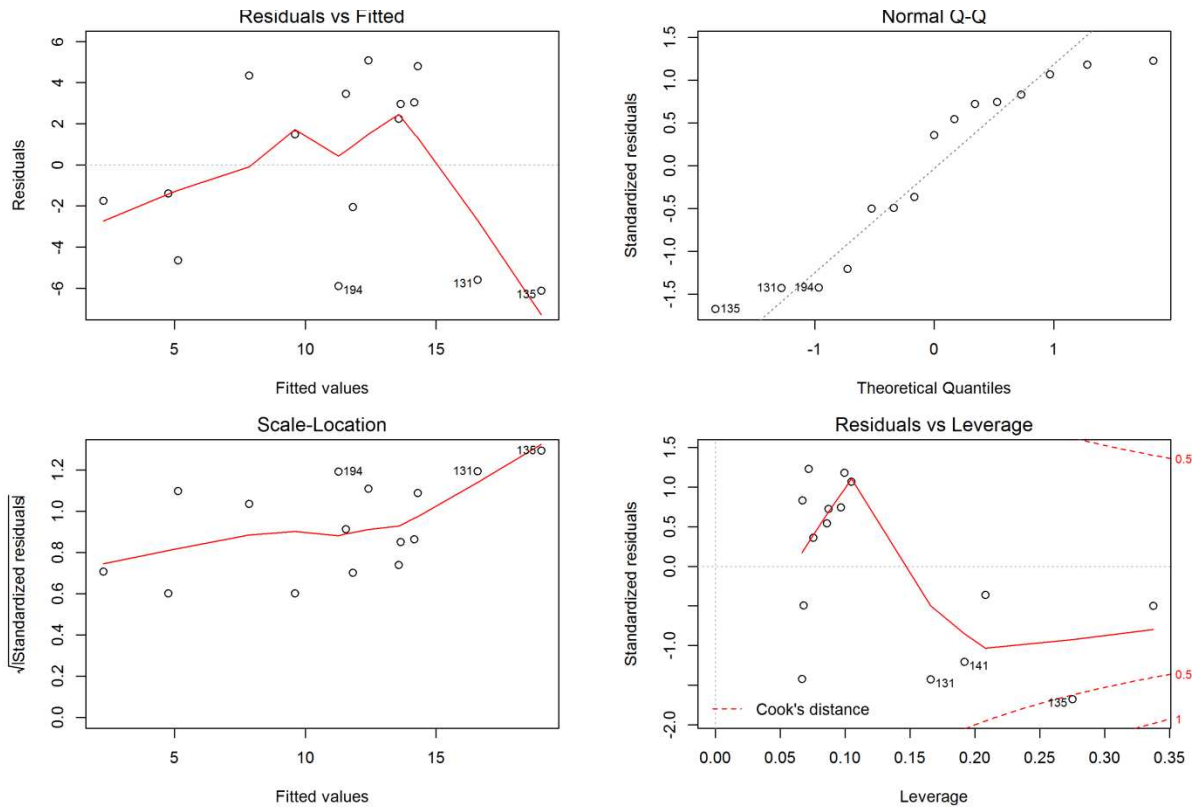


Figure 104. Diagnostics of  $C_{Se}$  vs  $C_{TDS}$  from deep and undrained groundwater with outliers removed.

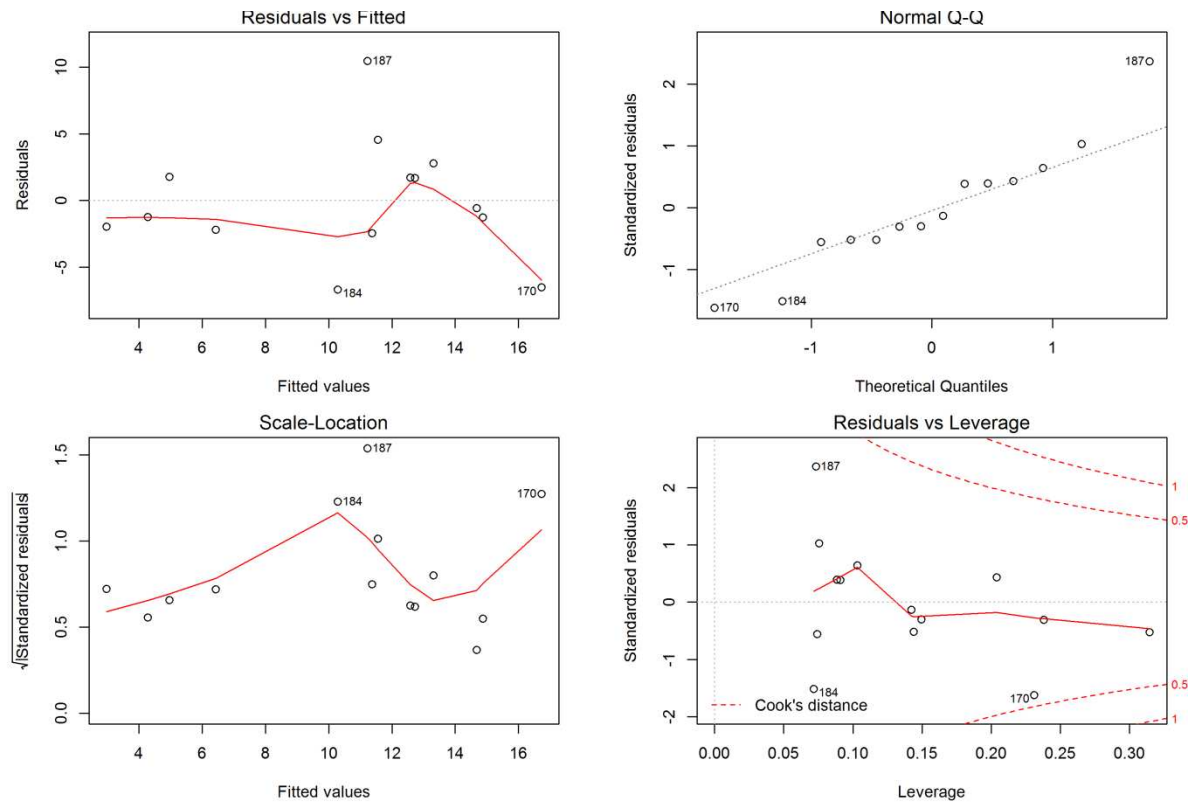


Figure 105. Diagnostics of  $C_{Se}$  vs  $C_{TDS}$  from shallow and undrained groundwater with outliers removed.

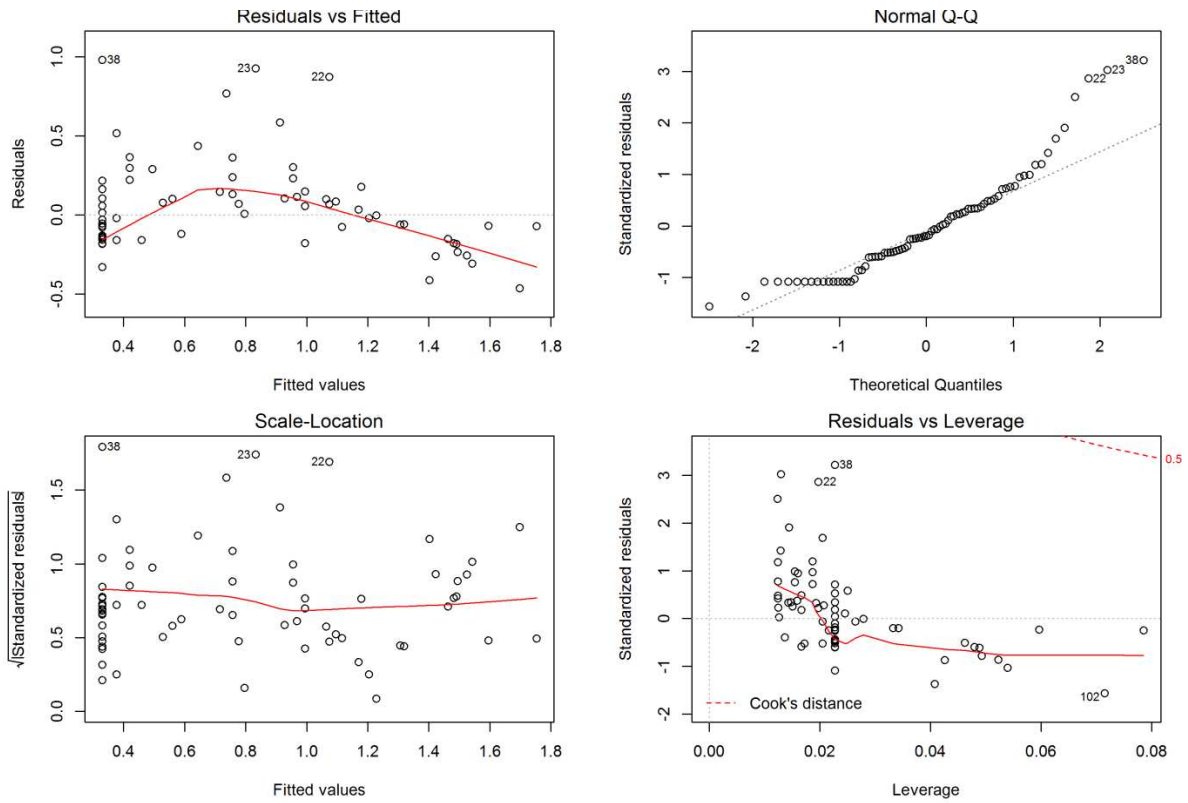


Figure 106. Diagnostics of  $C_{Se}$  vs  $C_N$  for groundwater dataset.

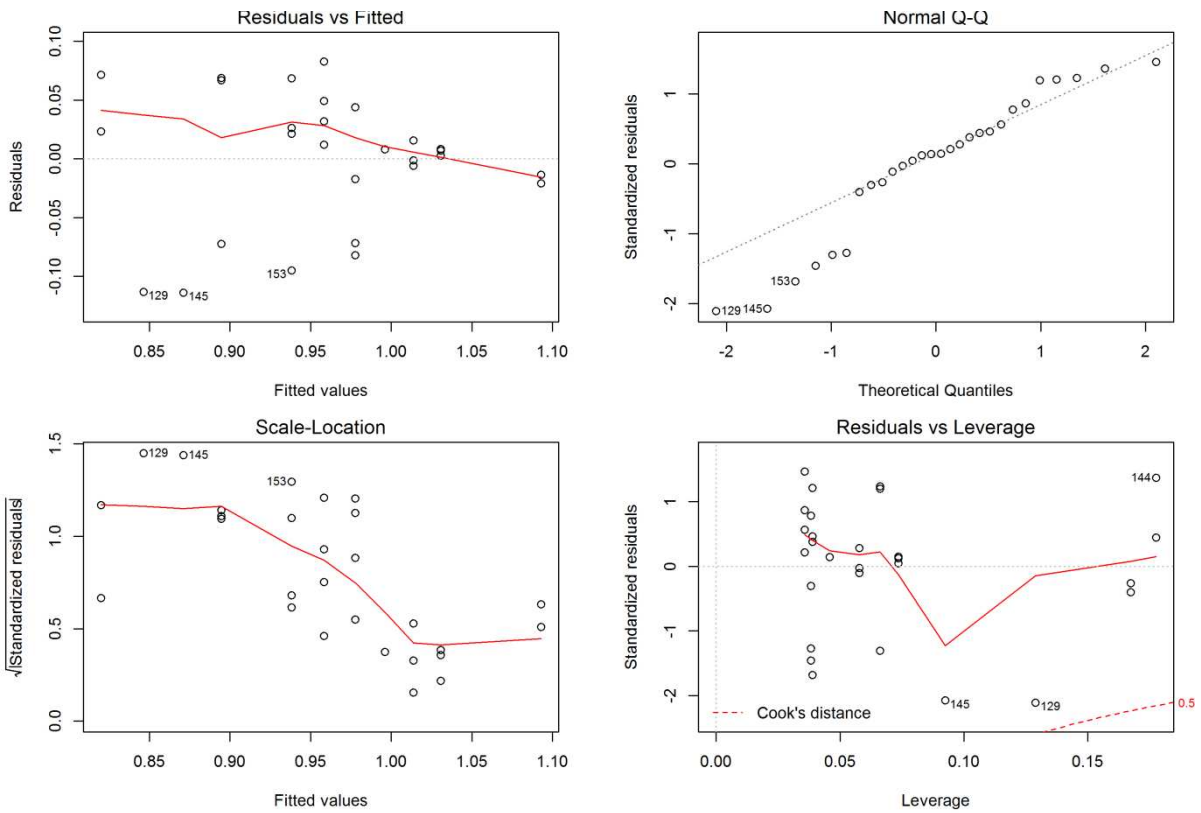


Figure 107. Diagnostics of  $C_{Se}$  vs  $C_N$  for surface water dataset.

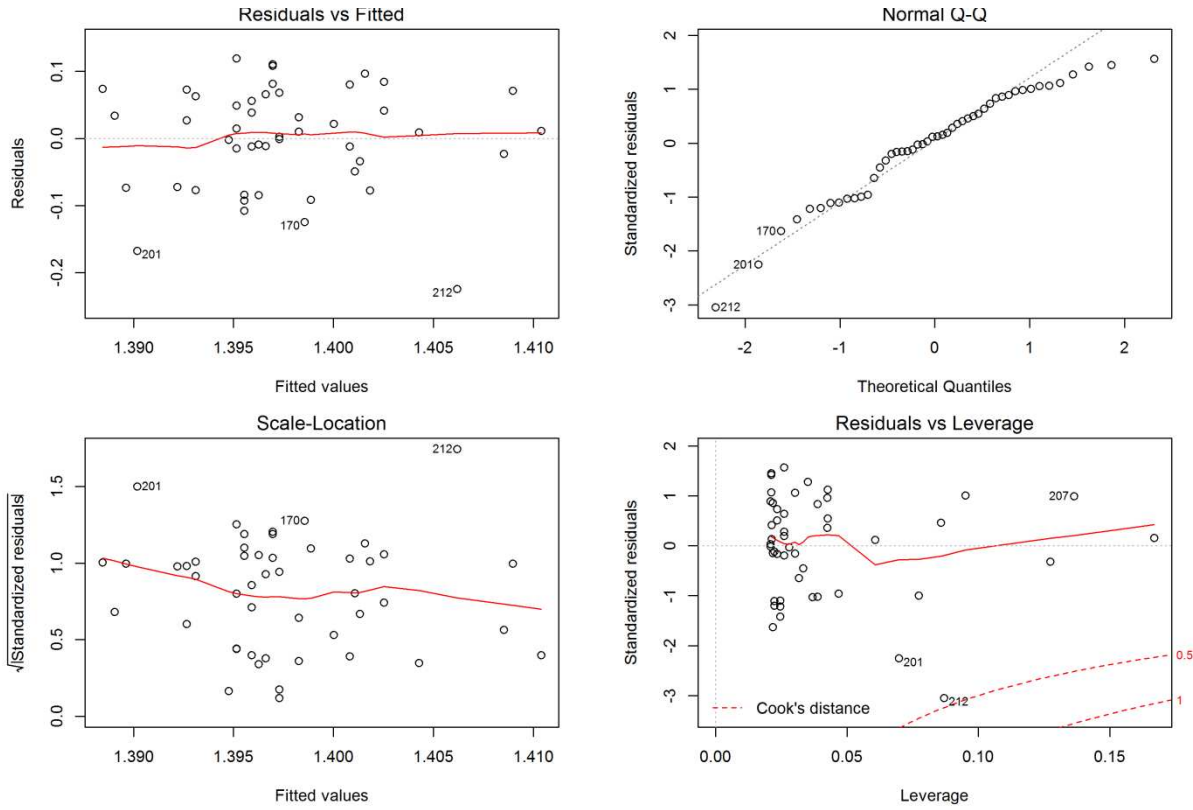


Figure 108. Diagnostics of  $C_{Se}$  vs  $C_N$  for tile drain dataset.

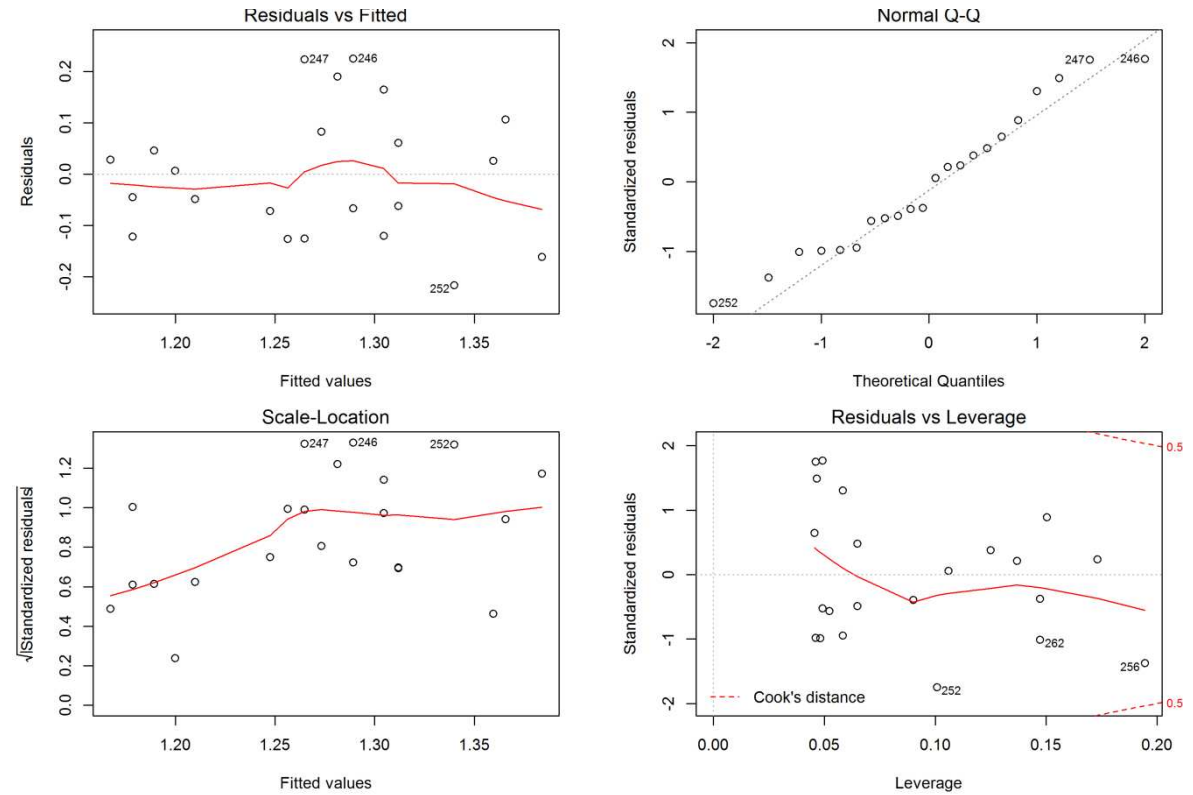


Figure 109. Diagnostics of  $C_{Se}$  vs  $C_N$  for the mixed tailwater and tile drain water dataset.

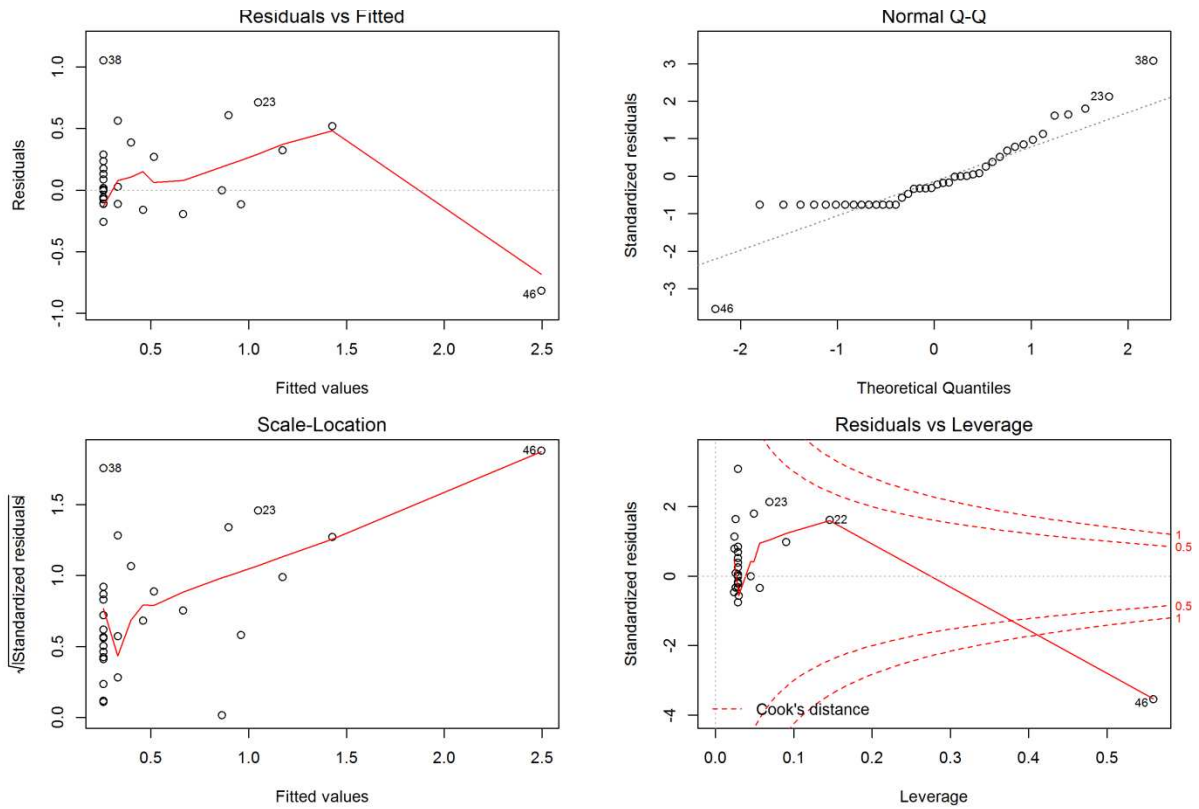


Figure 110. Diagnostics of  $C_{Se}$  vs  $C_N$  for groundwater with drains present.

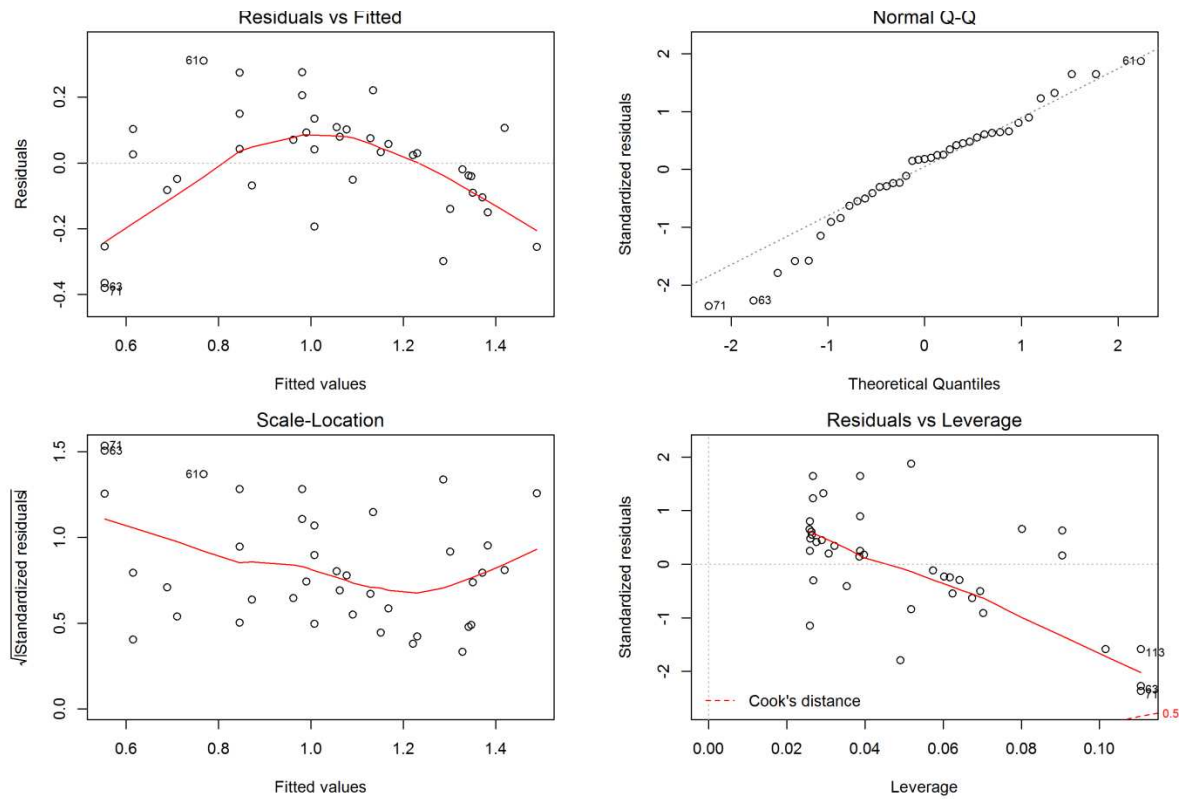


Figure 111. Diagnostics of  $C_{Se}$  vs  $C_N$  for groundwater with no drains present.

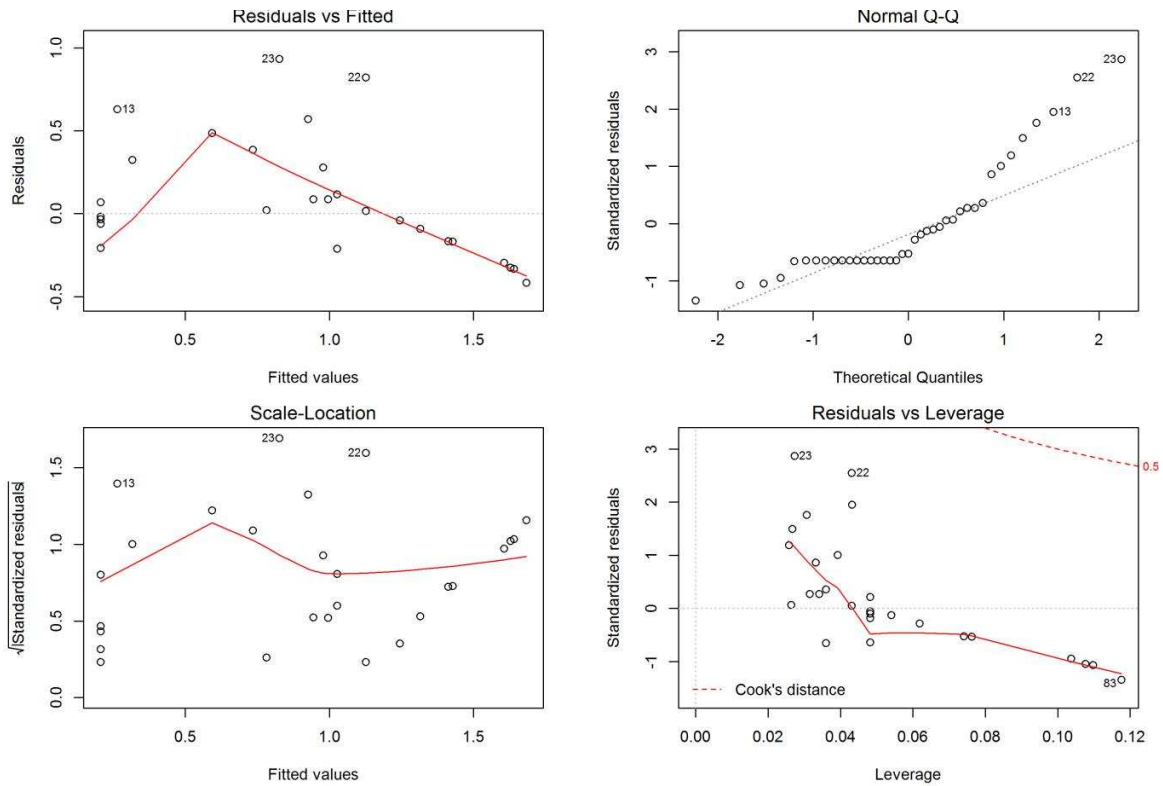


Figure 112. Diagnostics of  $C_{Se}$  vs  $C_N$  for deep groundwater.

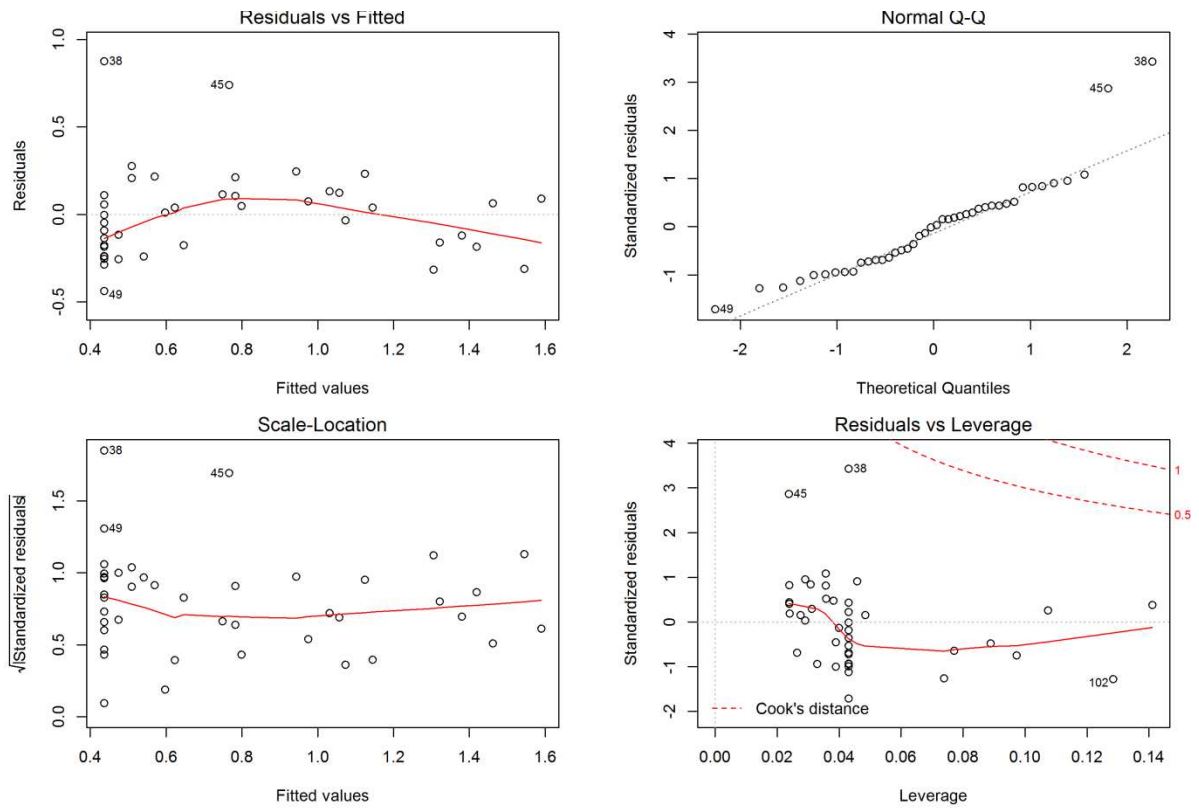


Figure 113. Diagnostics of  $C_{Se}$  vs  $C_N$  for shallow groundwater.

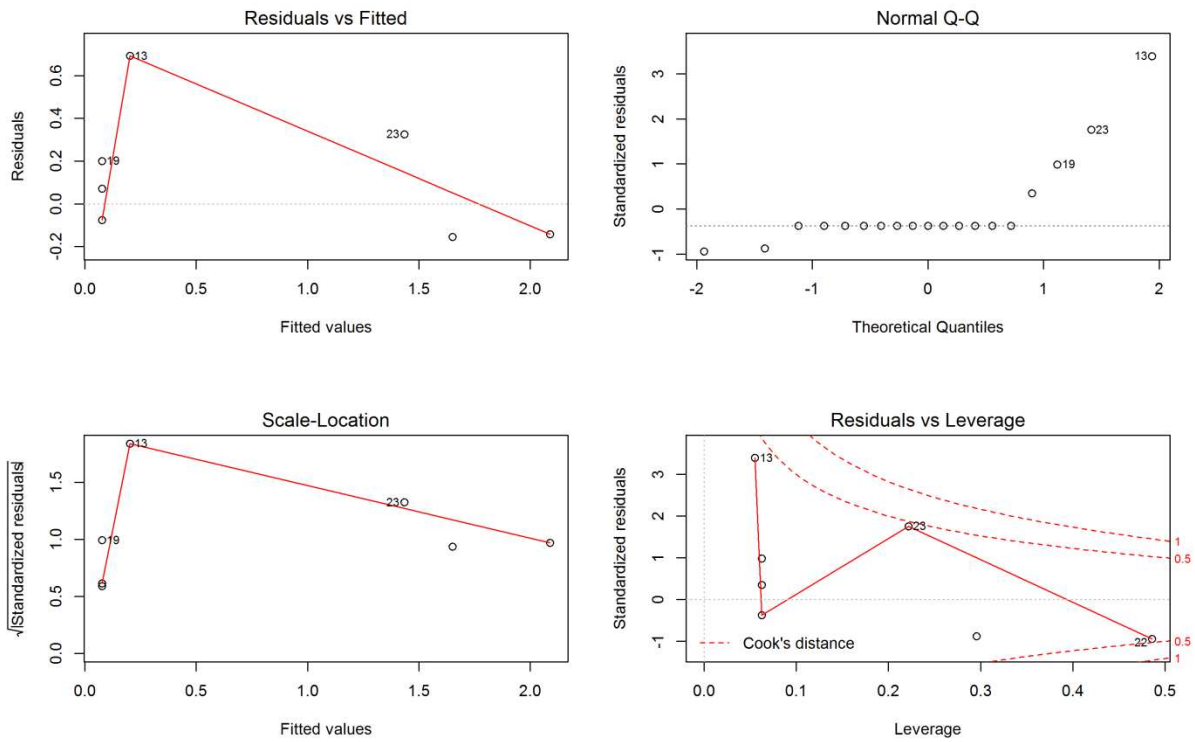


Figure 114. Diagnostics of  $C_{Se}$  vs  $C_N$  for deep drained ground water.

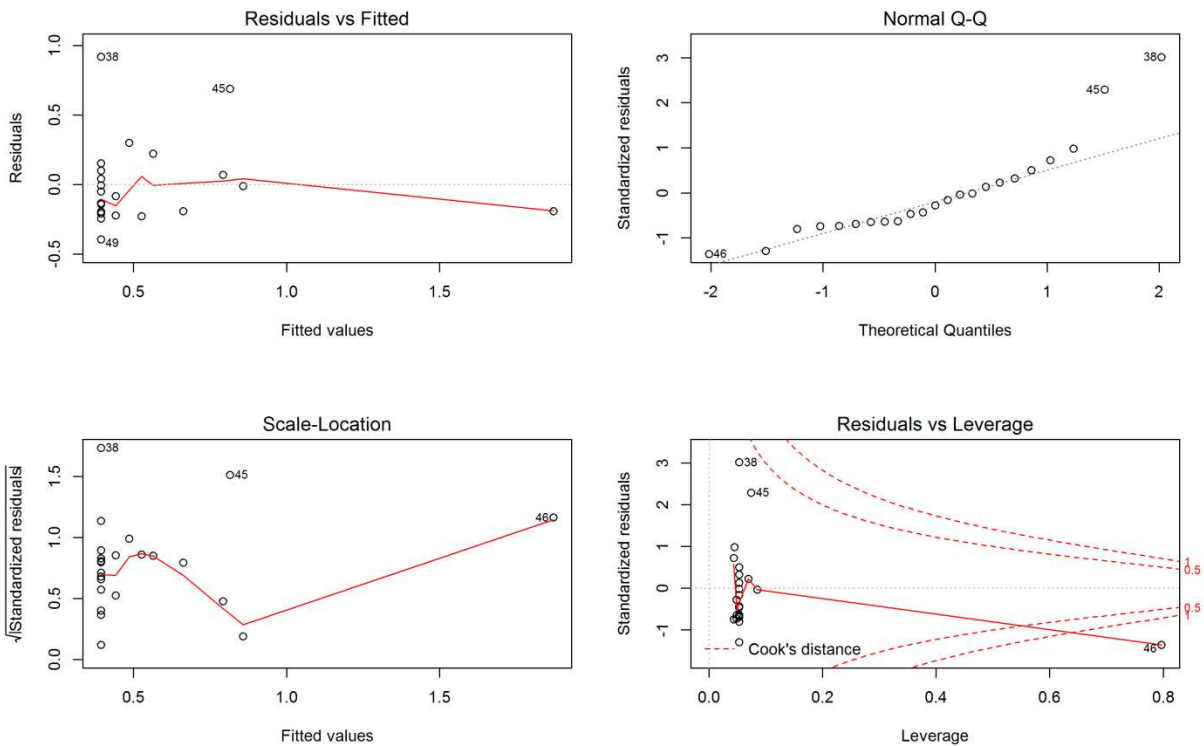


Figure 115. Diagnostics of  $C_{Se}$  vs  $C_N$  for shallow drained groundwater.

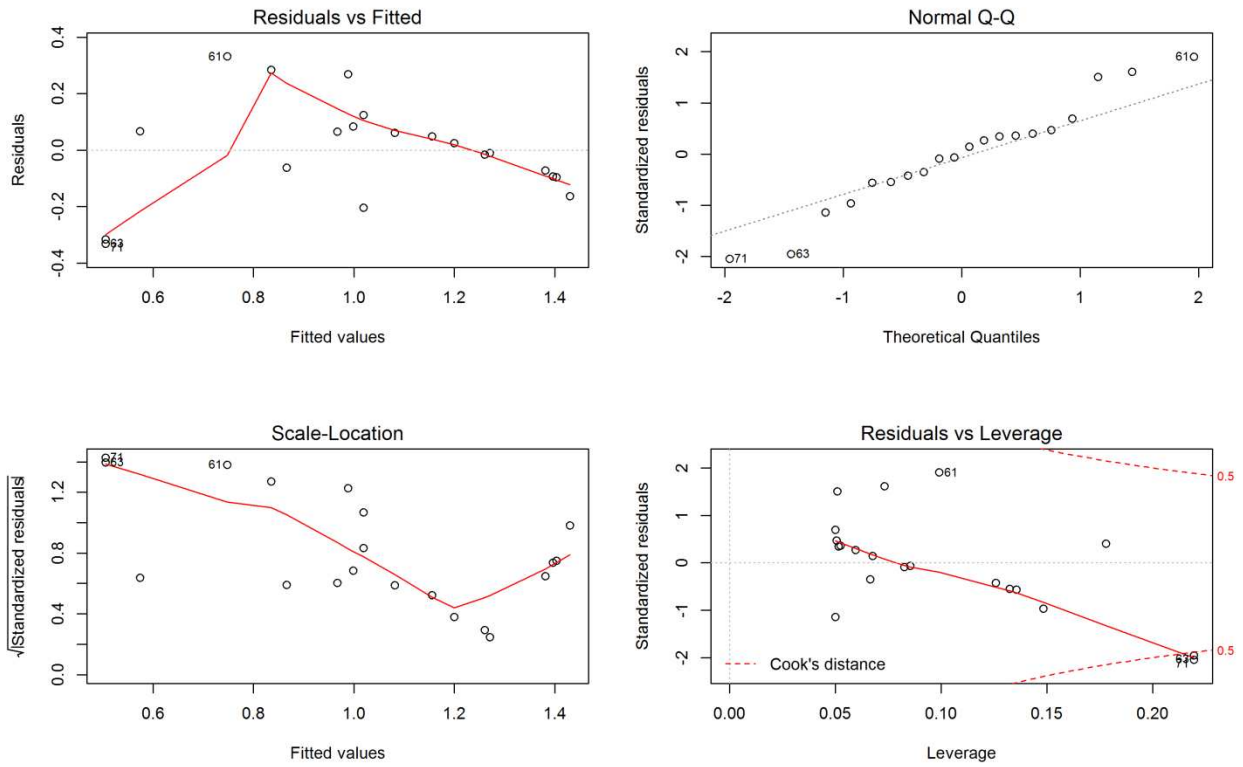


Figure 116. Diagnostics of  $C_{Se}$  vs  $C_N$  for deep undrained groundwater.

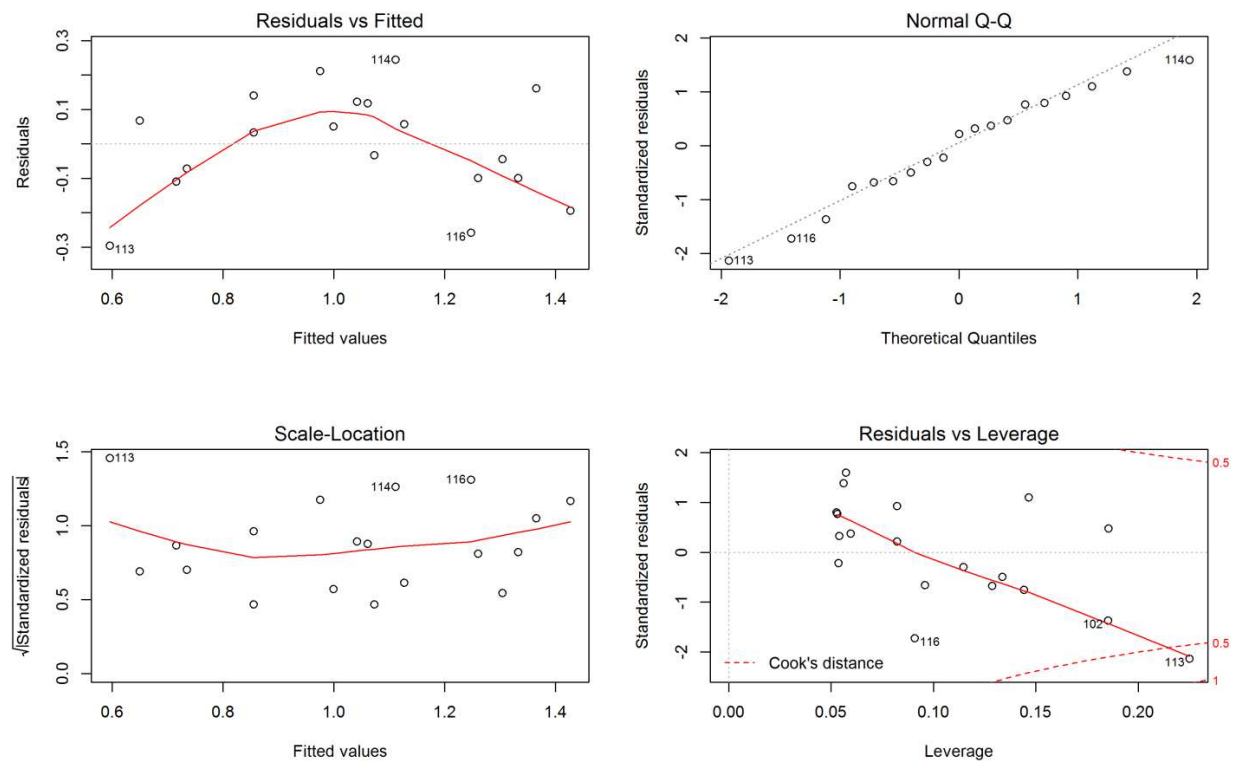


Figure 117. Diagnostics of  $C_{Se}$  vs  $C_N$  for shallow undrained groundwater.

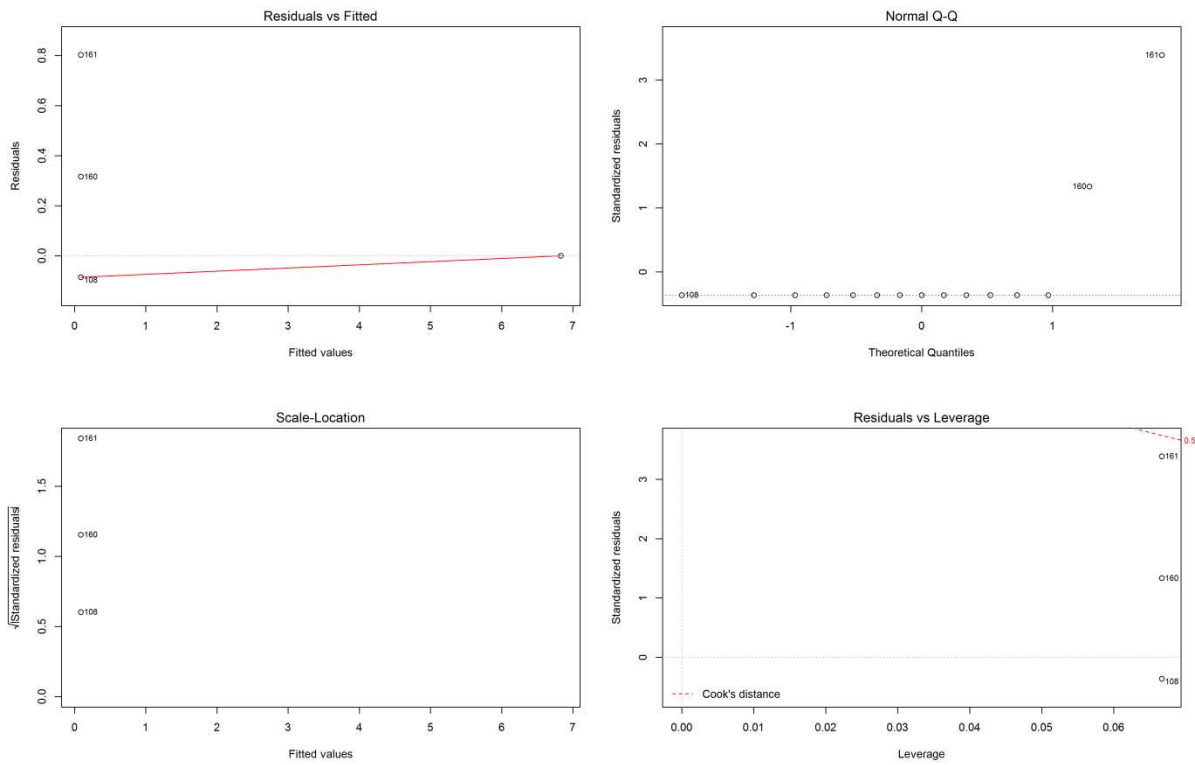


Figure 118. Diagnostics of  $C_{Se}$  vs  $C_N$  for deep, drained groundwater with outliers removed.

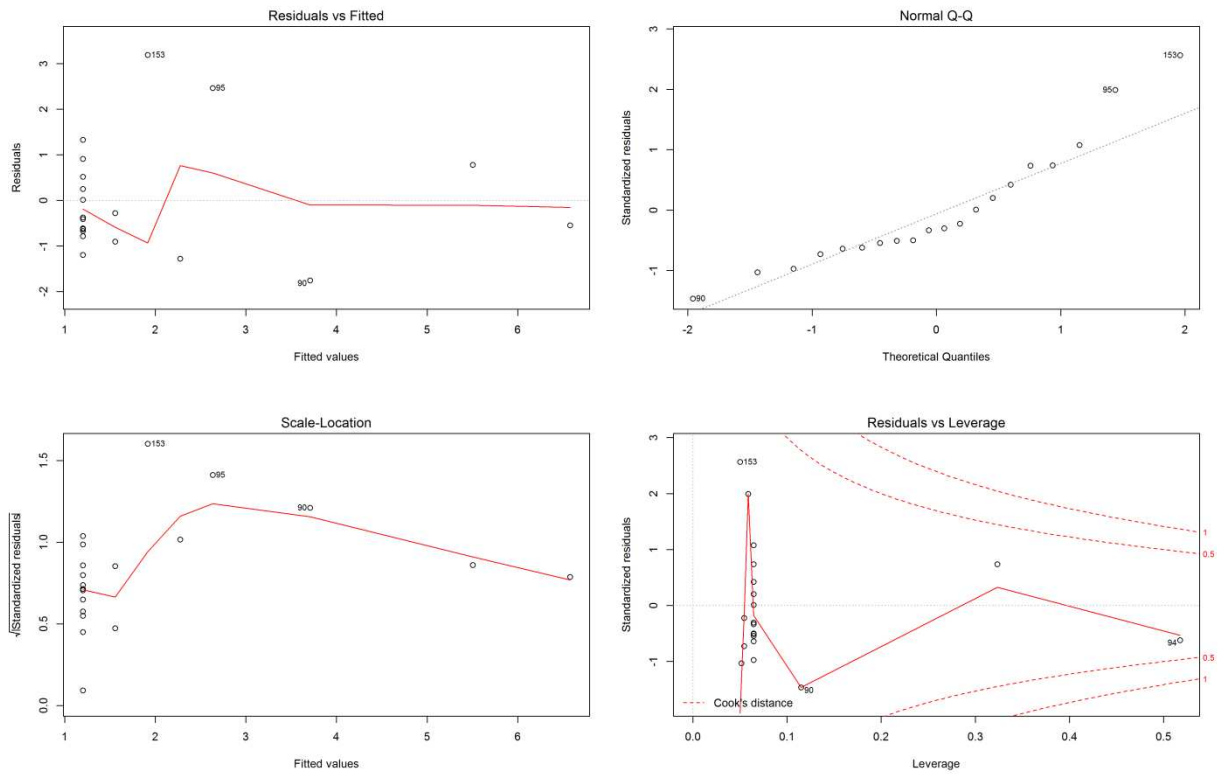


Figure 119. Diagnostics of  $C_{Se}$  vs  $C_N$  for shallow, drained groundwater with outliers removed.

APPENDIX E: STATISTICAL DIAGNOSTICS FOR ANOVA STATISTICS FOR COMPARISON  
OF FIELD-SCALE TDS MASS BALANCE POPULATIONS

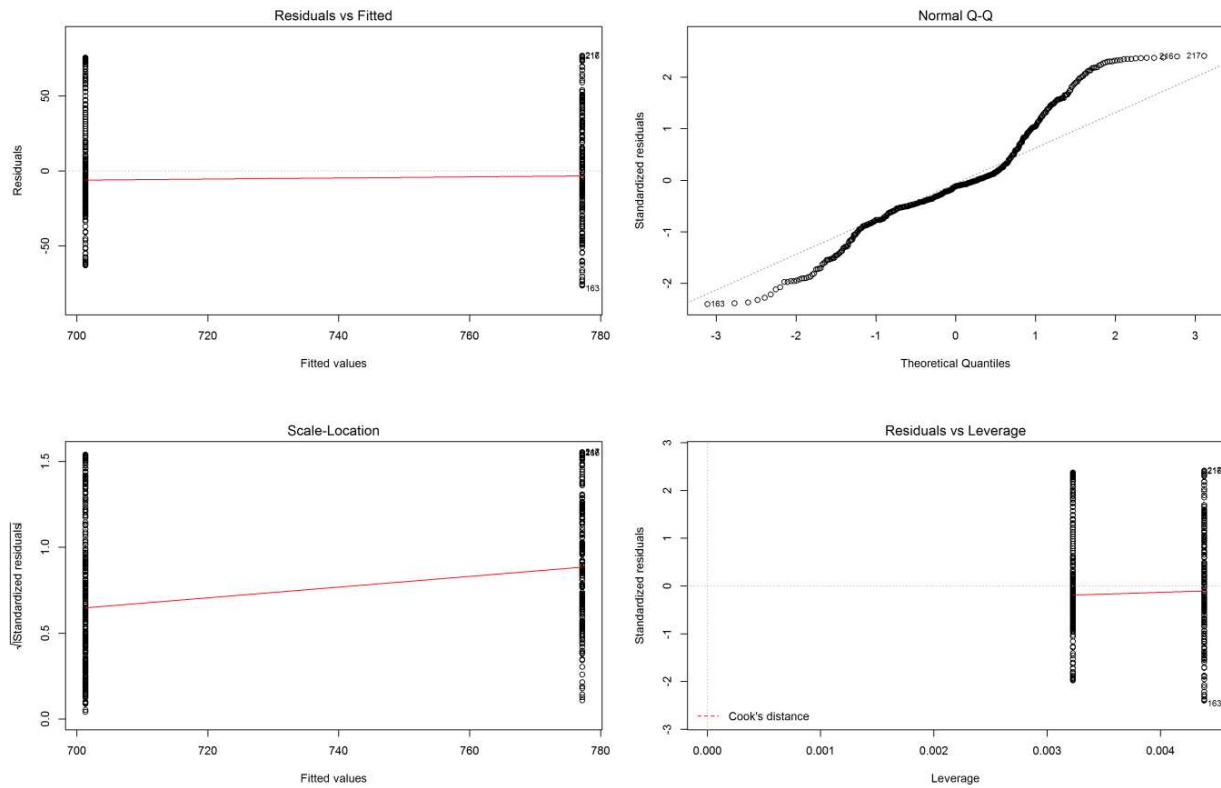


Figure 120. Diagnostic plots of  $C_{TDS}$  for applied water and tailwater for field DA7.

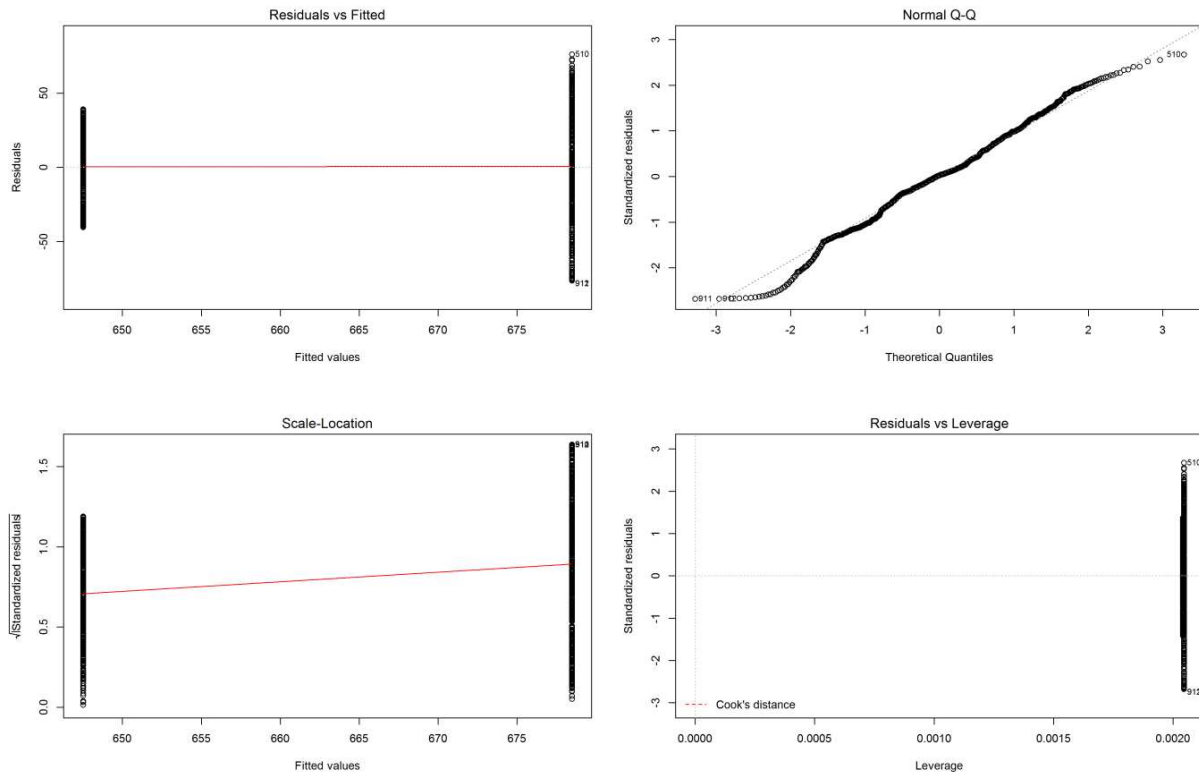


Figure 121. Diagnostic plots of  $C_{TDS}$  for applied water and tailwater for field Muth2.

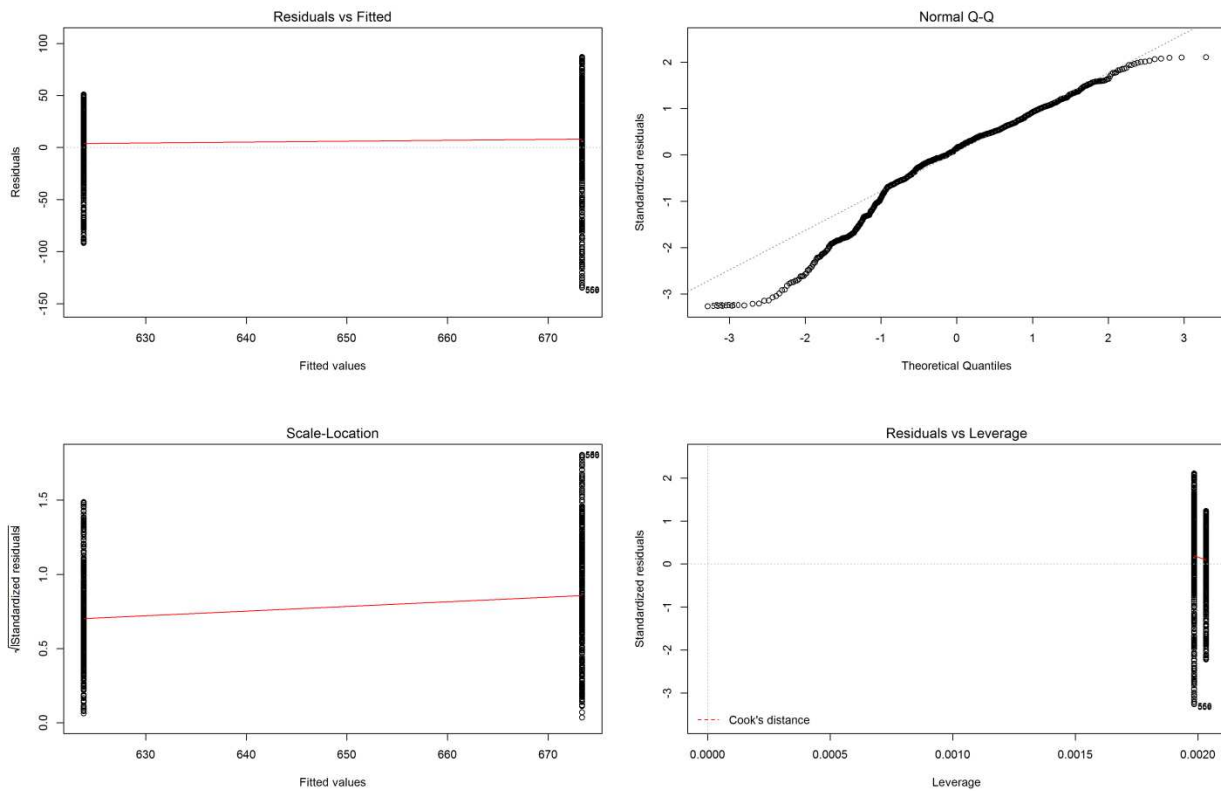


Figure 122. Diagnostic plots of  $C_{TDS}$  for applied water and tailwater for field Muth9.

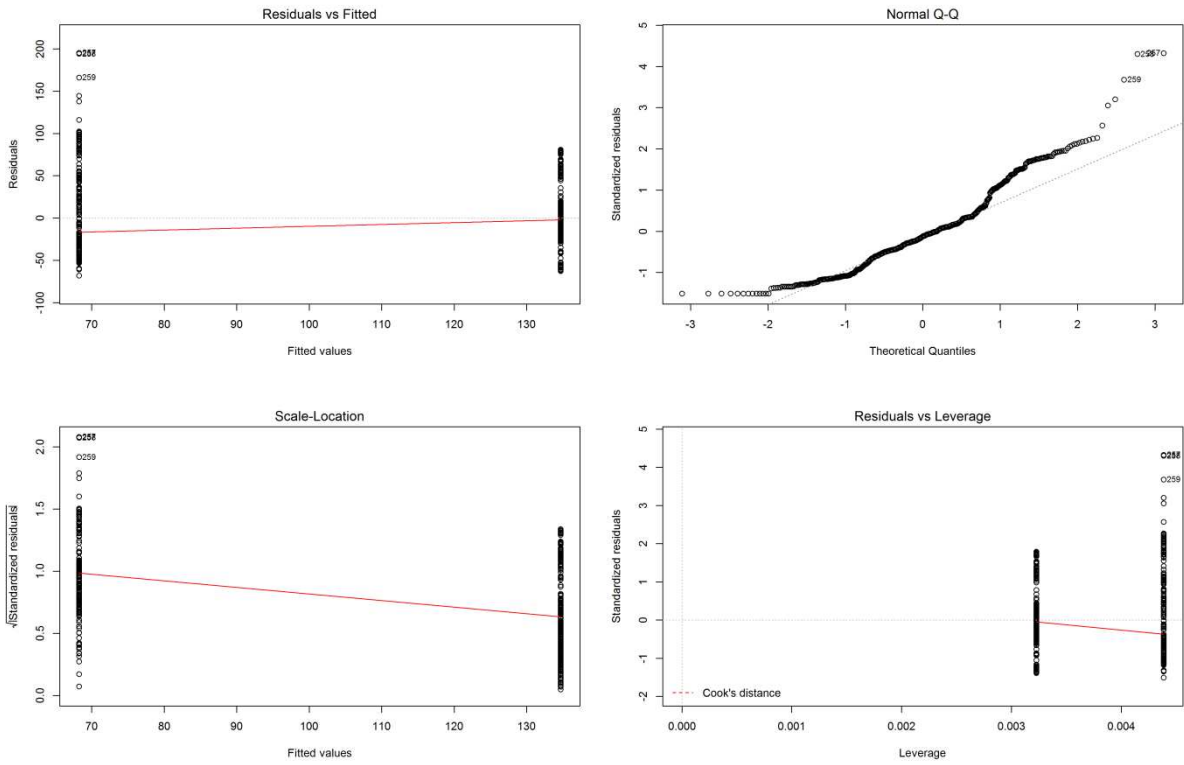


Figure 123. Diagnostic plots of TDS mass loading rate for applied water and tailwater for field DA7.

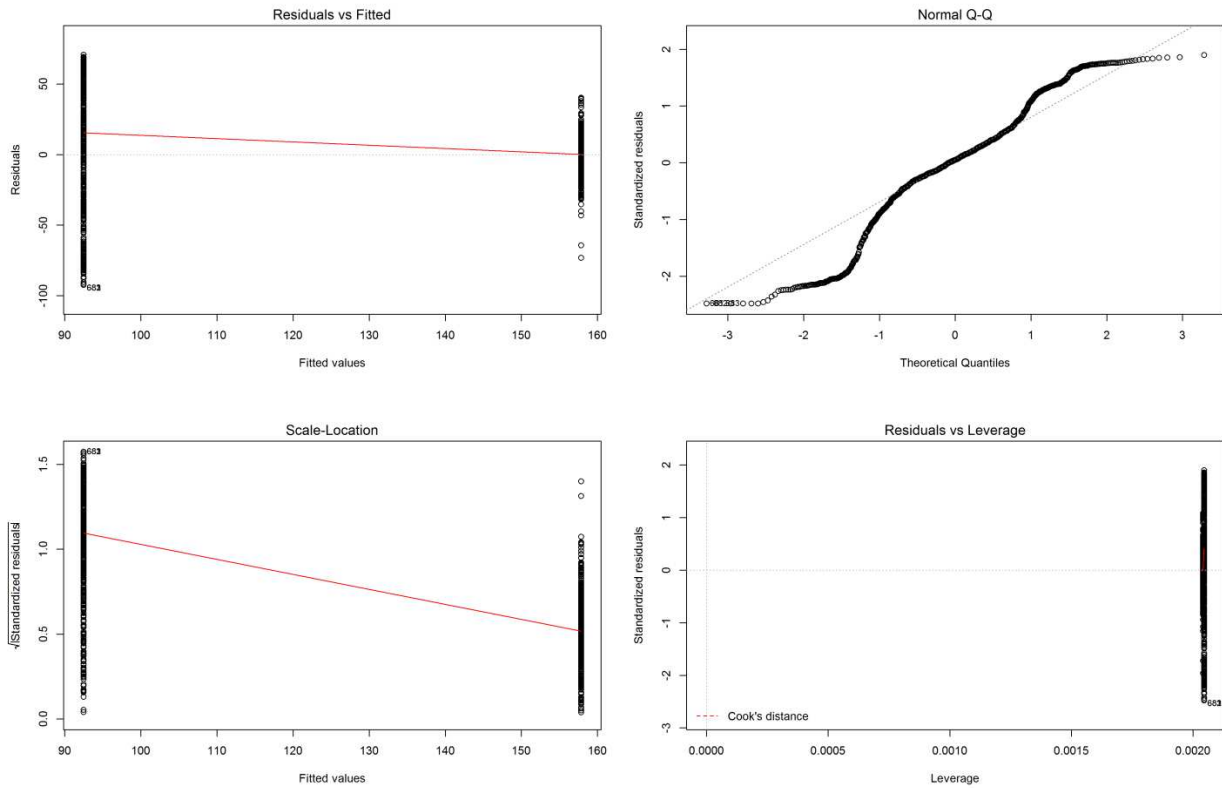


Figure 124. Diagnostic plots of TDS mass loading rate for applied water and tailwater for field Muth2.

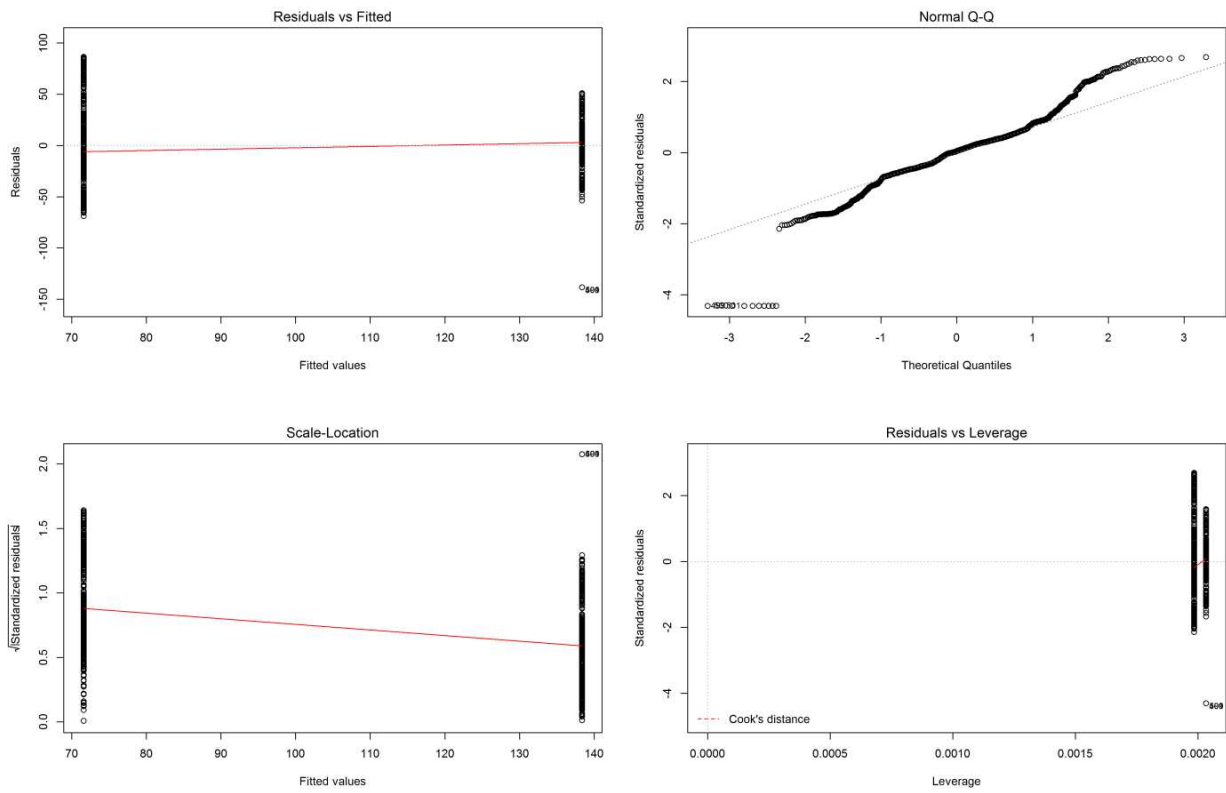


Figure 125. Diagnostic plots of TDS mass loading rate for applied water and tailwater for field Muth9.

*APPENDIX F: STATISTICAL DIAGNOSTICS FOR ANOVA STATISTICS FOR COMPARISON  
OF FIELD-SCALE SELENIUM MASS BALANCE POPULATIONS*

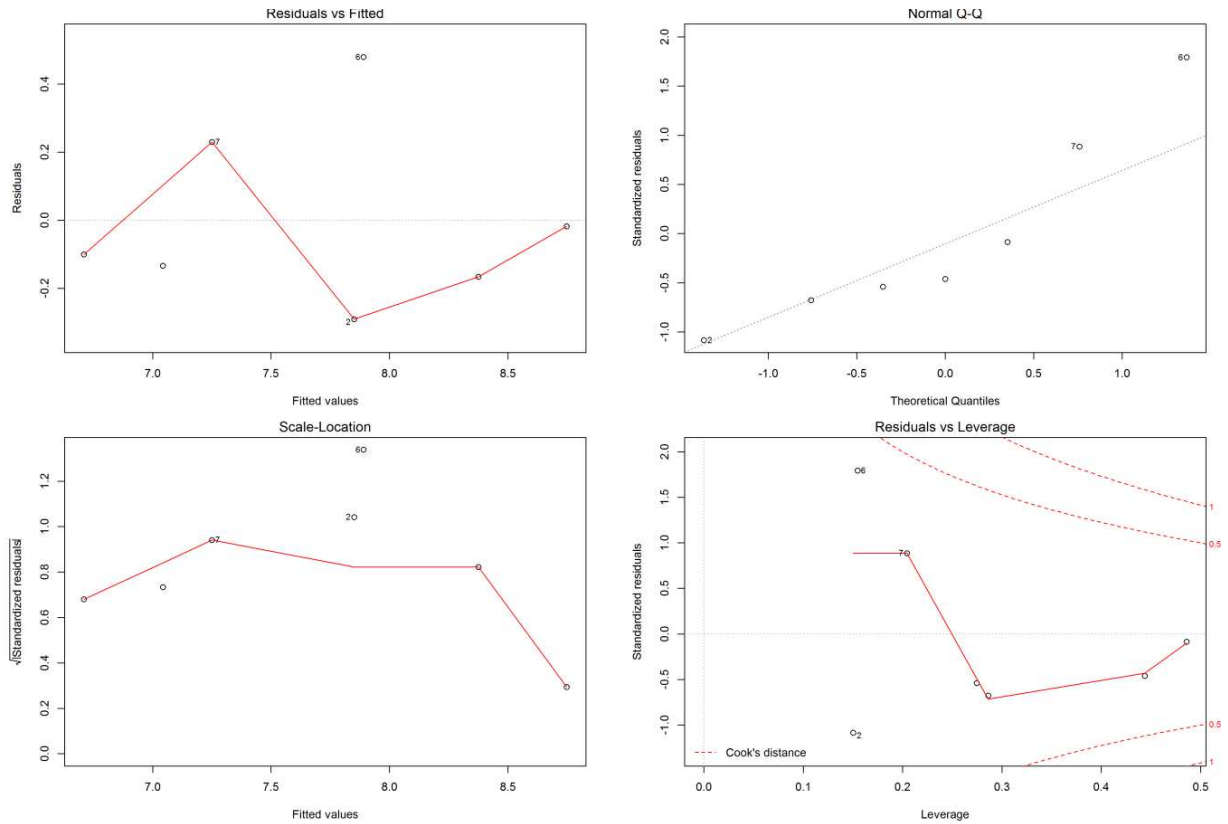


Figure 126. Diagnostic plots of  $C_{Se}$  vs  $C_{TDS}$  linear regression for applied water.

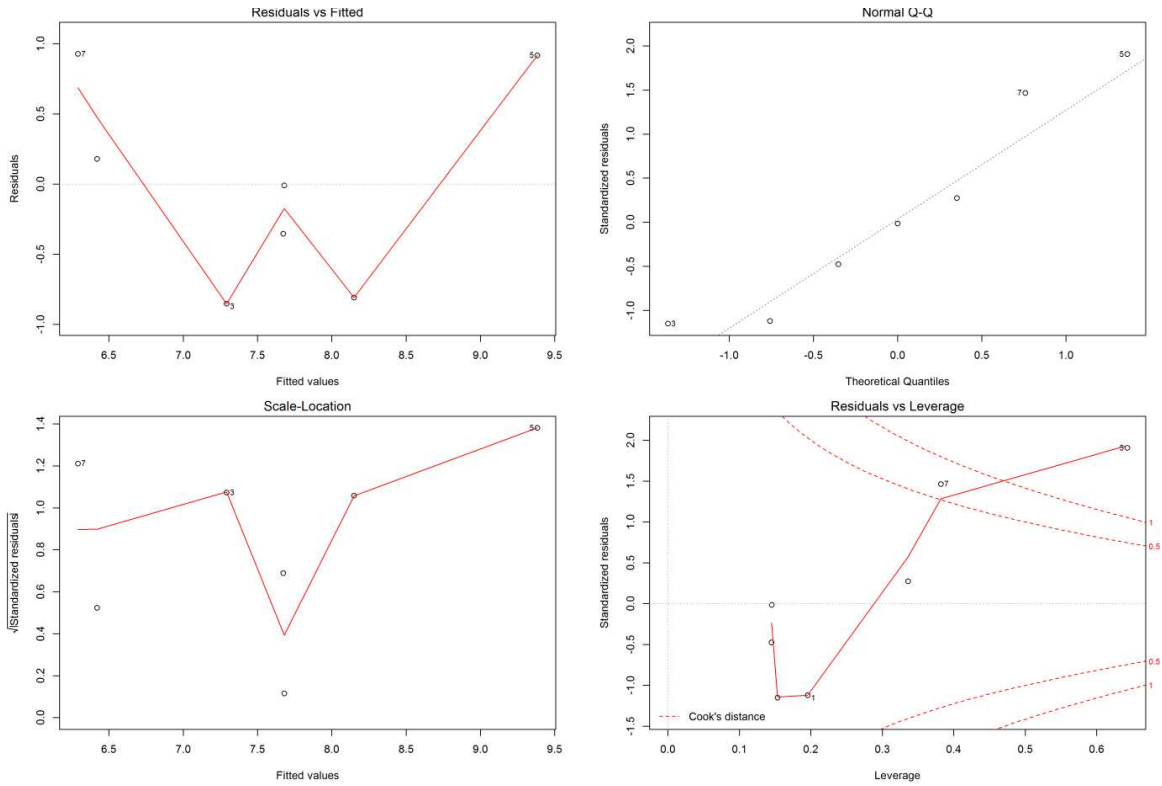


Figure 127. Diagnostic plots of  $C_{Se}$  vs  $C_{TDS}$  linear regression for tailwater.

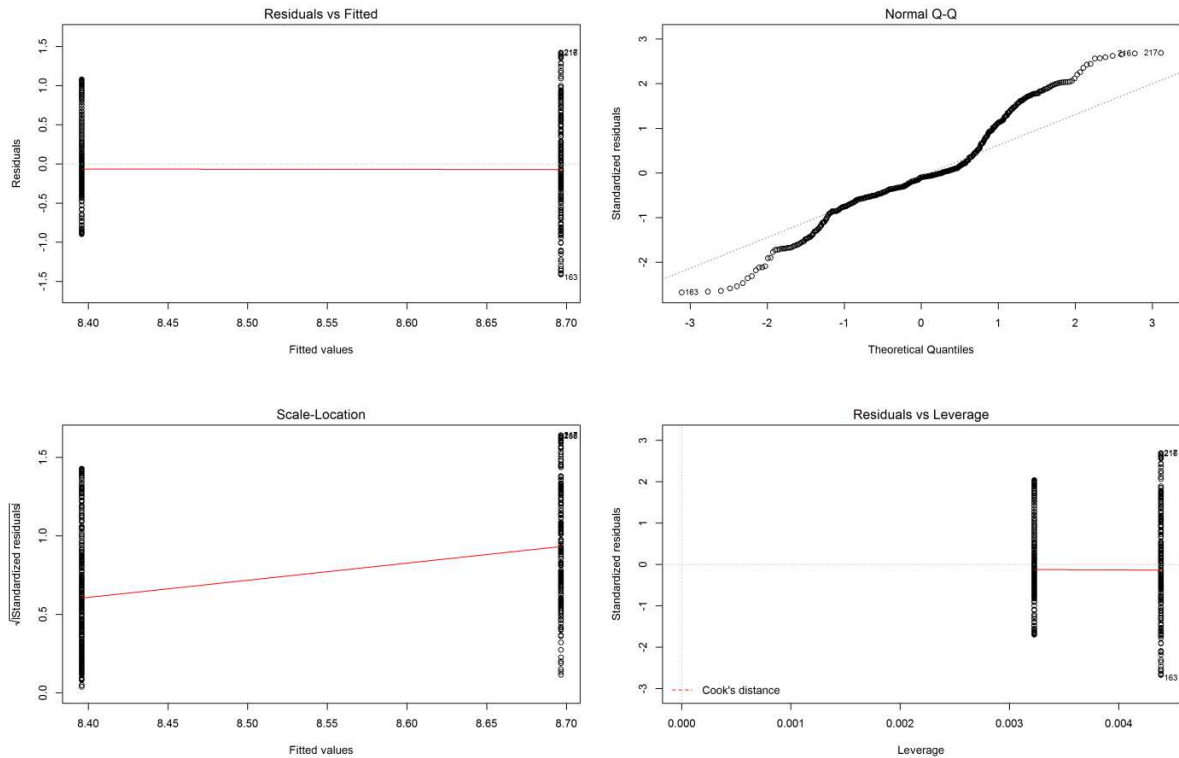


Figure 128. Diagnostic plots of  $C_{Se}$  for applied water and tailwater for field DA7.

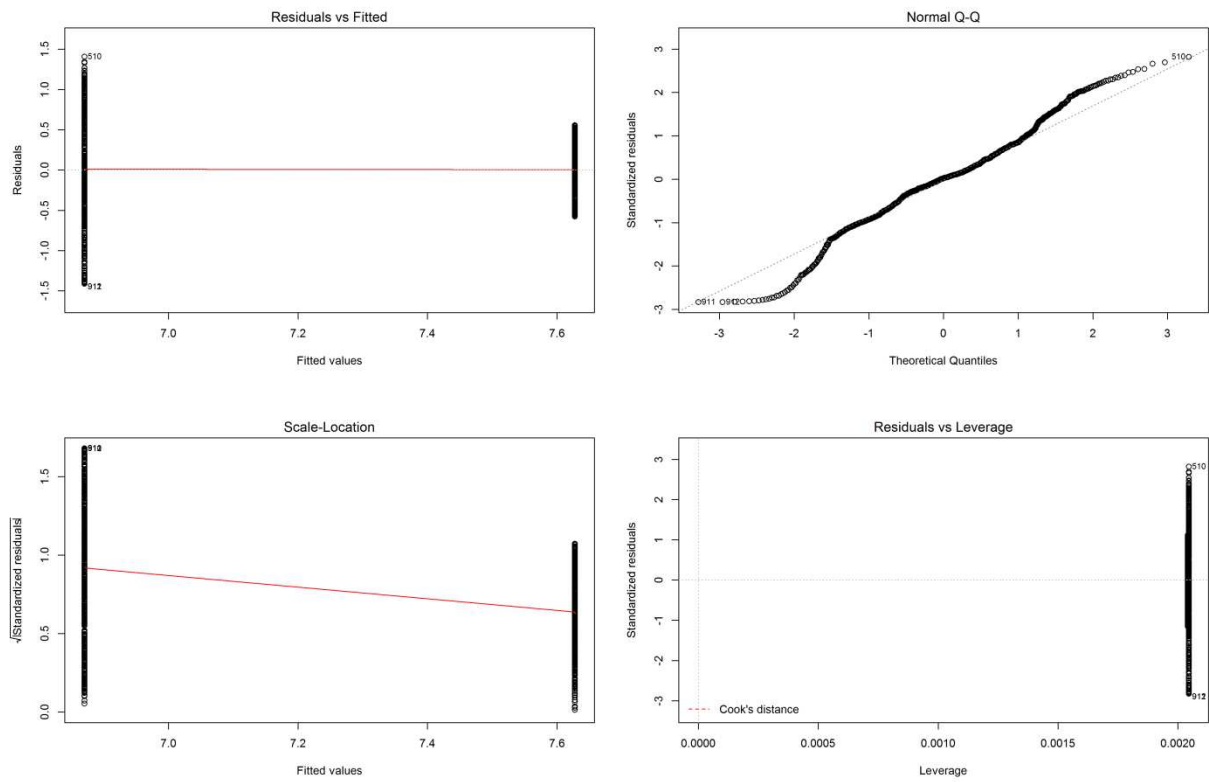


Figure 129. Diagnostic plots of  $C_{Se}$  for applied water and tailwater for field Muth2.

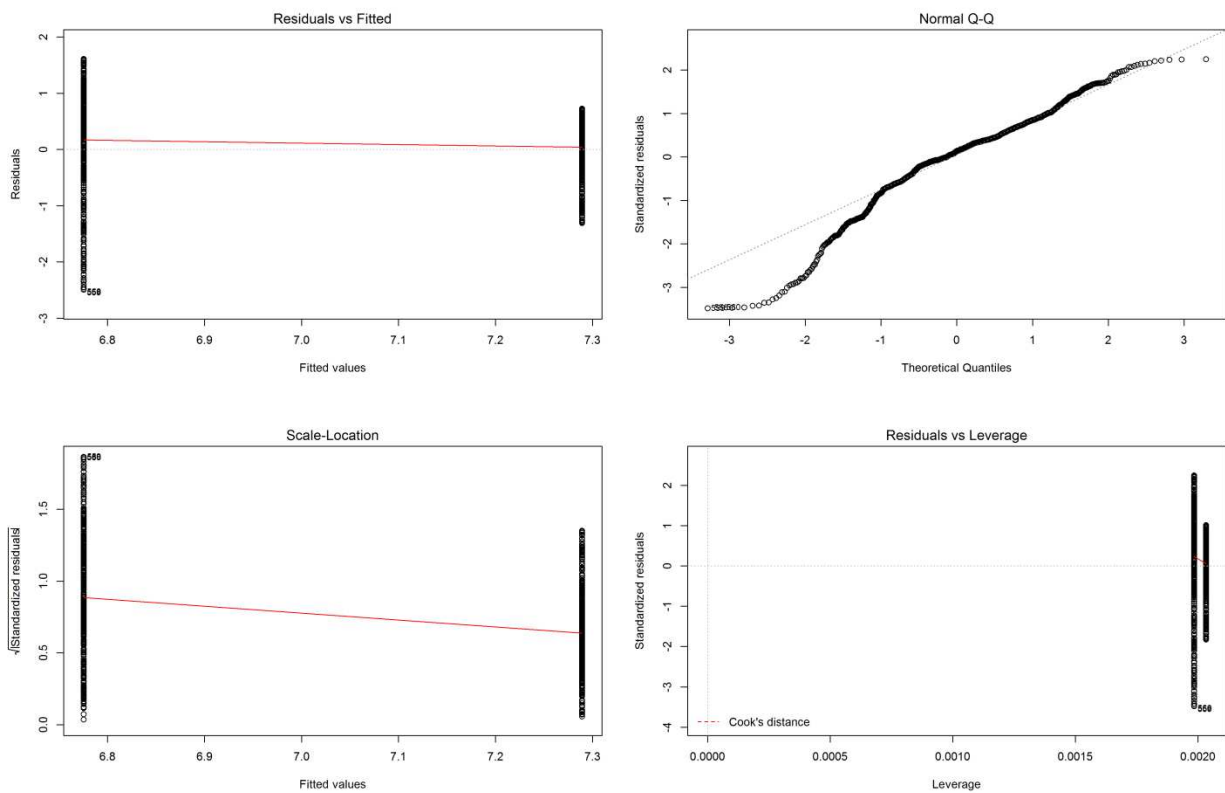


Figure 130. Diagnostic plots of  $C_{Se}$  for applied water and tailwater for field Muth9.

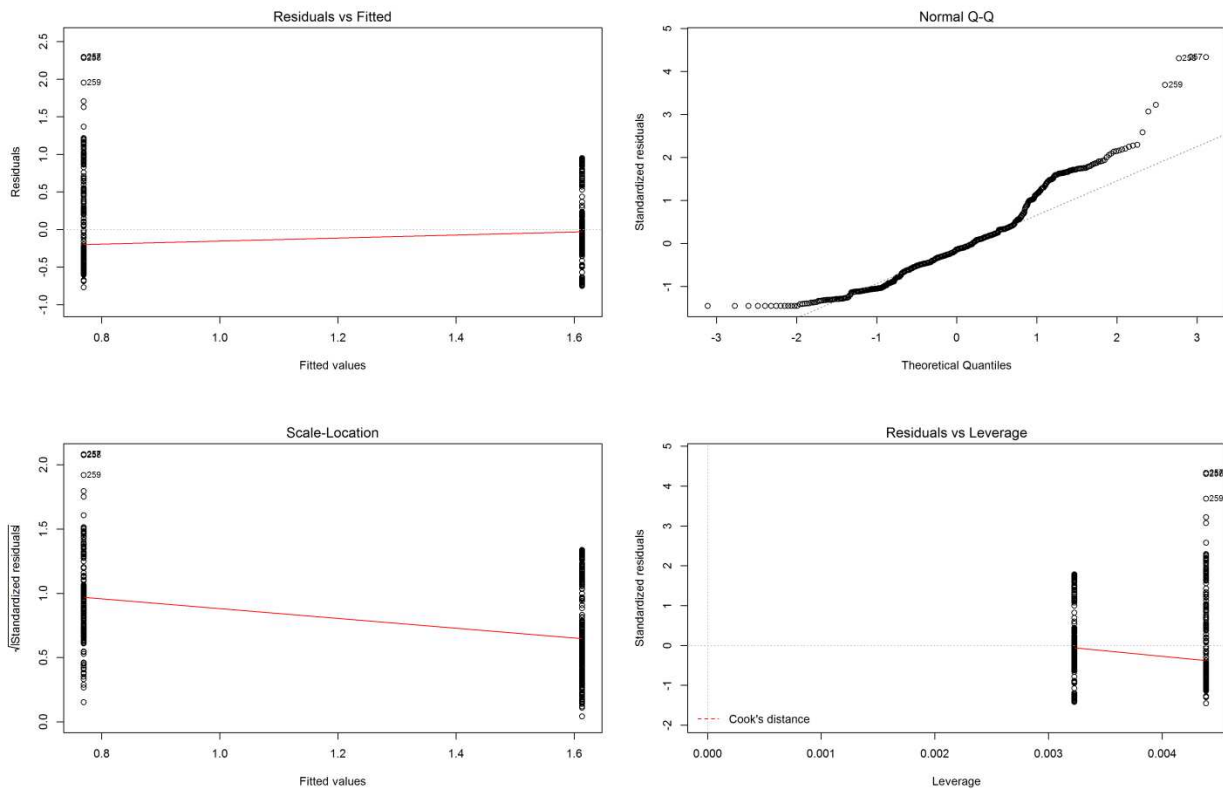


Figure 131. Diagnostic plots of dissolved Se mass loading rate for applied water and tailwater for field DA7.

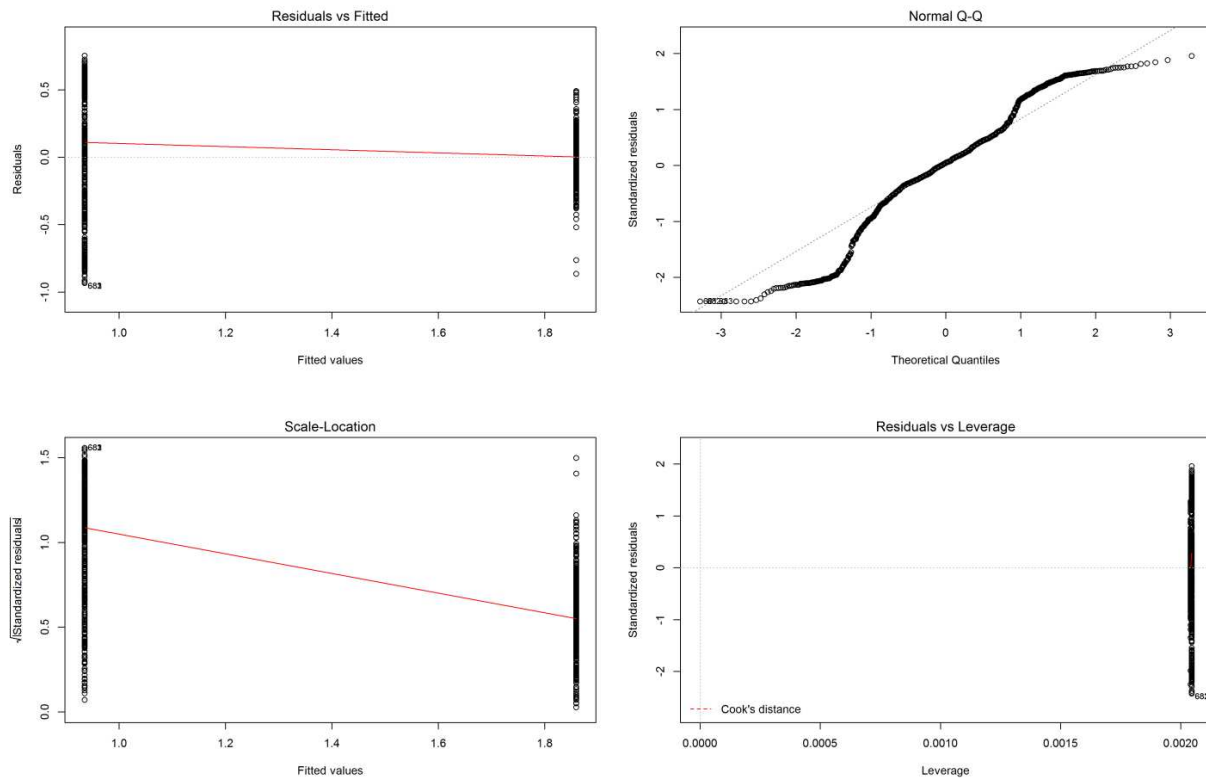


Figure 132. Diagnostic plots of dissolved Se mass loading rate for applied water and tailwater for field Muth2.

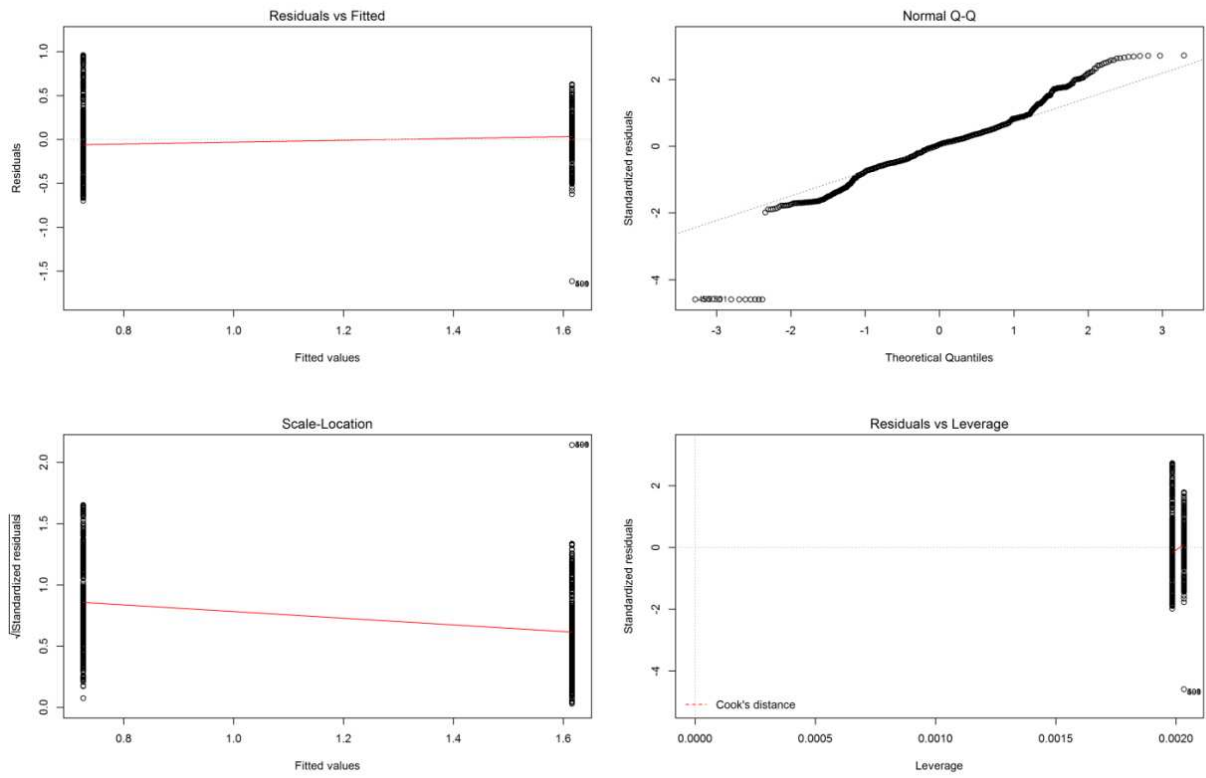


Figure 133. Diagnostic plots of dissolved Se mass loading rate for applied water and tailwater for field Muth9.

*APPENDIX G: STATISTICAL DIAGNOSTICS FOR ANOVA STATISTICS AND LINEAR  
REGRESSIONS OF SOIL SALINITY SURVEY AND MASS BALANCE*

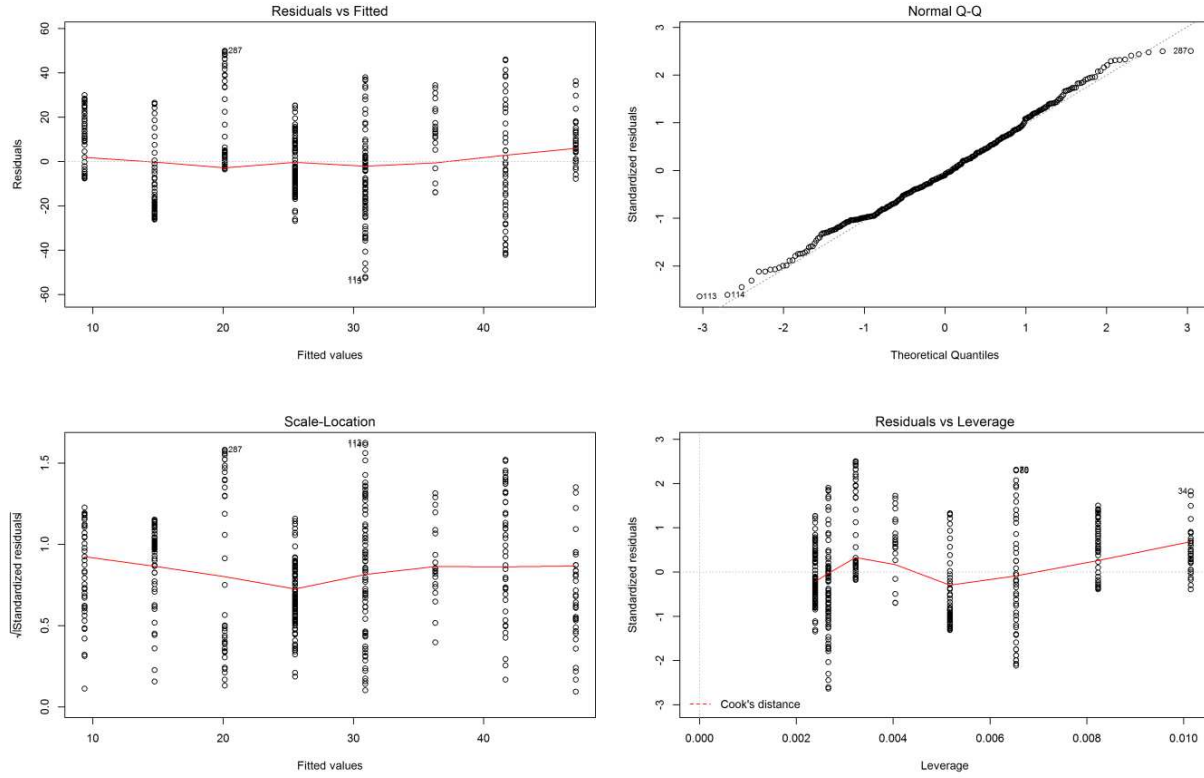


Figure 134. Diagnostic plots of the difference between applied water and tailwater  $C_{TDS}$  for each siphon interval for field Muth2.

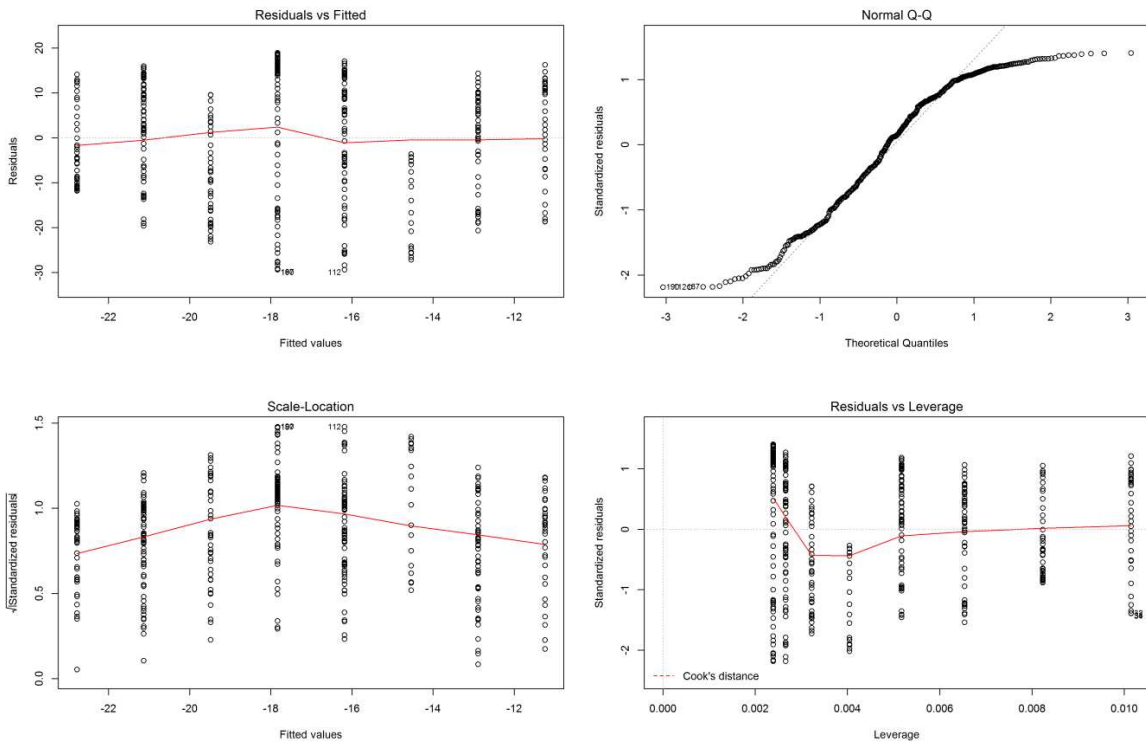


Figure 135. Diagnostic plots of the difference between applied water and tailwater TDS mass for each siphon interval for field Muth2.

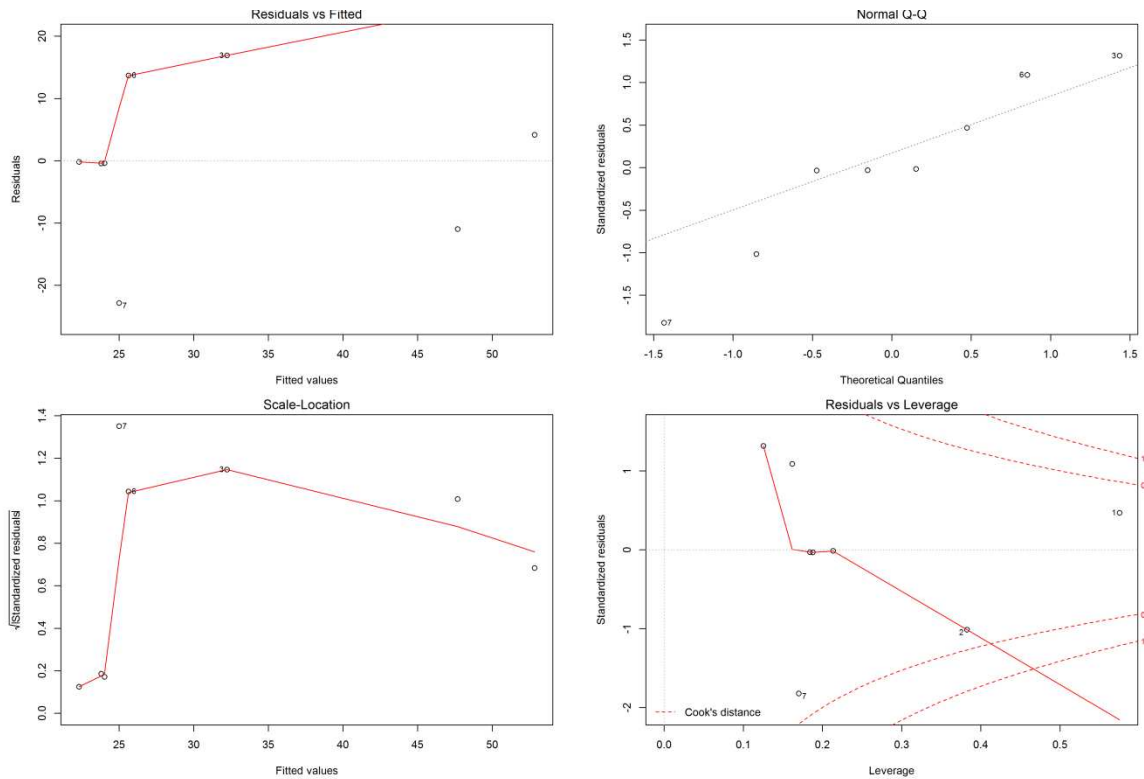


Figure 136. Diagnostic plots for the linear regression of the average difference of TDS concentration from applied water and tailwater vs average ECE of each siphon interval for field Muth2.

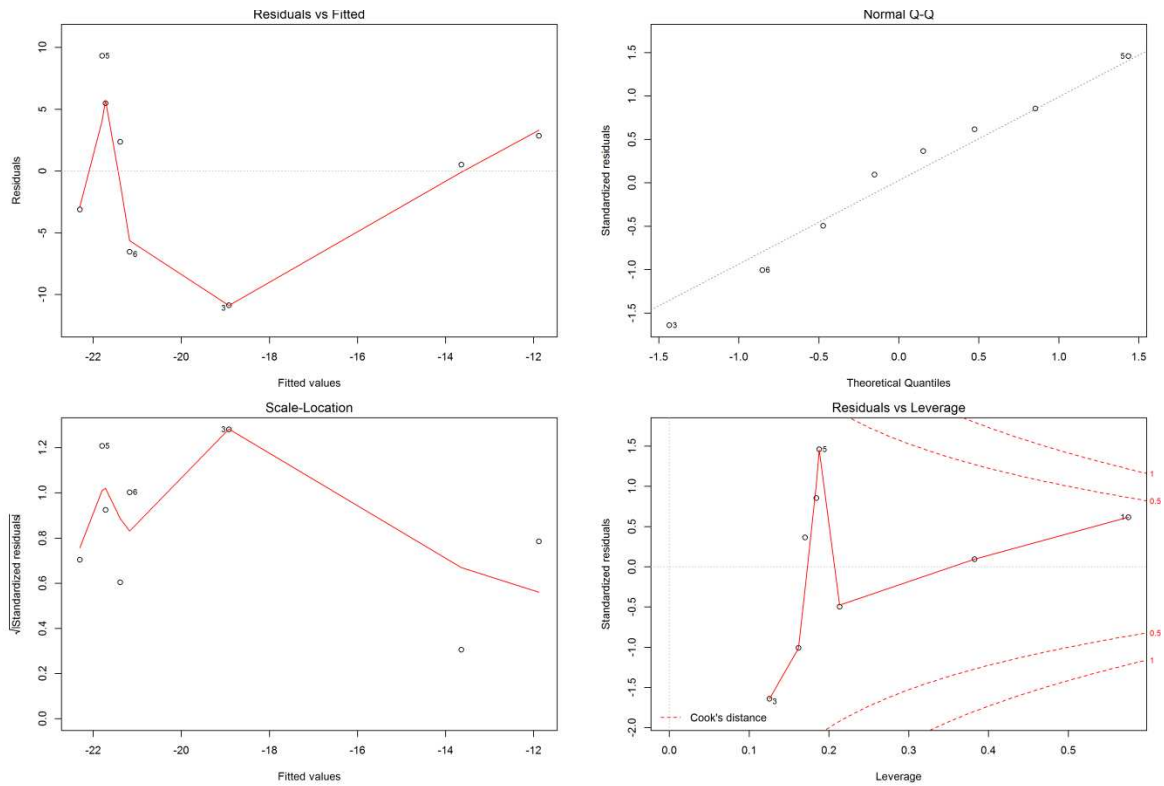


Figure 137. Diagnostic plots for the linear regression of the average difference of TDS mass from applied water and tailwater vs average ECE of each siphon interval for field Muth2.

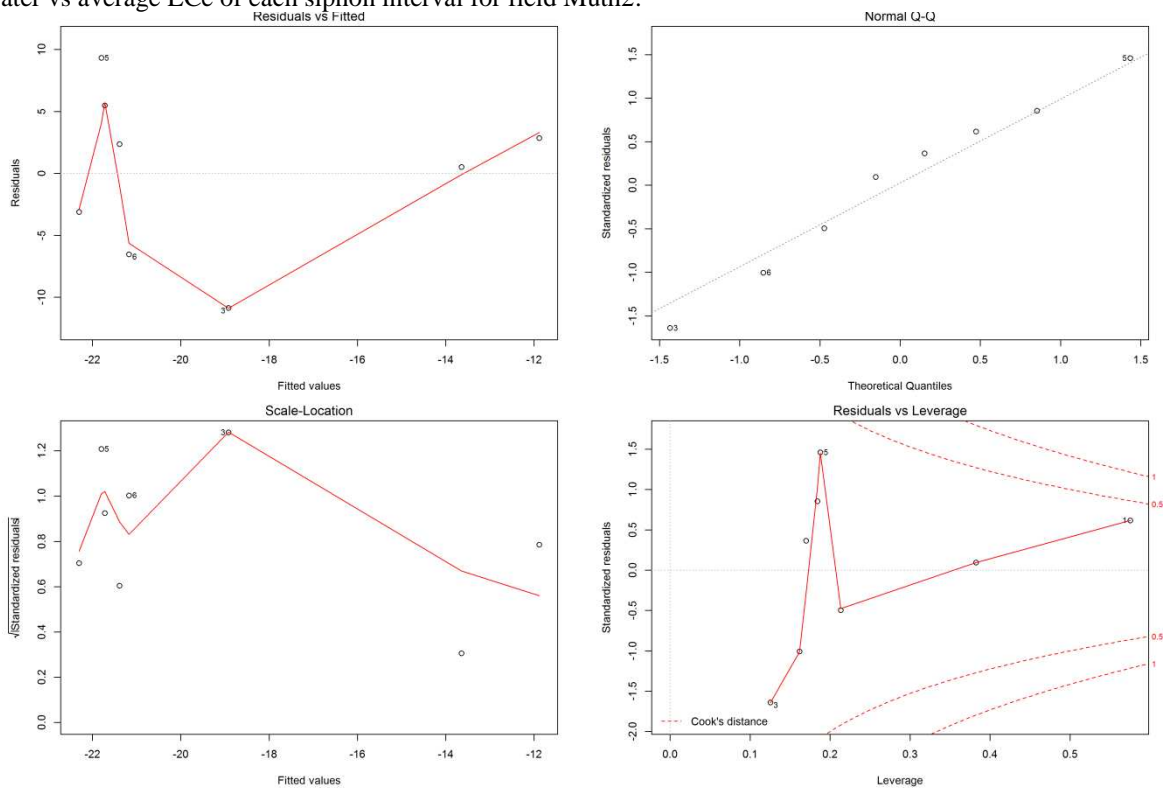


Figure 138. Diagnostic plots for the linear regression of the average difference of TDS mass from applied water and tailwater vs the volume of irrigated water for each siphon interval for field Muth2.